NEW NANOCOMPOSITE MATERIALS FROM KAOLINITE AS A MINERAL PRECURSOR

by

James J. Tunney

A thesis presented to the
School of Graduate Studies and Research
University of Ottawa

In partial fulfillment of the requirements
for the degree of

Ph.D. in Chemistry

Ottawa-Carleton Chemistry Institute
Ottawa, Ontario
August 1995

Ph.D. Candidate
James Joseph Tunney

Research Supervisor
Professor Christian Detellier

ISBN 0-612-15684-2

Canada

UNIVERSITÉ D'OTTAWA
UNIVERSITY OF OTTAWA

NEW NANOCOMPOSITE MATERIALS FROM KAOLINITE AS A MINERAL PRECURSOR

by

James J. Tunney

ACKNOWLEDGEMENTS

First and foremost, I would very much like to thank my research supervisor, Professor Christian Detellier for his steadfast support, encouragement and great enthusiasm throughout my Ph.D. studies.

I would also like to thank all my colleagues in Dr. Detellier's lab and in the chemistry department whom I had the pleasure of working with during my time at the University of Ottawa. Specifically, I would like to acknowledge Louis Mercier, Laila Raki and Hongbai Lao for helpful discussions, Johan Blixt for computer help, Corinne Bensimon and Ron Conlon for recording some of the X-Ray diffraction patterns, and Glen Facey for recording most of the solid state NMR spectra.

Finally, I would like to acknowledge all my family for their encouragement throughout my studies, especially my wife, Rita, for her great patience and support throughout my studies. It is to her that I dedicate this thesis.

ABSTRACT

New thermally resistant nanocomposite organokaolinite materials have been prepared and characterized. The preparation method for these materials generally involves first expanding the kaolinite interlayers with an intercalating agent such as dimethyl sulfoxide, followed by reaction with a given reagent in the interlayer space of the expanded kaolinite. In many cases the interlamellar surface of kaolinite was chemically modified through the grafting of organic units on the mineral surface. One new class of organokaolinite material was proposed to be formed through the interlayer condensation reaction between an alcohol group of the attacking species and an interlayer surface aluminol group of the kaolinite host to form Al-O-C linkages between the mineral and the organic components. In this manner, new chemically robust methoxy and ethylene glycol functionalized organokaolinites were prepared, with basal spacing of 8.2 Å and 9.4 Å respectively.

Furthermore, a new family of oxyethylene ($-OCH_2CH_2-$) based organokaolinite material was prepared and characterized. These materials include the species 15-crown-5 and 18-crown-6 as well as polyethylene glycol chains (MW 3400) which have been successfully incorporated into the interlayers of kaolinite. The products exhibit well defined basal spacings ranging from 10.8 Å to 11.2 Å, indicative of a 3.6-4.0 Å layer expansion due to a flattened monolayer arrangement of the oxyethylene units. The materials were generally stable up to temperatures greater than 250°C in both nitrogen

and air atmospheres, but the oxyethylene component could be leached out in refluxing water.

Finally, some promising exploratory work involving the functionalization of the interlamellar surface of kaolinite with aminoalcohols, carboxylic acid derivatives and other reagents is presented.

TABLE OF CONTENTS

LIST OF FIGURES

LIST OF TABLES

SYMBOLS AND ABBREVIATIONS

Clays:

Kao	kaolinite
Hal	halloysite
Sep	sepiolite
KGa-1	well-crystallized kaolinite from Georgia

Chemical Reagents:

DMSO	dimethyl sulfoxide
NMF	N-methylformamide
Hz	hydrazine
HOAc	acetic acid
KOAc	potassium acetate
MeOH	methanol
EtOH	ethanol
EG	ethylene glycol
MEO	2-methoxyethanol
EOA	ethanolamine (2-aminoethanol)
1,2 PD	1,2 propanediol
1,3 PD	1,3 propanediol
1,2 BD	1,2 butanediol
1,3 BD	1,3 butanediol
1,4 BD	1,4 butanediol
2,3 BD	2,3 butanediol
1,5 PD	1,5 propanediol
DiEG	diethylene glycol
DiEGBE	diethylene glycol mono n-butyl ether
TriEG	triethylene glycol
TriEGMME	triethylene glycol monomethyl ether
TetraEG	tetraethylene glycol
PEG	polyethylene glycol
PEG 1000	polyethylene glycol (average MW = 1000)
PEG 3400	polyethylene glycol (average MW = 3400)
PEO	polyethylene oxide
15C5	15-crown-5
18C6	18-crown-6
OEU	oxyethylene unit (OCH_2CH_2)
PDMS	polydimethylsiloxane

Organoclays:

Kao-DMSO	kaolinite-dimethyl sulfoxide
Kao-NMF	kaolinite-N-methylformamide
Kao-Hz	kaolinite-hydrazine
Kao-KOAc	kaolinite-potassium acetate
Hal-DMSO	halloysite-dimethyl sulfoxide
Hal-NMF	halloysite-N-methylformamide
Kao-MeOH	kaolinite-methanol
Kao-EG	kaolinite-ethylene glycol
Kao-Glycerol	kaolinite-glycerol
Kao-H_2O	kaolinite-hydrate
Kao-1,2 PD	kaolinite-1,2 propanediol
Kao-1,3 PD	kaolinite-1,3 propanediol
Kao-1,2 BD	kaolinite-1,2 butanediol
Kao-1,3 BD	kaolinite-1,3 butanediol
Kao-1,4 BD	kaolinite-1,4 butanediol
Kao-1,5 BD	kaolinite-1,5 butanediol
Kao-DiEGMBE	kaolinite-diethylene glycol mono n-butyl ether
Kao-TriEGMME	kaolinite-triethylene glycol monomethyl ether
Kao-MEO	kaolinite-2-methoxyethanol
Kao-EOA	kaolinite-ethanolamine
Kao-3,1 AP	kaolinite-3,1 aminopropanol
Kao-HOAc	kaolinite-acetic acid
Kao-PrOAc	kaolinite-propionic acid
Kao-DiEG	kaolinite-diethylene glycol
Kao-TriEG	kaolinite-triethylene glycol
Kao-TetraEG	kaolinite-tetraethylene glycol
Kao-PEG 1000	kaolinite-(polyethylene glycol MW 1000)
Kao-PEG 3400	kaolinite-(polyethylene glycol MW 3400)
Kao-15C5	kaolinite-15-crown-5
Kao-18C6	kaolinite-18-crown-6

Miscellaneous:

CEC	cation exchange capacity
CPK	Corey-Pauling precision molecular model
GC-MS	gas chromatography mass spectrometry
XRF	X-ray fluorescenece
XRD	X-ray diffraction
d_{001}	basal spacing
I.R.	intercalation ratio

K	residual kaolinite (XRD)
IR	infrared spectroscopy
FTIR	fourier transform infrared spectroscopy
NMR	nuclear magnetic resonance
MAS	magic angle spinning
CP/MAS	cross polarization magic angle spinning
DD/MAS	dipolar dephasing magic angle spinning
τ	dipolar dephasing time
I_0	intensity of signal without dipolar dephasing.
I_{DD}	intensity of signal with dipolar dephasing.
T_2	tranverse relaxation
TGA	thermogravimetric analysis
DGA	differential gravimetric analysis
DSC	differential scanning calorimetry
DTA	differential thermal analysis
endo.	endotherm
exo.	exotherm

Chapter 1

Introduction

1.1 A Brief Description of the Clay Minerals

Clay minerals are naturally occurring minerals which are usually formed as a result of the weathering of rocks, usually feldspars. The environmental conditions in which this weathering process takes place governs the type of clay which is formed. The clays then either remain where they are to give rise to "residual clays" or they are transported by water, wind and/or ice to be deposited as beds of clay in the sea or in lakes, or as land deposits. Clay minerals belong to the family of minerals called phyllosilicates (Greek: phyllon= leaf), or sheet silicates. As the name suggests, most of the members of this group have a platy morphology.

1.1.1 Structure [1-3]

Layer silicates may be thought of as being composed from two types of extended 2-dimensional units. The first is a sheet of corner-linked tetrahedra, and the second is a sheet of edge-linked octahedra. The manner in which these two units are joined and arranged determines the type of clay mineral. A clay layer is made up of two or three of these sheets which are joined together. The layers then stack one upon the other.

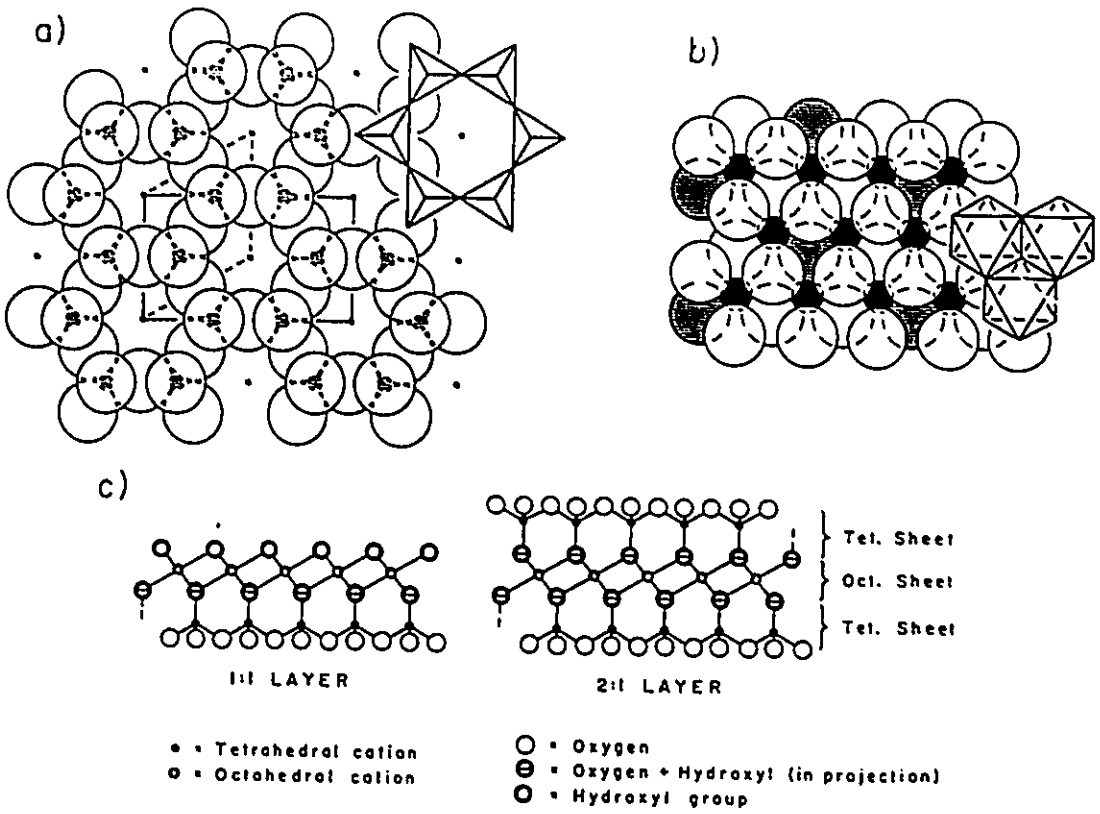

Figure 1.1: (a) Idealized tetrahedral sheet with hexagonal (dashed line) and orthogonal (full line) cells. (b) Idealized octahedral sheet with OH groups of lower anion plane (dashed circles) shown shaded. For a 1:1 layer upper anion plane (full circles) will be entirely OH groups. For a 2:1 layer upper anion plane will be of same composition as lower anion plane. (c) Combination of sheets to form 1:1 and 2:1 layers. (reproduced with permission from reference 2)

The tetrahedral sheet structural unit is composed primarily of Si^{4+} cations in tetrahedral coordination with oxygen. Al^{3+} or Fe^{3+} may often substitute for Si^{4+} in the tetrahedral sheet, thus imparting a net negative charge to the tetrahedral sheet. Each tetrahedron can be thought to rest on a triangular face with the oxygens on all three corners being shared with neighbouring tetrahedra. The fourth apical oxygen points upward, perpendicular to the base. Under conditions of zero strain, this sheet would be hexagonal, with the Si-O bond distance equal to 1.62 Å and the O-O distance equal to 2.64 Å. This idealized hexagonal pattern can be visualized in Figure **1.1 a**. Although tetrahedral sheets do not exist in an unconstrained state in minerals, Bailey has estimated their ideal lateral dimension in the free state as $b = 9.15 \pm 0.06$ Å [2].

The octahedral sheet consists of two planes of closest-packed oxygen or hydroxyl ions with cations occupying the resulting octahedral sites between the two planes (Figure **1.1 b**). The cations are usually Al^{3+} or Mg^{2+} although many transition metal cations and even Li^{+} may also be found in the octahedral holes. The minerals gibbsite ($Al(OH)_3$) and brucite ($Mg(OH)_2$) are the two prototypes commonly used to describe respectively dioctahedral and trioctahedral clay minerals. In gibbsite, two out of three octahedral holes are occupied by Al^{3+} cations, whereas in brucite, all three octahedral holes are occupied by Mg^{2+}. In these free octahedral sheets, the lateral b-dimension of the unit cells are 8.64 Å for the dioctahedral gibbsite and 9.36 Å for the trioctahedral brucite [2].

The tetrahedral and octahedral sheets are joined together by the replacement of two out of three hydroxyls in one of the octahedral planes by the apical oxygens of the tetrahedral sheet. The third hydroxyl fits into the middle of the hexagonal ring of the

tetrahedral sheet. When one tetrahedral and one octahedral sheet are joined together, this is called a 1:1 layer silicate structure (Figure **1.1 c**). When an additional tetrahedral layer is joined in the same manner to the free hydroxyl surface of the 1:1 layer silicate structure, a 2:1 layer silicate structure is formed (Figure **1.1 c**).

The lateral dimensions of the tetrahedral sheet rarely fit that of the octahedral sheet. A tetrahedral sheet containing only silicon has an ideal lateral b dimension intermediate between those of the ideal octahedral sheets containing only Mg (brucite) or only Al (gibbsite). The misfit is approximately 3-5 % for these cases [2]. This means that distortions or adjustments to the tetrahedral and/or octahedral sheets are necessary in order to join the sheets together. This can be accomplished in ways such as through the rotation or tilting of the tetrahedra or through the thickening or thinning of octahedral or tetrahedral sheets. It should also be noted that isomorphic substitution of Al^{3+} for Si^{4+} in the tetrahedral sheet has the effect of increasing the b dimension somewhat in response to the larger Al^{3+} ion.

When tetrahedral and octahedral layers are assembled into layers, they may be electrically neutral or they may be negatively charged. This is a direct consequence of isomorphic substitution of a lower valent cation in the octahedral and/or tetrahedral sheets. This can be the result of Al^{3+} or Fe^{3+} for Si^{4+} in the tetrahedral sheet, or for example, Mg^{2+} substituting for Al^{3+} in a dioctahedral sheet. When the clay layer possesses a net negative charge, it must be balanced by an interlayer cation. This interlayer cation is usually Na^{+} or Ca^{2+}, but other cations may be found in the

interlayers. These counter cations are often in a hydrated form and may be readily exchanged with other cations.

1.1.2 Polytypism [1]

Polytypism is a result of the different stacking arrangements of identical layers. When discussing polytypes in clay minerals, it is generally assumed that the stacking of layers in polytypes may be regular or random. In ordered stacking, the relationship of one layer to another can be explained on the basis of a rotation of some integral value of 60 °, which is repeated from one layer to another. In random stacking, rotation from one layer to another must also be an integral value of 60 °, only in this case the integer multipliers are random.

Another type of stacking, termed turbostratic is a highly disordered stacking arrangement in which there is little or no regular amount of rotation relating one layer to the next. It can be thought of as resembling a pile of cards lying flat on each other but with little or no alignment of the edges.

1.1.3 Classification of the Clay Minerals [2,4]

The clay minerals may be classified on the basis of layer type (1:1 or 2:1), layer charge and type of interlayers. Recently, the Clay Minerals Society Nomenclature Committee has decided to further classify the clay minerals on the basis of their

superstructures [4]. These include the planar hydrous phyllosilicates (Table **1.1**) and the non-planar hydrous phyllosilicates (Table **1.2**).

1.1.3.1 Planar Hydrous Phyllosilicates

This division of the clay minerals is arranged into eight main groups with subgroups being determined on the basis of the octahedral character (dioctahedral or trioctahedral with 2.5 cations as the boundary). Species in a given subgroup are distinguished by different compositions, stacking arrangements or octahedral vacancy sequences. The structures of some of the major non-modulated hydrous phyllosilicates groups are given in Figure **1.2**. These include the neutral kaolin, pyrophyllite and talc groups, as well as the mica, smectite and chlorite groups which all possess negative layer charges. Mica has a high charge density ($x \approx 1.0$) and the layers are held rigidly shut with the interlayer cation (usually potassium) held in 12-fold coordination with the oxygens of the two tetrahedral sheet surfaces. Smectites by contrast, have a lower charge density ($x \approx 0.25$-0.6) than do micas, and have exchangeable interlayer cations. These interlayer cations exist in nature in a hydrated state. Chlorites, like micas and smectites are also made up of negatively 2:1 layers, only here the negative charge of the 2:1 layers are counterbalanced not by interlayer cations but by positively charged interlayer octahedral hydroxide sheets. The di-trioctahedral chlorite sudoite for example, has negatively charged dioctahedral 2:1 layers and positively charged interlayer trioctahedral hydroxide sheets.

Layer Type	Interlayer Material[1]	Group	Octahedral Character	Species[2]
1:1	None or H_2O only ($x \approx 0$)	Serpentine-Kaolin	Trioctahedral Dioctahedral Di-trioctahedral	Lizardite, Berthierite, Amesite Kaolinite, Dickite, Nacrite, Halloysite (planar) Odinite
2:1	None ($x \approx 0$)	Talc-Pyrophyllite	Trioctahedral Dioctahedral	Talc, Willemsite, Kerolite, Pimelite Pyrophyllite, Ferripyrophyllite
	Hydrated exchangeable cations ($x \approx 0.2$-0.6)	Smectite	Trioctahedral Dioctahedral	Saponite, Hectorite, Sauconite Montmorillonite, Beidellite, Nontronite
	Hydrated exchangeable cations ($x \approx 0.6$-0.9)	Vermiculite	Trioctahedral Dioctahedral	Trioctahedral Vermiculite Dioctahedral Vermiculite
	Non-hydrated monovalent cations ($x \approx 0.6$-1.0)	True (flexible) Mica	Trioctahedral Dioctahedral	Biotite, Phlogopite, Lepidolite Muscovite, Illite, Glauconite
	Non-hydrated divalent cations ($x \approx 1.8$-2.0)	Brittle mica	Trioctahedral Dioctahedral	Clintonite, Anandite, Bityite Margarite
	Hydroxide sheet ($x \approx$ variable)	Chlorite	Trioctahedral Dioctahedral Di-trioctahedral	Clinochlore, Chamosite, Ninite Donbassite Cookeite, Sudoite
2:1	Regularly Interstratified ($x \approx$ variable)	Variable	Trioctahedral Dioctahedral	Corrensite, Hydrobiotite Rectorite

Table 1.1: Classification of Planar Hydrous Phyllosilicates. [1] x is net layer charge per $O_{10}(OH)_2$ formula unit. [2] only some examples are given. (adapted from reference 3)

Layer Type	Modulated Component	Linkage Configuration	Unit Layer, c sin ß value	Traditional Affiliation	Species[1]
A. Modulated Structures					
1:1	Tet. Sheet	Strips	7 Å	Serpentine	Antigorite, Bemenite
		Islands	7 Å	Serpentine	Greenalite, Caryopilite, Pyrosmalite
2:1	Tet. Sheet	Strips	9.5 Å	Talk	Minnesotaite
			12.5 Å	Mica	Ganophyllite, Eggletonite
		Islands	9.6-12.5 Å	Mica/complex	Zussmanite, Parssettenite
		Other	12.3 Å	None	Bannisterite
			14 Å	Chlorite	Gonyerite
	Oct. Sheet	Strips	12.7-13.4 Å	Pyribole	Sepiolite, Palygorskite, Loughlinite
B. Rolled and Spheroidal Structures					
1:1	None	Trioctahedral	-	Serpentine	Chrysotile, Pecoraite
		Dioctahedral	-	Kaolin	Halloysite (non-planar)

Table 1.2: Classification of non-planar hydrous phyllosilicates. [1] only some examples are given. (adapted from reference 3)

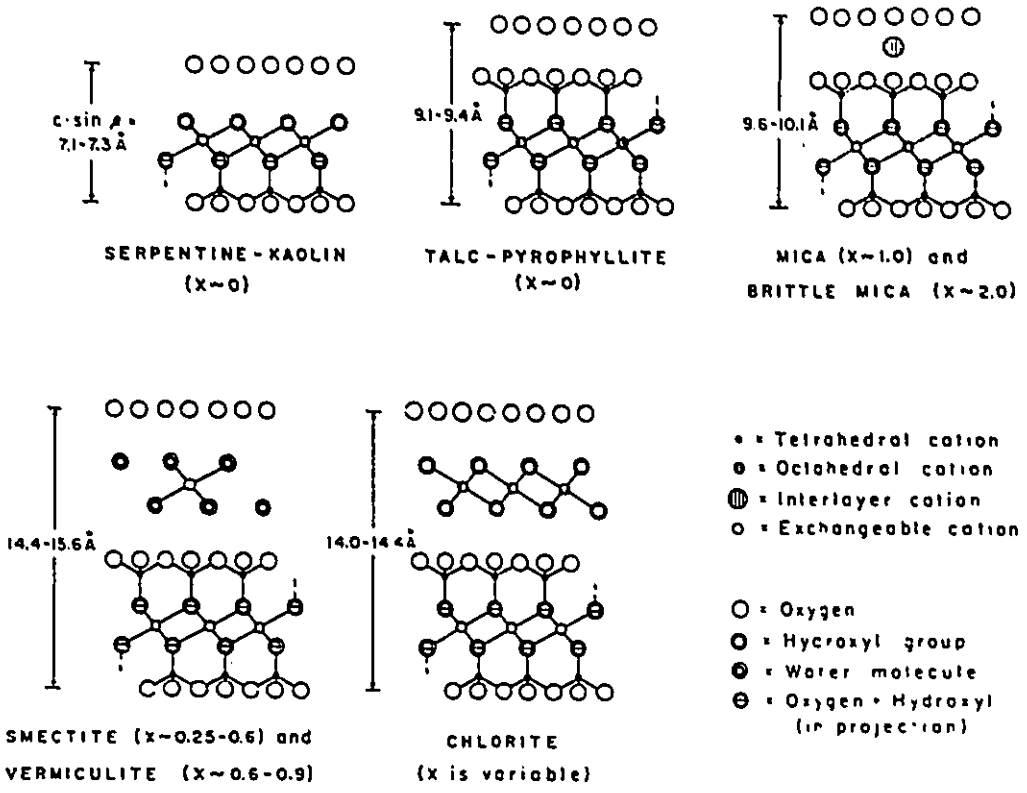

Figure 1.2: [010] view of structures of major non-modulated hydrous phyllosilicate groups. (reproduced with permission from reference 2)

1.1.3.2 Non-Planar Hydrous Phyllosilicates

Modulated layer silicates are those minerals in which there is a periodic perturbation of the basic silicate structure [4,5]. The classification scheme given in Table **1.2** is derived by considering the nature of the periodicity and the relationship of the perturbation to the basic 1:1 or 2:1 structure. Differing compositions and further structural variations within the subdivisions determine the species. Structural models of the tetrahedrally modulated layer silicates palygorskite and sepiolite are given in Figure **1.3.** It should be noted that both of these structures have a continuous two-dimensional tetrahedral sheet, but unlike the planar 2:1 hydrous phyllosilicates, they lack a continuous octahedral sheet. The structures of these minerals may be described as containing strips of 2:1 phyllosilicate structure, one strip being linked to the next by inversion of SiO_4 tetrahedra along a set of Si-O-Si bonds. These strips extend parallel along the x-axis (out of the page) forming a framework of rectangular channels between opposing 2:1 ribbons [6]. This is a good example of the structural complexity which can be found in many of the clay minerals.

Rolled forms, such as coils and spheroids, are not thought to be periodic within the layers over the entire extent of the crystal, as are the modulated layer silicates [4]. For example, if one considers non-planar halloysite which is made up of kaolinite-like layers rolled up into a cylinder in a spiralling pattern, it is clear that the radius is continuously varying and non-periodic. These structures do nonetheless, have a periodicity at the unit cell level. The minerals allophane and imogolite may also be tentatively placed into this

last grouping along with non-planar halloysite since there are many structural similarities. Both allophane and imogolite are structurally and chemically very similar to the 1:1 kaolins, yet they are found in the form of 35-50 Å diameter hollow spheres (allophane) and 18.3-20.2 Å tubes with a distance of 21-23 Å between the axes of the tubes (imogolite) [1,7].

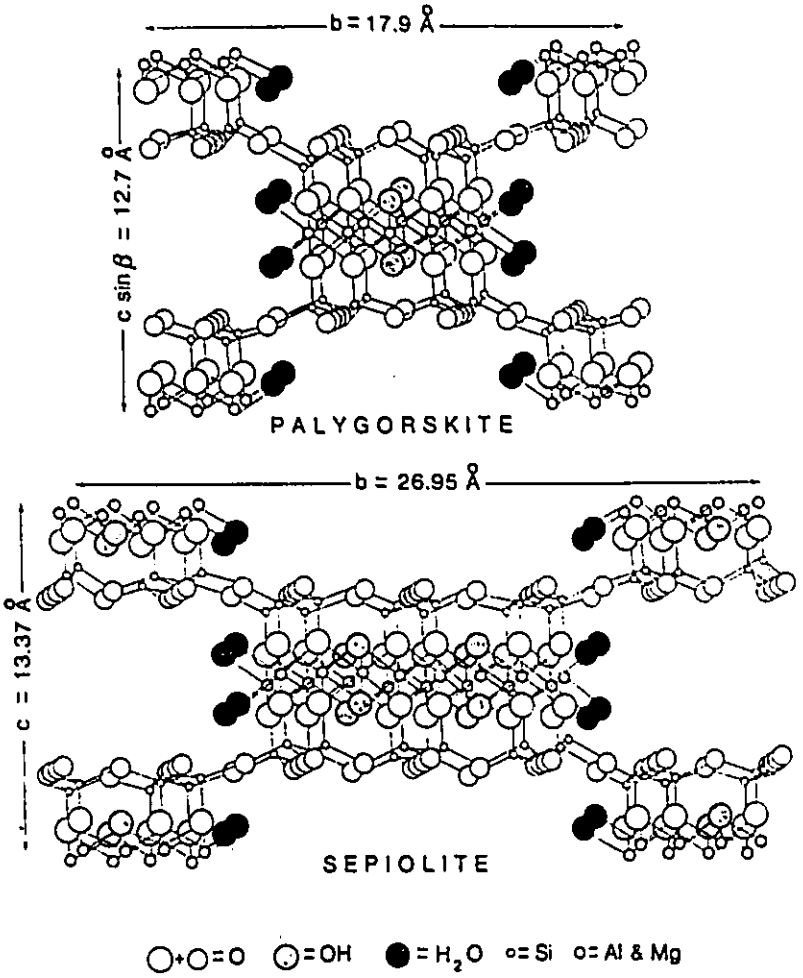

Figure 1.3: Schematic structure of palygorskite and sepiolite. (reproduced with permission from reference 6)

1.2 Kaolin Minerals

The origin of the word kaolin is believed to be derived from one of two sources, both involving derivations of the Chinese word "Kauling". In one interpretation, kaolin takes its name from the Chinese word for "high ridge" from where it was mined for many centuries near Jauchau Fu [8,9]. An alternate interpretation is that kaolin takes its name from the locality of Kauling in Kiangsi Province where it was also mined from the 11th century until 1964 [10,11]. Kaolin is also known to many as China clay. The origin of this expression is also unclear, although some trace its origin to Marco Polo, who brought back large ceramic urns from China and referred to these articles as "Chinaware". When kaolin was discovered in Cornwall, England, and was found to be similar to the type of clay used in China to make Chinaware, it was therefore called "China Clay" [8]. Other commercial terms associated with various types of kaolinitic clays are ballclays, fireclays, flintclays and underclays. Each of these terms describe kaolins with certain physical properties and uses primarily in the ceramics and refractory industries [1,8].

Kaolin is one of the most important natural industrial substances. In 1987, it was estimated that the worldwide production of kaolin was 20 million tons [8], which works out to a worldwide average of about 4 kg per person. Approximately 60 % of this was used in the paper industry, where kaolin is used as a filler in the interstices of the cellulose fibres that form the paper sheet and as a coating on the surface of the sheet to improve

the fidelity of printing using coloured inks. Other major uses of kaolin are in the ceramics, paints, rubbers, plastics and catalysis industries.

The kaolins are dioctahedral 1:1 hydrous phyllosilicates (Tables **1.1** and **1.2**) and are made up of the minerals kaolinite, halloysite, dickite and nacrite. All of these minerals have the approximate composition $Al_2Si_2O_5(OH)_4$ and are neutral. Small quantities of iron, titanium, potassium and magnesium are normally found in natural kaolins. Traces of other minerals such as vermiculite, mica or smectites may also be detected by XRD and these impurities are thought to contribute to the small negative charge found on some kaolinites [12].

Of the four kaolin minerals, kaolinite is by far the most ubiquitous. It is found primarily in soils and permeable bedrock in warm and moist regions. It is formed mainly as a weathering product or by hydrothermal alteration [10]. The most common parent minerals from which the kaolin minerals form, are feldspars and muscovite. For example, the transformation of potassium feldspar into kaolinite occurs by intense weathering of the feldspar and leaching of potassium and SiO_2 according to the following reaction [8]:

Potash Feldspar		Water		Kaolinite		Silica		Potash
$2\ KAlSi_3O_8$	+	$3\ H_2O$	→	$Al_2Si_2O_5(OH)_4$	+	$4SiO_2$	+	$2K(OH)$

In this process, all of the potassium is lost in solution and the much less soluble kaolinite and silica are left behind.

The formation of the rarer minerals dickite and nacrite, is believed to be restricted almost exclusively to hydrothermal occurrences [1,8]. The conditions for the formation of halloysite versus kaolinite are not entirely understood. It has been suggested that halloysite is simply a highly disordered form of kaolinite, disordered enough to allow water into the interlayers (see section **1.3**) [13]. It has also been suggested that halloysite is composed of a tetrahedral sheet with a greater amount of aluminum for silicon substitution than is found for the other kaolin minerals. This causes bending of the layers into a tubular morphology [8,14].

1.2.1 Polytypism in the Kaolin Minerals

All the kaolin minerals are made up of nearly identical 7.2 Å thick 1:1 layers of composition $Al_2Si_2O_5(OH)_4$. Nonetheless, it has been shown that many different polytypes for the kaolin minerals are possible [2]. Newnham for example claimed that six 1-layer and 108 2-layer structures were theoretically possible [15]. Zvyagin [16] later showed that only 52 theoretical dioctahedral structures with periodicities between one and six layers were possible since some of Newnham's theoretical structures were equivalent to one another. Thus far only three of the polytype structures have been conclusively shown to exist, presumably due to relative stability considerations [3,10]. These structures are those corresponding to kaolinite, dickite and nacrite. The stacking arrangement and exact structure of halloysite in both its collapsed 7 Å form and its expanded 10 Å hydrated form is still poorly understood [10,13].

In order to understand some of the factors which govern the determination of polytypes in the dioctahedral kaolins, it is useful to first consider the simpler case involving the trioctahedral serpentine minerals. This situation is simpler because there are no octahedral vacancies which may distort and break the symmetry of the structures. Here, the three octahedral cations may occupy one of two sets of positions above the oxygen/hydroxyl plane between the tetrahedral and octahedral sheets. This is illustrated in Figure **1.4** which discriminates between these two sets of positions as set I and set II. Depending on the set of positions that the octahedral cations occupy, the octahedral sheets have slants that differ by $\pm$ 60 ° or 180 ° relative to fixed axes [2,3]. This also implies that I transforms to set II by simple layer rotations of $\pm$ 60 ° or 180 °, so these two sets are in fact equivalent. The importance of these two sets comes from whether the same set of three octahedral positions is occupied in each successive layer or whether there is an alternation.

The positions of the adjacent layers has been shown to be determined largely by the formation of long hydrogen bonds between the basal tetrahedral oxygen surface of one layer with the octahedral hydroxyl surface of another layer [17,18]. This is shown in Figure **1.5** where the tetrahedral oxygen atoms are paired with the octahedral hydroxyl groups. It should be noted that other geometric pairing patterns are possible. Bailey [2,3,18] has shown that for planar structures, interlayer hydrogen bonds can be formed through the exact superposition of the hexagonal rings in the tetrahedral sheets of successive layers or through various interlayer shifts along the fixed hexagonal X and Y axes (see Figure **1.5** for X and Y coordinates).

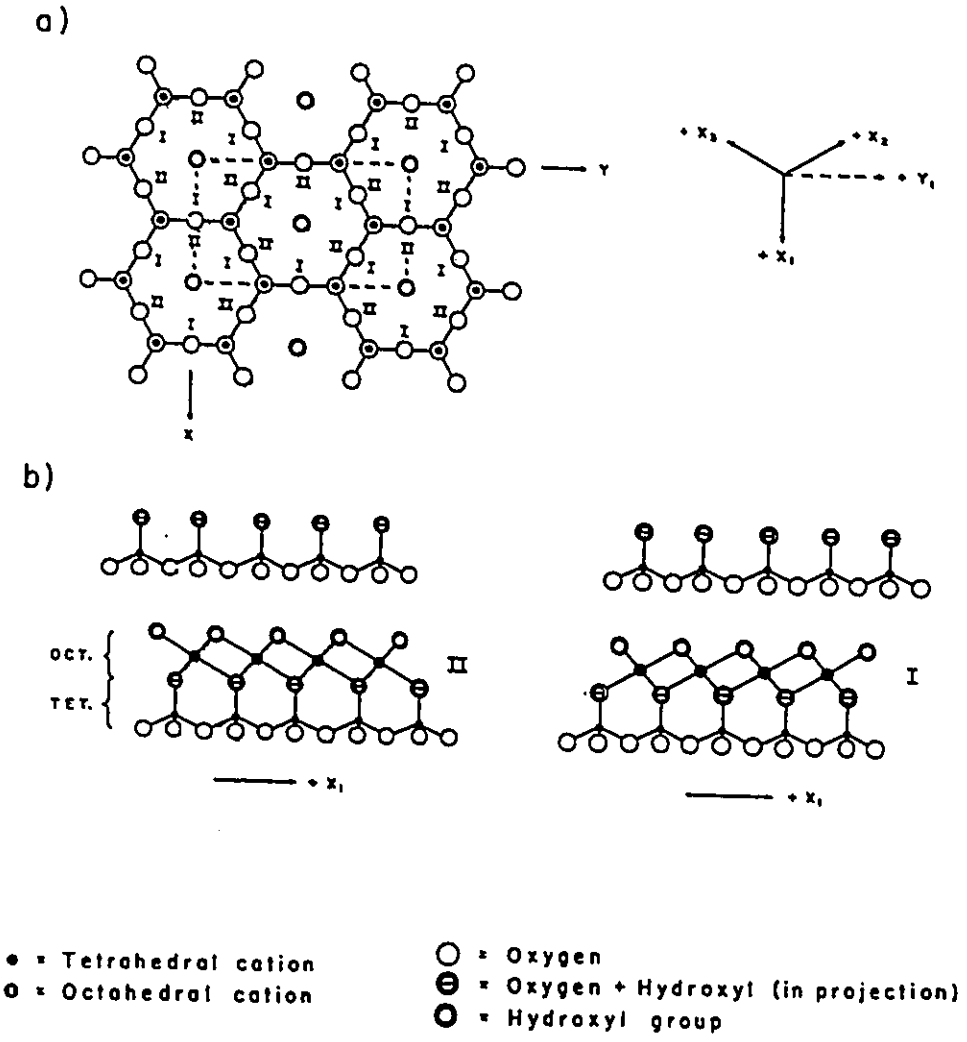

Figure 1.4: (a) Definition of I and II sets of octahedral cation positions above a tetrahedral set for a 1:1 layer, relative to a fixed set of hexagonal axes. (b) Octahedral sheets slant in opposite directions relative to a fixed X_1 direction for occupancy of I or II set of octahedral cation positions (reproduced with permission from reference 3)

Twelve standard trioctahedral 1:1 polytypes, plus four enantiomorphic structures were derived by making certain limiting assumptions [3,18]. These assumptions include undistorted tetrahedral and octahedral sheets, regular layer stacking and importantly, only one type of relative layer superposition within the same crystal. The 12 standard polytypes are shown diagrammatically in Figure 1.6. Each ideal polytype is specified by a symbol consisting of a number to indicate the number of layers in the repeating unit along Z and letters to indicate the resulting lattice symmetry. Subscripts are used to differentiate structures that have the same periodicity and symmetry.

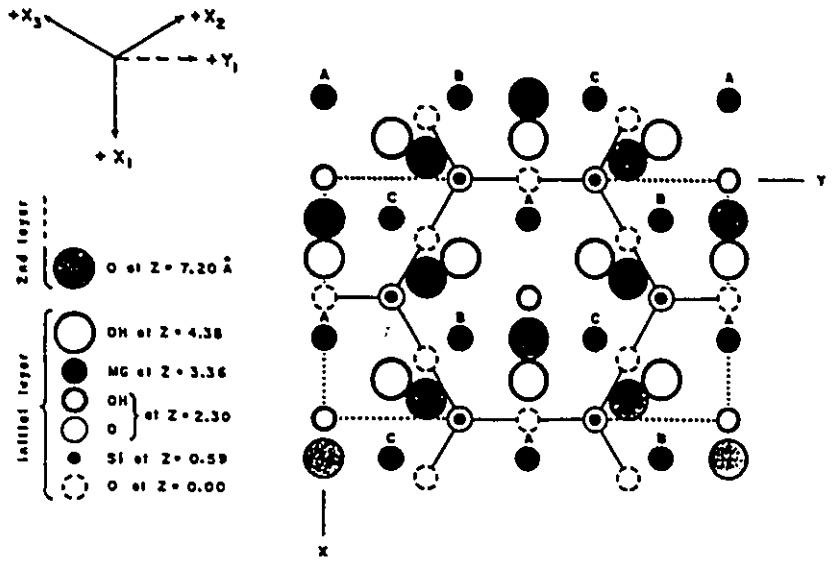

Figure 1.5: Pairing of tetrahedral oxygen atoms (stipled) at the base of an upper 1:1 layer with the octahedral OH groups (large double circles) on the upper surface of the layer below. (reproduced with permission from reference 3)

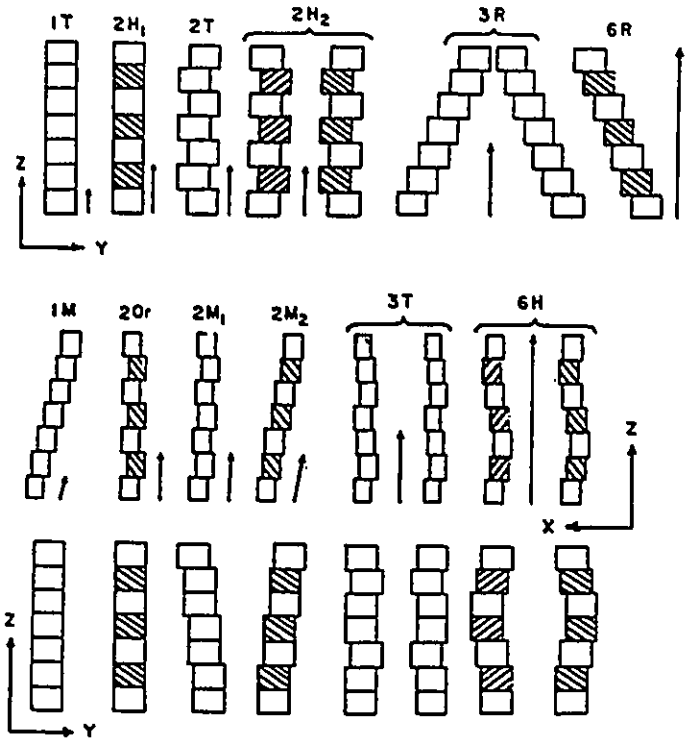

Figure 1.6: XZ and YX projections of 12 standard polytypes plus 4 enantiomorphic structures (linked by brackets). Blank and ruled rectangles represent layers with octahedral cations in sets II and I, respectively. Thin arrows indicate periodicity along Z. (reproduced with permission from reference 3)

The situation for the dioctahedral kaolin minerals is complicated by the presence of an octahedral vacancy site. The relative position of this vacancy site from layer to layer provides another degree of variability in the kaolin minerals. In any given layer, the vacancy may occur in the A,B or C positions shown in Figure 1.5. Sites B and C are enantiomorphic since they lie on opposite sides of a mirror plane, whereas site A lies on the mirror plane itself. This is shown more clearly in Figure 1.7 which shows the disposition of the octahedral sites in three successive 1:1 layers with either of the three possible sites vacant. For the kaolin group minerals, the vacant site is not A as in the micas, but either the enantiomorphic sites B or C.

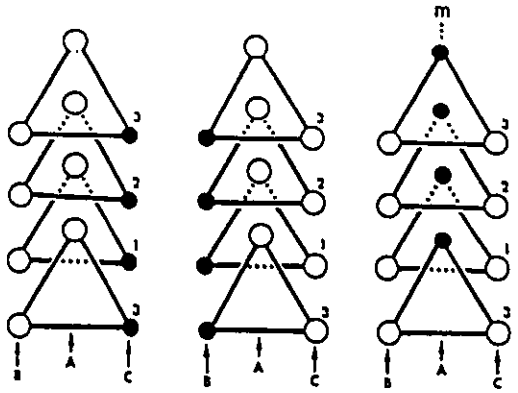

Figure 1.7: Three views projected onto (001) of the octahedral sites in kaolinite and dickite showing the possible placement of the vacant octahedral site. In each of these views the X direction is down and the Y direction is across from left to right. (reproduced with permission from reference 10)

This along with the distortions in the hexagonal pattern that are caused by the relative enlargement of the vacant site compared to the two occupied sites [2], cause symmetry changes in kaolinite, dickite and nacrite relative to those of the corresponding trioctahedral 1:1 structures [3,17]. Moreover, the presence of this vacant site also changes the layer periodicities of dickite and nacrite.

In kaolinite, the vacant octahedral site is believed to be either in position B or its mirror image, position C [2,3,17], although it has been proposed on the basis of XRD patterns that if the real distorted structure of kaolinite is considered, the vacant site must be B and not C [10,19]. This gives kaolinite a 1M (Figure **1.6**) stacking sequence of layers with a triclinic symmetry imposed by the loss of the symmetry plane that relates B to C (and by also by structural distortions). Between each layer there is a -a/3 shift with respect to one another. Kaolinite has thus been designated by the structural symbol $1Tc = [1M_{ord}]$ [3,17].

In dickite, the stacking sequence is 1M just like with kaolinite, only here the vacant site alternates regularly between sites B and C in adjacent layers to create a two-layer superlattice of monoclinic symmetry (space group Cc). This is reflected in dickite's designated structural symbol, $2M = [1M_{ord.}]$ [3,17].

Finally, with nacrite, the sequence of layers is that of the standard trioctahedral 6R polytype (Figure **1.6**). However, the vacant octahedral site varies regularly in successive layers in such a way that the symmetry is reduced from rhombohedral to monoclinic, and an inclined Z-axis can be selected in which there is a true two layer periodicity [2,3]. Nacrite is designated by the structural symbol $2M = [6R_{ord}]$ [3,17].

1.2.2 Structural Model for Kaolinite

Since most of the work involved the use of kaolinite as the mineral precursor material, it is useful to describe some of the work that has been done pertaining to the structural elucidation of kaolinite. Since Pauling first deduced the basic structure of kaolinite by analogy with other phyllosilicates [20], many researchers have tried to verify this proposed basic structure, determine its space group, and locate all the atoms which make up the unit cell of kaolinite. The relevant work that has been done pertaining to this subject up until 1988 has been nicely summarized by Giese [10].

While it is accepted that kaolinite is triclinic, there has been considerable controversy regarding the space group assignment of kaolinite. Suitch and Young [21] and Young and Hewat [22] had proposed a primitive lattice space group P1 based on X-ray and neutron diffraction refinement studies. On the other hand, Bish and von Dreele [23] have insisted on the more commonly accepted C1 as the space group. This is important since the choice of a P1 lattice requires twice the number of independent atoms in a more asymmetric unit cell by allowing crystallographically identical atoms in C1 to occupy non-equivalent sites in P1. While it is accepted that the non hydrogen atoms of the structure largely obey C-centring, Young and co-workers concluded that the hydroxyl groups which were equivalent in C1 were inequivalent in P1 [21,22].

A major criticism of the crystal structure proposed by Young and Hewat has been the presence of several unrealistic Si-O and Al-O internuclear distances, as well as infrared spectroscopic data which is inconsistent with the P1 structure [10,23]. In a recent

development, Bish has used neutron diffraction data taken at 1.5 K, in order to refine the kaolinite structure to a C1 lattice [24]. This fit was found to be better than that which was obtained using a P1 lattice. At present, the consensus seems to be that there is no need to use the lower symmetry P1 space group since the C1 space group model fits both diffraction and spectroscopic data quite well. It is therefore this model which will be assumed.

The unit cell parameters for the non hydrogen atoms refinement of a highly ordered kaolinite using a C1 space group, are given below [23].

a = 5.1554 Å	α = 91.700 °
b = 8.9448 Å	ß = 104.862 °
c = 7.4048 Å	Γ = 89.822 °

This refinement indicates that Si-O distances are 1.60-1.63 Å, Al-O distances are 1.87-1.97 Å, and the tetrahedral rotation angle is 6.9 °. The distance between surface tetrahedral basal oxygens is 2.58-2.63 Å, whereas the distance between surface hydroxyls from the octahedral sheet is 2.78-2.81 Å. The tetrahedral basal oxygen plane is corrugated with one oxygen approximately 0.16 Å higher in the cell (away from the interlayer) than the other two. Based on the recent neutron diffraction results of Bish [24] taken at 1.5 K, it appears that the inner OH group is in the plane of the layers, and the three inner-surface OH groups make angles of 60-73 ° with the (001) plane. The long hydrogen bonds between layers were found to be between 2.95-3.09 Å. It was proposed that differences in the distance of the three interlayer hydrogen bonds might also account for the presence of the three interlamellar v(OH) bands. This is in contrast to the

conventional view that these bands are due to the coupling of the surface hydroxyl stretching vibrations [25,26].

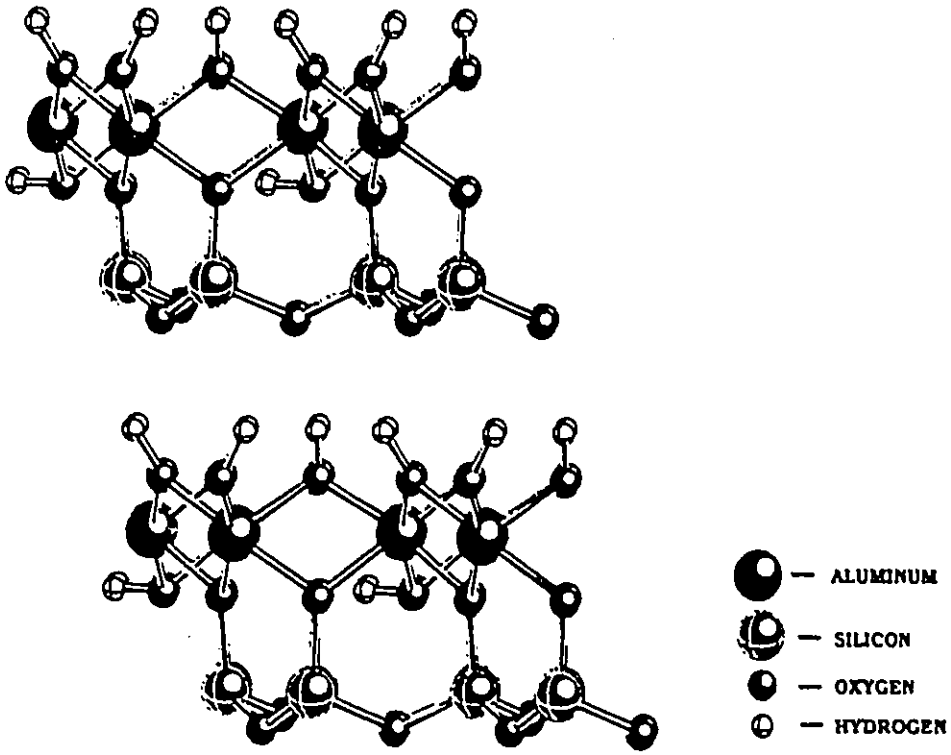

Figure 1.8: A representation of the kaolinite structure with non-hydrogen atoms placed at the experimental positions of Bish and von Dreele[23], and hydrogen positions assumed or derived from Hess and Saunders[27]. (reproduced with permission from reference 27)

The structural model for kaolinite which was given by Hess and Saunders [27] using the non hydrogen parameters of Bish and von Dreele [23] is shown in Figure **1.8**. The hydrogen atom positions were calculated using a periodic ab initio Hartree-Fock method. The position of the inner O-H group was found to be in fairly good agreement with that reported by Bish [24]. The inner surface hydroxyls are shown in this representation to be 58 ° with respect to the (001) plane which is slightly less than that found by Bish [24].

The above representation of the structure of kaolinite is of course idealized, whereas in reality kaolinite is an imperfect material covering a broad range of structural disorders. Disorder is important, since not only does this greatly influence the diffraction patterns generated by the material, it also affects many of the physico-chemical properties such as particle size, and intercalation chemistry [28,29]. Depending on the origin of the kaolinite itself, structural disorder is present in widely varying degrees [10,13]. Ideally, successive layers of kaolinite are thought to have the B octahedral positions vacant with interlayer shifts of -a/3 (see section **1.2.1**). Structural disorder may be caused by interlayer translations other than the normal - a/3 or by disorder in the placement of octahedral vacancies. Recent work suggests that for the kaolinites which were studied, the most common defects are interlayer translations which are as a first approximation the vector sum of -a/3 and b/3 layer translations [30,31].

1.3 Intercalation Chemistry of the Kaolin Minerals

Of the four kaolin minerals, only halloysite exists in nature as a hydrate, with water molecules occupying the interlayers of the mineral. This results in an expansion from the normal 7 Å c-spacing found for all of the kaolin minerals to 10 Å. As a result, halloysite may be termed halloysite 7 Å or halloysite 10 Å. Halloysite is also known to intercalate a wide range of organic compounds [32-34]. In contrast, the other kaolin minerals, kaolinite, dickite and nacrite for a long while were thought to be completely non-expandable with respect to both water intercalation and intercalation with organic compounds.

This situation changed with the discovery by Wada that kaolinite may be intercalated with potassium acetate and other salts of organic acids of low molecular weight [35]. Since then, there has been a vast body of research pertaining to the intercalation chemistry of kaolinite. This has been reviewed a number of times over the last three decades [28,36,37]. For the purpose of this work, it is the intercalation chemistry of kaolinite which will be focussed on, and indeed, this is the most studied of the kaolin minerals.

1.3.1 Intercalation of Organic Guest Molecules into Kaolinite

It is possible to intercalate organic compounds into kaolinite in one of two ways: directly (Figure **1.9**) or indirectly (Figure **1.10**). The direct route involves the preparation

of the organokaolinite intercalation compound through the direct reaction of the mineral with the organic substance. This may be done from the liquid, from the melt, by grinding the two solids together, or from a concentrated solution [28,37]. Some of the more common organokaolinite intercalates which are formed in this manner involve the direct reaction of DMSO [38-46], NMF [40,46-49], urea [50,51], hydrazine [44,50-53], formamide [40,44,46,47,49-51,54], pyridine n-oxide [40,44], potassium acetate [35,50,51,55] and ammonium acetate [55] with kaolinite. Compounds which intercalate directly into kaolinite have certain properties including high dipole moments and a tendency to form strong hydrogen bonds. Included in this group are various ionic species such as potassium, rubidium and cesium carboxylic acid salts [56]. Recent work has also shown that inorganic salts such as NaCl [57], CsBr [58], CsCl [59] and other alkali halides [60] may be directly intercalated into kaolinite by grinding the salt with kaolinite.

Many more organokaolinite intercalation compounds may be formed indirectly by the replacement of a previously intercalated molecule with another molecule (Figure **1.10**). Weiss and co-workers have intercalated a wide range of alkali and alkaline halides, amino acids, amines and other organic molecules in this manner by using either hydrazine or ammonium acetate as an "entraining" agent to first open up the layers, followed by its displacement with the desired compound [37,55,56].

Polar molecules such as acetone [40], ethylene glycol [38], glycerol [38], acetonitrile [38] and nitrobenzene [38] have been intercalated by the displacement of previously intercalated DMSO. Lactams such as 2-pyrrolidine and 2-piperidone were intercalated via the displacement of previously intercalated NMF [61].

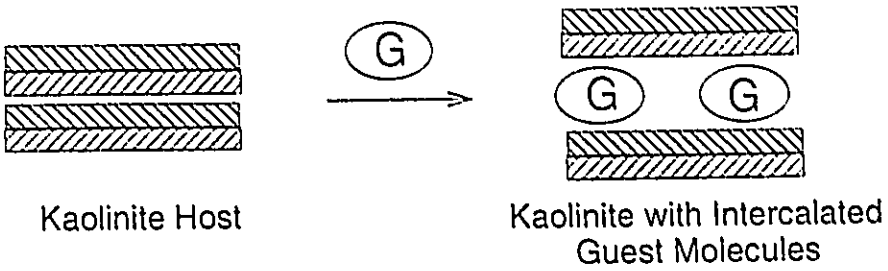

Figure 1.9: Scheme for the direct intercalation of guest molecules into the interlayers of kaolinite.

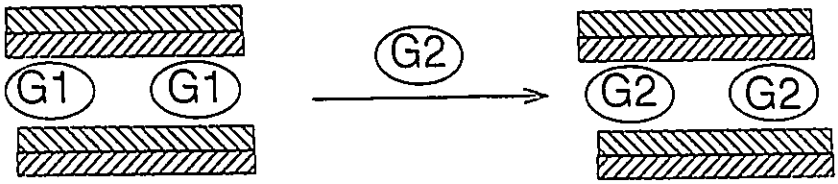

Figure 1.10: Scheme for the indirect intercalation of guest molecules into the interlayers of kaolinite through the displacement of one guest molecule (G1) with another (G2).

As stated previously, among the kaolin minerals only halloysite is known to naturally intercalate water into its interlayers [10]. Nonetheless, it is possible to form hydrates of kaolinite indirectly by displacing another intercalated molecule. Range *et al* [62,63] reported the formation of a 10 Å hydrated kaolinite via the displacement of hydrazine. Similarly, Raythatha and Lipsicas have prepared a 10 Å hydrate from Kao-DMSO without a preliminary fluoride treatment by first washing the Kao-DMSO with methanol and then with water. Upon air drying, this collapses to form an air stable 8.6 Å hydrate. The existence of a number of different "synthetic" hydrates of kaolinite was reported by Costanzo and co-workers [64-68]. These hydrates were prepared by the partial replacement of interlayer hydroxyl groups with fluorine after the expansion of the interlayers with DMSO, and then the replacement of interlayer DMSO with water. These synthetic hydrates include an 8.4 Å hydrate, an 8.6 Å hydrate, and two types of 10 Å hydrates.

There has been some interest in using these hydrated kaolinites as starting materials for the preparation of new types of intercalation compounds. Sugahara *et al* [69] have prepared pyridine and mono-substituted pyridine derivatives of kaolinite by the replacement of interlayer water from a 10 Å synthetically hydrated kaolinite. Costanzo and Giese have prepared numerous new intercalates from the 8.4 Å synthetically hydrated kaolinite [70]. In this case, the interlayer water was not displaced but remained cointercalated with the organic guest species. Finally, Wada *et al* have used an 8.6 Å hydrate of kaolinite as a starting material for the high pressure intercalation of acetone [71].

New directions were opened up for the intercalation chemistry of kaolinite when polymer based organokaolinites were prepared for the first time using an indirect method [72,73]. Kaolinite-polyacrylonitrile was prepared by first displacing previously intercalated NMF with acryamide monomer using a 10 % acrylamide solution. Interlayer polymerization was then induced by heating at 300 °C for 1 hr, yielding an organokaolinite nanocomposite with a basal spacing of 11.4 Å [72]. In a similar manner kaolinite-polyacetonitrile was prepared from an ammonium acetate intercalate of kaolinite [73]. Unlike most organokaolinite intercalates, these materials were resistant to thermal decomposition up to 300 °C and the kaolinite-polyacrylamide was also reported to be stable with respect to washing with water for 30 minutes.

Thus far, all of the intercalation compounds of kaolinite, seem to involve weakly bound guest species. As such they may be easily leached out by washing with water or other suitable solvents, and are generally susceptible to thermal decomposition at temperatures less than 200 °C. Exceptions to this include the kaolinite-polymer complexes described above, and the alkali halide intercalates which are stable up to the dehydroxylation temperature of the kaolinite host (about 500 °C) and even higher [57,60]. However, these kaolinite-alkali halide intercalates are not stable with respect to water washing.

The formation of a thermally stable kaolinite-$(HBO_2)_n$ intercalate was reported in which the intercalating agent was thought to consist of polymerized $[B(O,OH)_3]$ and $[B(O,OH)_4]$ groups which are rigidly fixed through chemical bonds to the interlayer

surface of kaolinite [74]. This material was stable with respect to water washing at room temperature, and retained its layer structure up to 600 °C.

The concept of chemically grafting organic species onto the interlamellar surfaces of clay minerals has been explored to a certain extent for several clay minerals [28,75,76]. This generally involves the attachment of organic species via Si-O-Si or Si-O-C bridges. Specifically, the silylation of montmorillonite [77-79] and sepiolite [80-83] have especially been investigated. Very little has been done involving the derivatization of kaolinite. Kuroda and Kato [84] were successful in their attempt at the formation of a trimethylsilylation derivative of halloysite in which the trimethylsilyl groups were attached via Si-O-Si$(CH_3)_3$ linkages and the aluminum octahedral sheet was decomposed. Their attempt to do the same for kaolinite was not successful, probably due to the inability of the attacking species (HCl) to penetrate the interlayers. Ruiz-Hitzky and Fripiat [81] were able to react trimethylchlorosilane and methylvinyldichlorosilane with Si-OH groups on the crystal edges of kaolinite to the extent that the carbon content of the derivative was about 1%, but no interlayer grafting was achieved.

1.3.2 Interlayer Cohesion Energy in Kaolinite

Before considering the mechanism of the intercalation process in kaolinite, the energetics involved with separating two adjacent kaolinite layers should first be understood. The energy versus separation curve from 0.01 Å to 10.0 Å for two kaolinite layers has been estimated by Giese based on a calculated electrostatic model [85]. He found

that this interaction was important over long distances, but the slope of the curve was steepest for the first few Angstroms [85,86]. This explains why it is most difficult to expand a fully collapsed kaolinite. Subsequent expansion should become easier once the layers have been opened up even slightly. The energy required to separate individual kaolinite layers to a distance of 10 Å was estimated to be in the order of 300 kJ per $Al_2Si_2O_5(OH)_4$ unit [85].

Cruz *et al* [87] have also estimated the interlayer cohesion energy of kaolinite using a different approach. They separated the interlayer bonding energy of kaolinite into three components: 1) van der Waals' attractive forces between layers, 2) hydrogen bonding between octahedral hydroxyl groups on one layer and tetrahedral oxygen atoms on the adjacent layer and, 3) electrostatic interactions arising from the dipolar nature of kaolinite. Calculations based on some simplifying assumptions provided a value in the order of 200 kJ per $Al_2Si_2O_5(OH)_4$ unit, with the main contribution being due to the electrostatic energy term.

The electrostatic term was due mainly to the electrostatic component of long interlayer hydrogen bonds. Therefore, the driving force of the intercalation process may be envisaged as the solvation of dipolar kaolinite layers. Molecules which form strong hydrogen bonds with the interlamellar kaolinite surface, and which have high dielectric constants and dipole moments should be favoured for the intercalation process.

1.3.3 Mechanism of Intercalation

At present, the intercalation behaviour of kaolinite is not entirely interpreted. All intercalative processes must involve the expansion of the individual layers in order to accommodate the guest molecule. In order for intercalation to occur, the energy that is required to separate the kaolinite layers must be balanced in some manner, usually through strong host-guest interactions [87].

The extent of intercalation in kaolinite can be estimated by XRD using what is known as the intercalation ratio. Here one compares the relative intensities of the d_{001} reflections ($I_{(001)}$) corresponding to both the expanded modified phase ($I_{(001)\ complex}$; $d_{001} > 7.2$ Å) and unmodified kaolinite phase ($I_{(001)\ kaolinite}$; $d_{001} \approx 7.2$ Å). Applying the following formula gives the intercalation ratio, I.R. [36]:

$$Intercalation\ Ratio = \frac{I_{(001)\,complex}}{I_{(001)\,complex} + I_{(001)\,kaolinite}} \qquad (1.1)$$

It should be stressed that the I.R. is not strictly speaking quantitative since one should in principle, correct for the variation of the scattering, Lorentz and polarization factors at low angles [1,2]. The I.R. is nonetheless extensively used when studying organokaolinites since it provides a readily measurable qualitative estimate of the extent of modification.

The layer expansion is estimated from the d_{001} XRD reflections of the modified phase. For layered materials exhibiting long range order along the directions

perpendicular to layers (in the c-direction for kaolinite) more than one $d_{(00l)}$ reflection may be observed. It is therefore desirable to take all of these reflections into account when calculating the distance between two consecutive unit layers. This may be calculated by indexing the $d_{(00l)}$ reflections of the phase in question and applying Equation **1.2**, where $d_{(00l)}$ is the d-value associated with the (00l) reflection.

$$\bar{d} = \frac{\sum_{l=0}^{k} l * d_{00l}}{k} \qquad (1.2)$$

Concerning the mechanism of intercalation, it is widely believed that the intercalation reaction begins at the edges of the kaolinite crystal, with the intercalating molecules then penetrating towards the interior of the crystal with the same rate between each pair of layers [28]. The constant rate assumption is necessary in order to explain the fact that during the course of the intercalation process, one does not observe an XRD pattern indicative of an interlayering phenomena, where one has a random stacking of expanded and non-expanded layers. The molecules act as wedges on the kaolinite crystal and cause the layers to be elastically deformed at the interphase.

Many factors have been attributed to influencing the reaction rate. These include particle size of the kaolinite, degree of crystallinity of the kaolinite, reaction temperature, concentration of the intercalating material and the degree of association of the reactant in the solvent mixture [29,40,48].

A competing model for the intercalation mechanism of kaolinite is based on the idea that macroscopically, kaolinite may in fact be made up of one or more screw-

dislocation axes [88,89]. This is supported by studies which have shown growth spirals of various types on the basal planes of kaolinite crystals [90]. In this mechanism, the organic molecules would first enter via edge dislocations. The molecules would then diffuse through the crystal layer by layer, since these are connected in a manner similar to a spiral staircase (Figure 1.11). Expansion of the layers would therefore take place in an orderly manner as the reaction proceeds. This mechanism is consistent with the formation of an ordered complex at all stages of the intercalation process. Kaolinite would thus act like an "elastic spring" during the intercalation and deintercalation of guest species.

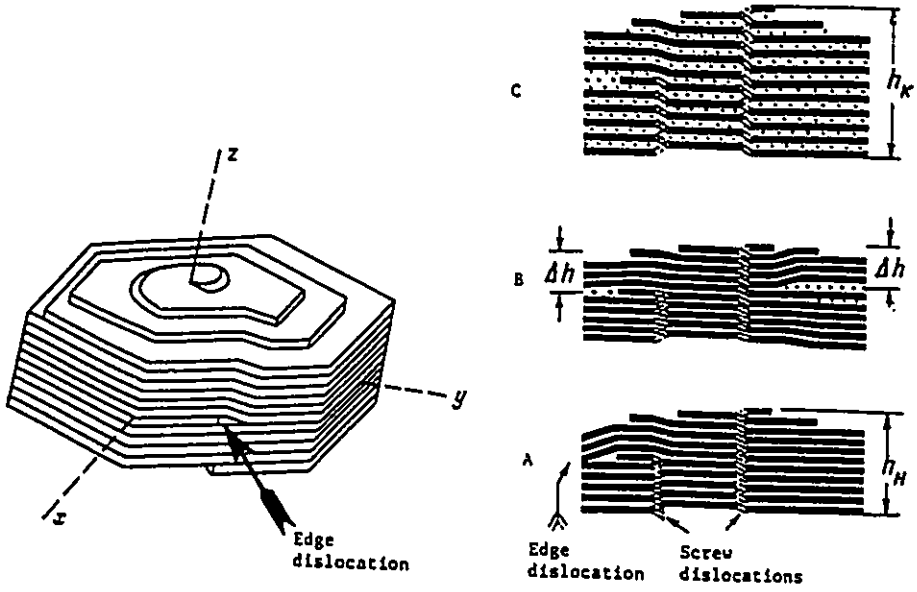

Figure 1.11: Scheme for the intercalation of organic molecules into a kaolinite crystal based on a defect mechanism. (reproduced with permission from reference 88)

1.4 Application of Clay Minerals in the Design of Novel Nanocomposite Materials

Clay minerals have certain properties, including ion exchange capacities, anisotropic two dimensional structures, high surface areas and high surface reactivities which make them useful precursors for the design and preparation of new technologically interesting nanocomposite materials. The term nanocomposite indicates that different phases, usually inorganic and organic, are intimately mixed at the molecular, or nanometre scale. As such, nanocomposite hybrid materials often exhibit properties which are intermediate between the components which make up the material. For example the thermal and mechanical resistance of inorganics may combine with the flexibility and chemical diversity of the organic phase. This synergism may also extend to the electric and optical properties of the two phases. In the following sections, some of the applications of clay minerals as precursors for the design and preparation of nanocomposite materials will be outlined.

1.4.1 Catalysis

There has been a considerable amount of work involved with the modification of clay minerals to yield new catalytically active materials [91,92]. Clays are catalysts by themselves, with both Brønsted and Lewis acid sites, but considerable improvements in catalytic strength and selectivity can be achieved through the modification of the clay.

Much of the recent work has centered around the "pillaring" of smectite clays with catalytically active metal oxide clusters, such as the Al-13 Keggin ion $(Al_{13}O_4(OH)_{24}(H_2O)_{12}^{7+})$ [91,93-95] and zirconium oxide [93,96-98] clusters. These materials are prepared by first exchanging the countercation of the smectite (usually Na^+) with cationic metal oxide clusters, followed by calcination at 400-500 °C. This results in a microporous material which is composed of smectite clay layers which are pillared with catalytically active metal oxide clusters (Figure **1.12**). In a novel approach, Pinnavaia and coworkers have prepared a new type of pillared material, termed "tubular silicate-layered silicate" , where smectite layers appear to be pillared by cylindrical fibres of the mineral imogolite [99].

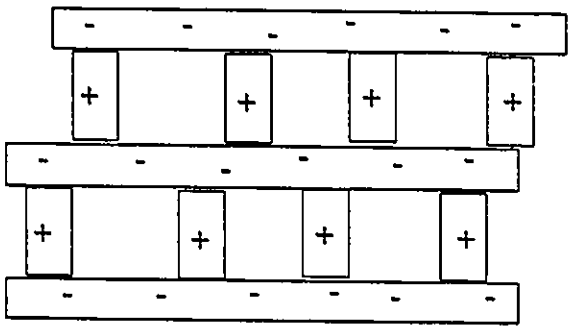

Figure 1.12: Schematic representation of a smectite pillared clay.

1.4.2 Separation Science

The use of modified clays for use in separation science as sorbents and molecular sieves has been extensively investigated. Barrer was the first to explore in detail this potential [100-103]. In many of these applications, organosmectite clays are prepared by ion exchange with organic cations. Depending on the charge density of the clay, and the nature of the organic cation, microporous materials may be prepared which may be used for the separation of gases [104-106].

1.4.3 Carbon-Mineral Nanocomposite Materials

Workers have also used the two-dimensional interlayer spaces of clays as a templates for the preparation of very thin sheets of carbonaceous materials sandwiched between inorganic aluminosilicate layers [107-109]. In this approach, one first intercalates significant amount of organic material (usually a polymer) into the interlayer space of the clay, and then the organic material is pyrolysed by heating to high temperatures (>500 °C) under nitrogen atmosphere. At this point the product is a carbon-mineral nanocomposite. If one wishes, the interlayer carbonaceous material which results may be removed by the dissolution of the inorganic aluminosilicate phase. This methodology is being employed to create very thin sheets of graphite [107,108] and ultramicroporous carbon-mineral materials which may adsorb significant amounts of hydrogen gas [109]. At present, only smectite clays have been investigated as templates for these reactions.

1.4.4 Polymer-Mineral Nanocomposite Materials

An area of study which has recently gained considerable attention involves the preparation of new polymer-mineral nanocomposites [110-118]. The interaction between polymers and clay minerals has been well studied over the years [119], but it is only recently that true nanocomposite polymer-clay materials have been prepared. Much of this interest is centered on efforts to enhance the thermal and mechanical properties of polymers. It has been shown for example, that the glass transition temperature of polymers may be inhibited upon nanocomposite formation with smectite clay [115]. Other efforts involve the preparation of anisotropic ionic conductors through the interlayer incorporation of polyethylene oxide chains into smectite clays [116,118,120]. Once again, very little has been done using kaolinite as a precursor for this new class of materials, beyond the interlamellar polymerization of acetonitrile [73] and acrylamide [72].

1.4.5 Optic and Photosensitive Materials

The use of smectite clays as supports for photoactive catalysts has been reviewed by Thomas [121]. Some recent work has focussed on using clays to organize photoactive molecules in two dimensional arrays, for use in "photochemical hole burning" [122,123], and as non-linear optic (NLO) active materials where the NLO active component (p-nitroaniline) is aligned in the interlayers of the smectite with the aid of an electric field [124].

1.5 Recent Pertinent Developments in Materials Science

There are a number of recent developments in materials science which may be especially interesting if one is to consider the role that kaolinite might play as a precursor for technologically relevant nanocomposite materials. For many years materials scientists were constrained by the inability to rationally design materials with pore sizes greater than that afforded by the zeolites (< 15 Å). This scenario changed with the development of new mesoporous structures with pore sizes ranging from 16 to 100 Å [125,126]. The proposed mechanism for the formation of these materials involved a liquid crystal templating mechanism, whereby the inorganic phase would crystallize around supramolecular liquid crystal organic assemblies. The great success in creating materials with a controlled uniform pore size and composition would seem to make some of the appeal of using clay minerals as precursor materials for the design of porous structures obsolete. Inagaki *et al* [127] however, have shown that the layered silicate kanemite, may be used as a precursor for mesoporous structures. It is possible that other layered structures may also play this role. Indeed, it is currently believed that layered phases are precursors for the formation of these mesoporous structures [128-130]. Very recently, it was demonstrated that "porous clay heterostructures" could be prepared with pore sizes ranging from 14-22 Å [131]. These structures consisted of porous silicate superstructures sandwiched between smectite clay layers. This approach was based on a surfactant mediated interlamellar hydrolysis and polymerization of inorganic precursors such as tetraethylorthosilicate, within the galleries of smectite clays.

In order to make full use of the anisotropic two-dimensional properties of many clay minerals, it should be possible to create robust ordered thin films in the macroscopic state. Such smectite films have been prepared by cross-linking the individual clay particles with phosphoric acid [132,133]. The term "molecular ceramics" has been coined to describe the way that these clay plates are ordered at the molecular level to give a thin film. The swelling and ion exchange properties of the smectite clay are mostly retained in the form of a chemically and mechanically robust film. Kleinfeld and Ferguson have also created multilayered nanostructured films on silicon wafers by sequentially adsorbing a cationic polyelectrolyte and individual sheets of negatively charged hectorite plates [134]. Uses of clay minerals involving thin films is expected to become increasingly important in the future.

1.6 Research Rationale and Purpose

Upon surveying the recent literature, it is apparent that the vast majority of what has been done regarding the use of clay minerals as precursors for preparation of new technologically interesting nanocomposite materials involves the use of 2:1 layered smectites. This is undoubtedly a result of the many advantages that are associated with smectites. Their interlayers readily expand in water and other solvents thus providing ready access to a very large internal surface area. The interlayer cations, which balance the net negative charge of smectites, can be easily exchanged with a plethora of both inorganic and organic cations. By carefully choosing the type of smectite, one can also

tailor the charge density of the material, or impart various catalytic properties to the material by selecting a material with transition metals which are isomorphically substituted into the clay structure.

The kaolin minerals, by contrast, are essentially neutral, have very small cation exchange capacities, and are much more difficult to expand. In fact, it is generally not possible to completely expand all the interlayers of kaolinite. It is not surprising therefore, that smectites are the clay minerals of choice as precursors for the development of many new microporous and catalytic materials.

Kaolinite however, has certain advantages which make it an ideal candidate as a precursor for the preparation of some types of nanocomposite materials. Like the smectites, kaolinite is readily available at a very cheap price. It is a big industrial product, with extensive use in the pulp and paper and ceramics industries. Kaolinite has a greater theoretical internal surface area per unit mass than do the smectites (1000 m^2/g versus about 700 m^2/g) and it exhibits a much greater crystallinity than do the smectites. From a practical point of view, the high degree of ordering characteristic of kaolinite make the analysis of host-guest interactions easier. Some intercalates of kaolinite, Kao-DMSO for example [43], exhibit ordering in both the c-direction and in the ab-plane. Deductions can be made regarding the nature and conformation of the guest species relatively easily on the basis of powder XRD, IR and NMR.

Unlike smectites, which have only one type of interlamellar surface, the kaolin minerals possess two types of surfaces (Figure **1.8**). The first is the silicate surface which is also found in the smectites and is composed of $(Si\text{-}O)_6$- macrorings. The second is the

hydroxylated aluminate surface. These two surfaces stack one upon the other in a repeating manner thus providing an anisotropic dipolar interlayer environment. Herein, lies the most powerful advantage of kaolinite as a nanocomposite precursor material. Not only does the hydroxylated aluminate surface provide an abundance of reactive hydroxyl groups for guest species to stick to or attach themselves to, but the dipolar interlamellar environment induced by this second surface may cause the spontaneous poling of polar guest species in an ordered and reproducible manner.

The 1:1 layered clays are alone among the clay mineral to possess a dipolar unit cell. Indeed, as far as we know, all expandable layered materials possess only one type of interlamellar surface and possess no interlayer dipole. The trioctahedral 1:1 layered serpentines are of limited interest since they are not known to expand, and the individual unit cells are arranged in the crystallites in such a way so as to create cylindrical fibres or corrugated structures (Table **1.2**) in which the individual unit cell dipoles cancel out within the crystallite. Kaolinite crystallites are generally found to be in the form of platelets (Table **1.1**), so it is reasonable to assume that within the individual crystallites of kaolinite, one has an assembly of oriented dipoles. This situation is enticing, if one wishes to create nanocomposite materials based on organized dipolar assemblies of alternating organic and inorganic layers (Figure **1.13**). It is clear that kaolinite could provide an attractive precursor for such materials if some of the problems surrounding the difficulty in expanding the interlayers of kaolinite could be solved.

Thus far, most of the vast body of research pertaining to the interlamellar chemistry of kaolinite involves the use of "soft" methods of intercalation. Typically, this

involves the intercalation of non-destructive reagents at temperatures less than 100 °C, and at atmospheric pressures. Relatively little has been done to explore the interlamellar chemistry of kaolinite using harsher reaction regimes. In order to utilize some of the unique advantages that kaolinite has as a precursor material for the preparation of nanocomposite dipolar assemblies, one must first expand the interlamellar chemistry of kaolinite still further. New methods should be found for the incorporation of guest molecules into the interlayers of kaolinite and new interlamellar surface modification reactions should be found whereby organic groups may be rigidly fixed in the interlayer spaces.

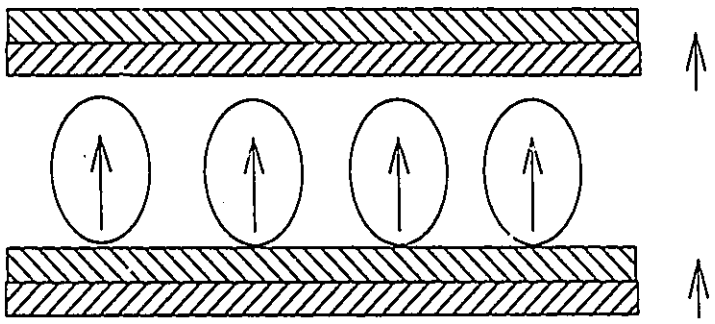

Figure 1.13: Schematic representation of the spontaneous alignment of a dipolar guest molecule in the dipolar interlayers of kaolinite.

With this in mind, the broad purpose of this research was to explore and extend the interlamellar chemistry through the preparation and characterization of new kaolinite based nanocomposite materials using harsher methodologies than previously employed. Specifically, one wishes to prepare organokaolinite materials where organic units would be covalently grafted to the interlayers of kaolinite, yielding thermally robust materials resistant to decomposition.

Chapter 2

Preparation of a New Class of Organokaolinite Hybrid Material: The Interlamellar Grafting of Alcohols onto Kaolinite

2.1 Introduction

Organomineral derivatives are of interest because they have the surface properties and reactivity corresponding to the grafted organic molecules, while maintaining the mechanical and thermal properties of the mineral framework [28]. Many strategies have been employed for the organic derivatization of inorganic surfaces. For example, the most common surface modification approach involves the use of organochlorosilane reagents to graft organic units on silanol groups of various minerals [75,77,80,82,135-137].

The surface modification of inorganic materials through the formation of surface ether linkages (≡S-O-R) has been reported for a number of materials [28,138]. Many of these reactions are formed through the surface condensation reaction of alcohols, whereby an alcohol group (R-OH) reacts with a surface hydroxyl (≡S-OH) to give the condensation products, ≡S-O-R and H_2O. Reactions in which surface ether linkages are formed have been reported for silica [139-143], alumina [144-150], gibbsite and boehmite [151-157], $Ni(OH)_2$ [158], H-magadiite ($H_4Si_{14}O_{30}$) [159], zeolites [160-165] and sepiolite [28].

For kaolinite, despite the presence of large numbers of interlayer aluminol groups (about 13 OH/nm^2 for the hydroxyl surface), there have been no reports of the interlamellar

grafting of surface ether groups via Al-O-R bonds. Ruiz-Hitzky and Fripiat [81] and Porro and Paccini [166] have reported the silylation of the external surfaces of kaolin clays, but to the best of our knowledge there has been no report of the silylation of the interlayer hydroxyl groups. Ovramenko *et al* have reported the grafting of borates to the interlamellar surface of kaolinite to yield a material which is thermally stable up to 400 °C and which is resistant to water washing [74].

The formation of layered organoboehmite derivatives where the organic units have been attached via Al-O-C bonds has been reported [151,152,155,157]. This is especially relevant for kaolinite since like kaolinite, boehmite is made up of sheets of octahedrally coordinated aluminum with interlayer surface aluminol groups. In both cases, the layers are held together by interlayer hydrogen bonds. Kubo and Ushida [151] have reported the preparation of an organoboehmite material whose approximate composition is $AlO(OH)_{0.5}(OCH_3)_{0.5}$. This material was formed through the high temperature (200 °C), high pressure (100 kg/cm^2) reaction of $Al(OH)_3$ with methanol in an autoclave. More recently, in a series of papers, Inoue and co-workers have described the preparation and characterization of various diol [152,155,157] and aminoalcohol [157] derivatives of boehmite from a gibbsite ($Al(OH)_3$) starting material. Once again, these reactions took place at high temperature in an autoclave. It was proposed that these materials were formed via the interlayer surface condensation reaction of Al-OH and the corresponding alcohol to give Al-O-R surface ether functionalities. Similar organoboehmite materials were also formed through the sol-gel reaction of aluminum alkoxides with glycols [153,154,167].

By analogy with boehmite, it should be possible to functionalize the interlayer hydroxyl surface of kaolinite through the condensation of alcohol groups, if sufficient access could be provided to the interlayer spaces of this mineral. This could be accomplished by first intercalating the interlayers of kaolinite with an appropriate guest molecule followed by the high temperature condensation reaction with an excess of the alcohol. This proposed reaction scheme is illustrated in Figure 2.1. A number of attempts were made to derivatize the hydroxyl surface of kaolinite based on this proposed reaction sequence. Many of these attempts are described in this chapter.

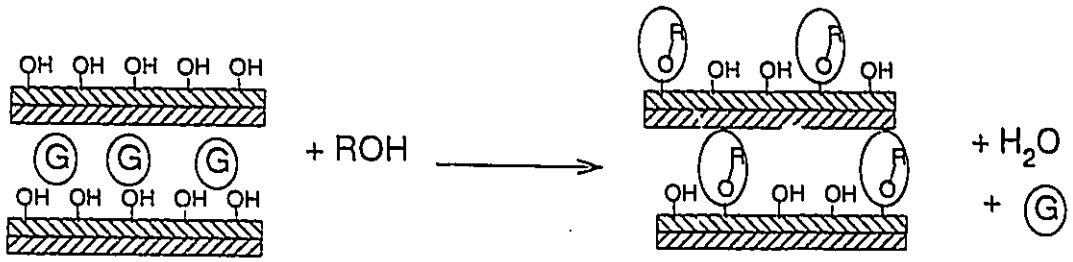

Figure 2.1: Proposed reaction scheme for the functionalization of kaolinite through the condensation of alcohols on the hydroxyl surface of kaolinite.

2.2 Results and Discussion

2.2.1 Methoxy Functionalization of Kaolinite

2.2.1.1 Preparation

A number of attempts were made to react the interlayer hydroxide surface of kaolinite with methanol at high temperatures. These results are summarized in Table **2.1.**

Starting Material	Reaction Conditions[1]			XRD Characterization[1]	
	Rxn Code	Temp.	Duration	d-spacing	I.R.[2]
		°C	hrs	Å	-
Kao-DMSO	**2-1-1**	190-270	89	8.17	0.89
Kao-DMSO	**2-1-2**	190-230	35	8.63	0.93
Kao-DMSO	**2-1-3**	155-160	42	N.R.	
Kao-NMF	**2-1-4**	190-200	20	8.53	0.91
Kaolinite	**2-1-5**	200-215	120	N.R.	

Table 2.1: Reaction summary for the preparation of Kao-MeOH with XRD basal spacing and intercalation ratio characterizations. (1) Reaction conditions and product characterizations are more fully explained in Section **6.5.1.** (2) Intercalation Ratio; N.R. indicates that no reaction occurred.

It was found that when the kaolinite was first intercalated with either dimethylsulfoxide (DMSO) or N-methylformamide (NMF) and then exposed to methanol at high temperatures and pressures in an autoclave, a new product was formed which is characterized by a basal spacing ranging between 8.17 Å (Rxn **2-1-1**) and 8.63 Å (Rxn **2-1-2**), depending on the reaction conditions. When the reaction temperature was in the range of 155-160 °C and the reaction time 42 hours (Rxn **2-1-3**), no reaction occurred. Under these conditions, the unmodified Kao-DMSO starting material (basal spacing= 11.2 Å), was the only observed product.

A control experiment (Rxn **2-1-5**), where kaolinite was used instead of the DMSO or NMF intercalates of kaolinite showed that no reaction occurred. Access must first be provided to the interlayer spaces of kaolinite. When access is provided, the condensation of methanol molecules on the interlayer hydroxyl surface of kaolinite may occur, with the subsequent formation of water and the displacement of intercalated guest species (DMSO or NMF) in the starting material. A schematic representation of the Kao-MeOH product is given in Figure **2.2**.

The water contents of the solvent before (0.03 %) and after reaction (2.2 %) for Rxn **2-1-1** were monitored by Karl-Fischer titration. This increase in water content is greater than one expects if the sole source of water production is assumed to be through the covalent grafting of methoxy groups onto the hydroxyl surface of kaolinite. On this basis, the expected water content for the mother liquor was calculated to be less than 1.0 %, even if 100 % of the interlayer hydroxyl groups of the kaolinite surface were functionalized with methoxide groups. So, it would appear that while the formation of water is consistent with

the proposed surface condensation grafting mechanism, it cannot account for the formation of all of the water. It is probable that dimethylether and other condensation products were formed during the course of this high temperature sealed reaction. The formation of organic condensation products from methanol using alumina [148] and pillared clays [168] as catalysts has been reported. The presence of secondary condensation reaction products was qualitatively confirmed by GC-MS analysis of the mother liquor which showed the presence of dimethyl ether and 2-methoxyethanol (Section **6.5.1.1**).

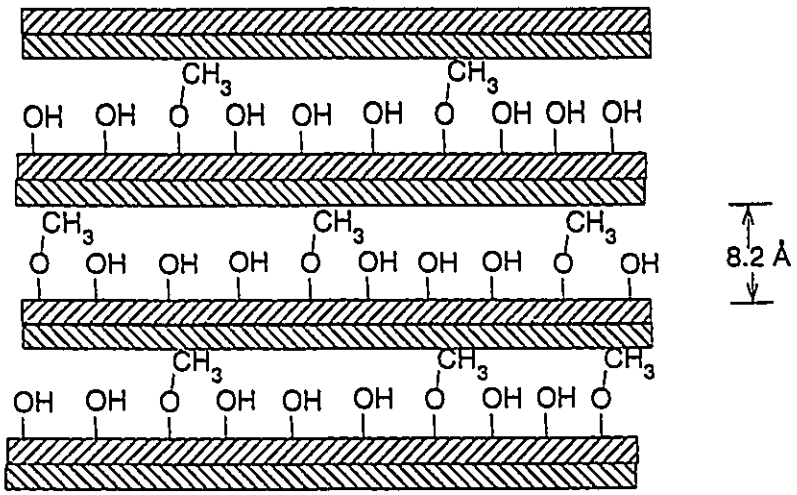

Figure 2.2: Schematic representation of Kao-MeOH 8.2 Å.

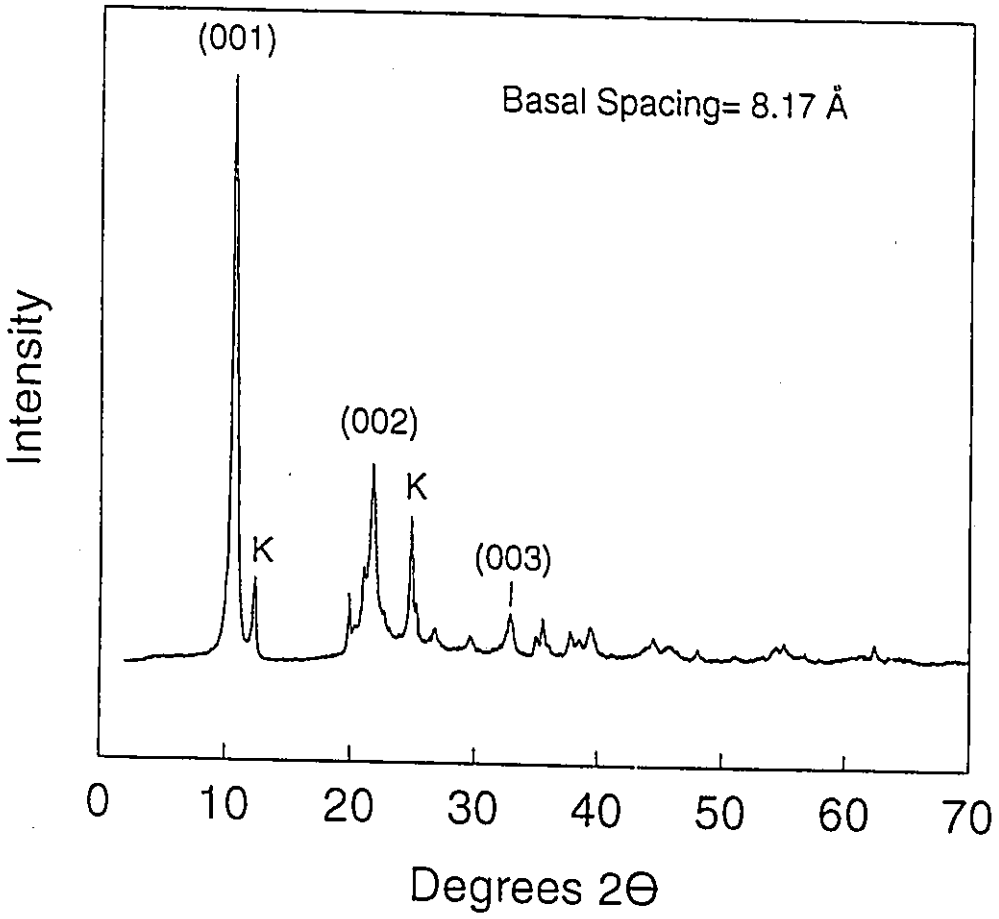

Figure 2.3: XRD pattern (2-70 °2Θ) of Kao-MeOH 8.2 Å (2-1-1). (K) indicates residual kaolinite.

The basal spacing of the methoxy modified kaolinite (Kao-MeOH), from Rxn **2-1-1** is 8.2 Å, which represents a 1.0 Å layer expansion from the 7.2 Å basal spacing of the parent kaolinite material. The XRD of this product (Figure **2.3**) shows that approximately 90 % modification was achieved, judging by the intercalation ratio (I.R.). A number of basal reflections could be indexed. Since the minimum clearance space for a methanol molecule trapped between two layers has been estimated to be 3.7 Å [34], it is unlikely that methanol is simply loosely intercalated in the interlayer spaces of kaolinite. The very small basal spacing observed may be attributed to the methyl group keying into the $-(SiO-)_6$ macroring of the silicate sheet in the adjacent layer. Precedents for this keying in phenomena for kaolinite are well known [36,42,43,53,69].

A halloysite-methanol intercalation compound with a basal spacing of 10.6 Å was reported by MacEwen [32,33]. Carr and Chih later reported a 9.5 Å basal spacing for a methanol treated hydrated halloysite complex [34], which they attributed to a partial dehydration of the complex rather than to a true halloysite-methanol complex. More recently, Costanzo and Giese [68], on the basis of IR results, have reported the formation of a disordered methanol intercalate of an 8.4 Å synthetically hydrated kaolinite. In this case the XRD pattern of the complex could not be measured because deintercalation of the methanol proceeded too rapidly under ambient conditions. Similarly, the intercalation of methanol into an 8.6 Å synthetically hydrated kaolinite was reported to yield an intercalate with a basal spacing of 10.95 Å [71]. In all cases, methanol intercalated kaolinite or halloysite exhibit much larger basal spacings than that observed for the 8.2 Å phase, and were unstable in ambient conditions.

The layer expansions reported for other methoxy functionalized layered materials such as boehmite [151], FeOCl [169], $Ni(OH)_2$ [158] are much larger than the 1.0 Å observed here, due in part to the fact that there are methoxy groups on both the bottom and top interlamellar surfaces of these materials and not just one of the surfaces as is the case for kaolinite.

The relationship between the 8.17 Å phase (Rxn **2-1-1**) and the 8.63 Å (Rxn **2-1-2**) phase is thought to be related to the presence of co-intercalated water. Support for this hypothesis is provided from IR (Section **2.1.1.2**) and TGA (Section **2.1.1.3**) results and from the observation that when the 8.17 Å phase is washed with water for 72 hours at room temperature, a product with a d_{001} reflection at 8.6 Å is observed by XRD (Figure **2.4**). IR and TGA data for the water washed sample are also very similar to that of the 8.63 Å (Rxn **2-1-2**) and 8.53 Å (Rxn **2-1-4**) phases.

Sample	Sample Description	d_{001}	Intercalation Ratio
a	Kao-DMSO starting material	11.14	0.98
b	Kao-MeOH 8.2 Å (Rxn **2-1-1**)	8.20	0.89
c	(b) + water (Rxn **2-2-9**)	8.62	0.86
d	(c) + heating at 150 °C for 4 hours	8.10	0.82

Table 2.2: Summary of XRD data showing the effects of water washing on the methoxy functionalized kaolinite product of Rxn **2-1-1** (see section **6.5.1.9**).

It is significant that the preparation of a synthetic 8.6 Å hydrated phase of kaolinite has been previously reported [64,70]. Here, it was first necessary to replace some of the hydroxyl groups with fluorine in order to reduce interlayer cohesive forces. By replacing a number of the hydroxyl groups with methoxy functionalities, this same reduction in cohesive energy may have resulted in the intercalation of water to form an 8.6 Å methoxy hydrate phase of kaolinite. Upon heating the 8.6 Å phase at 150 °C in an oven for 4 hours, the 8.2 Å phase, which was measured at d_{001} = 8.10 Å was regenerated. These treatments are summarized in Table **2.2.**

The above results suggest that some of the methoxy functionalities were hydrolysed upon prolonged exposure to intercalated water. Comparison of the relative intensities of the v(CH) stretching intensities of the products before and after washing also suggests that some hydrolysis of the methoxy functionalities had occurred (Figure **2.5**).

On the basis of elemental analysis, an approximate chemical formula of $Si_2Al_2O_5(OH)_{3.5}(OCH_3)_{0.5}$ for Kao-MeOH 8.2 Å (Rxn **2-1-1**) can be estimated (%C: calc.: 2.26; found: 2.17; %H: calc.: 1.89; found 2.00). X-ray fluorescence data confirmed that the Si/Al ratio of the product (Si/Al=1.13) was essentially unchanged from that of the parent kaolinite material (Si/Al=1.20) given the precision of the XRF analysis technique under the conditions employed. The Si/Al ratio is ideally 1.0 for both materials and more precise X-ray fluorescence data using a much larger sample size has confirmed that the parent kaolinite has a Si/Al ratio of 0.99 (Section **6.3.1**).

Alternately, if one solely considers the 17.85% weight loss which was observed upon calcination of Kao-MeOH 8.2 Å at 1150 °C in air atmosphere, one obtains the formula

$Si_2Al_2O_5(OH)_{3.13}(OCH_3)_{0.87}$. This discrepancy may be explained on the basis that during the combustion process in the elemental analysis, carbonaceous material formed in the interlayers of kaolinite and became trapped in the mineral matrix (see Section **2.2.1.3** for more details), and so some of the organic material was not combusted, leading to a lower than expected carbon content. This phenomena of carbon-mineral nanocomposite formation was observed for many other thermally robust organokaolinites. Only through prolonged combustion in air atmosphere at temperatures in excess of 1050 °C can one totally combust all the organic material. It is therefore this latter formula ($Si_2Al_2O_5(OH)_{3.13}(OCH_3)_{0.87}$) which is thought to be a more accurate representation of the chemical formula.

This implies that about one out of three of the surface hydroxyl groups have been replaced with methoxide groups. For comparison, approximately one half of the hydroxyl groups were replaced with methoxide for the methoxy functionalized boehmite derivative [151], and one third of the surface hydroxyls were replaced in $Ni[(OH)_{2/3}(OCH_3)_{1/3}]_2$ [158]. Since the distance between adjacent surface hydroxyl groups in kaolinite is approximately 2.8 Å [23], and since the van der Waals diameter of a methyl group is 3.9 Å [158], it is highly improbable to obtain a completely methoxylated surface. Assuming ideal hexagonal symmetry with interhydroxyl distances of 2.8 Å, replacement of one third of the interlayer hydroxyls with methoxy groups in an idealized hexagonal 2-dimensional ordering would give intermethoxy distances of approximately 4.9 Å. This is greater than the 3.9 Å minimum distance required.

The replacement of one third of the hydroxyl groups for methoxy groups would also correspond to a ratio of one methoxy group per $-(SiO-)_6$ macroring. This would allow every methoxy group to be keyed into one $-(SiO-)_6$ macroring of the silicate surface of the adjacent

layer, and could account for the very low 1.0 Å layer expansion which was observed. On this basis, the upper limit for the methoxy functionalization of kaolinite should be $Si_2Al_2O_5(OH)_{3.0}(OCH_3)_{1.0}$.

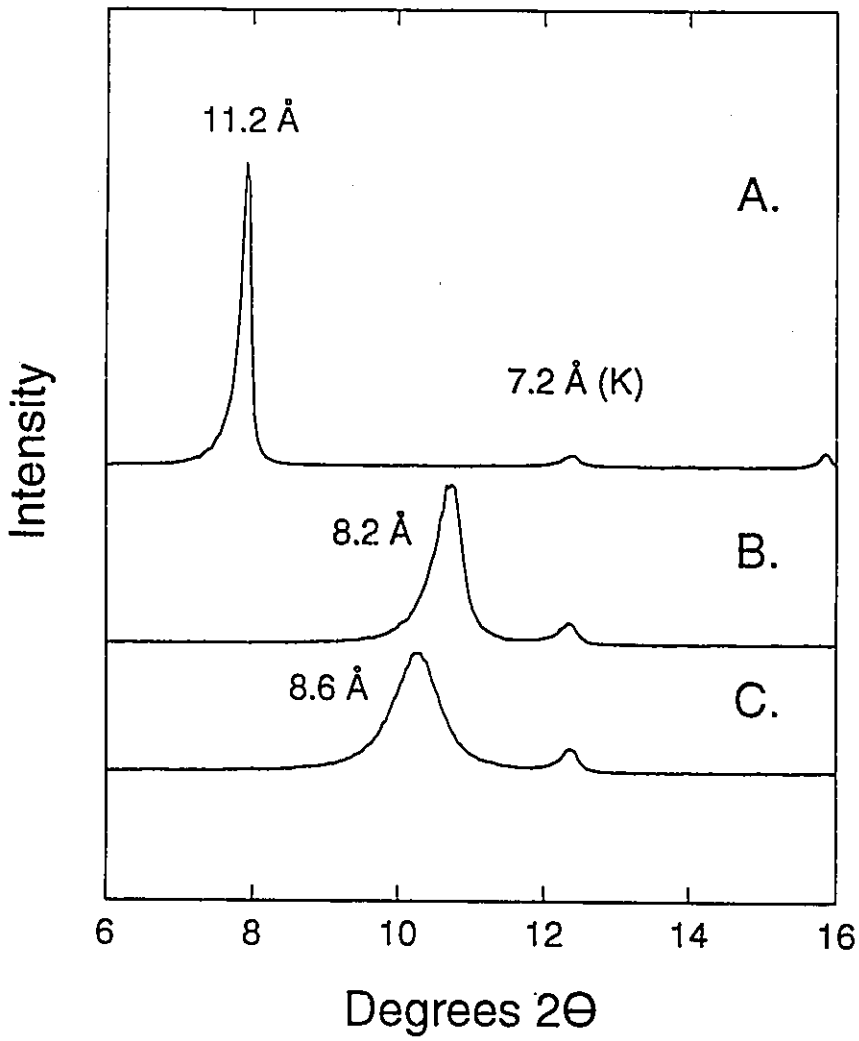

Figure 2.4: XRD patterns (6-16 °2Θ) of: (**A**) Kao-DMSO starting material; (**B**) Kao-MeOH 8.2 Å (2-1-1); (**C**) **B** + water washing for 72 hrs at room temperature. (K) indicates residual kaolinite

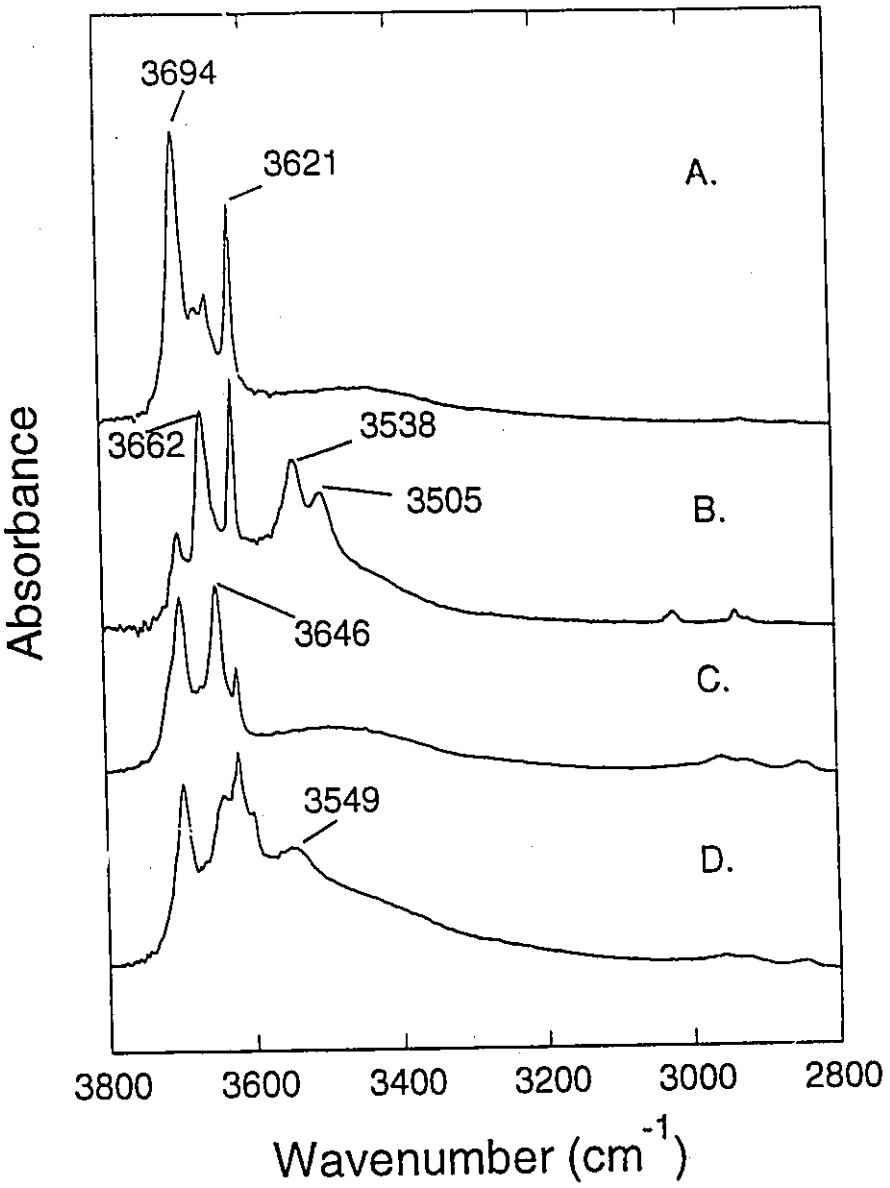

Figure 2.5: FTIR spectra (3800-2800 cm^{-1}) of: **(A)** Kaolinite; **(B)** Kao-DMSO; **(C)** Kao-MeOH 8.2 Å **(2-1-1)**; **(D) C** + water washing for 72 hrs at room temperature **(2-1-9)**. Note: The relative absorbance scales of the spectra have been adjusted in order to facilitate comparison.

2.2.1.2 IR Analysis

The infrared OH stretching region of kaolinite is very sensitive to the effects of interlayer modification [36]. Consequently, interlayer methoxy functionalization of the hydroxyl surface should have a major influence on the diagnostic OH stretching pattern of kaolinite. This is indeed shown to be the case in Figure **2.5**, where it is readily observed that the OH stretching pattern of Kao-MeOH 8.2 Å (**C**) is very different from that of either the parent kaolinite material (**A**) or Kao-DMSO (**B**). The band at 3694 cm^{-1} which is attributable to one of the stretching modes of the surface hydroxyl groups of kaolinite remains at roughly the same frequency, albeit at somewhat weaker relative intensity. The inner hydroxyl stretching vibration at 3621 cm^{-1} is also unshifted compared to kaolinite although once again, the relative intensity of this band appears to be diminished somewhat.

The major difference between the IR spectra of kaolinite (Figure **2.5 A**) and Kao-MeOH 8.2 Å (Figure **2.5 C**) is the appearance of a band at 3646 cm^{-1} for Kao-MeOH 8.2 Å. This is assigned to the OH stretching motion of weakly perturbed surface Al-OH groups. Some care must be taken in this assignment, since the ν(OH) band of CH_3OH monomer in CCl_4 solution has been found to be at a nearly identical frequency of 3645 cm^{-1} [149]. The assignment of this band due to the presence of isolated CH_3OH monomer is ruled out on the basis that it is extremely unlikely that weakly interacting CH_3OH molecules with no hydrogen bonding interactions could exist within the aluminosilicate mineral matrix.

It is noteworthy that no low energy bands due to guest molecules hydrogen bonded to the surface hydroxyls are observed as is the case for Kao-DMSO (Figure **2.5 B**) where H-bonded surface hydroxyl bands are observed at 3538 cm^{-1} and 3505 cm^{-1}. Nor is there any conclusive evidence for C-OH stretching bands due to hydrogen bonded intercalated methanol. The weak broad band which one observes between 3350-3600 cm^{-1} is of the same intensity as for kaolinite and can be attributed to externally adsorbed water in either the clay or the KBr matrix. The absence of an alcohol v(OH) stretching band is consistent with the condensation of methanol on the hydroxyl surface to yield a surface methoxide group.

Further evidence for grafting is also seen from the C-H stretching region of Kao-MeOH (Figure **2.5 c**), where one observes three bands at 2957 cm^{-1} (w), 2927 cm^{-1} (w) and 2849 cm^{-1} (w) corresponding to the symmetric and antisymmetric C-H stretching bands of the surface methoxide group. Neat methanol, by contrast has two C-H stretching bands at 2942 cm^{-1} and 2832 cm^{-1}, whereas methanol in dilute CCl_4 solution has v(CH) bands at 2977 cm^{-1}, 2938 cm^{-1}, and 2830 cm^{-1} [149]. For comparison, both methoxyboehmite ($AlO(OH)_{0.5}(OCH_3)_{0.5}$) [151] and aluminum methoxide [170] have two CH stretching bands at 2940 cm^{-1} and 2840 cm^{-1}.

Methanol adsorbed on alumina activated at 500 °C exhibits at least three surface species, each with a characteristic v(CH) IR pattern [149]. Bands attributed to the presence of a "bridging methoxide" group on alumina have been assigned at 2970 cm^{-1}, 2955 cm^{-1} and 2844 cm^{-1}, whereas bands due to a "coordinated form" have been assigned at 2960 cm^{-1} and 2850 cm^{-1} [149]. These latter values are similar to those originally reported by Greenler who assigned C-H stretching bands at 2950 cm^{-1} and 2840 cm^{-1} for an alumina methoxide

species [144]. All this indicates that the position of the ν(CH) bands for Kao-MeOH 8.2 Å is consistent with methoxide species. Moreover, the appearance of an ill-defined $\delta(CH_3)$ band at 1460 cm^{-1} (vw) is also consistent with the presence of methoxide species [149].

Other regions of the IR spectra show that the kaolinite host mineral has been perturbed. The very strong Si-O lattice vibration bands of kaolinite (1010 cm^{-1} and 1032 cm^{-1}) were replaced by bands at 1033 cm^{-1} and 1050 cm^{-1} for Kao-MeOH 8.2 Å, and the δ(Al-OH) in-plane bending vibration of the inner hydroxyl of kaolinite [25] was also perturbed from 915 cm^{-1} in kaolinite to 910 cm^{-1} in Kao-MeOH 8.2 Å. The δ(Al-OH) in-plane bending vibration of the surface hydroxyls of kaolinite [45] at 938 cm^{-1} was no longer observed in the case of Kao-MeOH 8.2 Å.

Other kaolinite lattice vibrations have also been perturbed. Kaolinite bands at 790 cm^{-1} (w), 755 cm^{-1} (w) and 694 cm^{-1} (m) have been replaced by new bands at 818 (vw), 802 (w), 743 (w) and 678 (m). The 16 cm^{-1} shift of the 694 cm^{-1} band to lower frequency at 678 cm^{-1} may be especially significant. It was noted by Farmer [26] that this band, which was attributed to a perpendicular vibration of the hydroxide sheet of kaolinite is shifted 13 cm^{-1} to lower frequencies upon deuteration due to the higher mass of the deuteroxyl group versus the hydroxyl group. One would expect this same trend if the hydroxyl groups were instead replaced with methoxide groups, and indeed this is what is observed.

2.2.1.3 Thermogravimetric Analysis

The thermal stability of the Kao-MeOH 8.2 Å product was quite remarkable for an organomineral material. The material did not begin to decompose until about 370 °C, and when decomposition of the organic material did occur, it overlapped with the dehydroxylation of the kaolinite lattice (see Section **6.5.1.1**). This thermal event was characterized by an endothermic peak temperature of 515 °C, which is 23 degrees lower than the peak dehydroxylation temperature of the kaolinite starting material (538 °C). With the onset of this thermal decomposition, the product blackened, indicating the formation of carbonaceous material. The product remained black even in air atmosphere until greater than 1000 °C when the carbonaceous material was burnt off. Between 920 and 1050 °C there was an exothermic event, with a peak temperature of 1009 °C assigned to a structural reorganization of the metakaolinite-like aluminosilicate mineral matrix. In the pure kaolinite parent material, this exothermic event was found to occur at 1003°C, and no weight loss was associated with this event. By contrast, for Kao-MeOH 8.2 Å in air atmosphere, one observed a 1.4 % weight loss between 920-1050 °C which is associated with this structural reorganization. It is also at this temperature range that the product regains its off-white colour. All this suggests that the carbonaceous material which was trapped in the metakaolinite matrix during the dehydroxylation step ($\approx$ 400-550 °C) was released during the structural reorganization ($\approx$ 1000 °C), and then combusted in the air atmosphere, leading to the observed 1.4 % weight loss. As previously mentioned, the formation of a thermally

stable carbon-mineral nanocomposite material was also often the source of inaccurate elemental analysis determinations for carbon and hydrogen.

The TGA pattern of Kao-MeOH 8.6 Å (Rxn **2-1-2**) was very similar to that of Kao-MeOH 8.2 Å (Rxn **2-2-1**) except that there was a greater weight loss at low temperatures (< 250 °C) due presumably to the presence of cointercalated water. For Kao-MeOH 8.6 Å, from 20-250 °C, one observed an approximate weight loss of 1.7 % compared to only 0.2% for Kao-MeOH 8.2 Å.

2.2.1.4 NMR Analysis

A ^{13}C CP/MAS NMR spectra of the Kao-MeOH 8.2 Å product was obtained in order to obtain more information regarding the nature of the organic component of this organokaolinite. Figure **2.6** shows that only one resonance at 51.1 ppm is present, as one might expect for a methoxy functionalized kaolinite. This represents a slight downfield chemical shift compared to liquid methanol (49.3 ppm [160]). The difference between the ^{13}C chemical shifts of aluminum alkoxides and the corresponding free alcohol is quite small [154,171]. It was noted by Inoue *et al* [154] that the chemical shifts the methyl and methine carbons of $Al(OPr^i)_3$ are quite similar to those of 2-propanol (δ 25.1 and 63.4 for methyl and methine carbons, respectively). In following by ^{13}C solution state NMR the sol-gel synthesis of aluminum oxide from mixtures containing $Al(O\text{-}s\text{-}Bu)_3$, acetic acid, and *sec*-butyl alcohol, Rezgui *et al* found that the methine ^{13}C resonance of *sec*-butyl alcohol ($CH_3CH_2{}^{13}CHOHCH_3$) at 69 ppm was shifted only slightly to 73 ppm when in the form of an aluminum alkoxide

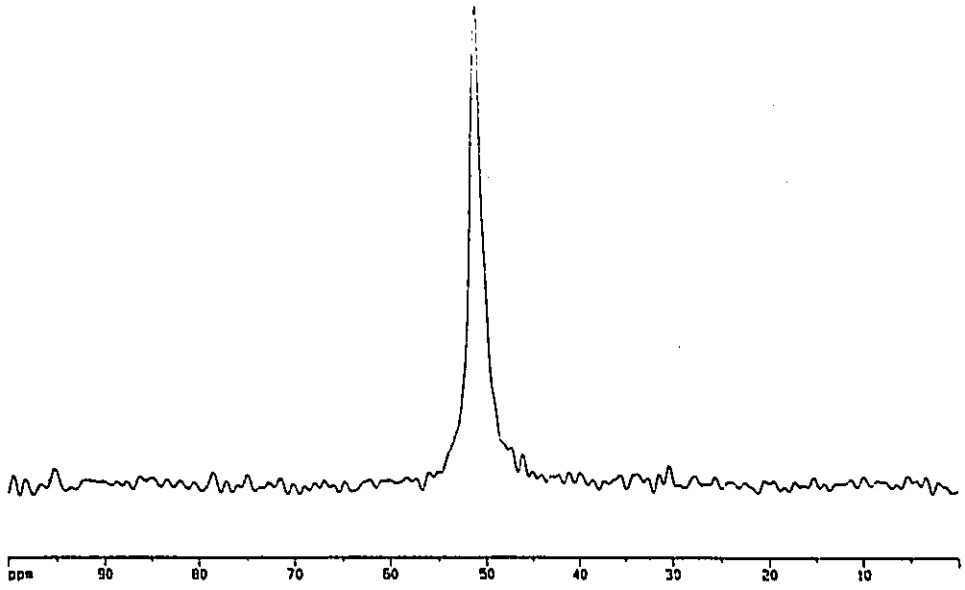

Figure 2.6: ^{13}C CP/MAS NMR of Kao-MeOH 8.2 Å (2-1-1). (Bruker ASX-200; 50.32 MHz; spinning rate= 4 KHz; referenced to hexamethylbenzene at 14.9 ppm)

ligand ($\equiv$Al-O-$^{13}CHCH_3$-CH_2CH_3) [171]. This suggests that it is difficult to differentiate between a methoxide group and a methanol group solely on the basis of chemical shift, especially if the linewidth is fairly broad as is the case for Kao-MeOH 8.2 Å ($v_{1/2}$= 75 Hz).

The ^{13}C chemical shifts of $Al(OCH_3)_3$, methoxylated alumina and methoxylated boehmite are unreported, but the ^{13}C CP/MAS NMR spectra of methanol adsorbed onto zeolites has been reported [160,161,163]. Methanol adsorbed on zeolite H-Y exhibits two resonances [163]. The resonance at 50.1 ppm was attributed to two types of species, a mobile

species due to surface adsorbed methanol, and a rigidly bound methoxy species. The peak at 55.7 ppm was also attributed to a rigidly fixed methoxyl group, on a different site. For methanol adsorbed onto zeolite ZSM-5, a peak at 50.8 ppm was attributed surface adsorbed methanol and not to methoxide species [160]. The zeolite experience suggests that it is clear that it is difficult to make a reliable assignment for the formation of a surface methoxide group solely on the basis of the ^{13}C NMR chemical shift.

^{29}Si CP/MAS NMR (39.76 MHz) of the Kao-MeOH product showed a single resonance at -92.6 ppm ($\nu_{1/2}$= 100 Hz) which compares to a resonance at -91.2 ppm ($\nu_{1/2}$= 80 Hz) for kaolinite. This 1.4 ppm upfield shift is diagnostic of a perturbation of the silicate surface to a more shielded environment, but no major structural changes have taken place. The silicon atoms have remained in tetrahedral Q3(OAl) sites [172]. These results are in accord with the ^{29}Si chemical shifts observed for organokaolinite intercalates [42,44].

2.2.2 Functionalization of Kaolinite with Polyols

2.2.2.1 Preparation

A number of attempts were made to functionalize kaolinite with other monoalcohols such as ethanol, decanol and benzyl alcohol, but all attempts met with failure presumably due to the difficulty of these less polar larger molecules to enter into the interlayer spaces of kaolinite (see Section **6.5.1**). Considerable success was obtained, however, using a number of small polyols to functionalize kaolinite (Table **2.3**). Further attempts to

Product[1]	Basal Spacing[2] (Å)		
	Found	Literature	Estimated[5]
Kaolinite-Ethylene Glycol **(2-2-1)**	9.40	10.9[3]	11.2
Kaolinite-1,3 Propanediol **(2-2-6)**	9.82	11.0[4]	11.2
Kaolinite-1,2 Propanediol **(2-2-8)**	10.84	11.6[4]	11.4
Kaolinite-1,4 Butanediol **(2-2-10)**	NR	-	-
Kaolinite-1,2 Butanediol **(2-2-11)**	11.36	-	-
Kaolinite-1,3 Butanediol **(2-2-13)**	11.36	10.7 (d)[4]	11.2
Kaolinite-2,3 Butanediol **(2-2-15)**	NR	-	-
Kaolinite-1,5 Pentanediol **(2-2-17)**	NR	-	-
Kaolinite-Glycerol **(2-2-19)**	11.06	11.1 [3]	11.6

Table 2.3: Summary of products formed through the functionalization of kaolinite with polyols. (1) See section **6.5.2** for reaction details and product characterizations. (2) This is the basal spacing of the modified organokaolinite phase. In all cases, the product contained variable amounts of the 7.2 Å kaolinite parent material. (3) Taken from reference 38. (The reference mineral was kaolinite). (4) Taken from reference 34 (The reference mineral was halloysite). (5) Based on estimates from reference 34. (d) diffuse reflection. (NR) indicates that no intercalation reaction took place.

intercalate/graft sugars (glucose, methyl-glucoside, α-cyclodextrin) into the interlayer space of kaolinite were unsuccessful due presumably to the difficulty in diffusing these large molecules into the constrained spaces of kaolinite, even after having first swollen the layers with hydrazine or DMSO.

It is apparent from Table **2.3** that the greatest success was obtained with small polyol reagents such as ethylene glycol, propanediols and glycerol. For the larger butanediols, only the 1,3 and 1,2 butanediols yielded products. 1,4 butanediol and 2,3 butanediol failed to react with either Kao-DMSO or Kao-NMF under the refluxing condition employed. It is known that the intercalation of organic molecules into kaolinite is favoured by small polar molecules with more than one functionality [28,36]. These results support this trend. The fact that only two of the four butanediols could be intercalated into the kaolinite structure can be rationalized by the necessity for the various isomers to orient themselves in the interlayer space of kaolinite, such that favourable interaction with the clay surfaces are possible.

For all of the organokaolinite materials which were successfully prepared from polyols, one dimensional stacking order (along the c-axis) was observed by XRD. In all cases at least three (00l) reflections could be observed (see Section **6.5.2**).

From Table **2.3** one sees that there exists in some cases literature precedents for the formation of these products, with either kaolinite or the related mineral halloysite as the parent mineral. In the cases of Kao-EG 9.4 Å, Kao-1,3 PD 9.8 Å and Kao-1,2 PD 10.8 Å, the literature values for the basal spacings were substantially greater than those which were obtained in this study, indicating that different organokaolinite phases had been formed than previously reported. In the case of Kao-Glycerol, a product exhibiting an identical basal

spacing to that previously reported was formed, and for Kao-1,3 BD, a product was observed whose basal spacing was actually greater than that previously reported for a 1,3 butanediol treated halloysite (Hal-1,3 BD). In this last example, the basal reflection was noted by the authors to be very diffuse and asymmetric, indicative of substantial interlayering, so this 10.7 Å basal reflection reported for Halloysite-1,3 Butanediol must therefore be treated with caution.

The conditions that were employed in the preparation of the materials of this study were generally more severe than those reported in the literature [34,38]. Long reaction times (> 16 hours) under high temperature (190-240 °C) reflux conditions were usually employed. However, in the case of Kao-EG, almost identical conditions were employed in the formation of a 10.9 Å ethylene glycol phase of kaolinite [38] and the 9.4 Å phase which was observed in this work. The relationship between these two phases was the subject of considerable study in order to remove the apparent contradiction. This is discussed in detail in Chapter 3. For now, it is sufficient to assume that the 9.4 Å phase is an organokaolinite phase in which the ethylene glycol moieties are grafted to the interlayers of kaolinite via Al-O-C bonds, whereas the 10.8 Å phase is an organokaolinite phase where the EG units are merely intercalated into the interlayers of kaolinite and are held in place by a hydrogen bonding network. The existence of distinct grafted and intercalated phases results also in different basal spacings that were observed for both Kao-1,3 PD 9.8 Å and Kao-1,2 PD 10.8 Å, compared to the literature values of the corresponding organohalloysites (Table 2.3).

The basal spacings of the grafted phases are expected to be less than those calculated based on the intercalation of completely flattened organic molecules. The data from Table

2.3 supports the hypothesis that grafted phases were formed in the cases of Kao-EG 9.4 Å, Kao-1,3 PD 9.8 Å and Kao-1,2 PD 10.8 Å. It is likely that substantial "keying in" of the organic unit into the kaolinite structure is taking place, similar to what was proposed for Kao-MeOH 8.2 Å.

In the case of Kao-Glycerol, Kao-1,2 BD and Kao-1,3 BD, it is not clear on the basis of their basal spacings if an organokaolinite material was formed in which the alcohols were attached via Al-O-C bonds. The 11.06 Å basal spacing of Kao-Glycerol for example, is not out of line with what one might expect on the basis of a glycerol molecule sandwiched between two kaolinite layer. The same can be said of Kao-1,2 BD and Kao-1,3 BD, whose 11.36 Å basal spacing seemingly implies that no grafting has taken place, and only loosely intercalated butanediol molecules are present in the interlayers.

2.2.2.2 IR Analysis

Infrared spectroscopy served to confirm the functionalization of kaolinite with the various polyols. It also provided some information regarding the nature of the guest species and the perturbation of the host kaolinite material. The IR results are summarized in section 6.5.2 as part of the product characterization, and will not be discussed in detail here.

In all cases where modification was deemed to have been successful by XRD (Table 2.3), one observed clear evidence of modification by IR. Specifically, the OH stretching patterns were greatly modified from that of either kaolinite or of the Kao-DMSO and Kao-NMF staring materials. Evidence for H-bonding between the kaolinite host and the polyol

guests was seen as ν(OH) kaolinite bands which had been shifted to lower energies and also as ill-defined hydrogen bonded ν(OH) alcohol bands at still lower energies.

For example, Kao-1,3 PD has ν(OH) bands at 3694 cm^{-1} (m), 3632 cm^{-1} (m), 3621 cm^{-1} (m), 3550 (m,br) and 3440 cm^{-1} (m,br). The kaolinite bands at 3694 cm^{-1} and 3621 cm^{-1} are unperturbed in Kao-1,3 PD, although the 3694 cm^{-1} band in Kao-1,3 PD is much less intense than in kaolinite. The bands at 3632 cm^{-1} and 3550 cm^{-1} are assigned to perturbed surface hydroxyl groups, whereas the broad band at 3440 cm^{-1} is assigned to the hydrogen bonded alcohol groups of the organic unit.

One also observes well defined C-H stretching bands indicative of the presence of the interlayer organic species. Using Kao-1,3 PD once again as an example, one observes two well defined ν(CH) bands at 2968 cm^{-1} (w), and 2890 cm^{-1} (w) corresponding respectively to the antisymmetric and symmetric C-H stretching bands of the grafted 1,3 propanediol units.

2.2.2.3 NMR Analysis

The presence of the organic component was confirmed by ^{13}C CP/MAS spectra for Kao-EG 9.4 Å, Kao-1,3 PD 9.8 Å and Kao-1,2 PD 10.8 Å (see section **6.5.2**). The ^{13}C spectra were characterized by broad resonances, but were consistent with the presence of either intercalated or grafted alcohol units. ^{29}Si CP/MAS were also taken for these samples and the results are summarized in Table **2.4**.

These results are similar to those obtained by Thompson [44] who found that the intercalation of polar organic molecules into kaolinite tended to decrease the linewidths of the ^{29}Si resonance as well as shifting the resonance slightly upfield. In all cases only one ^{29}Si resonance was observed, even for kaolinite, where it has been reported that there are two resonances [42,44,172,173]. The failure to observe two ^{29}Si resonances for kaolinite may be due to the low field at which the spectra was taken, and may explain the broadness of this resonance. It has been proposed that the degeneracy of the silicon environments caused by the expansion of the kaolinite structure shows that interlayer H-bonding is the main cause of Si site differentiation in kaolinite [42,44].

Product	Chemical Shift (ppm relative to TMS)	$\nu_{1/2}$ (Hz)
Kaolinite	-91.3	90
Kao-DMSO	-92.9	35
Kao-EG 9.4 Å (2-2-2)	-92.6	50
Kao-1,2 PD 10.8 Å (2-2-6)	-93.2	65
Kao-1,3 PD 9.8 Å (2-2-8)	-92.7	85

Table 2.4: ^{29}Si NMR chemical shifts and signal widths at half height ($\nu_{1/2}$). These spectra were performed on a Bruker CXP-180 at 35.76 MHz using the CP/MAS (^{1}H-^{29}Si) technique and spinning at 4 KHz.

2.2.2.4 Thermogravimetric Analysis

TGA showed that many of the polyol functionalized kaolinites exhibited thermal stabilities much beyond that expected for organokaolinite intercalates. The details of the thermal analyses of the products are given in section **6.5.2** as part of the product characterizations, and this is summarized in Table **2.5**. In general, there was a small weight loss at temperatures less than 200 °C due to surface adsorbed water and perhaps loosely adsorbed or intercalated organics. At higher temperatures, from 200-600 °C there was a complicated multistep decomposition process due to the pyrolysis or combustion of the organic species and to the dehydroxylation of the kaolinite host. Finally, at much higher temperatures (950-1200 °C), one observed an additional much smaller weight loss, usually characterized by two exothermic transitions between 1000-1050 °C.

Irreversible structural collapse of the polyol organokaolinite materials did not begin until temperatures in excess of 250 °C. The peak endotherms corresponding to the decomposition of the organic components were between 380-450 °C which suggests the presence a strongly bound organic units in the interlayers of kaolinite. If the intercalated guest species were held in place by an electrostatic or hydrogen bonding network with the host material, one would expect the interlayer organic material to volatilize at a much lower temperature. In Kao-DMSO for example, which is one of the most stable organokaolinite intercalates, complete desorption occurs before 250 °C and one observed two endothermic peaks at 131 °C and 215 °C corresponding to the volatilization of DMSO (Section **6.4.1**).

No combustion or pyrolysis of the interlayer DMSO occurs, as is the case for many of the polyol based organokaolinites.

Product[1]	Peak Organic Decomposition Temperature[2] (°C)	Peak Dehydroxylation Temperature[2] (°C)	Total TGA Wt. Loss[3] (%)
Kaolinite	-	538	13.6
Kao-EG 9.4 Å (3-2-1)	444	554	23.2
Kao-1,3 PD 9.8 Å (2-2-7)	411	517	22.3
Kao-1,2 PD 10.8 Å (2-2-8)	405	517	26.3
Kao-1,2 BD 11.4 Å (2-2-11)	386	513	29.9
Kao-1,3 BD 11.4 Å (2-2-13)	387	497	30.6

Table 2.5: Summary of thermogravimetric analysis for polyalcohol based organokaolinites. All TGA\DSC runs were done under N_2 atmosphere. (1) The codes after the product names refer to the reaction number. (2) These peak decomposition temperatures are taken from the corresponding DSC endothermic minima. (3) The TGA weight loss refers to the total weight loss after heating up to 1200 °C in nitrogen atmosphere.

For Kao-EG 9.4 Å and Kao-1,3 PD 9.8 Å, only a small weight losses were observed before 300 °C (less than 2 %), and the peak DSC organic decomposition temperatures were higher than those of Kao-1,2 BD and Kao-1,3 BD. For Kao-1,2 BD and Kao-1,3 BD, the relatively large weight loss at temperatures less than 300 °C (5-8 %) may plausibly be attributed to the presence of more loosely bound intercalated molecules. The presence of intercalated diols would also explain the much higher basal spacings which were observed for these two organokaolinites (d=11.37 Å for both). However, the fact that the peak DSC

decomposition temperatures for Kao-1,2 BD and Kao-1,3 BD were at 386 °C and 387 °C respectively, suggests that some strongly bound grafted species was also present.

2.2.3 Functionalization of Kaolinite with Alcoholethers

2.2.3.1 Preparation

A number of alcoholether based organokaolinites were prepared using the same methods as for the polyols, whereby either Kao-DMSO or Kao-NMF were reacted with an excess of the reagent usually at refluxing conditions. A summary of the alcoholether based organokaolinites prepared along with the XRD basal spacings of the modified phase is given in Table **2.6**.

Product[1]	Basal Spacing[2] (Å)
Kaolinite-2-methoxyethanol **(2-3-1)**	10.57
Kaolinite-diethylene glycol monobutyl ether **(2-3-3)**	10.94
Kaolinite-triethylene glycol monomethyl ether **(2-3-5)**	10.99

Table 2.6: Summary of the products formed through the functionalization of kaolinite with alcoholethers. (1) See section **6.5.3** for reaction details and product characterizations. Codes refer to reaction number. (2) This is the basal spacing of the modified organokaolinite phase.

While the preparation of only three alcoholether based organokaolinites is shown above, it is evident that it is relatively easy to modify the interlayers of kaolinite by inserting various alcohol ether chains. In particular, kaolinite seems to have a certain affinity for alcohol ether structures based on repeating oxyethylene units. A consequence of this, the preparation of a new family of oxyethylene based organokaolinites, will be discussed in Chapter 4.

The preparation of the products shown in Table **2.6** have not been previously prepared, although the preparation of a 2-methoxyethanol (MEO) intercalate of halloysite (Hal-EOA) has been reported by both Carr and Chih [34] and MacEwen [33]. Carr and Chih reported a basal spacing of 11.0 Å whereas MacEwen reported a smaller basal spacing of 10.7 Å. The minimum clearance space necessary for the insertion of 2-methoxyethanol was calculated to be 4.4 Å [34] which would correspond to a basal spacing of 11.6 Å. This is significantly larger than the 10.57 Å basal spacing which was found in this study. This smaller than expected basal spacing value may be explained either by the grafting of the 2-methoxyethanol groups onto the interlayers of kaolinite via Al-O-C bonds or alternatively, by significant keying in of the intercalated 2-methoxyethanol molecules into the kaolinite structure.

The basal spacings which were observed for the other organokaolinites (Kao-DiEGMBE 10.9 Å and Kao-TriEGMME 11.0 Å) were in accord with what one might expect for a flattened monolayer arrangement of the intercalated molecules.

2.2.3.2 Characterization

IR spectroscopy confirmed that for all of the products described in Table **2.6**, new organokaolinite materials were formed which exhibited perturbed O-H stretching patterns compared to kaolinite. One also observed the presence of C-H stretching (2800-3000 cm^{-1}) and C-H deformation bands (1200-1600 cm^{-1}) for these products as well as some perturbations of many of the lattice vibration bands of kaolinite (see Section **6.5.3**).

Thermogravimetric analysis of Kao-MEO 10.6 Å shows that this material is quite stable with respect to heating, and does not begin to decompose in nitrogen atmosphere until greater than 300 °C. The peak endotherm assigned to the decomposition of organic material is at 412 °C. The decomposition of Kao-DiEGMBE 10.9 Å in air atmosphere shows a strong exothermic peak at 317 °C due to the combustion of interlayer organic material. For both of these materials one observes additional endotherms at temperatures slightly less (450-530 °C) than the dehydroxylation temperature of kaolinite (538 °C) as well as weak exotherms near 1000 °C, similar to that of kaolinite, although somewhat weaker.

^{13}C CP/MAS NMR results for Kao-MEO 10.6 Å were consistent with the presence of 2-methoxyethanol in the interlayers of kaolinite, in that one was able to observe two broad resonances, one at 74.2 ppm ($v_{1/2}$= 240 Hz) and another at 62.0 ppm ($v_{1/2}$= 180 Hz). The ^{29}Si CP/MAS NMR spectra of Kao-MEO 10.6 Å showed the presence of two resonances, the first at -91.6 ppm due presumably to residual unreacted kaolinite, and the second at -93.1 ppm due to Kao-MEO 10.6 Å. This is in accord with the ^{29}Si chemical shifts that were observed for some of the polyol functionalized kaolinites (Table **2.4**).

2.3 Conclusions

It has been shown that it is possible to modify the interlayers of kaolinite with a wide range of small aliphatic alcohols. These modification reactions involved the reaction of Kao-DMSO or Kao-NMF with the alcohol reagent at high temperatures. It is proposed that the alcohols are grafted to the hydroxyl surface of kaolinite through an alcohol condensation reaction whereby Al-O-C bonds are formed. This new class of organokaolinite hybrid exhibited thermal stability in excess of that for other organokaolinite intercalates, and for the most part did not decompose in nitrogen atmosphere until greater than 250 °C. It was found that kaolinite functionalization was favoured for alcohol reagents which were not overly hydrophobic and possessed additional ether or alcohol functionalities.

Many of the organokaolinites exhibited basal spacings which were less than those calculated on the basis that the intercalated molecule would adopt a minimum height flattened monolayer conformation. This observation is consistent with the covalent grafting hypothesis, and may account for the fact that in some cases, the basal spacings which were obtained for these organokaolinites, were less than those previously reported for the corresponding organokaolinite or organohalloysite intercalates. For example, this is particularly striking in the cases of the ethylene glycol functionalized kaolinite (Kao-EG 9.4 Å) whose 9.4 Å basal spacing is much less than the literature reported value of 10.9 Å.

All this represents a significant departure from the conventional intercalation chemistry of kaolinite. No longer is it sufficient to consider the intercalation chemistry of kaolinite solely in terms of relatively weak host-guest hydrogen bonding interactions. One

must also consider the possibility of guest molecules, in this case alcohols, reacting with the hydroxyl interlayer surface of kaolinite to form a new class of organokaolinite nanocomposite material whose thermal and chemical properties differ from those of classical organokaolinites.

Chapter 3

Preparation and Characterization of Two Distinct Ethylene Glycol Organokaolinite Phases

3.1 Introduction

In Chapter 2, the covalent grafting of organic units to the interlamellar surface of kaolinite was described. This involved the attachment of various alcohols to the aluminate surface of kaolinite via Al-O-C bonds. Many of these organokaolinite materials possessed basal spacings in excess of that expected on the basis of intercalated organic molecules, and literature precedents suggested that in some cases, it should be possible to obtain two distinct modification phases. For example, it should be possible to selectively prepare either the Kao-EG 9.4 Å grafted phase described in Chapter 2 or a Kao-EG 10.8 Å intercalated phase described in the literature [38,63]. It is interesting that Camazano and Garcia [38] used virtually identical conditions in the synthesis of their intercalated Kao-EG 10.8 Å phase as was used in the synthesis of the Kao-EG 9.4 Å grafted phase. The question naturally arises: what governs the formation of the intercalated Kao-EG 10.8 Å phase over that of the grafted Kao-EG 9.4 Å phase? In this chapter, an attempt is made to answer this question as well as to better characterize these two phases. In the process, it is wished to better rationalize some of the chemistry which can occur between alcohols and the interlamellar surfaces of kaolinite and possibly other similar materials.

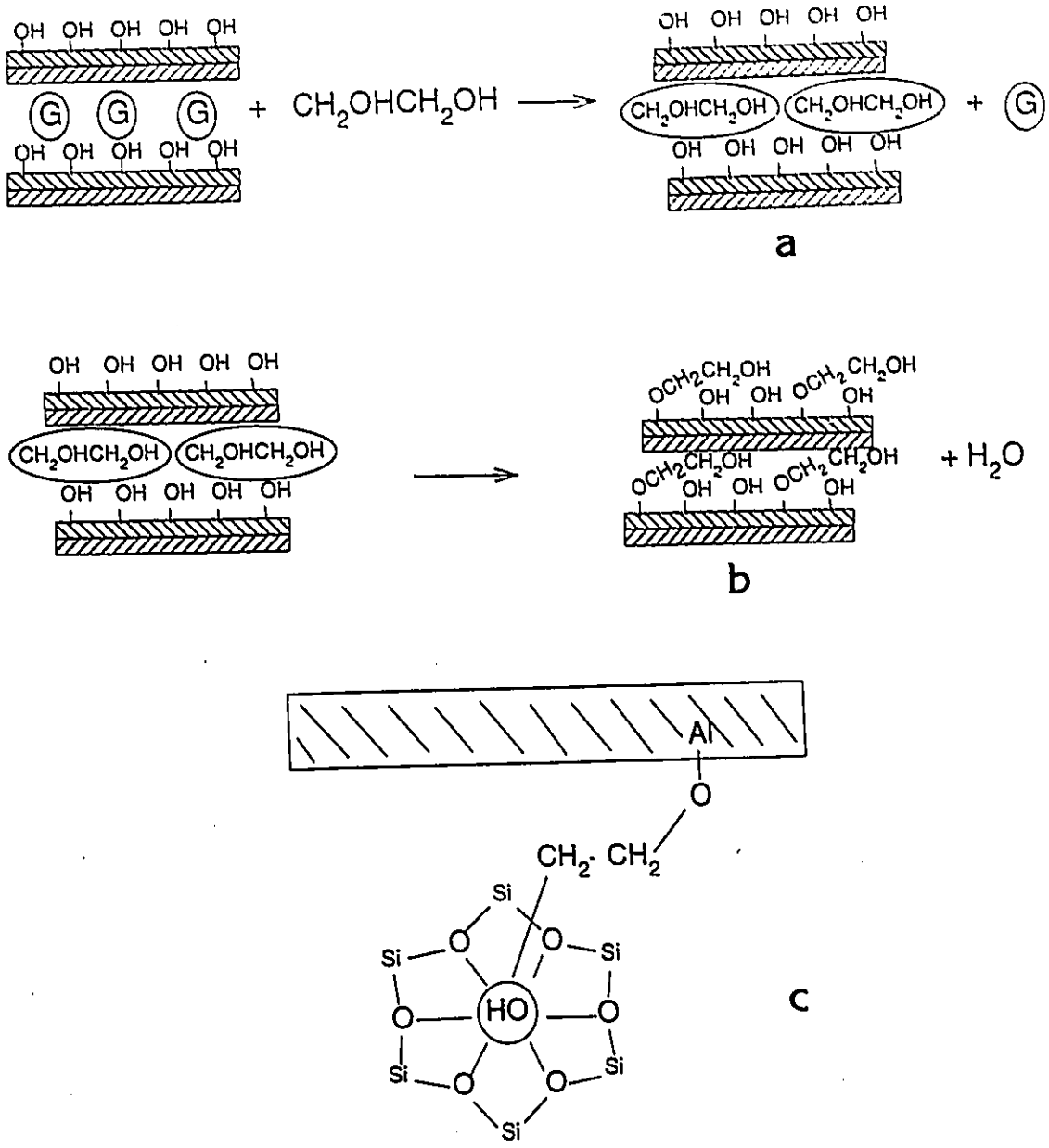

Figure 3.1: Proposed Mechanism for the Formation of Kao-EG 10.8 Å (a) and Kao-EG 9.4 Å (b). (c) Structural model for Kao-EG 9.4 Å showing the "keying in" of the free alcohol end of the EG unit into the $(Si\text{-}O\text{-})_6$ macroring of the silicate surface.

3.2 Results and Discussion

3.2.1 Preparation

3.2.1.1 Preparation of Kao-EG 10.8 Å

If one wishes to compare Kao-EG 9.4 Å with Kao-EG 10.8 Å it is necessary to first verify that it is possible to individually prepare both phases. Kao-EG 9.4 Å had already been previously prepared a number of times (Section **6.5.2**) using a variety of preparation methods. It was also possible to prepare the halloysite analogue of Kao-EG 9.4 Å (Hal-EG 9.4 Å), in the same manner by refluxing Hal-DMSO in ethylene glycol for 40 hours (Section **6.6.7**). As for Kao-EG 10.8 Å, its preparation had been previously reported in the literature[38,175], so it was decided to repeat these preparations. Attempts to prepare Kao-EG 10.8 Å using the preparation method of Camazano and Garcia [38] whereby Kao-DMSO was refluxed in an excess of EG consistently yielded Kao-EG 9.4 Å. Eventually, the preparation of Kao-EG 10.8 Å from Kao-DMSO was finally achieved by modifying this preparation method somewhat. A small excess of reagent grade ethylene glycol was reacted with Kao-DMSO (1 g/1 g) in a sealed glass ampoule for 3 days at 140-190 °C (Rxn **3-1-1**). It was also possible to prepare Kao-EG 10.8 Å by reacting Kao-hydrazine (Rxn **3-1-2**) with ethylene glycol in a manner similar to that described by Range *et al* [63]. Attempts to prepare Kao-EG 10.8 Å via the gas phase displacement of intercalated DMSO or NMF with EG were unsuccessful (Rxns **3-1-3** and **3-1-4**).

3.2.1.2 The Role of Water in Determining the Reaction Products

Once the preparation of Kao-EG 10.8 Å was confirmed, some of the factors which might influence the formation of one ethylene glycol organokaolinite over another were investigated. The proposed mechanism shown in Figure **3.1** indicates that water is a reaction product. It is thus reasonable to assume that if one could control the water content in the reaction media, it should be possible to exert some control over the nature of the organokaolinite product. Increasing water content should drive the product towards the formation of Kao-EG 10.8 Å whereas dry reaction conditions should favour the formation of Kao-EG 9.4 Å.

To test this hypothesis, a series of experiments were performed whereby the initial water content of the reaction media was varied from close to 0 % by volume to 20 % by volume. The powder XRD patterns of the products of these trials are shown in Figure **3.2**. It was found that by changing the water content of the reaction media it was indeed possible to change the nature of the products. The results taken from Figure **3.2** are summarized in Table **3.1**. The product distribution which was estimated based on the relative intensities of the basal peaks of the various product phases was found to be a function of the water content of the reaction media.

When Kao-DMSO was refluxed in relatively dry ethylene glycol (Rxn **3-2-1**), the main product was the 9.4 Å ethylene glycol modified organo-kaolinite Kao-EG 9.4 Å. Residual unexpanded kaolinite contaminates the product in this and all other trials, and is seen as the superposition of the powder XRD patterns of unexpanded kaolinite onto that of

the principal product(s). This is not surprising since the Kao-DMSO starting material contains approximately 7 % unexpanded kaolinite as judged by comparing the relative heights of the basal reflections of the DMSO intercalated (d_{001} = 11.2 Å) and unexpanded (d_{001} = 7.2 Å) kaolinite.

Reaction	Percentage of Water in Reaction Mixture[1].	Relative Intensities of d_{001} XRD Peaks of Products (as a percentage of the total intensity).		
		Kao-EG 10.8 Å phase	Kao-EG 9.4 Å phase	Residual kaolinite 7.2 Å phase
3-2-1	0.0	-	93.7	6.3
3-2-2[2]	1.0	32.3	61.3	3.9
3-2-3	2.0	38.7	53.9	7.4
3-2-4	5.0	87.3	-	12.7
3-2-5	10.0	87.7	-	12.3
3-2-6	20.0	12.2	-	87.8

Table 3.1: Data showing the dependence of product formation on the water content of the reaction mixture. The trials involved refluxing Kao-DMSO with the given ethylene glycol\water mixtures and is described in the experimental section. The product distribution was analyzed by measuring the relative intensities of the basal spacing peaks with the sum total basal spacing intensity normalized to 100. (1) The reaction mixtures were prepared by adding a given volume of water to dry ethylene glycol (<.05 % by Karl Fischer titration). The percentage of water is taken as the percent volume of water per sum total volume before mixing. (2) The product distribution does not sum to 100% since an additional 2.5 % is in the form of a 8.5 Å hydrate of kaolinite.

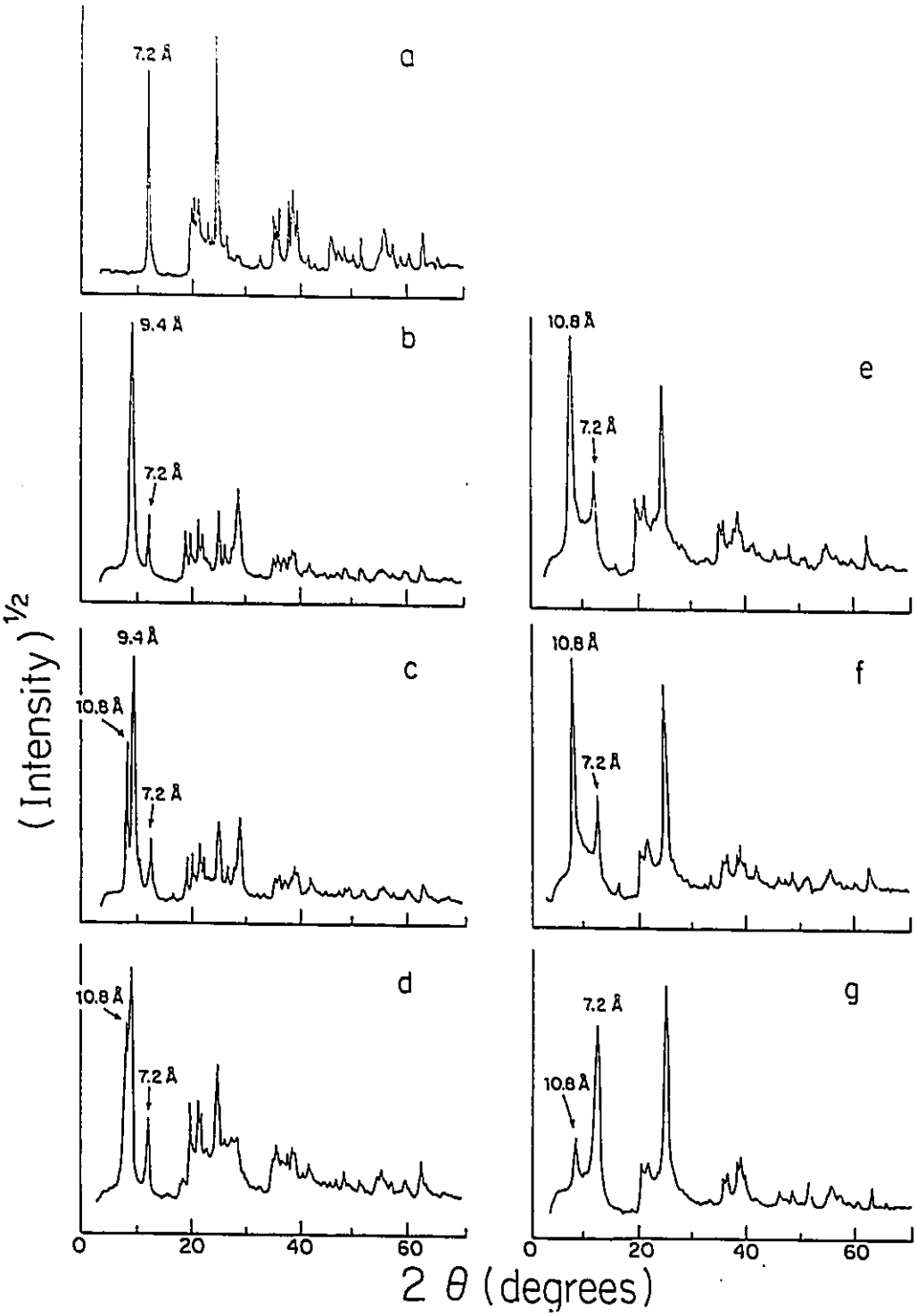

Figure 3.2: Powder XRD patterns of: Kaolinite 7.2 Å (a) and Kao-EG samples prepared with 0 % (b), 1 % (c), 2 % (d), 5 % (e), 10 % (f) and 20 % (g) by volume water added to the refluxing ethylene glycol/ Kaolinite-DMSO reaction mixture (see Section 6.6.2).

As the water content is increased, another ethylene glycol modified organokaolinite is observed with a characteristic basal spacing of 10.8 Å (Kao-EG 10.8 Å). In reactions 3-2-2 and 3-2-3, at low concentrations of water (1% and 2% by volume respectively), the Kao-EG 9.4 Å phase is still predominant, but as the water content is increased still further to 5% and 10 % (3-3-4 and 3-2-5), Kao-EG 10.8 Å becomes the predominant product and the Kao-EG 9.4 Å phase cannot even be detected. At still higher concentrations of water (3-2-6), the yield of Kao-EG 10.8 Å is dramatically reduced and the formation of unexpanded kaolinite material becomes the principal phase. This shows that there is an optimum water content for the reaction media if one wishes to maximize the yield of Kao-EG 10.8 Å. In contrast, to maximize the yield of the Kao-EG 9.4 Å phase, it is required that the reaction media consist of dry ethylene glycol.

From the series of experiments summarized in Table 2.1, it is clear that the concentration of water plays an important role in determining the product distribution. One would expect that excess water would drive the reaction towards the unmodified hydroxylated surface and free alcohol whereas a low concentration of water should favour the formation of the grafted surface ether. Assuming that the forward reaction is endothermic, one would also expect that heating would drive the reaction towards the formation of the ≡Al-O-R surface ether species. This simplistic model therefore can rationalize the roles of water content and of heat in determining which type of ethylene glycol organo-kaolinite is formed.

3.2.1.3 Changes in Kao-EG Product Distribution Over Time

For products **3-2-2** and **3-2-3**, it was found that powder XRD patterns changed over time. One day after preparation, only the 9.4 Å phase could be detected, but after three months both the 9.4 Å and the 10.8 Å phases could be observed. Product **3-2-6** also changed over time. Initially, the 10.8 Å phase could not be seen at all. Instead there was a large broad peak at a d-spacing of 7.3 Å and a small unresolved peak at 14.6 Å. The powder XRD patterns of the products formed in the other trials changed relatively little after 3 months.

In some cases, it appears that the sample must be given sufficient time to equilibrate so that the different phases may form. It is believed in the case of products **3-2-2** and **3-2-3**, that water trapped in the interlamellar space during formation of the Kao-EG 9.4 Å phase slowly hydrolysed some of the Al-O-R bonds yielding intercalated ethylene glycol in the process. Eventually the intercalated Kao-EG 10.8 Å phase could separate enough from the 9.4 Å phase to be observed by powder XRD and yield a second detectable ethylene glycol organokaolinite phase. It is important to note that it is only water already trapped in the interlamellar space of kaolinite which may enact hydrolysis. External water, or water molecules outside the interlamellar space cannot penetrate these spaces. If no water is present in the interlamellar space as is the case for product **3-2-1**, no hydrolysis occurs and the Kao-EG 10.8 Å phase does not form even after sitting for three months.

3.2.2 Product Characterization

Characterization of the Kao-EG 9.4 Å and the Kao-EG 10.8 Å phases were hampered by the fact that it was not possible to obtain solely one phase. Nonetheless, it was possible through use of an assortment of techniques to gain some insight into the structures of these two phases as well as the relationship between the two. It was decided to more fully characterize the products of **3-2-1**, **3-2-4** and **3-2-5** (see Table **3.1** and Figures **3.2 b**, **e** and **f**) since these runs had the highest yields of Kao-EG 9.4 Å (**3-2-1**) and Kao-EG 10.8 Å (**3-2-4** and **3-2-5**).

3.2.2.1 Thermogravimetric Analysis

The TGA curves for kaolinite, Kao-EG 9.4 Å and Kao-EG 10.8 Å are given in Figure **3-3**. Kaolinite exhibits a single weight loss of 13.1 % from 400 to 700 °C ($T_{ons.}$ = 478 °C) corresponding to the loss of water in the dehydroxylation reaction of the crystal lattice in the kaolinite-metakaolinite phase transition [176]. The corresponding DSC run (not shown) showed an endothermic transition at 538 °C (peak minimum) corresponding to the 13.1 % weight loss as well as a sharp exothermic transition at 1003 °C (peak maximum) corresponding plausibly to a structural reorganization (no weight change).

Kao-EG 10.8 Å exhibits a weight loss 5.4 % at an onset temperature of 124 °C and a slow two step weight loss of 14.5 % commencing at around 240 °C and ending at 620 °C. The first decomposition in this two step process occurs in the range of 240-440 °C

($T_{ons.}$ =343 °C) and involves a 5.1 % weight loss. The second decomposition step occurs in the range 440-620 °C ($T_{ons.}$ = 486 °C) and involves a weight loss of 9.4 %. From 620 °C to 1200 °C an additional 4.2 % weight loss occurs. The DSC run (not shown) gives endothermic minima at 160 °C, 426 °C, and 524 °C corresponding to the 5.4, 5.1 and 9.4 % weight losses. In addition to the exothermic peak maximum at 1003 °C (metakaolinite structural organization), there is an additional smaller exotherm maximum at 1025 °C.

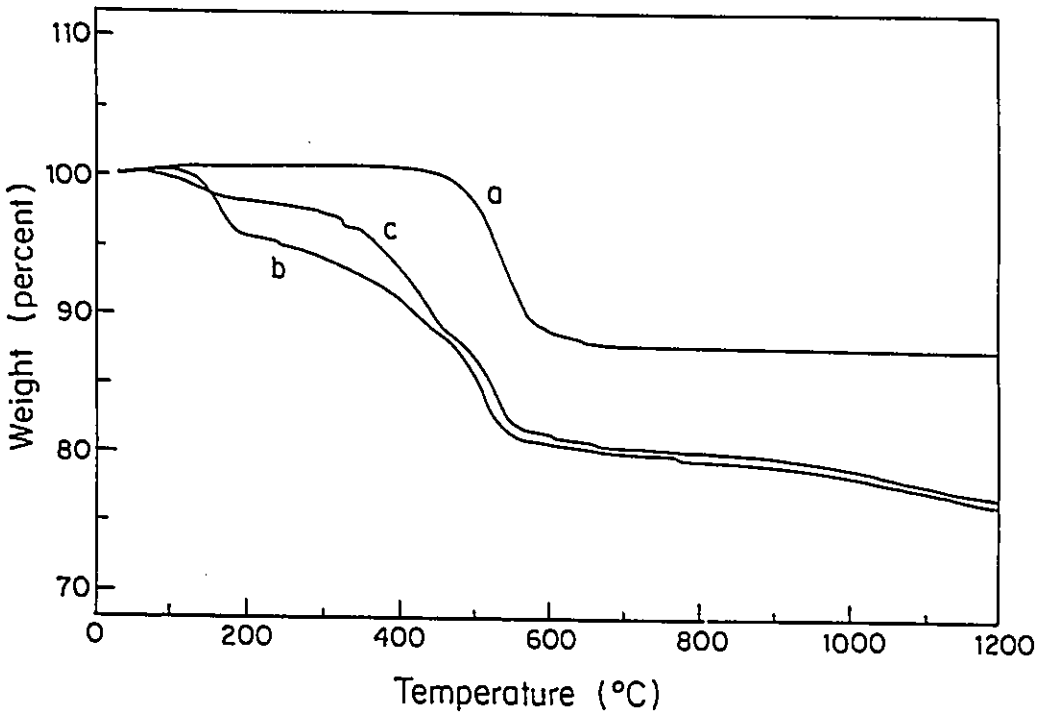

Figure 3.3: TGA results for: (a) Kaolinite 7.2 Å; (b) Kao-EG 10.8 Å (3-2-5) and (c) Kao-EG 9.4 Å (3-2-1).

Kao-EG 9.4 Å experiences its first weight loss of 2.1 % in what appears to be a two step process from 60-200 °C. The DSC run shows a 2-stage endothermic event with peaks at 100 °C and 145 °C. The next weight loss involves another 2-stage decomposition between 200 °C and 620 °C. The first stage occurs from 200-470 °C ($T_{ons.}$ = 346 °C; 9.8 % weight loss) and the second stage occurs from 470-620 °C ($T_{ons.}$ = 507 °C; 7.2 % weight loss). The DSC run show endothermic minima at 444 °C and 554 °C as well as an exotherm at 528 °C. Finally, from 620 °C to 1200 °C there is a gradual 4.3 % weight loss. DSC show two exotherms at 1004 °C and 1029 °C similar to what was obtained for Kao-EG 10.8 Å except that in this case, the 1029 °C exotherm is larger than the 1004 °C exotherm.

On the basis of the TGA data (percentage of weight loss of water and organics to form metakaolinite $Al_2O_3.2SiO_2$), the following formula can be calculated: $Al_2Si_2O_5(OH)_{3.2}(OCH_2CH_2OH)_{0.8}$. This is in good agreement with X-ray fluorescence data (SiO_2: calc.: 40.9 %; found: 39.7 %; Al_2O_3: calc.: 34.8 %; found: 34.4 %) and chemical analysis data (C: calc.: 6.55 %; found: 6.51 %; H: calc.: 2.46 %; found 2.48 %).

The TGA data shows that the Kao-EG 9.4 Å phase and the Kao-EG 10.8 Å behave differently with respect to their thermal decomposition sequence. Kao-EG 10.8 Å begins decomposition much earlier than Kao-EG 9.4 Å, presumably due to the loss of intercalated H_2O and EG. It appears that not all of the EG is removed from Kao-EG 10.8 Å during this first deintercalation step (<200 °C) and in fact some of the residual EG is in the form of grafted EG units.

In an attempt to confirm this and better understand what phases are formed once the volatile component (<200 °C) is expelled, an experiment was performed whereby small

portions (100 mg) of kaolinite, Kao-EG 10.8 Å and Kao-EG 9.4 Å were heated in a furnace at 200 °C for 1 hr, followed by XRD and infrared analysis before and after thermal treatment. These results are shown in Figures **3.4** and **3.5**. From these figures, it is clear that whereas kaolinite and Kao-EG 9.4 Å change little upon thermal treatment, Kao-EG 10.8 Å is transformed into Kao-EG 9.4 Å.

3.2.2.2 Powder XRD

Figures **3.2 a-f** show the XRD pattern of the various products formed by varying the water content of the reaction media. In Figures **3.2 b** (0 % water content) **3.2 e** and **3.2 f** (5% and 10% water content respectively) the XRD patterns show a superposition of two separate phases. In the case of Figure **3.2 b**, the Kao-EG 9.4 Å phase is superimposed on the residual kaolinite phase. Both the d_{002} (18.9 °2Θ) and the d_{003} (28.5 °2Θ) peaks are clearly observable in addition to the intense d_{001} peak (9.3 °2Θ) thus indicating a relatively low stacking disorder. The same can also be said for the principal Kao-EG 10.8 Å phase in Figure **3.2 f**, where the d_{001} (8.2 °2Θ), d_{002} (16.4 °2Θ) and d_{003} (24.7 °Θ) reflections can be identified. Here, the d_{003} reflection overlaps somewhat with the d_{002} (24.9 °2Θ) reflection of the residual kaolinite.

In Figures **3.4 a-c**, the 4-14 °2Θ XRD patterns illustrates the effects of heating at 200°C on the Kao-EG 9.4 Å and Kao-EG 10.8 Å phases. There is no change in the d_{001} peak of kaolinite upon heating at 200 °C (Figure **3.4 a**). Both the position (d= 7.14 Å), and the peak width (0.16 °2Θ) remain constant upon heating.

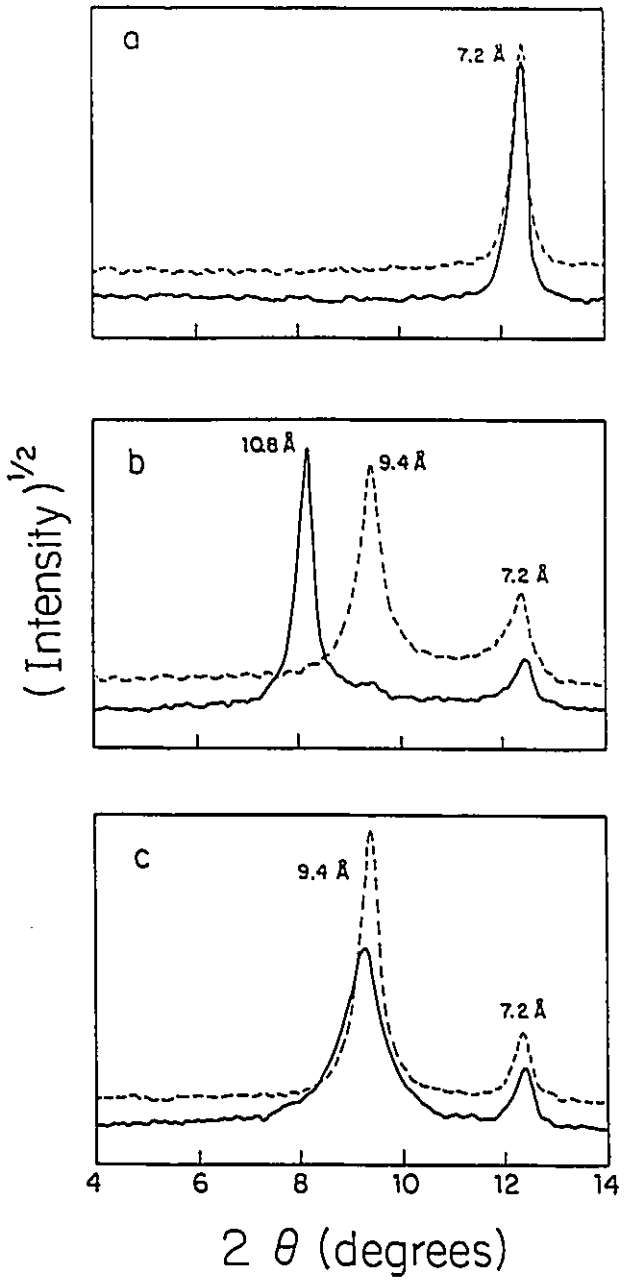

Figure 3.4: XRD patterns 4-14 degrees 2Θ before (——) and after (- - - -) heating at 200 °C for one hour for: **(a)** Kaolinite 7.2 Å; **(b)** Kao-EG 10.8 Å **(3-2-4)**; **(c)** Kao-EG 9.4 Å **(3-2-1)**.

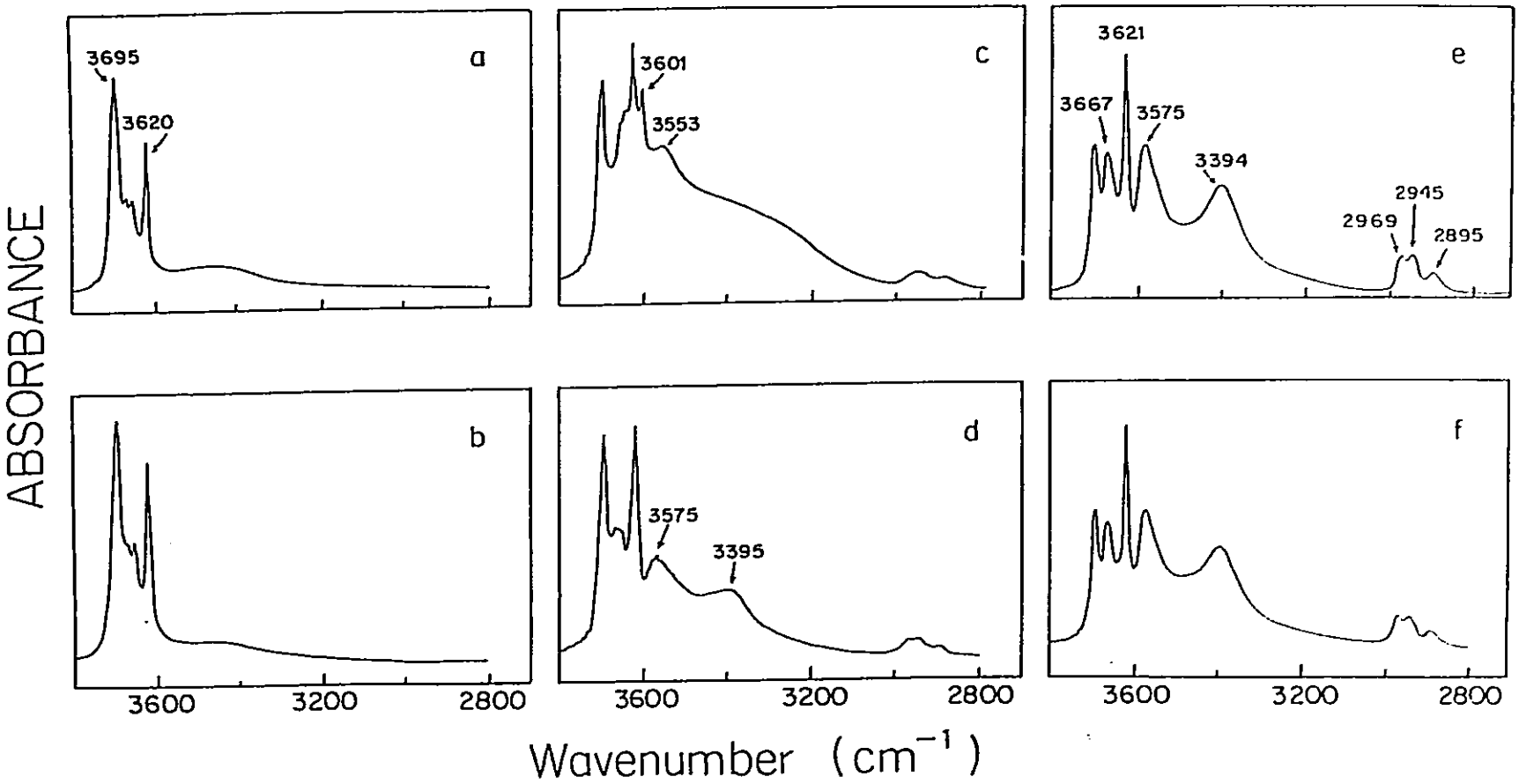

Figure 3.5: FTIR (3800-2800 cm^{-1}) of the O-H and C-H stretching region of: (a) Kaolinite 7.2 Å; (b) Kaolinite after heating at 200 °C 1 hr; (c) Kao-EG 10.8 Å (3-2-4); (d) Kao-EG 10.8 Å (3-2-4) after heating at 200 °C 1hr.; (e) Kao-EG 9.4 Å (3-2-1); (f) Kao-EG 9.4 Å (3-2-1) after heating at 200 °C 1 hr. Note: The relative absorbance scales of the spectra have been adjusted in order to facilitate comparison.

In the case of Kao-EG 10.8 Å (**3-2-4**), it was found that thermal treatment caused significant changes in the XRD pattern (Figures **3.4 b**). The peak at d= 10.75 Å (8.2 °2Θ) was eliminated upon heating at 200 °C and instead, the peak at d= 9.4 Å (9.4 °2Θ) was drastically increased in relative intensity from 2.1 to 100.0. The relative intensity of the residual kaolinite d_{001} peak at d= 7.14 (12.4 °2Θ) also increased in relative intensity from 4.6 to 17.5 upon heating at 200 °C.

For Kao-EG 9.4 Å (**3-2-1**), heating at 200 °C caused a slight shift in the d_{001} peak position from 9.52 Å (9.3 °2Θ) to 9.39 Å (9.4 °2Θ), but the main difference was the reduction in peak width from 0.36 to 0.24 °2Θ (Figure **3.4 c**). Heating Kao-EG 9.4 Å at 600-700 °C in air atmosphere (Section **6.6.4**) produced an XRD amorphous black powder, whose IR spectra closely approximated that of metakaolinite. Very weak C-H stretching bands could still be observed at 2962 cm^{-1}, 2925 cm^{-1} and 2872 cm^{-1}, but no ^{13}C CP-MAS signal could be observed even after one hour acquisition time. The amorphous carbonaceous material which was formed, as evidenced by the black colour of the product and the residual CH stretching intensity, is made up of carbons with a very broad range of chemical shifts, and so it is difficult to observe by ^{13}C CP/MAS NMR.

3.2.2.3 IR Analysis

Figures **3.5 a-f** show the effects of heating to 200 °C on the C-H and O-H stretching regions of the infrared spectrum. The characteristic O-H stretching pattern of the parent kaolinite remained unchanged upon heating (Figures **3.5 a,b**). The 3695 cm^{-1}, 3669 cm^{-1}, and

3652 cm^{-1} peaks have been assigned to the interlamellar surface O-H stretching vibrations of the Al-OH surface of kaolinite [41,177]. The 3620 cm^{-1} peak is the O-H stretching frequency corresponding to the internal hydroxyl group of the kaolinite.

Upon modification of Kao-EG 10.8 Å as the main phase one sees a corresponding change in the infrared O-H and C-H stretching region (Figure **3.5 c**). The 3620 cm^{-1} peak corresponding to the O-H stretching frequency of the internal hydroxyls of kaolinite remains unchanged since modification takes place in the interlayers and not in the structure itself. The 3695 cm^{-1} peak decreased in intensity as a series of ill defined bands at 3651 cm^{-1}, 3640cm^{-1}, 3601 cm^{-1} and 3553 cm^{-1} appeared, superimposed on a broad hydrogen bonded OH stretching beginning at 3100 cm^{-1}. In addition, two broad, low intensity bands in the C-H stretching region appeared at about 2880 cm^{-1} and 2950 cm^{-1}. This corresponds roughly to the symmetric and antisymmetric C-H stretching bands of neat ethylene glycol (2874 cm^{-1} and 2941 cm^{-1}). It is also noteworthy that there is virtually no intensity at 1650 cm^{-1} (not shown) thus ruling out the possibility of significant amounts of water being intercalated into the interlamellar space of kaolinite since this is the area where the bending deformation δ(H-O-H) of water occurs.

Upon heating at 200 °C, the infrared pattern of the Kao-EG 10.8 Å product changed significantly (Figure **3.5 d**), in accordance with what was seen by XRD (Figure **3.4 b**). Both IR and XRD confirmed that the Kao-EG 10.8 Å phase had been converted almost quantitatively to the Kao-EG 9.4 Å phase. This can be seen by the similarity between the infrared spectra in Figure **3.5 d** and that of the Kao-EG 9.4 Å product in Figures **3.5 e** and

3.5 f. In contrast to the Kao-EG 10.8 Å product, the infrared pattern of the Kao-EG 9.4 Å product remains essentially unchanged upon heat treatment at 200 °C (Figures **3.5 e, f**).

For the Kao-EG 9.4 Å product, there exists five distinct OH stretching frequencies. The 3620 cm^{-1} peak remains virtually unchanged from kaolinite since the internal structural hydroxyl group is removed from the site of modification. The 3695 cm^{-1} and the 3667 cm^{-1} bands are due to the interlamellar surface hydroxyls of the Al-OH kaolinite sheet. The peak at 3575 cm^{-1} is proposed to be due to the hydrogen bonded component of the interlamellar surface hydroxyls of kaolinite. This hydrogen bonding involves the ethylene glycol moiety, which in turn has a hydrogen bonded O-H stretching frequency at still lower energy at 3394 cm^{-1}. The presence of this alcohol ν(OH) band at 3394 cm^{-1} is consistent with the model proposed in Figure **3.1** where only one end of the EG unit is grafted. If both ends were grafted, one should not observe this band.

As for the C-H stretching region, there now appears to be three distinct C-H stretching bands at 2895 cm^{-1}, 2945 cm^{-1} and 2969 cm^{-1}. This contrasts with the situation for neat ethylene glycol and the Kao-EG 10.8 Å product (Figure **3.5 c**) where only two bands, indicative of the symmetric and antisymmetric C-H stretching modes, were observed. The presence of a third C-H stretching band in Kao-EG 9.4 Å may be indicative of two non-identical CH_2 fragments as would be expected if only one end of the EG unit was grafted.

The alumino-silicate framework of kaolinite absorbs strongly in the region 1000-1200 cm^{-1}, and neat ethylene glycol is characterized by two absorption bands, due to the C-C-O stretchings at 1087 cm^{-1} and 1044 cm^{-1}. In the case of three aluminum alkoxides, the Al-O-C linkage was characterized by the presence of a band in the region 1030 to 1070 cm^{-1} [178].

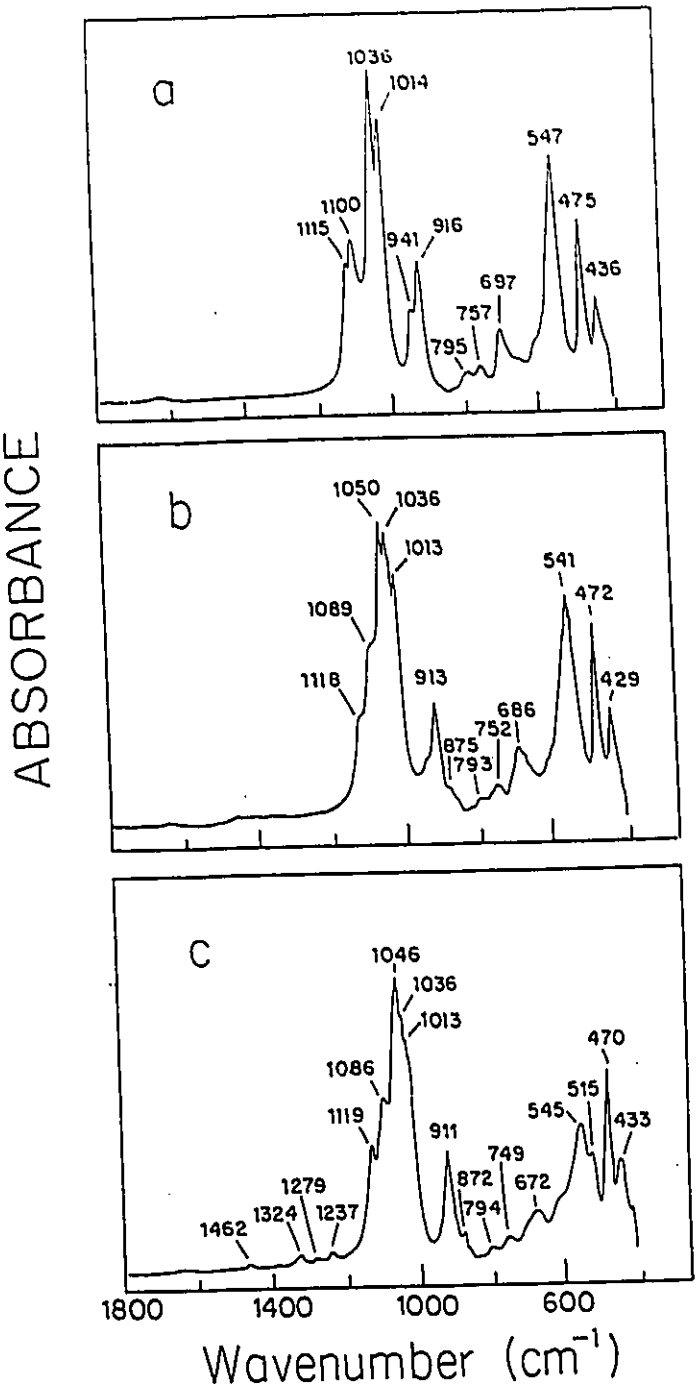

Figure 3.6: FTIR of the lattice vibrations region (1800-400 cm^{-1}) of: (a) Kaolinite; (b) Kao-EG 10.8 Å; (c) Kao-EG 9.4 Å. Note: The relative absorbance scales of the spectra have been adjusted in order to facilitate comparison.

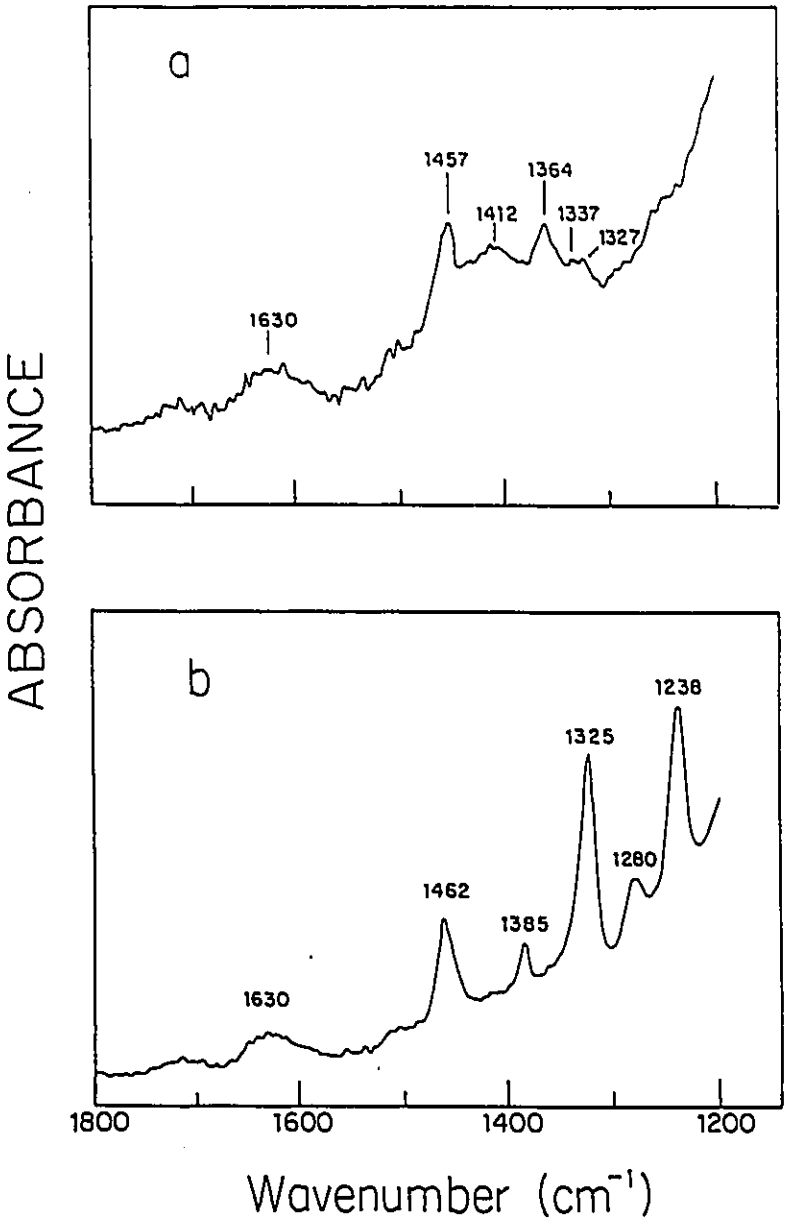

Figure 3.7: FTIR of the C-H deformation region (1800-1200 cm^{-1}) of: (a) Kao-EG 10.8 Å; (b) Kao-EG 9.4 Å. Note: The relative absorbance scales of the spectra have been adjusted in order to facilitate comparison.

The presence of a band at 1100 cm^{-1} was recently mentioned as being characteristic of a barium aluminate glycolate [179]. In both Kao-EG 9.4 Å and Kao-EG 10.8 Å, the region 1000-1200 cm^{-1} is strongly modified (Figure **3.6**), showing, in first approximation, the superposition of the spectra of kaolinite host and ethylene glycol guest.

Figure **3.6** also shows that other lattice vibrations in kaolinite have been modified as well. The δ(Al-OH) band due to the inner surface hydroxyls of kaolinite at 941 cm^{-1} (Figure **3.6 a**) is much reduced in intensity for Kao-EG 10.8 Å (Figure **3.6 b**), and is entirely missing in Kao-EG 9.4 Å (Figure **3.6 c**). This is consistent with the hypothesis that some grafting of EG units has occurred on the hydroxyl surface of kaolinite to give Al-O-R linkages thus removing Al-OH groups.

The 697 cm^{-1} band of kaolinite which has been attributed to the perpendicular vibration of the hydroxide sheet of kaolinite [26] is red shifted 11 cm^{-1} to 686 cm^{-1} for Kao-EG 10.8 Å and 25 cm^{-1} to 672 cm^{-1} for Kao-EG 9.4 Å. The shift to lower frequencies of this band was observed for deuterated kaolinite and was attributed to the larger mass of the deuteroxyl compared to the hydroxyl [26]. This phenomena which was also observed for Kao-MeOH 8.2 Å (Section **2.2.1.2**) is plausibly due to the presence of a larger mass attached to the hydroxyl surface (Al-OCH_2R vs Al-OH), although it may simply be due to a strong perturbation caused by the presence of interlayer EG units.

In general, the absorption bands are narrower for the 9.4 Å phase compared to the 10.8 Å one, showing a strong rigidification of the organic units in Kao-EG 9.4 Å. This is particularly striking in the region of the CH_2 deformation bands, between 1200 cm^{-1} and 1500 cm^{-1} (Figure **3.7**). Five bands of weak (w) or very weak (vw) intensity can be clearly

identified on the Kao-EG 9.4 Å spectrum, at 1238 cm^{-1} (w), 1280 cm^{-1} (vw), 1325 cm^{-1} (w), 1385 cm^{-1} (vw) and 1462 cm^{-1} (w) (Figure **3.7 b**). This region is diagnostic of the conformation, gauche or trans, of the ethyleneoxy, O-CH_2CH_2-O groups. The clear presence of a band at 1325 cm^{-1} suggests the trans conformation, since in previous work, involving polyethylene oxide (PEO) chains, the lack of a band at 1322 cm^{-1} was assumed to be diagnostic of ethyleneoxy units in the gauche conformation [118]. This was assumed on the basis of the vibrational spectra of PEO.Hg salt complexes, whose structure is known from X-ray analysis to be in a planar zig-zag conformation in which the ethyleneoxy groups are in trans and gauche conformations. The presence of a band at 1322 cm^{-1} was attributed to the trans conformation of the -O-CH_2CH_2-O- unit.

This and other IR data for Kao-EG 9.4 Å supports the hypothesis that the O-CH_2CH_2-O unit is in a trans conformation with one end grafted to form an Al-O-C bond, while the free OH group is keyed into the $(\text{-Si-O-})_6$ macroring of the silicate side by hydrogen bonding. In contrast, IR data for the Kao-EG 10.8 Å phase suggests that EG is loosely intercalated, held in place by hydrogen bonding with the kaolinite host. It is much more disordered compared to Kao-EG 9.4 Å.

3.2.2.4 NMR Analysis

Figure **3.8** shows the ^{13}C CP/MAS and DD/MAS NMR spectra of Kao-EG 9.4 Å (**3-2-1**) taken at 75.37 MHz. A relatively broad signal ($v_{1/2}$= 190 Hz) is observed at 64 ppm. No other ^{13}C resonances were detected due to residual interlayer DMSO (^{13}C methyl

resonance expected near 40 ppm) or polyethylene glycol oligomerization products (^{13}C ether resonance expected near 70 ppm). The dipolar dephasing experiment eliminates almost completely the signal, showing the presence of very rigid organic units.

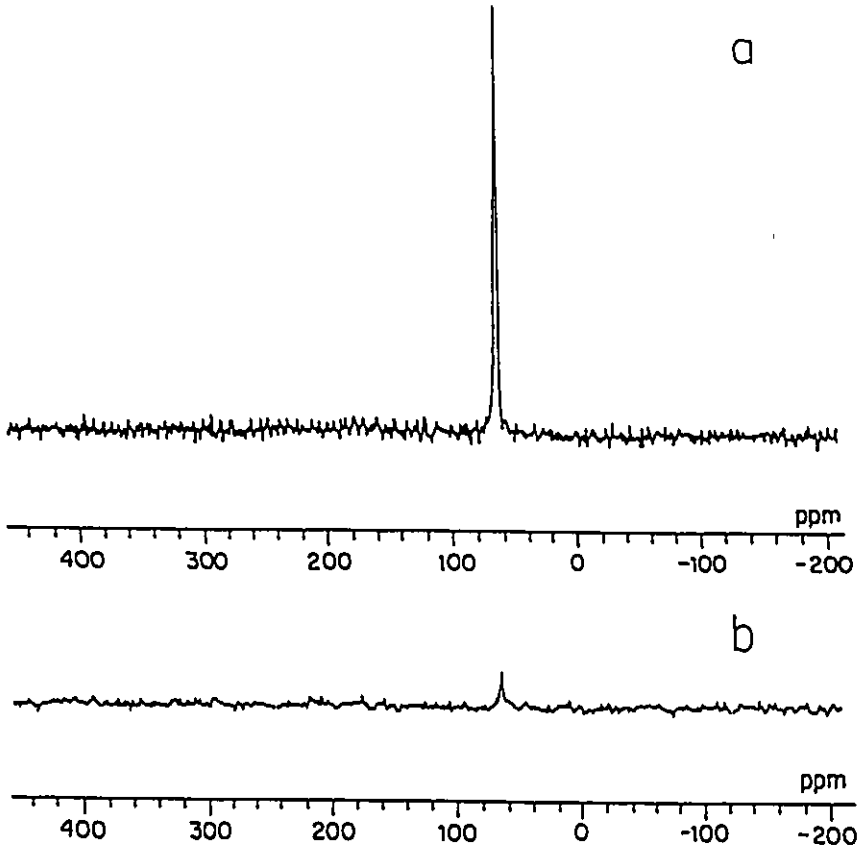

Figure 3.8: ^{13}C CP/MAS spectra of the product Kao-EG 9.4 Å (3-2-1): (a) without dipolar dephasing; (b) with 40 μs dipolar dephasing. These spectra were taken on a Chemagnetics CMX-300 with a spinning rate of 7 KHz at a frequency of 75.4 MHz.

A comparison of the ^{13}C CP/MAS and DD/MAS NMR of both Kao-EG 9.4 Å (3-2-1) and Kao-EG 10.8 Å (3-2-5) performed under identical conditions at lower frequency (50.32 MHz) was made. The results are summarized in Table 3.2. Both Kao-EG 9.4 Å and Kao-EG 10.8 Å were found to have a chemical shift of about 65 ppm. This compares to a chemical shift of 62.2 ppm for aqueous ethylene glycol. The linewidths for these resonances are markedly different, with Kao-EG 9.4 Å exhibiting a linewidth of 120 Hz and that of Kao-EG 10.8 Å, 55 Hz. Motional averaging is thought to be responsible for the decreased linewidth in the case of Kao-EG 10.8 Å. This observation was supported by the DD/MAS experiment which showed that after 40 μs of dephasing, I_{DD}/I_o for Kao-EG 9.4 Å was only about 0.24, whereas for Kao-EG 10.8 Å, this was found to be 0.61. This confirms that the EG unit in Kao-EG 9.4 Å is much more rigid than the EG unit in Kao-EG 10.8 Å and supports the

Product	$\delta^{13}C$	$\nu_{1/2}$	I_{DD}/I_o
	ppm	Hz	
Kao-EG 10.8 Å	65	55	0.61
Kao-EG 9.4 Å	65	120	0.24

Table 3.2: ^{13}C CP/MAS and DD/CPMAS results for Kao-EG 9.4 Å (3-2-1) and Kao-EG 10.8 Å (3-2-5). Spectra were performed on a Bruker MSL-200 at ^{13}C frequency of 50.29 MHz; spinning rate= 4 KHz. Dipolar dephasing time was 40 μs.

hypothesis that Kao-EG 9.4 Å is an ≡Al-O-CH_2CH_2OH grafted phase whereas Kao-EG 10.8 Å it is an the intercalated phase.

Only one relatively broad signal could be observed on the ^{13}C CP/MAS NMR spectrum of Kao-EG 9.4 Å (Figure **3.8**). This is in apparent contradiction with what is expected on the basis of the proposed model (Figure **3.1**), where the two carbons of the grafted ethylene glycol units should be inequivalent. Similarly, Inoue *et al* [154] have shown that the products obtained by the reaction of $Al(OPr^i)_3$, in which the diol units were proposed to be attached via Al-O-C bonds on one end only, all exhibit single ^{13}C resonances around 60 ppm. These data show that the effects on the ^{13}C NMR chemical shifts of an aluminate (^{13}C-O-Al) or of a hydroxyl (^{13}C-O-H) substituent are unfortunately very similar (see Section **2.2.1.4**).

So, while the ^{13}C NMR spectra shows unambiguously the complete replacement of DMSO molecules by ethylene glycol, as well as the absence of any oligomerization or polymerization products (see Chapter **4**), it does not provide definite evidence for the formation of an Al-O-C linkage.

The ^{29}Si MAS NMR spectrum (at 35.76 MHz) of kaolinite and of Kao-EG 9.4 Å show single resonances centered at -91.3 ppm and -92.6 ppm respectively (see Table **2.4**). These data, characteristic of the Q3(OAl) kaolinite structure [172,180] are in accord with other organokaolinites [181]. The 1.3 ppm upfield shift is in agreement with a perturbation of the H-bond network in the interlamellar region, with no major structural change in the tetrahedral silicate sheet.

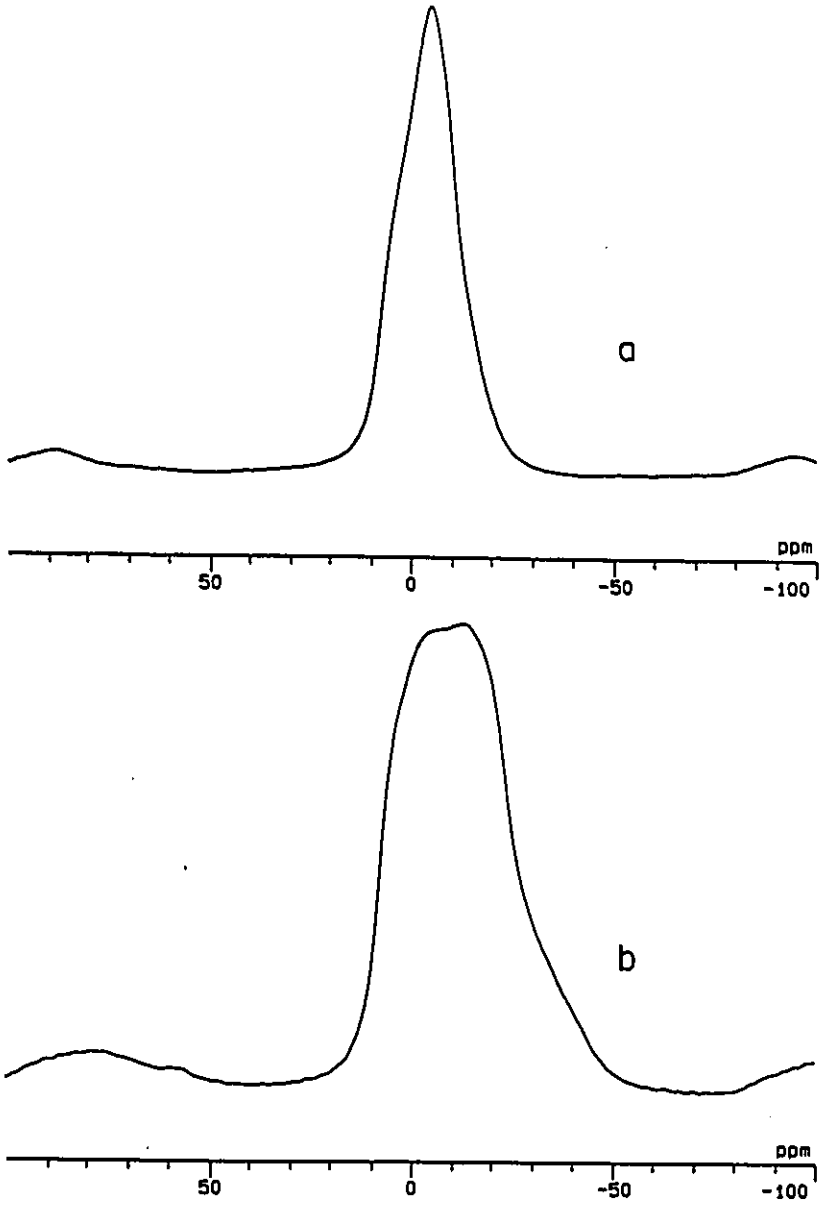

Figure 3.9: ^{27}Al MAS NMR spectra (Chemagnetics CMX-300, 78.1 MHz, spinning rate 7 KHz) of: (a) Kaolinite 7.2 Å; (b) Kao-EG 9.4 Å (3-2-1).

In contrast with the ^{29}Si MAS NMR results, were the ^{27}Al MAS NMR results (Figure **3.9**). The ^{27}Al resonance of kaolinite (at 78.1 MHz) is at -3 ppm, characteristic of the Al octahedral coordination [172,182]. The spectrum of Kao-EG 9.4 Å, centered at -8 ppm was strongly broadened. This broadening was smaller on lower field spectra (46.86 MHz), which rules out an interpretation of the 78.1 MHz spectrum broadening based on an increase of the second order quadrupolar interactions. Rather, the spectrum could be interpreted as the result of an increase of the chemical shift dispersion, showing the superposition of a higher field resonance on the signal of residual Al-OH units. This is in agreement with the grafting of EG units on the aluminum hydroxide sheet, to form Al-O-C bonds.

3.2.3 Chemical Stability of Kao-EG 9.4 Å

The Kao-EG 9.4 Å phase was found to be remarkably resistant to decomposition by solvent leaching. This was the case for both water and organic solvents. A number of attempts were made to open up the interlayers of Kao-EG 9.4 Å by exposing Kao-EG 9.4 Å to organic solvents at room temperature and in refluxing conditions (Section **6.6.3.1**). The room temperature exposure (14 days) of Kao-EG 9.4 Å to DMSO, ethyl acetate, 1,4 dioxane, methanol, hexane and acetic acid had no effect whatsoever on the product indicating that no swelling of the layers had occurred. Likewise, refluxing Kao-EG 9.4 Å in toluene and 1,2-dimethoxyethane had no effect on Kao-EG 9.4 Å. Even refluxing Kao-EG 9.4 Å in a 90:10 mixture of ethylene glycol:water for 16 hours was unable to cause significant

decomposition or expansion of the Kao-EG 9.4 Å phase to yield either the Kao-EG 10.8 Å phase or the 7.2 Å collapsed kaolinite phase.

A refluxing mixture of approximately 5% water in DMSO was however able to cause decomposition of the Kao-EG 9.4 Å phase (Section **6.6.3.2**). This mixture could hydrolyse and displace the interlamellar ethylene glycol units to yield as the main phase the 11.2 Å Kao-DMSO phase as well as residual Kao-EG 9.4 Å and 7.2 Å kaolinite.

One of the most interesting features of Kao-EG 9.4 Å is its remarkable resistance to hydrolysis. One would normally expect a surface ether linkage to be susceptible to water hydrolysis. This is apparently not the case, since it was found that even upon refluxing Kao-EG 9.4 Å (**3-2-1**) in water for twenty hours, almost no decomposition of the Kao-EG 9.4 Å phase could be detected as judged by comparing the O-H stretching region of the infrared spectra before and after refluxing in water (Section **6.6.5.1**). Washing Kao-EG 9.4 Å in D_2O for three days (Section **6.6.5.2**) showed only very slight evidence of deuterium exchange for the hydroxyl groups. Very weak (vw) or extremely weak (vvw) infrared O-D bands could be observed at 2755 cm^{-1} (vvw), 2735 cm^{-1} (vvw), 2707 cm^{-1} (vw), 2675 cm^{-1} (vw), 2637 cm^{-1} (vw) and 2519 cm^{-1} (vw). This indicates that most of the interlayer hydroxyl groups are inaccessible to water molecules under ambient conditions. When this same deuteration experiment was performed on Kao-EG 10.8 Å (products **3-1-2** and **3-2-4**) it was found that structural collapse back down to kaolinite occurred after heating, and significant deuteration of the hydroxyls in kaolinite had taken place, judging by the intensities of the O-D stretching bands at 2728 cm^{-1} and 2674 cm^{-1} (Sections **6.6.1.2** and **6.6.2.4**).

Using more drastic conditions, namely reacting the product with water in an autoclave at 200°C for 72 hours (Section **6.6.5.3**), a partial decomposition could be observed. The recovered solid phase consisted of a mixture of kaolinite and of the starting material. The solution (supernatant), contained only ethylene glycol as organic material. One could not detect by ^{13}C NMR any trace of other organic material. This result rules out the possibility of the formation and the presence of oligoethyleneglycols or of polyethyleneglycol in the interlayer spaces of kaolinite.

It appears that upon formation of the Kao-EG 9.4 Å phase, the interlamellar spaces of this organokaolinite become relatively inaccessible to water and thus water hydrolysis. Hydrolysis may occur only by using extreme reaction conditions such as reacting with water at 200 °C, or by refluxing in a 95:5 mixture of DMSO:H_2O. This is reasonable if one considers that in kaolinite itself, the interlayers are also inaccessible to water due to the strong interlayer cohesive forces (Section **1.3.2**). For example, no deuteration of the interlayer hydroxyl groups occur at room temperature in kaolinite even upon prolonged exposure to D_2O [183].

For Kao-EG 9.4 Å it was proposed that one end of the ethylene glycol was grafted onto the aluminate hydroxyl surface via an Al-O-C linkage, whereas the other hydroxyl end was keyed into the $(\text{-Si-O-})_6$ macroring, with the alcohol group being hydrogen bonded to the six basal oxygens which make up the macroring. Based of the calculated chemical formula for Kao-EG 9.4 Å of $Al_2Si_2O_5(OH)_{3.2}(OCH_2CH_2OH)_{0.8}$, one would expect 0.8 EG units per macroring, and on this basis, one expects very strong cohesive forces caused by the hydrogen bonding between the oxygens of the macroring and the free alcohol group of

the EG unit. For this reason, the interlayers would become inaccessible to water and other solvents.

3.2.4 Formation of an 8.4 Å Hydrate from Kao-EG 10.8 Å

3.2.4.1 Introduction

Interlayer water in the kaolin minerals has attracted considerable attention over the years [10]. Halloysite is known to readily intercalate water to yield a 10 Å hydrated phase and an 8.35 Å hydrate of nacrite has been prepared by first intercalating with potassium acetate and then washing with water [184]. Kaolinite does not naturally exist in a hydrated form, and hydrates that may be formed by displacing a previously intercalated species by washing with water are not stable and quickly decompose.

Costanzo and coworkers have prepared various synthetic hydrates of kaolinite by first treating the Kao-DMSO intercalate with ammonium fluoride to exchange some of the interlamellar hydroxyl groups with fluoride and then washing with water [65-68]. They succeeded in forming both 8.4 Å and 8.6 Å monohydrates of kaolinite as well as two types of 10 Å dihydrates. The stable 8.4 Å hydrate could only be formed if 20 % or more of the surface hydroxyls could be replaced with fluorine. The water molecule in the 8.4 Å hydrate was found to be keyed into the silicate sheet and was termed "hole water". Water in the 10 Å hydrate was found in both the "hole" environment and the more weakly bound "associated" environment.

3.2.4.2 Preparation and XRD Characterization

The preparation of an 8.4 Å hydrate from Kao-EG 10.8 Å (**3-1-1**) by washing with water at room temperature is described in Section **6.6.6**. It should be noted that in some instances washing Kao-EG 10.8 Å with water yielded only a collapsed kaolinite characterized by a broad basal spacing ranging from 7.2-7.3 Å. It is not clear which factors govern the formation of an 8.4 Å hydrate of kaolinite or the collapsed 7.2 Å kaolinite, although it may have to do with slight variations in both the Kao-EG 10.8 Å product and the water washing methods. It is reasonable to assume that in order for the intercalated EG molecules to be displaced by water molecules, diffusion of EG molecules out of the interlayer spaces of kaolinite should not be significantly greater than the diffusion of water molecules into the interlayer spaces. If these diffusion rates are not properly matched, it is possible that irreversible collapse of the kaolinite layers may occur before water molecules are able to displace the intercalated EG molecules. In the following discussion only the displacement of EG by H_2O to yield an 8.4 Å hydrate of kaolinite will be considered.

The XRD (2-70 °2Θ) patterns of kaolinite, Kao-EG 10.8 Å and the Kao-H_2O 8.4 Å (EG) product are shown in Figure **3.10**. Upon water washing of Kao-EG 10.8 Å, the structure collapsed to form an 8.4 Å hydrate of kaolinite (Kao-H_2O 8.4 Å (EG)). This can be observed in Figure **3.10 c**, where the d_{001} peak of Kao-EG 10.8 Å (Figure **3.10 b**) is replaced by an asymmetric peak at d= 8.38 Å. In all cases the peak at d= 7.12 Å due to the unexpanded kaolinite remains unchanged. The 8.4 Å hydrated phase was quite stable

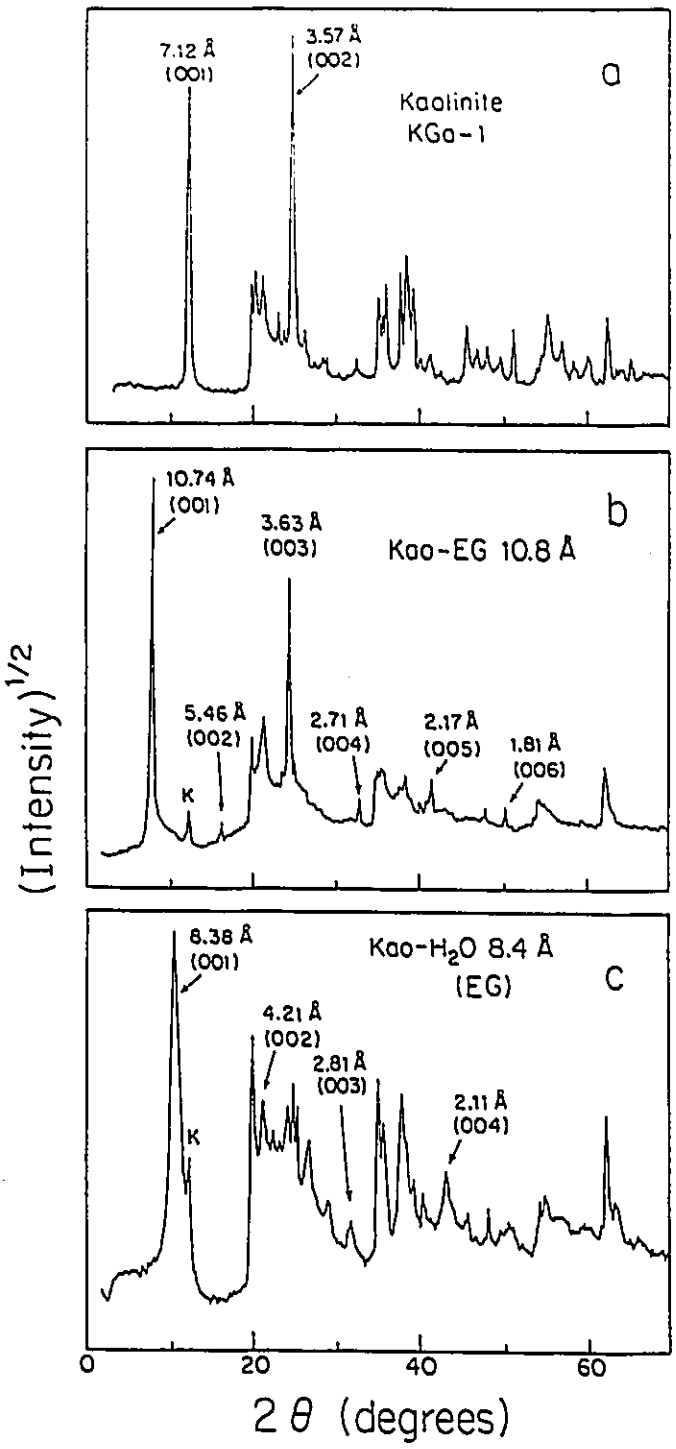

Figure 3.10: XRD pattern (2°-70° 2Θ) of: **(a)** Kaolinite 7.2 Å **(b)** Kao-EG 10.8 Å before water washing **(c)** Kao-H_2O 8.4 Å (EG). (K = d_{001} peak due to residual kaolinite)

since even after one day standing in air, it was found that decomposition of the hydrate had not occurred and the XRD pattern remained unchanged.

The XRD pattern (2-70 °2Θ) showed that the 8.4 Å hydrate was the principal phase with an intercalation ratio of 86 % based on the relative intensities of the d_{001} peaks of the hydrated (d= 8.38 Å) and dehydrated (d= 7.12 Å) kaolinite. Reflections corresponding to what are likely the d_{002}, d_{003} and d_{004} peaks of 8.4 Å hydrate were also observed. The relative broadness of these peaks suggest that this 8.4 Å hydrate is not as ordered as the 8.4 Å

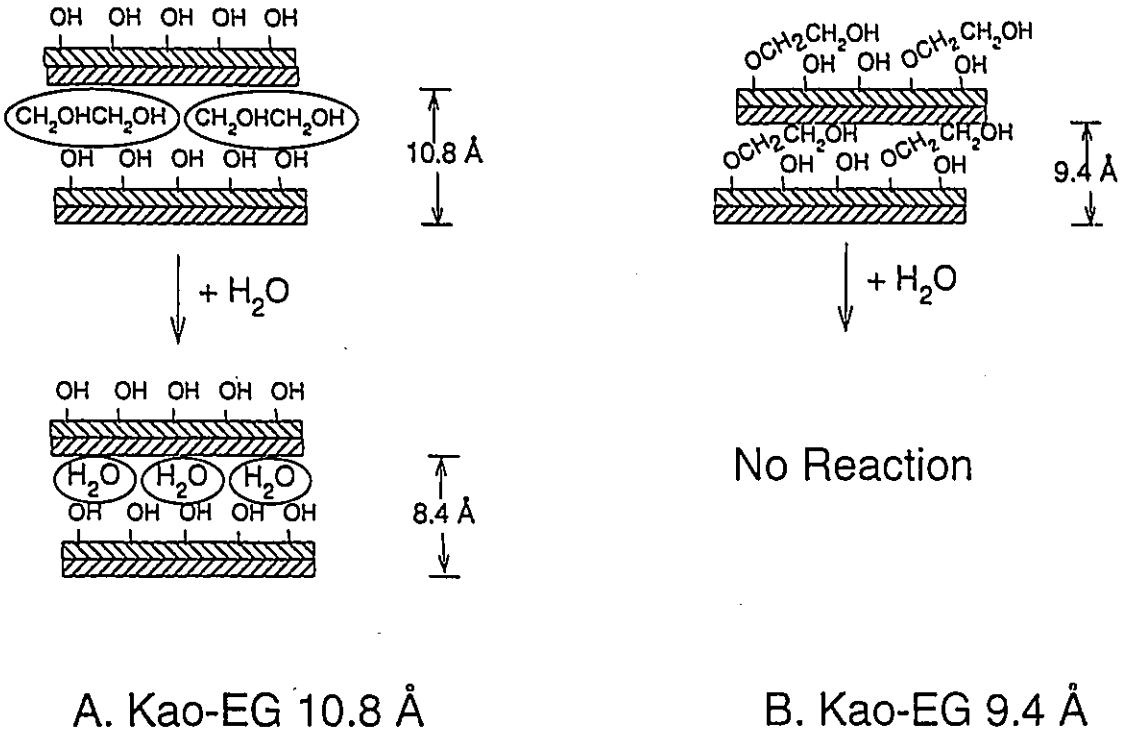

Figure 3.11: Diagrammatic representation of the effects of water washing on Kao-EG 10.8 Å compared to Kao-EG 9.4 Å.

partially fluorinated hydrate of kaolinite (Kao(F)-H_2O 8.4 Å) [68]. In addition, the intensities of the peaks generated by the Kao(F)-H_2O 8.4 Å appear to be significantly different from those seen for Kao-H_2O 8.4 Å (EG) hydrate (Figure **3.10 c**), suggesting that some structural differences exist between the two types of 8.4 Å hydrate.

The formation of a stable 8.4 Å hydrate of kaolinite from Kao-EG 10.8 Å contrasts strongly with what was observed for Kao-EG 9.4 Å. This situation is illustrated diagrammatically in Figure **3.11**. These observations are in accord with Kao-EG 10.8 Å being an EG intercalated phase, and Kao-EG 9.4 Å being a grafted phase, whose layers are sealed shut to water under ambient conditions (much like kaolinite itself).

3.2.4.3 TGA Analysis

TGA/DSC results for Kao-H_2O 8.4 Å (EG) showed a slow, weakly endothermic 4% weight loss due to the loss of interlayer water and possibly residual ethylene glycol beginning immediately upon heating and finally reaching a plateau near 300 °C (T_{ons} = 78 °C, T_{peak} = 150 °C). There was another much more dramatic endothermic weight loss of 13 % between 400 and 600 °C due to the kaolinite-metakaolinite transition (T_{ons}= 480 °C, T_{peak} = 526 °C). Finally there was an exothermic transition between 980 and 1030 °C (T_{ons}= 998 °C, T_{peak}= 1009 °C) which corresponds to a structural reorganization of metakaolinite. There was no associated weight loss for this last thermal event.

If one assumes that only water occupies the interlayer spaces, and that all the interlayer water was lost in the first endothermic transition, one finds that there are 0.60

water molecules per $Al_2Si_2O_5(OH)_4$ unit. This is slightly less than the 0.78 water molecules per $Al_2Si_2O_5(OH)_4$ unit that Wada found for the 8.4 Å hydrate of nacrite [184].

3.2.4.4 IR Analysis

The IR spectra of the O-H and C-H stretching region of the Kao-EG 10.8 Å phase both before and after water washing supported the XRD results that an ordered hydrate had been formed. Figure **3.12 a** shows the characteristic O-H stretching region of well-crystallized kaolinite KGa-1. Upon formation of Kao-EG 10.8 Å one observes the pattern shown in Figure **3.12 b**. The O-H stretching pattern has changed due to intercalation of ethylene glycol, and an ill defined C-H stretching pattern due to the intercalated ethylene glycol units appear. Upon washing with water, one sees the appearance of an O-H stretching band at 3550 cm^{-1} (Figures **3.12 c, d**), as well as the water deformation vibration near 1655 cm^{-1} (not shown). In some instances, a sharp peak at 3599 cm^{-1} is also observed for Kao-H_2O 8.4 Å (EG) (Figure **3.12 d**). The difference between the spectra in Figures **3.12 c** and **3.12 d** could plausibly be due to some heterogeneity in the bulk sample. This inhomogeneity could not be detected by XRD analysis, which showed that different samples taken from the bulk material yielded nearly identical XRD patterns, showing as the principal phase Kao-H_2O 8.4 Å (EG).

The IR spectra of Kao-H_2O 8.4 Å (EG) (Figures **3.12 c, d**) appeared very different than the IR spectra shown for Kao(F)-H_2O 8.4 Å [68]. Costanzo and Giese found that the O-H stretching band at 3620 cm^{-1} due to the inner O-H of kaolinite was red-shifted to 3612 cm^{-1}

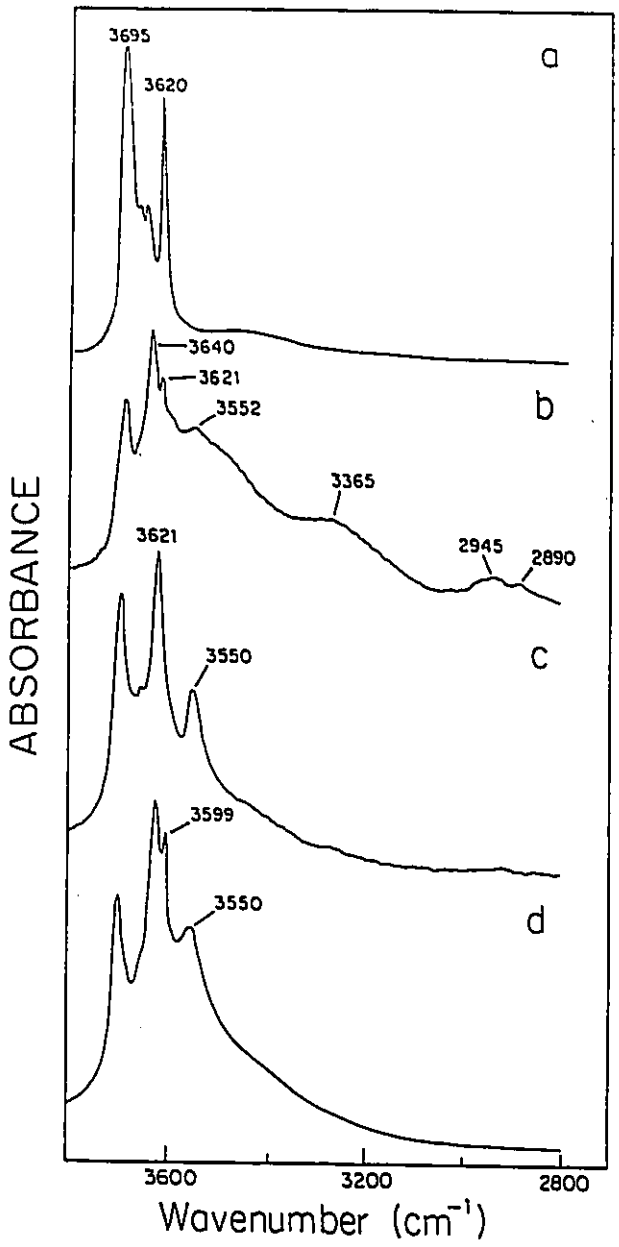

Figure 3.12: Infrared spectra (3800-2800 cm^{-1}) of: (a) Kaolinite 7.2 Å (b) Kao-EG 10.8 Å; (c,d) Kao-H_2O 8.4 Å (EG) (FTIR spectra of two samples taken from the same bulk product). Note: The relative absorbance scales of the spectra have been adjusted in order to facilitate comparison.

for the Kao(F)-H_2O 8.4 Å. They also observed a moderately intense band at 3655 cm^{-1} and a sharp peak due to the deformation vibration of water at 1580 cm^{-1}. These bands were not observed for the 8.4 Å hydrate formed from Kao-EG 10.8 Å. This supports the XRD data in showing that there are significant differences between these two types of 8.4 Å hydrates. This appears to relate to differences in their interlayer bonding schemes, as exhibited by their different infrared spectra.

The local environment of the intercalated water in Kao-H_2O 8.4 Å (EG) may resemble more closely that of the 8.4 Å hydrate of nacrite [184], where in both cases fairly sharp absorptions at 1655 cm^{-1} due to the deformation of water molecules could be observed. In contrast, the deformation band of water adsorbed on the external surface of kaolinite is normally at 1630 cm^{-1}. Wada noted that for water dissolved in various solvents, "its deformation band shifts progressively upward as the base strength of the solvent increases".

This absorption band appeared much sharper when the O-H stretching band at 3599 cm^{-1} could not be observed as was the case in Figure **3.12 c**. When the band at 3599 cm^{-1} could be observed (Figure **3.12 d**), the H-O-H deformation band was much broader and slightly lower in energy (1647 cm^{-1}). Also associated with the appearance of this 3599 cm^{-1} band, was a sharp band at 968 cm^{-1} in place of the band at 940 cm^{-1} normally attributed to the Al-O-H deformation of the inner surface hydroxyl groups of kaolinite [25]. This would seem to indicate strong interaction between intercalated water and the aluminate surface of kaolinite. In contrast, the Al-O-H deformation due to the inner O-H group of kaolinite (914 cm^{-1}) regardless of the presence (Figure **3.12 d**) or absence (Figure **3.12 c**) of a band at 3599

cm^{-1} was perturbed only very slightly to 910 cm^{-1}. Wada also noticed a shift from 935 cm^{-1} to 970 cm^{-1} upon going from nacrite to the 8.4 Å hydrated nacrite [184].

3.3 Conclusions

Two types of ethylene glycol organokaolinites could be prepared by refluxing the kaolinite-DMSO intercalate in ethylene glycol:water solutions. It was found that the concentration of water in the ethylene glycol reaction media played a crucial role in governing which of the two phases predominated. Water favours Kao-EG 10.8 Å formation, while anhydrous conditions favour the formation of Kao-EG 9.4 Å.

These two phases were characterized by FTIR, TGA/DSC and X-Ray techniques. The Kao-EG 9.4 Å phase was characterized by a d_{001} of 9.4 Å, is resistant to decomposition by hydrolysis in pure water and ethylene glycol:water (90:10). It is hypothesized that Kao-EG 10.8 Å is the true ethylene glycol intercalated phase, while Kao-EG 9.4 Å is a grafted phase resulting from the product of the condensation reaction between an aluminol group on the interlamellar surface of kaolinite and the alcohol group of ethylene glycol. Ethylene glycol units are attached to the interlamellar surface of kaolinite via Al-O-C bonds.

By washing Kao-EG 10.8 Å with water, it was possible to prepare an 8.4 Å hydrate of kaolinite. The product exhibited well defined IR and XRD patterns. This material began decomposition upon heating but the interlayer water was not fully removed until above 200°C.

Chapter 4

New Oxyethylene Based Organokaolinite Intercalation Compounds

4.1 Introduction

Molecules such as crown ethers and polyethylene oxide (PEO) are well-known for their alkali and alkaline cation complexing abilities. PEO readily complexes with inorganic alkali and alkaline salts to form solid state polymer-salt complexes at room temperature and has been extensively studied for its potential as a solid electrolyte material for use in solid-state batteries and electrochromics [185,186]. PEO and simple crown ethers such as 18-Crown-6 and 15-Crown-5, can be thought of as assemblies of oxyethylene ($-CH_2CH_2O-$) units (OEU) which are formed from the condensation of ethylene glycol (EG) monomers.

Over the last few years, there has been considerable interest in the intercalation of PEO in layered structures [110,115-118,120,187-192]. The two dimensional confinement of PEO in an inorganic lattice can lead to certain desirable anisotropic ionic conduction properties. Some of the layered materials which have been intercalated with PEO, or its smaller molecular weight analogue, polyethylene glycol (PEG), include zirconium phosphate [191,192], V_2O_5 [193], MPS_3 (M=Mn,Cd) [189], MoS_2 [190], and smectite clays [115-118,187,188]. The conformations that the PEO adopts in the confined spaces of these inorganic matrices are quite variable. For example PEO intercalated in V_2O_5 is thought to be in a straight chain conformation [193], whereas in MPS_3 [189] and MoS_2 [190], the PEO chains are thought to adopt a bilayer

arrangement. Finally, in some smectite clays, the PEO was hypothesized to form helices, in which the interlayer cation is found within the helix [118].

The orientation of crown ethers within the interlayers of smectites was also found to be variable. Depending on the crown ether itself, the type of interlayer cation, and the charge density of the smectite, the crown ether could adopt monolayer or bilayer orientations which were either parallel or tilted with respect to the clay layers [194].

The preparation of two dimensional inorganic-polymer nanocomposites generally involves either polymer intercalation from solution or intercalation of a suitable monomer and its subsequent polymerization. A research group at Toyota for example, has prepared a number of nanoscale polymer-clay hybrid composites using these techniques [113,195-197]. Many of these composite hybrids were found to exhibit much improved mechanical and thermal properties. Recently workers have started looking at alternate preparation methods, where the polymer is inserted directly into the layered material without the use of a solvent. Giannelis and coworkers have prepared a series of two-dimensional nanostructures based on the direct polymer melt intercalation of organically modified smectites [115]. A PEO-smectite nanocomposite with an identical XRD pattern to the PEO-smectite materials prepared via the solution intercalation method [118] was one of the materials prepared.

The direct incorporation of PEO or any other polymer into the structure of kaolinite has never been reported in the literature. Sugahara *et al* have nonetheless succeeded in preparing kaolinite-polyacrylonitrile [73] and kaolinite-polyacrylamide [72] nanocomposites by first intercalating the appropriate monomer into the interlayers and then inducing polymerization by thermal treatment.

For kaolinite, it has been shown that it is possible to prepare two distinct ethylene glycol phases of kaolinite, Kao-EG 9.4 Å and Kao-EG 10.8 Å (see Chapter 3). The Kao-EG 10.8 Å phase was believed to be the more weakly bound intercalated phase. A polytype of kaolinite, halloysite, was also reported to intercalate not only EG but also diethylene glycol (DiEG) and triethylene glycol (TriEG) [34]. From these data, it was logical to assume that larger molecules based on the oxyethylene unit, of which EG was the simplest unit, may also intercalate into the structure of kaolinite. With this idea in mind, it was attempted to intercalate successively larger oxyethylene based molecules into kaolinite. In this chapter, the preparation and characterization of a series of new oxyethyelene based organokaolinites is reported, including the preparation of kaolinite-PEG 3400, which is the first example of the direct intercalation of a polymer into kaolinite.

4.2 Results and Discussion

4.2.1 Preparation

The organoclays were typically prepared by first preparing the DMSO or NMF intercalate of kaolinite (see section **6.4**) and then reacting this directly with the oxyethylene species. Typically, 1-2 grams of either Kao-DMSO or Kao-NMF intercalate were mixed with an excess of the organic reagent. This was done directly in the melt of the appropriate organic reagent, without the use of a solvent. The mixture was maintained at a given temperature for a given period of time followed by the reaction workup. The reaction details

for the individual reactions are given in section **6.7**, and are summarized in Table **4.1**. The product codes and reaction conditions are given along with the interlayer d-spacing, intercalation ratio and calcined weight loss of the products. The interlayer or d-spacings were calculated from the first 5 or 6 (00l) reflections of the principal phase using equation **1.2** (section **1.3.3**).

The interlayer expansion for all these materials was comparable. Basal spacings ranged from a low of 10.85 Å for Kao-EG 10.8 Å to a high of 11.19 Å for Kao-PEG 3400. After subtracting for the 7.14 Å basal spacing of kaolinite, this corresponds to a clearance space of approximately 3.7 Å to 4.1 Å which is roughly what one might expect, based on CPK models for an oxyethylene unit sandwiched between two clay layers. Comparable values for the interlayer expansion of other layered materials due to the monolayer intercalation of molecules based on the oxyethylene unit can be found [34,188,193,198,199]. The XRD pattern of Kao-PEG 3400 (**4-8-A**) from 2 to 70 °2Θ is shown in Figure **4.1** showing 6 (00l) reflections. XRD patterns of the other kaolinite-oxyethylene materials are similar to this, and in all cases at least 4 (00l) reflections could be indexed.

Product		Reaction Conditions					Product Characterization		
Name	Code	Starting Material (S)	Reaction Media (R)	(R)/(S)	T_{rxn}	t_{rxn}	d_{001}[1]	I.R.[2]	Calcination Weight Loss[3]
				g/g	°C	hr	Å		Wt. %
Kao-EG 10.8 Å	4-1-A	Kao-DMSO	EG/H_2O (95/5)	50	185	20	10.85	0.95	-
Kao-DiEG	4-2-A	Kao-DMSO	DiEG	50	245	26	10.86	0.97	26.5
Kao-DiEG	4-2-B	Kao-NMF	DiEG	50	245	26	10.86	0.97	27.7
Kao-TriEG	4-3-A	Kao-DMSO	TriEG	50	285	18	10.93	0.96	29.9
Kao-TriEG	4-3-B	Kao-NMF	TriEG	50	285	18	10.92	0.95	28.2
Kao-TetraEG	4-4-A	Kao-NMF	TetraEG	40	150	48	10.99	0.96	27.3
Kao-15C5	4-5-A	Kao-DMSO	15C5	5	155	45	11.15	0.96	28.4
Kao-18C6	4-6-A	Kao-DMSO	18C6	6	190	16	11.15	0.97	29.6
Kao-PEG 1000	4-7-A	Kao-DMSO	PEG 1000	5	155	216	11.12	0.95	29.1
Kao-PEG 1000	4-7-B	Kao-NMF	PEG 1000	7	var	312	11.01	0.78	23.5
Kao-PEG 1000	4-7-C	Kaolinite	PEG 1000	8	200	144	7.16	0.00	-
Kao-PEG 3400	4-8-A	Kao-DMSO	PEG 3400	5	155	216	11.16	0.96	29.4
Kao-PEG 3400	4-8-B	Kao-DMSO	PEG 3400	4	195	116	11.19	0.97	30.4
Kao-PEG 3400	4-8-C	Kaolinite	PEG 3400	8	200	144	7.16	0.00	-

Table 4.1: Summary of the product codes, reaction conditions and preliminary characterizations for the various oxyethylene based organokaolinites prepared in this study. Reaction details of the various reactions are given in the experimental section. (1) d-spacing; (2) intercalation ratio; (3) based on the weight after calcination in air at 1100 °C; (var) indicates that the temperature was varied during the course of reaction.

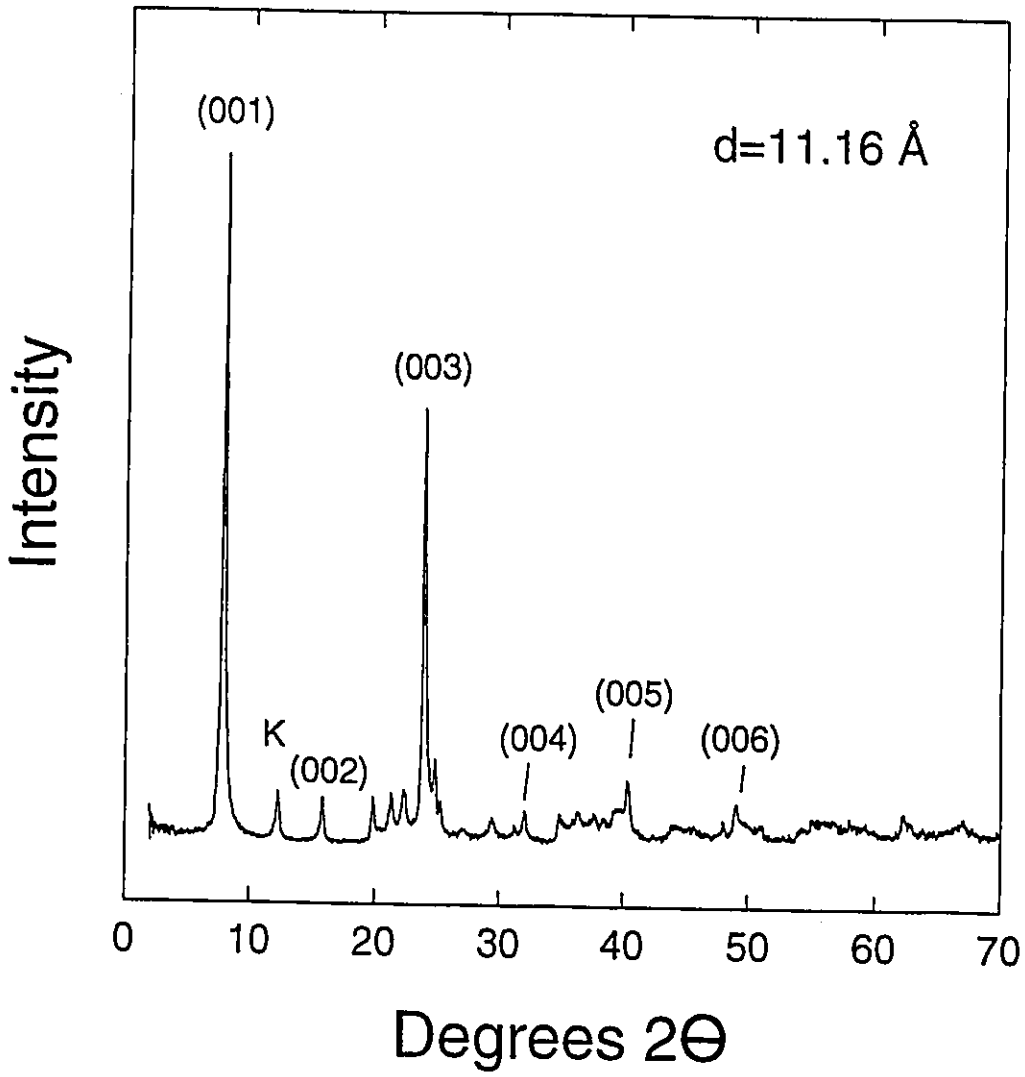

Figure 4.1: XRD pattern (2°-70° 2Θ) of Kao-PEG 3400 (**4-8-A**) dried at 100 °C for 3 hrs. (00l) peaks are indicated along with the residual (001) unexpanded kaolinite peak (K).

4.2.2 Reaction Kinetics

It was decided to do a preliminary kinetic study of the reaction of polyethylene glycol with Kao-DMSO and Kao-NMF mainly in order to obtain an estimate of how long it takes for the completion of the intercalation reactions. Other goals included determining what are the influences of the starting materials (Kao-NMF or Kao-DMSO) on the reaction products and yields, and what are the effect of temperature and polymer size on the reaction rates. This study was qualitative in nature.

The reaction of Kao-DMSO with PEG 3400 at 155 °C (**4-8-A**) was monitored with XRD and FTIR. At selected times during the course of the reaction, small aliquots were removed from the reaction mixture, and worked up by repeatedly washing with methanol followed by centrifugation, and air drying (see section **6.7.8.1** for details). The XRD and IR patterns of these samples were then measured. This was continued until the reaction was judged to be complete.

The change in the XRD patterns (6-18 °2Θ) as a function of reaction time for reaction **4-8-A** is shown in Figure **4.2**. Initially, one observes the XRD pattern of the Kao-DMSO starting material with reflections at d_{001}= 11.2 Å, d_{002}= 5.6 Å and the residual kaolinite (001) peak at d= 7.1 Å. After 1.5 hrs of reaction, the product becomes disordered, with two broad reflections at d= 11.1 Å and d= 8.5 Å along with the residual kaolinite peak at d= 7.1 Å. The (002) peak is barely noticeable at d= 5.6 Å. Upon further reaction, the peak at d= 11.1 Å begins to grow again, to give first an asymmetric peak with a shoulder at d= 9.9 Å, and then finally a well defined peak at d= 11.1 Å. The increase in

intensity of the (002) peak mimics that of the (001) peak. After 21 hrs of reaction time, the reaction appeared to be complete, judging by the XRD pattern.

In contrast, FTIR showed that the reaction was not yet complete. The reaction could also be followed by observing the disappearance of bands associated with intercalated DMSO and the subsequent appearance and evolution of bands associated with the presence of intercalated PEG 3400. The bands which were easiest to monitor were the band at 2927 cm^{-1} ($\nu_{asym.}$(C-H) Kao-PEG 3400) and the band at 3022 cm^{-1} ($\nu_{asym.}$(C-H) of Kao-DMSO). The intensity of the 2927 cm^{-1} band continued to grow slightly after 21 hrs reaction time at the expense of the band at 3022 cm^{-1}. Although no quantitative measurements of the band intensities were made, it was estimated that the reaction was not fully complete until 140 hrs.

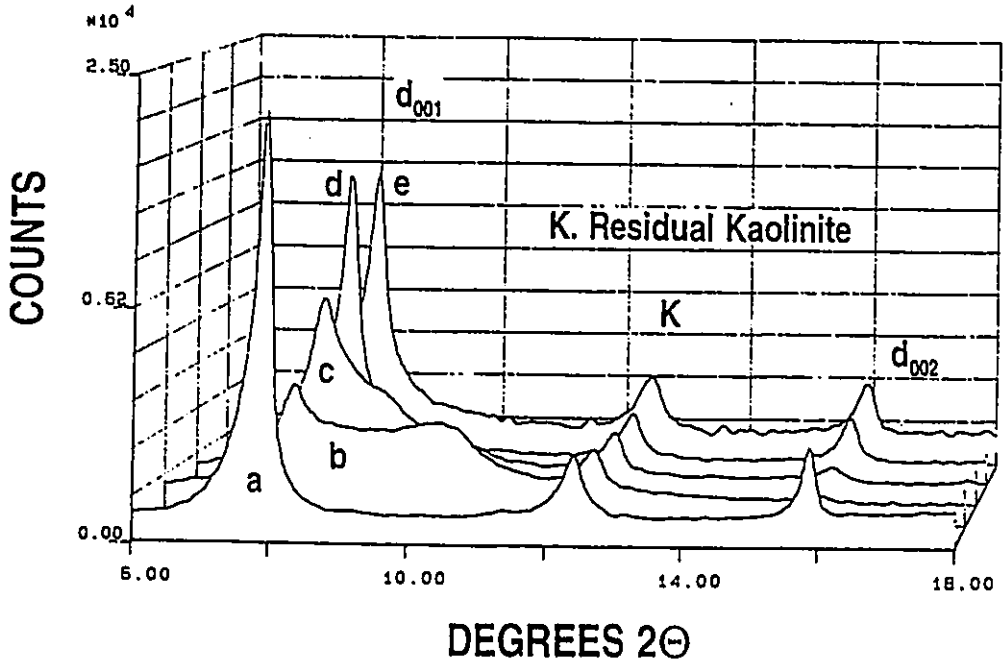

Figure 4.2: Reaction of Kao-DMSO with PEG 3400 at 155 °C (Rxn **4-8-A**) monitored by XRD: Kao-DMSO starting material (**a**); Rxn time = 1.5 hrs (**b**); 5.3 hrs (**c**); 21 hrs (**d**); 141 hrs (**e**).

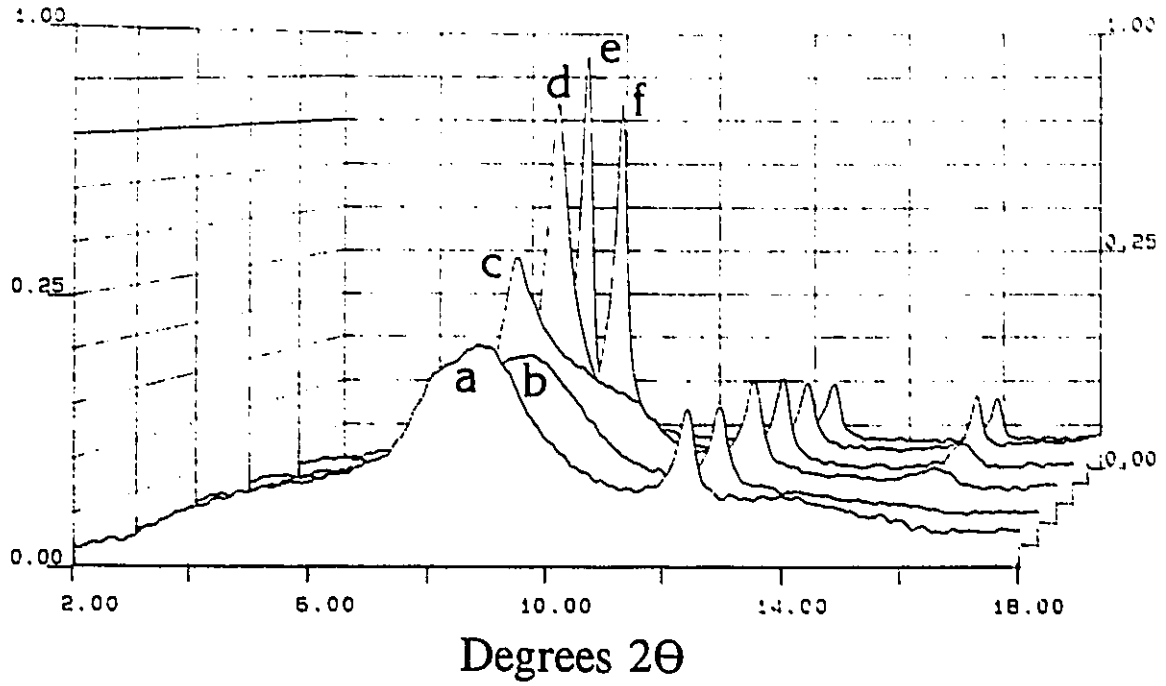

Figure 4.3: Reaction of Kao-DMSO with PEG 3400 at 195 °C (Rxn **4-8-B**) monitored by XRD: Rxn time = 1 hrs (**a**); 4 hrs (**b**); 8 hrs (**c**); 21 hrs (**d**); 45 hrs (**e**); 116 hrs (**f**).

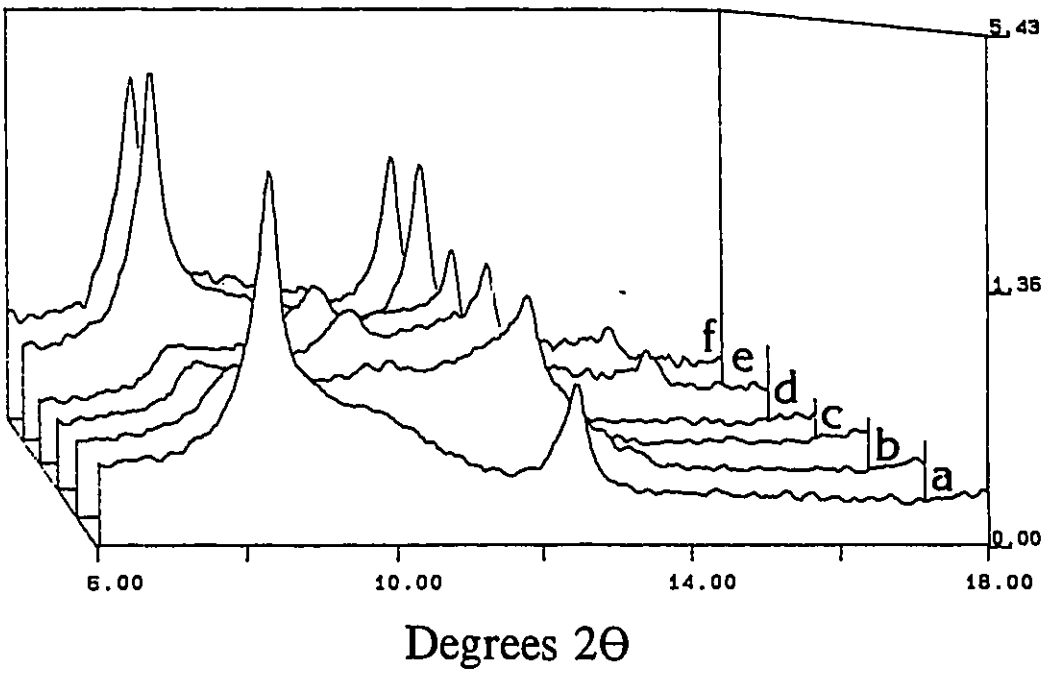

Figure 4.4: Reaction of Kao-NMF with PEG 1000 (Rxn **4-7-B**) monitored by XRD: Kao-NMF starting material (**a**); 2 days reaction at 70 °C (**b**); (**b**) + 4 days at 70 °C (**c**); (**c**) + 2 days ramping up to 130 °C (**d**); (**d**) + 2 days ramping up to 160 °C (**e**); (**e**) + 3 days at 160 °C (**f**).

The reaction of Kao-DMSO with PEG 3400 at 195 °C (**4-8-B**, see section **6.7.8.2**) was carried out in much the same way as for the same reaction at 155 °C (**4-8-A**), only in this case, the ratio of PEG 3400/Kao-DMSO was slightly less (4:1 vs 5:1). The increased reaction temperature did not appear to significantly influence the reaction rate, although this may be due in part to the smaller excess of PEG 3400 used for this reaction. Reaction appeared to be complete by XRD in about 21 hrs, but by FTIR did not appear to be finished until approximately 140 hrs. Once again, in the early stages of reaction (< 10 hrs), one observed a very broad XRD reflection between d= 7.1 Å and d= 11.1 Å (Figure **4.3**).

When Kao-DMSO was reacted with PEG 1000 at 155 °C (**4-7-A**, see section **6.7.7.1**) instead of PEG 3400 at the same temperature (**4-8-A**), a similar XRD reaction profile was observed, only this time the reaction appeared to proceed at a faster rate. Once again, evidence for an intermediate material exhibiting a broad reflection between d= 7.1 Å and d= 11.1 Å was observed (not shown). After 1.5 hrs of reaction time, this was evident in the form of an asymmetric peak at d= 11.1 Å with two overlapping shoulders at d= 10.0 Å and d= 8.7 Å. It appeared that the initial reaction stage where a more pronounced intermediate reflection might have been observed occurred before 1.5 hrs and was missed. In contrast to the reaction with PEG 3400 (**4-8-A**), this reaction appeared to be practically complete after 5.3 hrs, judging by the reemergence of an intense reflection at d= 11.1 Å. IR also indicated that the reaction with the smaller PEG 1000 occurred more rapidly than with PEG 3400. This is in accord with what one might intuitively expect on the basis of the relative sizes of PEG 3400 and PEG 1000 and the influence this would have on interlamellar diffusion.

It was attempted to prepare Kao-PEG 1000 and Kao-PEG 3400 using Kao-NMF as the starting material instead of Kao-DMSO. Several attempts failed, presumably due to the fact that the Kao-NMF structure collapsed before intercalation by PEG could occur. Partial success was achieved for the preparation of Kao-PEG 1000 only when the reaction temperature was slowly ramped up, so as to prevent the premature structural collapse of the starting material, thus allowing the replacement of NMF with PEG 1000 to occur in the interlayers.

The XRD reaction profile for Reaction **4-7-B** (section **6.7.7.2**) is shown at various reaction stages in Figure **4.4**. The Kao-NMF starting material which is characterized by a basal spacing of d= 10.8 Å, becomes disordered and once again we observe an intermediate reflection between d= 10.8 Å and d= 7.14 Å at about d= 8.6 Å, followed by the emergence of a peak at d= 11.0 Å corresponding to the formation of Kao-PEG 1000 product. IR confirmed the gradual interlayer displacement of NMF by PEG 1000. The final product showed traces of residual NMF in the interlayers, seen as very weak bands at 3418 cm^{-1} (ν(N-H)) and at 1660-1680 cm^{-1} (amide ν(C=O)). The intercalation ratio (I.R.) of the final product (I.R.= 0.78) proved to be much less than that which was obtained starting from Kao-DMSO (I.R.= 0.95). FTIR analysis of the final product also supported the XRD results that less PEG 1000 intercalation had occurred. This was evident in the O-H stretching region especially, which showed a pattern intermediate between that of kaolinite and that of Kao-PEG 1000 (**4-7-A**). Specifically, the band at 3695 cm^{-1}, which generally decreases in intensity upon interlamellar modification, was greater in intensity for the Kao-PEG 1000 product starting from Kao-NMF than for the product obtained using Kao-DMSO as the

starting material. The weight loss upon calcination (23.5 %) also confirmed that much less intercalation has occurred than for the reaction using Kao-DMSO as the starting material (29.1 %).

The most striking feature of the XRD kinetic profiles (Figures **4.2-4.4**) was the appearance of a broad reflection at about d= 8.5 Å. This is somewhat unexpected since both the Kao-DMSO starting material and the Kao-PEG 3400 final product have nearly identical d-spacings of d= 11.1-11.2 Å. If the reaction mechanism simply involved the displacement of DMSO molecules for PEG molecules, all the while maintaining the same d-spacing, one would expect to see relatively little change in the XRD patterns during the course of reaction. And if the displacement of DMSO by PEG were to occur by a mechanism whereby the PEG molecules first enter the interlayers and further expand the clay layers to higher d-spacings, and the DMSO molecules then diffuse out of the interlayers, one would expect to see a broad reflection at a d-value greater than 11.1 Å.

Alternately, if DMSO molecules were to begin to deintercalate before significant amounts of PEG could enter into the interlayers, one might expect to see some indication of the partial collapse of the structure. If this were the case, one should observe a broad reflection intermediate between the 11.1 Å d-spacing of both starting material and final product and the 7.14 Å d-spacing of fully collapsed kaolinite. Indeed, this is what is observed. Since it was shown that the direct reaction between kaolinite and PEG 1000 or PEG 3400 does not occur, even at high temperatures (**4-7-C** and **4-8-C**), it can be assumed that during the course of the reaction of Kao-DMSO and Kao-NMF with PEG, complete

structural collapse cannot occur or the reaction will no longer proceed. This is apparently what happened to some extent, for the reaction using Kao-NMF as the starting material.

To account for the broad intermediate reflection that is observed, it is thus necessary to invoke another mechanism than the simple interlayering between a fully expanded phase at 11.1 Å and a fully collapsed phase at 7.14 Å. It is conceivable that in the early stages of reaction, one observes instead, the interlayering between the starting material or the final product (which have similar d-spacings) and a "partially" collapsed kaolinite. It can be hypothesized that this intermediate material may consist of wedged shaped layers mixed with fully expanded layers. These wedge shaped layers would consist of one end of the clay plate being pried open with PEG and/or DMSO and the other end being shut.

It is believed that during the course of reaction, an equilibrium was established between DMSO and PEG in both the bulk and interlayer environments. Significant amounts of DMSO remained in the interlayers (see section **4.2.4**) partly as a result of the strong affinity which kaolinite has for DMSO. It should be possible to decrease the amount of residual interlayer DMSO by increasing the PEG/Kao-DMSO ratio of the reaction mixture, or even better, by removing DMSO product during the course of reaction by distillation.

It must be noted that these mechanistic insights were dependent on the analysis of samples which were prepared by first quenching the reaction in air at 20 °C, washed with methanol, followed by air drying. This treatment may have had some influence on the nature of the samples. Clearly an *in situ* approach would be invaluable in further exploring the mechanistic details of this interesting intercalative substitution reaction.

4.3.2 IR Analysis

In contrast to XRD, which provides some information regarding the long range ordering of organokaolinites, FTIR spectroscopy provides information about the short range ordering pertaining to the nature of the guest species and any host-guest interaction between kaolinite and the oxyethylene guest species. The analysis is broken down by region of interest.

O-H stretching region (3800-3200 cm^{-1}): Kaolinite is characterized by a diagnostic, signature O-H stretching pattern consisting of four bands at 3694 cm^{-1}, 3669 cm^{-1}, 3653 cm^{-1} and 3621 cm^{-1} (Figure **4.5 a**). The attribution of these bands has been the subject of extensive study [41,177,200-203]. The band at 3621 cm^{-1} has been unambiguously assigned to the stretching frequency of the internal hydroxyl group of kaolinite. This hydroxyl group is believed to be oriented almost parallel to the direction of the (001) layers, pointing in the direction of the unoccupied octahedral hole [24,27]. The inner-surface hydroxyl groups associated with the remaining bands (3694 cm^{-1}, 3669 cm^{-1} and 3653 cm^{-1}) are believed to make an angle of 60-73° with the (001) plane [24].

The inner hydroxyl stretching band at 3621 cm^{-1} is not usually influenced very much by interlamellar modification reactions since it is removed from the interlamellar surface. In contrast, the three inner-surface hydroxyl stretching bands are very much influenced by interlamellar modifications [36,39,47,50,51,61,69,204]. This can be readily observed for Kao-DMSO (Figure **4.5 b**). Here, the band at 3694 cm^{-1} is greatly reduced in intensity and one no longer

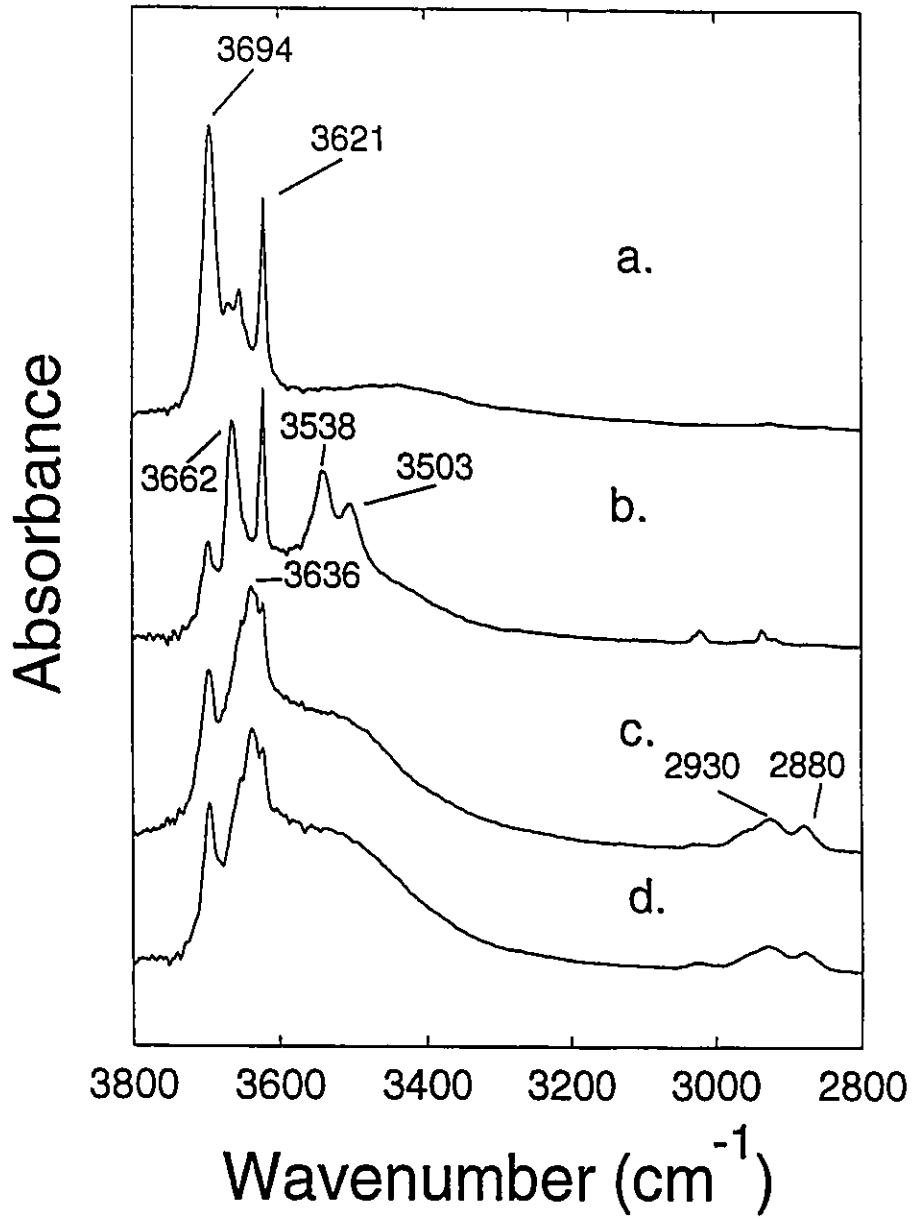

Figure 4.5: FTIR spectra (3800-2800 cm^{-1}) of Kaolinite (**a**); Kao-DMSO (**b**); Kao-PEG 3400 **4-8-A** (**c**); Kao-18C6 **4-6-A** (**d**). Note: The relative absorbance scales of the spectra have been adjusted in order to facilitate comparison.

sees the bands at 3669 cm^{-1} and 3653 cm^{-1}, and in their place one observes a band at 3662 cm^{-1}. Appearing at 3538 cm^{-1} and 3503 cm^{-1} are two new low frequency bands of interlamellar Al-O-H groups hydrogen bonded to the DMSO molecule [39,41].

The O-H stretching patterns of Kao-PEG 3400 (**4-8-A**) and Kao-18C6 (**4-6-A**) can be seen in Figures **4.5 c** and **4.5 d**. It is evident that O-H stretching patterns for Kao-PEG 3400 and Kao-18C6 are very similar to one another, and differ significantly from both kaolinite and Kao-DMSO. This result suggests that the nature of the interaction between the guest 18C6 and PEG 3400 molecules and the kaolinite hydroxyl surface is very similar.

For both Kao-18C6 and Kao-PEG 3400, the band at 3695 cm^{-1} is reduced in intensity with respect to kaolinite but not with respect to Kao-DMSO. There also appears a band at 3636 cm^{-1} along with a broad ill-defined band centered near 3525 cm^{-1}. As always, the band at 3621 cm^{-1} remains unperturbed.

All of the oxyethylene based organokaolinites exhibited similar O-H stretching patterns, except for those of the more hydroxylated oxyethylene based products such as Kao-EG 10.8 Å (**4-1-A**) and Kao-DiEG (**4-2-A, 4-2-B**). Here, one observes an additional lower frequency broad O-H stretching band between 3200 cm^{-1} and 3500 cm^{-1} which is assigned to the hydrogen bonded C-OH groups at the ends of the intercalated ethylene glycol and diethylene glycol molecules. Comparing the relative hydroxylation states of the oxyethylene molecules, Kao-EG 10.8 Å and Kao-DiEG have 2.0 and 1.0 hydroxyl groups per oxyethylene organic unit respectively, whereas Kao-18C6 and Kao-PEG 3400 have 0.0 and 0.03 hydroxyl groups per oxyethylene organic unit. As one might expect on the basis of their intermediate states of hydroxylation, Kao-TriEG and Kao-TetraEG (0.67 and 0.50 hydroxyls

per oxyethylene unit respectively) have O-H stretching patterns which appear to be intermediate between the two hydroxylation extremes.

C-H Stretching Region (2800-3100 cm^{-1}): The C-H stretching region is diagnostic of the incorporation of the oxyethylene-based organic unit. These bands, which are associated with the methylene groups of the oxyethylene molecules are perturbed upon intercalation into the interlayers of kaolinite. Close examination of this region also reveals the presence of residual interlayer DMSO or NMF.

In the case of Kao-EG 10.8 Å, Kao-DiEG, Kao-TriEG and Kao-TetraEG, the intercalated oxyethylene species show distinct asymmetric and symmetric C-H stretching bands at about 2940 cm^{-1} and 2880 cm^{-1} respectively. These frequencies are slightly higher than those of the corresponding bands for the neat liquids (approximately 10-20 cm^{-1} higher).

For Kao-PEG 1000, Kao-PEG 3400, Kao-15C5 and Kao-18C6, the C-H stretching bands are remarkably similar. This can be seen for Kao-PEG 3400 and Kao-18C6 in Figures **4.6 c** and **4.6 d**. In these cases, the C-H symmetric stretching band is found near 2880 cm^{-1} and the C-H asymmetric stretching band near 2930 cm^{-1} with a shoulder at about 2956 cm^{-1}. The very weak band near 3020 cm^{-1} for Kao-PEG 3400 and Kao-18C6 is due to the C-H asymmetric stretching of residual intercalated DMSO. For comparison, the C-H stretching pattern of Kao-DMSO (Figure **4.6 b**) shows three bands due the asymmetric and symmetric C-H stretching modes of the methyl groups at 3022 cm^{-1}, 2937 cm^{-1} and a very weak band at 2919 cm^{-1} [39].

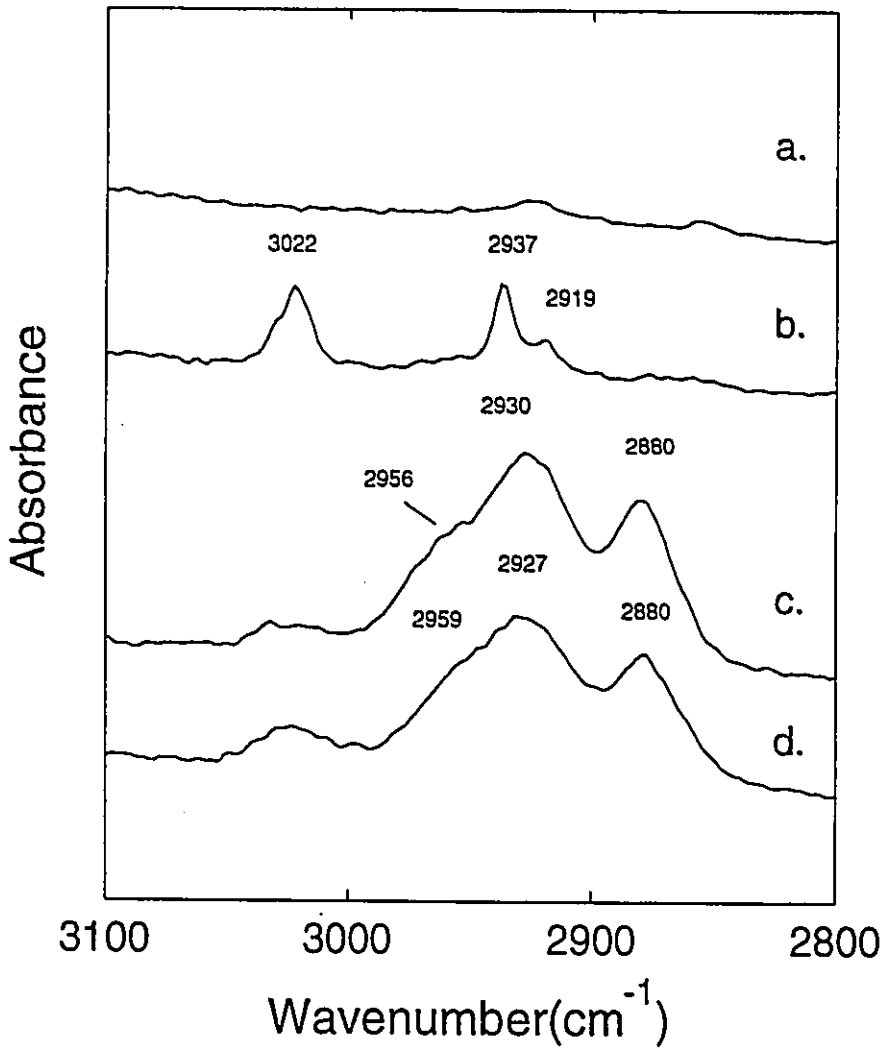

Figure 4.6: FTIR spectra (3100-2800 cm^{-1}) of Kaolinite (a); Kao-DMSO (b); Kao-PEG 3400 **4-8-A** (c); Kao-18C6 **4-6-A** (d). Note: The relative absorbance scales of the spectra have been adjusted in order to facilitate comparison.

For Kao-PEG 3400 it is evident that the C-H stretching bands were greatly perturbed upon intercalation. In pure solid PEG 3400, which is most likely a mixture of amorphous and crystalline phases similar to polyethylene oxide (PEO) [185], the symmetric and asymmetric C-H stretching modes are not resolved, and only one broad ill-defined band between 2800 and 3000 cm^{-1} centered at 2887 cm^{-1} is observed. Upon intercalation, one observes the splitting of this broad band at 2887 cm^{-1} into two and possibly three (if one includes the shoulder at 2956 cm^{-1}) distinct bands. Aranda and Ruiz-Hitzky observed a similar phenomenon for various PEO/M^{n+}-montmorillonite complexes [118]. They found that upon intercalation, the C-H stretching band of the PEO moiety was resolved into two well-defined bands of moderate intensity at approximately 2910 cm^{-1} and 2875 cm^{-1}. They also found that these bands were insensitive to the nature of the interlayer cation of the smectite. Polyether derivatives of zirconium phosphate yielded products which had C-H stretching patterns almost identical to those of Kao-PEG 3400 and Kao-18C6 with bands at 2880, 2920 and 2950 cm^{-1} [191].

Casal and Ruiz-Hitzky found that the C-H stretching bands of crown ethers incorporated into smectites were influenced by their interactions with the interlayer cations. These interactions were also thought to be responsible for the alignment of the crown ethers in the interlayer spaces of the smectite and thus the interlayer d-spacings [194,199,205]. Kaolinite, which has no interlayer cation may also intercalate 18-Crown-6 and 15-Crown-5 to produce materials with C-H stretching patterns which are virtually identical to that of Kao-PEG 3400 with two distinct bands at 2927 and 2880 cm^{-1} and what appears to be a shoulder at 2956 cm^{-1} (Figure **6d**). Interestingly, this pattern is very similar to that reported for 15-crown-5

intercalated as a monolayer into a Na^+-montmorillonite, which shows distinct bands at 2882 and 2921 cm^{-1} and a shoulder at 2959 cm^{-1} [205]. This similarity exists despite the fact that there can be no crown ether-cation interaction for Kao-18C6 or Kao-15C5, as is the case for 15C5/Na^+-montmorillonite. It is plausible nonetheless, that there exist some strong interaction between the crown ether and either the host kaolinite lattice or residual DMSO molecules to produce a similar effect on the C-H stretching bands.

HOH Bending Region (1680-1600 cm^{-1}): The δ(HOH) deformation band of water may be indicative of either surface adsorbed water or co-intercalated water. Wada has shown that the δ(HOH) band for water intercalated in kaolin minerals is at higher frequencies than for external physisorbed water (approximately 1650 cm^{-1} vs 1630 cm^{-1}) [184]. As one might expect, this band is also very sensitive to the method used for drying the sample. Since various drying methods were used, and the KBr pellets were prepared in varying degrees of humidity, the position and intensity of this band is variable. The presence of higher frequency δ(HOH) bands (> 1640 cm^{-1}) in some of the oxyethylene-based organokaolinites, suggests that under certain circumstances water may be co-intercalated to some extent with the oxyethylene unit. Kao-PEG 3400 and Kao-18C6 for example show an ill-defined δ(HOH) band between 1630-1650 cm^{-1}, probably corresponding to both surface adsorbed and co-intercalated water molecules (Figures **4.7 c** and **4.7 d** respectively).

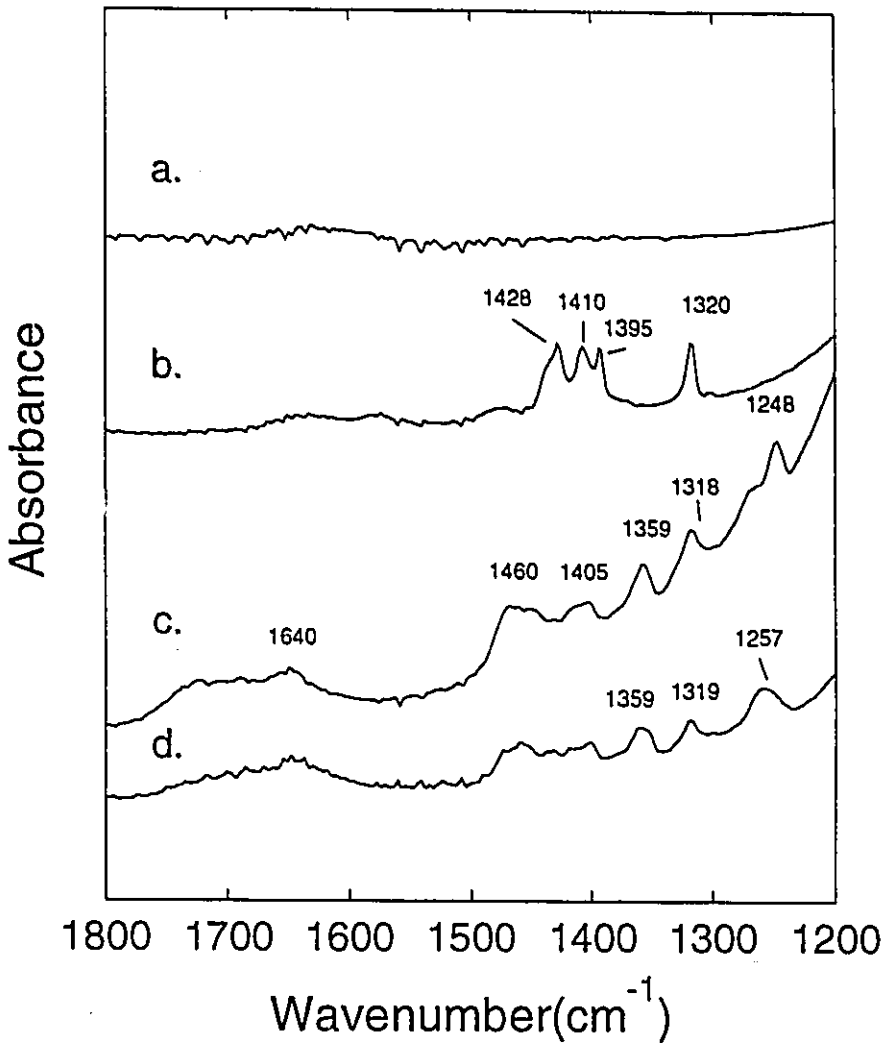

Figure 4.7: FTIR spectra (1800-1200 cm^{-1}) of Kaolinite (**a**); Kao-DMSO (**b**); Kao-PEG 3400 **4-8-A** (**c**); Kao-18C6 **4-6-A** (**d**). Note: The relative absorbance scales of the spectra have been adjusted in order to facilitate comparison.

C-H Deformation Region (1500-1200 cm^{-1}): Here one finds a number of bands indicative of various CH deformations originating from the oxyethylene species, or in some instances from residual intercalated DMSO or NMF. Close examination of this region may provide some insights into the structural conformations of interlayer oxyethylene species. All oxyethylene based organokaolinites studied showed characteristic bands due to CH_2 deformations of the oxyethylene groups.

Figures **4.7 a-d** shows the FTIR spectra (1800-1200 cm^{-1}) of kaolinite, Kao-DMSO, Kao-PEG 3400 and Kao-18C6 respectively. Kaolinite, as expected shows no C-H deformation bands at all. Kao-DMSO shows deformation bands at 1428, 1410, 1395 and 1320 cm^{-1} which have been previously assigned [39]. For Kao-PEG 3400 and Kao-18C6, the spectra appear to be very similar, with C-H deformation bands near 1460 cm^{-1}, 1405 cm^{-1}, 1359 cm^{-1} and 1318 cm^{-1}. This similarity breaks down for the C-H deformation bands between 1240 and 1270 cm^{-1}. Only one band is observed for Kao-18C6 at 1257 cm^{-1} whereas for Kao-PEG 3400 there appear two bands, one at 1248 cm^{-1} and a shoulder band at 1268 cm^{-1}.

For Kao-PEG 3400, the broad ill-defined band(s) between 1480-1440 centered about 1460 cm^{-1} can be attributed to CH_2 bending modes of the PEG chain based on literature assignments for PEO [206]. Similarly the band centered near 1405 cm^{-1} may be assigned to the CH_2 wagging mode of the oxyethylene units based the IR assignment for PEO [206], although this is complicated by the of presence of residual interlayer DMSO (see section **4.2.4**). Kao-DMSO has two absorption bands in this region (Figure **4.7 b**) which may overlap with the PEG band. The band at 1359 cm^{-1} can be assigned to a combination band made up of CH_2

wagging and C-C stretching modes [206]. A band in this region has also been observed for both crown ethers and PEO intercalated into smectites [118,205].

The attribution of the band at 1318 cm^{-1} for both Kao-PEG and Kao-18C6 was complicated once again, by the fact that Kao-DMSO has an absorption band in this region at 1320 cm^{-1}, and residual DMSO was shown to be present in the interlayers. The attribution of this band is important since the presence or absence of a band in this region may be indicative of the conformation of the oxyethylene species [118,186,207]. Nonetheless, it is believed that for at least Kao-PEG 3400, residual DMSO cannot be the sole contributor to the intensity of this band since this sample was shown to have a relatively small amounts of residual interlayer DMSO (see section **4.2.4**). In support of this, IR bands due to the presence of DMSO in Kao-PEG 3400 such as those at 3022 cm^{-1} (Figure **4.5 c**) and 1428 cm^{-1} (Figure **4.7 c**) have relatively insignificant intensities compared to the intensities of the bands associated uniquely with the presence of intercalated PEG 3400.

More conclusively, analysis of the Kao-PEG 3400 product when Kao-NMF was used as the starting material (**4-7-B**) showed that in addition to C-H deformation bands at 1248 cm^{-1}, 1358 cm^{-1} and 1460 cm^{-1}, a band at 1315 cm^{-1} was observed, although at slightly weaker relative intensity than the 1318 cm^{-1} band observed for Kao-PEG 3400 in Figure **6.4 c**. Kao-NMF was verified to have no absorption bands which might, like Kao-DMSO, interfere with the assignment of this band.

The presence of a band at 1326 cm^{-1} for molten PEO has been attributed to a combination of CH_2 wagging and twisting modes [207]. This band is not present for solid PEO presumably because in the solid state, the $-OCH_2CH_2O-$ groups are mainly in the gauche

conformation and the presence of a band in this region has been proposed to be due to -OCH_2CH_2O- groups in the trans conformation [186]. In fact, the lack of a band near 1322 cm^{-1} for PEO/M^{n+}-montmorillonite has been used as evidence supporting the hypothesis that the O-CH_2CH_2-O groups of the interlayer PEO chains are all in the gauche conformation [118]. For Kao-EG 9.4 Å, the presence of a band at 1325 cm^{-1} was also used to support the hypothesis that the ethylene glycol moiety was in the trans conformation [208] (see Chapter 3). The above discussion suggests that for Kao-PEG 3400, at least a portion of the oxyethylene units are in a trans conformation.

Finally, the band at 1257 cm^{-1} for Kao-18C6 and the bands at 1268 cm^{-1} and 1248 cm^{-1} for Kao-PEG 3400 are attributed to the CH_2 twisting vibrations of the oxyethylene units [206]. Similar bands were found for example, at 1265 cm^{-1} for an 18C6/Ba^{2+}-montmorillonite complex [205], and at 1274 cm^{-1} and 1248 cm^{-1} for PEO/Na^{+}-montmorillonite[118].

Kaolinite Lattice Vibrations (1200-800 cm^{-1}): This region provides information regarding any perturbations to the kaolinite lattice vibrations (1150-1000 cm^{-1}) and any changes in the Al-O-H bending modes of kaolinite (900-980 cm^{-1}). The C-O stretching intensity due to the oxyethylene groups is buried beneath the very intense lattice vibrations of the kaolinite host, although it probably contributes in some small way to the shape of the very intense bands between 1000 cm^{-1} and 1070 cm^{-1}. All the oxyethylene-based organokaolinites exhibited almost identical IR stretching patterns in this region.

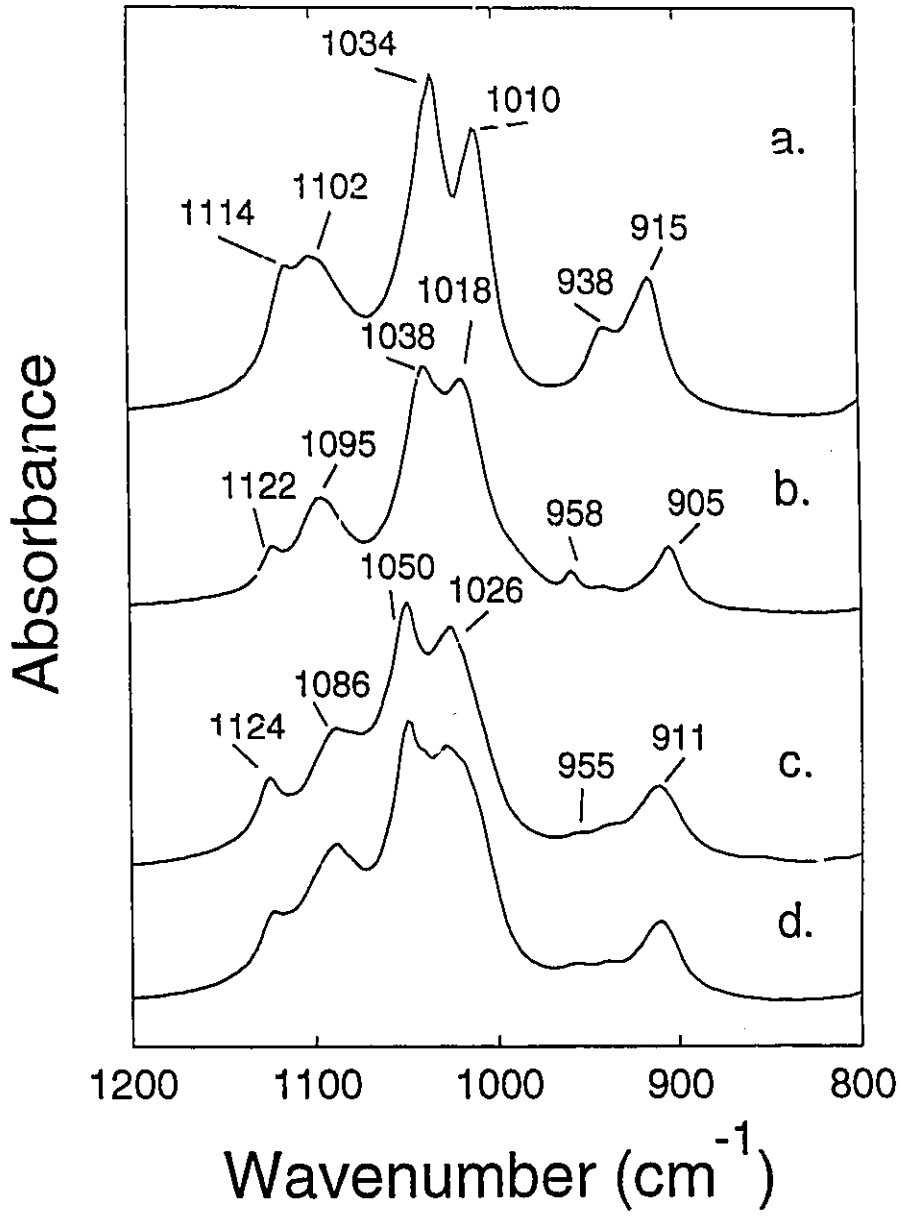

Figure 4.8: FTIR spectra (1200-800 cm^{-1}) of Kaolinite (a); Kao-DMSO (b); Kao-PEG 3400 **4-8-A** (c); Kao-18C6 **4-6-A** (d). Note: The relative absorbance scales of the spectra have been adjusted in order to facilitate comparison.

Figure **4.8 a-d** shows the differences in the IR patterns (1200-800 cm^{-1}) for kaolinite, Kao-DMSO, Kao-PEG 3400, and Kao-18C6 respectively. Examination of the patterns of both Kao-18C6 and Kao-PEG 3400 show strong signs of perturbation of the kaolinite lattice vibrations. The two most intense vibrations of kaolinite at 1034 cm^{-1} and 1010 cm^{-1} are both shifted to higher frequencies by 16 cm^{-1} for Kao-PEG 3400 and Kao-18C6. These bands have been previously assigned to the in-plane Si-O-Si stretching vibrations of kaolinite [25], and are often shifted slightly upon intercalation of guest species such as DMSO, as can be seen for the Kao-DMSO starting material, where these bands are blue-shifted slightly to 1038 cm^{-1} and 1018 cm^{-1} (Figure **4.8 b**). The fact that these bands are shifted to yet greater frequencies when PEG or 18C6 are intercalated, indicates plausibly a greater perturbation of the silicate surface on the part of the oxyethylene species, although intensity from the C-O stretching bands of the oxyethylene species may also contribute to these frequency shifts.

The perpendicular Si-O vibrations found in kaolinite at 1102 cm^{-1} and 1114 cm^{-1} [25] (Figure **4.8 a**) are once again more perturbed for both Kao-PEG 3400 and Kao-18C6 than for Kao-DMSO. In contrast to the in-plane Si-O-Si vibrations, where both bands are shifted to higher frequencies, here the band at 1102 cm-1 is shifted to lower frequency whereas the band at 1114 cm^{-1} is shifted to higher frequency. For Kao-PEG 3400 and Kao-18C6 these two bands are found at 1086 cm^{-1} and 1124 cm^{-1}, indicating shifts of -16 cm^{-1} and +10 cm^{-1} respectively compared to kaolinite.

The kaolinite band at 938 cm^{-1} has been assigned to the in-plane bending vibrations of surface hydroxyl groups whereas the band at 915 cm^{-1} has been assigned to the inner hydroxyl [25,200]. Upon intercalation of DMSO, the band at 938 cm^{-1} decreases greatly in

intensity and another band appears 20 cm^{-1} higher in frequency at 958 cm^{-1} (Figure **4.8 b**). This band probably results from either the effects of hydrogen bonding between the oxygen of DMSO and the hydroxyl surface of kaolinite on the Al-O-H bending mode, or from the CH_3 rocking vibration of the DMSO guest itself [39,41]. The band at 915 cm^{-1} is shifted 10 cm^{-1} to a lower frequency at 905 cm^{-1} presumably due to a repulsive interaction between one of the methyl groups of DMSO which is proposed to be keyed into the $(SiO\text{-})_n$ macro-ring of the silicate surface [39,42,43,45], and the internal hydroxyl of kaolinite.

For Kao-PEG 3400 and Kao-18C6, a band at 955 cm^{-1} appears, presumably due a shift to higher frequency of the 938 cm^{-1} band caused by hydrogen bonding between the hydroxyl surface and the oxygens of the oxyethylene species. The band at 955 cm^{-1} may also be due to a CH_2 rocking vibration of the oxyethylene unit which falls in this region for PEO [206]. For Kao-PEG 3400, Kao-18C6 and Kao-DMSO, a very weak band at approximately 938 cm^{-1} is observed due to residual unexpanded kaolinite.

For Kao-PEG and Kao-18C6, the inner hydroxyl band of kaolinite is not as perturbed as it was for Kao-DMSO. Here, one observes a negligible 4 cm^{-1} shift to lower frequency at 911 cm^{-1}. This is plausibly due to the inability of the oxyethylene species to key in as well to the $(SiO\text{-})_6$ macrorings of the silicate surface as DMSO.

4.2.4 Solid State ^{13}C NMR Studies

A series of ^{13}C CP/MAS and DD/MAS experiments were performed on many of the oxyethylene based organokaolinites in order to obtain some preliminary information regarding the interlayer structure and dynamics of the intercalated hosts. These results are summarized in Table **4.2**.

4.2.4.1 Identification of the Interlayer Species

Regarding the structure of the oxyethylene units, the chemical shift of the CH_2 groups of the oxyethylene unit should indicate if it is in the form of an end alcohol group (R-OH), or as a link in the ether chain (R-O-R). For example, the different ^{13}C chemical shift values of Kao-PEG 3400 ($\approx$ 70 ppm) compared with both Kao-EG 9.4 Å and Kao-EG 10.8 Å ($\approx$ 65 ppm) indicate that depolymerization of the PEG 3400 did not occur in the interlamellar space of kaolinite to yield an intercalated ethylene glycol monomer in either its 9.4 Å or 10.8 Å form. The polymer remains intact in the interlayers.

For the intermediate oxyethylene based organokaolinites, Kao-DiEG, Kao-TriEG and Kao-TetraEG, ^{13}C CP/MAS spectra showed both ether methylene resonances at about 68-71 ppm and alcohol methylene resonances due to the ends of the polyethylene glycol units at about 59-64 ppm. This suggests that the hydrolysis of ether groups to give alcohols or inversely, the condensation of alcohol groups to give ethers does not occur in the interlayers

Sample	Freq. (MHz)	Carbon Type	δ (ppm)	I_{DD}/I_o	$\nu_{1/2}$ (Hz)
Kao-EG 9.4 Å (3-2-1)	50.29	CH_2O-	65	0.24	120
Kao-EG 10.8 Å (4-1-A)	50.29	CH_2O-	65	0.61	55
Kao-DiEG (4-2-A)	50.33	CH_2O- CH_2O-	68 59	res res	415 380
Kao-TriEG (4-3-A)	50.33	CH_2O- CH_2O-	71 62	res res	420 275
Kao-TetraEG (4-4-A)[1]	50.33	CH_2O- CH_3 (NMF) C=O (NMF)	67 27 165	res 0.75 nd	730 115 200
Kao-15C5 (4-5-A)[1]	50.33	CH_2O- CH_2O- CH_3 (DMSO)	70 62 42	res res 0.85	400 - 115
Kao-18C6 (4-6-A)[1]	50.33	CH_2O- CH_2O- C=O (?) CH_3 (DMSO)	70 62(sh) 180 41	res res 0.85 0.78	390 - 150 130
Kao-PEG 1000 (4-7-A)[1]	50.33	CH_2O- CH_3 (DMSO)	70 42	res 0.73	415 115
Kao-PEG 3400 (4-8-A)[1]	50.33	CH_2O- CH_3 (DMSO)	70 42	res 0.48	450 150
PEG 3400	50.33	CH_2O-	73	0.26	755
PEG 1000	50.33	CH_2O-	73	0.18	40
Kao-DMSO	45.27	CH_3 (DMSO) CH_3 (DMSO)	43.7 42.7	0.58 0.60	80 80

Table 4.2: Summary of ^{13}C CP/MAS and DD/MAS results for the oxyethylene based organokaolinites. These were done on a number of instruments: Bruker instruments ASX-200 (50.33 MHz), MSL-200 (50.29 MHz) and CXP-180 (45.3 MHz). The spinning rates ranged from 4-5 KHz, and a dipolar dephasing time (τ) of 40 μs was used for the DD/CP-MAS experiments: (1) These samples had residual amounts of either DMSO or NMF in the kaolinite interlayers due to incomplete reaction; (res) residual signal ($I_{DD}/I_o < 0.10$); (nd) no signal ($I_{DD}/I_o \approx 0.00$); (sh) shoulder

of kaolinite. In contrast, various ion-exchanged montmorillonites were found to catalyze the condensation reaction of primary diols to give either oligomeric or cyclic ether products [209].

A distinguishing feature of the ^{13}C CP-MAS spectra of both Kao-18C6 and Kao-15C5 is the presence of two broad methylene resonances at about 70 and 62 ppm. This is unexpected since one would expect only one resonance at about 70 ppm due to ether carbons. The presence of an additional peak or shoulder at 62 ppm may be indicative of either an asymmetry in the crown ether caused by interaction with the host kaolinite material, or perhaps due to interaction with co-intercalated DMSO molecules. Also, one may not entirely rule out the possibility of the presence of a primary alcohol caused by the ring opening hydrolysis of the crown ether. For Kao-18C6 an unidentified very small peak at 180 ppm was also observed. This was most likely due to a carbonyl impurity of some sort.

The ^{13}C CP/MAS spectra of many of the oxyethylene based organokaolinites were complicated by the presence of large amounts of residual interlayer DMSO, as evidenced by resonances at 41-42 ppm. The OEU/DMSO ratio based on the ^{13}C CP/MAS peak integrations was crudely estimated to be 1.8 and 0.9 for Kao-18C6 and Kao-15C5 respectively, and 5.9 and 2.8 for Kao-PEG 3400 and Kao-PEG 1000. Traces of co-intercalated NMF were also found for Kao-TetraEG. It is noteworthy that in all cases where DMSO is co-intercalated with oxyethylene species, only one ^{13}C methyl resonance could be found for DMSO, whereas for the pure Kao-DMSO intercalate, two resonances were observed [42,43,45]. The implications of this will be discussed later (Section **4.2.4.2**).

4.2.4.2 Dynamic Considerations

For the dipolar dephasing technique, the ratio of I_{DD}/I_0, where I_{DD} and I_0 are the peak intensities of the ^{13}C resonance obtained respectively with and without dipolar dephasing conditions, is a semiquantitative measure of the dynamic state of the molecular group [210-212]. If a molecular group is rigidly bound, this ratio will be decreased, whereas molecular motion has the effect of increasing I_{DD}/I_0 up to a maximum value of unity. The dipolar dephasing technique may also be used to discriminate between carbons weakly coupled to protons such as quaternary carbons (both sp^3 and sp^2 carbons) from carbons strongly coupled to protons (methine and methylene carbons) [211]. The overall signal decay for carbons strongly coupled to protons has been shown to be best described by the following equation [211]:

$$I_{DD} = I_0 e^{-t^2/(2T_2^2)} \qquad (4.1)$$

Here, τ is the dipolar dephasing time and T_2 is the transverse relaxation time constant.

The DD/MAS results for all of the oxyethylene based organokaolinites except for Kao-EG 10.8 Å and to a lesser extent Kao-EG 9.4 Å showed only residual signal after 40 μs of dipolar dephasing (Table **4.2**). This is indicative of rigid oxyethylene species. The results for Kao-EG 9.4 Å and Kao-EG 10.8 Å are treated separately in chapter 3 and are provided here only for comparison. The DD/CP-MAS results for Kao-PEG 3400 and Kao-18C6 are illustrated below, as examples of the intercalation of PEG and crown ether molecules into kaolinite.

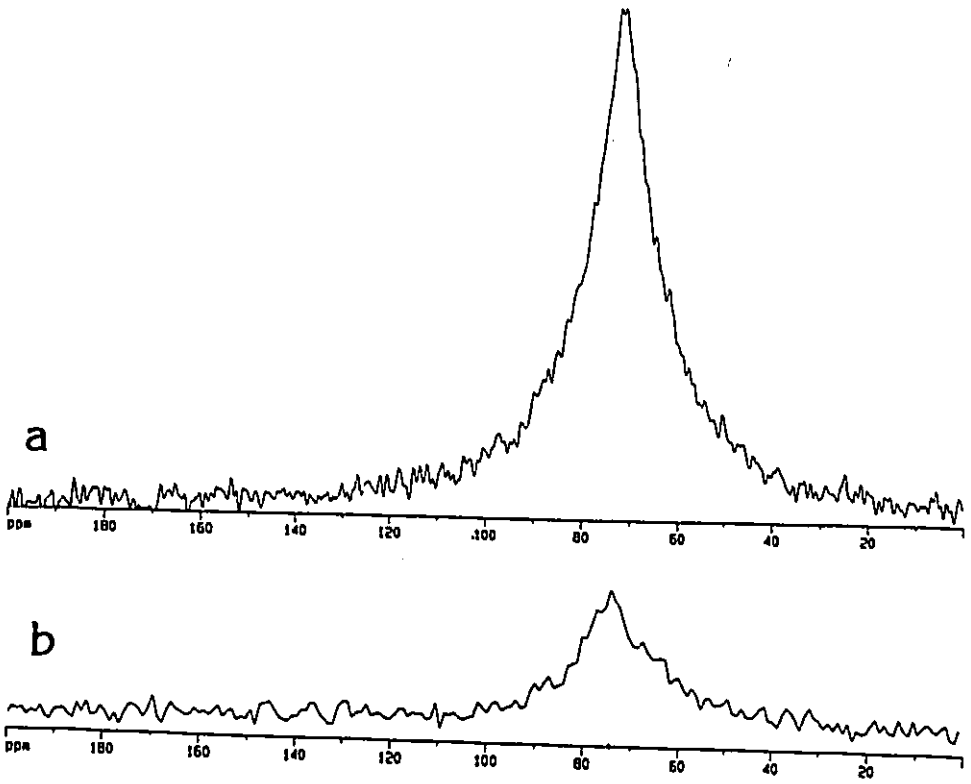

Figure 4.9: Solid State ^{13}C CP/MAS NMR spectra for PEG 3400: (a) no dipolar dephasing; (b) DD/MAS (τ= 40 μs).

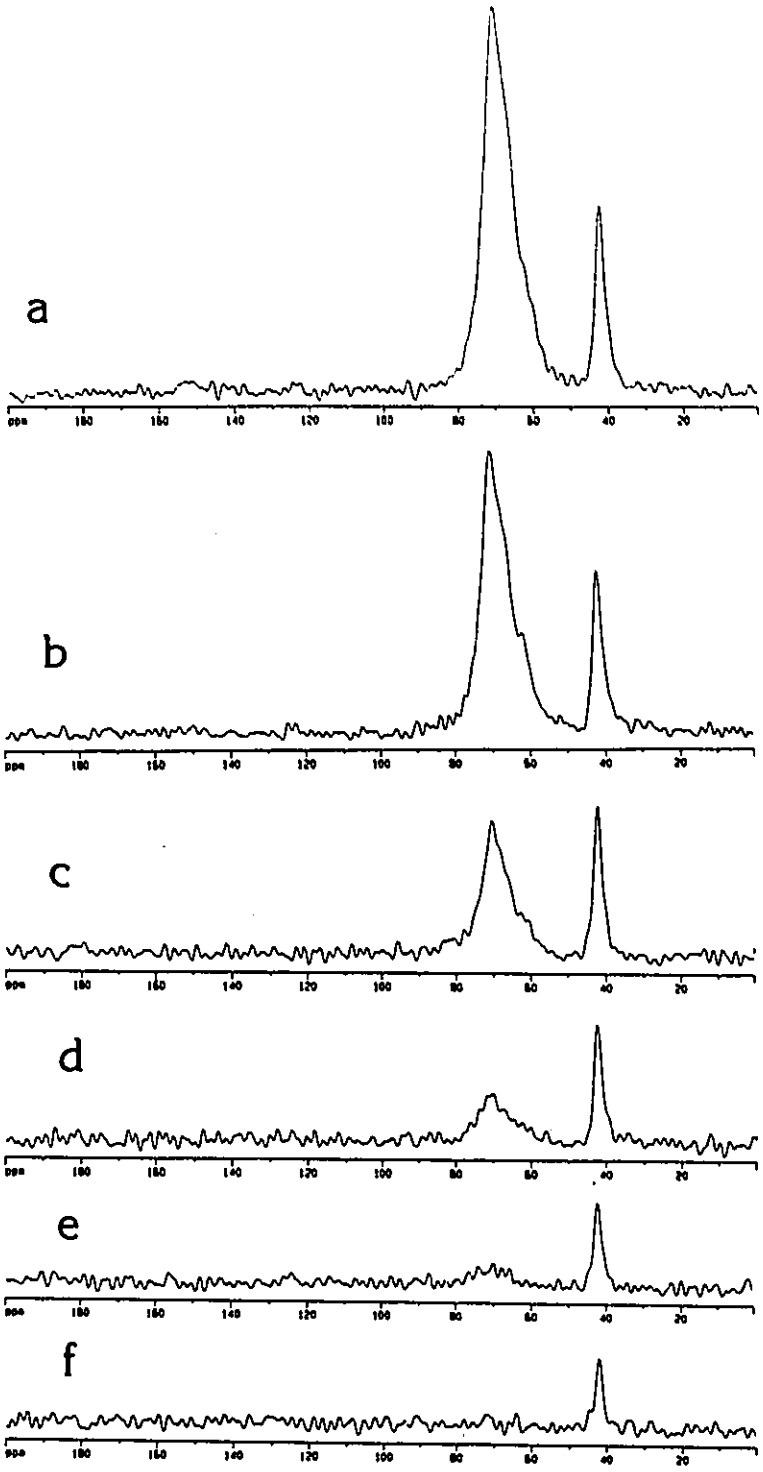

Figure 4.10: Solid State ^{13}C CP/MAS NMR spectra for Kao-PEG 3400 4-8-A: without dipolar dephasing (a); with dipolar dephasing: τ= 10 μs (b); 20 μs (c); 30 μs (d); 40 μs (e); 50 μs (f).

Polyethylene Glycol Intercalates: The ^{13}C CP/MAS NMR spectrum of pure polyethylene glycol has been previously reported [118]. Two signals at 70.6 and 71.9 ppm were detected, the first was due to a relatively narrow peak, and the second to a broader resonance (about 440 Hz). For polyethylene oxide intercalated into Na^+ hectorite (PEO/Na^+-hectorite), Aranda and Ruiz-Hitzky observed a single broad peak at around 70 ppm ($\nu_{1/2} \approx 440$ Hz at 100.63 MHz) which they attributed to a helicoidal PEO conformation where all the methylene groups exists in a gauche conformation [118]. In solution, PEO was reported to have a ^{13}C chemical shift between 71.5 and 72.4 ppm and it was determined that there was a concentration dependence on the chemical shift as well as a dependence on the average trans-gauche conformation [213].

In this study, PEG 3400 gave a resonance at about 72 ppm with a 1/2 height linewidth of 750 Hz (Figure **4.9 a**). This enormous linewidth is attributable to polymer molecular motion interfering with the efficiency of the proton decoupling [214]. By contrast, PEG 1000 gave a much narrower resonance at 72.9 ppm with a 1/2 height linewidth of only 40 Hz. This is a good example of the influence that chain length may have on polymer mobility. PEG 3400 and PEG 1000 were both found to be relatively mobile in the solid state since after 40 μs of dipolar dephasing, a significant signal could still be detected, with I_{DD}/I_o equal to 0.26 for PEG 3400 (Figure **4.9 b**) and 0.18 for PEG 1000 (not shown). It is somewhat surprising that I_{DD}/I_o was found to be greater for PEG 3400 than for PEG 1000, since this would seem to imply that the larger polymer, PEG 3400, is more mobile than the smaller one, PEG 1000. One must consider however, the relative linewidths and lineshapes of the two polymer resonances. PEG 1000 exhibited a narrow (40 Hz) and symmetric

resonance, whereas PEG 3400 did not. This dissimilarity may cause some difficulty in the interpretation of the relative magnitudes of the effects of dipolar dephasing for the two PEG samples.

For Kao-PEG 3400, the resonance at about 70 ppm (Figure **4.10 a**) which is due to the methylene groups of the polyethylene glycol chain, is not significantly shifted from that of the bulk polymer (Figure **4.9 a**). However, the linewidth of this resonance was diminished upon polymer incorporation, from about 750 Hz to 450 Hz. This decrease in linewidth can plausibly be attributed to the fact that upon intercalation, the molecular motion of the polymer no longer interferes as much with the proton decoupling. The decreased linewidth is not thought to be due to any increase in polymer crystallinity.

In a series of experiments, the dipolar dephasing time (τ) was varied from 0 μs to 50 μs for the Kao-PEG 3400 sample, and the variation in intensity was monitored (Figure **4.10**). This qualitatively showed that the polymer chains in the interlamellar spaces of kaolinite are more constrained and less mobile than in its bulk form. After 40 μs dephasing time, only a residual signal for Kao-PEG 3400 could be detected ($I_{DD}/I_O < 0.10$). These results are plotted in Figure **4.11** as the I_{DD}/I_O ratio vs the dipolar dephasing time. In order to test the validity of Equation **4.1** this same data was then replotted in Figure **4.12** as $\ln(I_{DD}/I_O)$ vs τ^2 to see if this results in a straight line with slope equal to $-1/(2T_2^2)$ as predicted by Equation **4.1**. This showed that for small values of τ, the graph was fairly linear with a T_2 value of approximately 15 μs but for higher values of τ this linearity seemed to break down, possibly due to the difficulty in obtaining accurate intensity estimates of the residual dipolar dephased peaks. $1/T_2$ may be considered to be a root mean squared average of w_i properly weighted

by the fraction of molecules with a given orientation having the dipolar modulation frequency, w_1 [211].

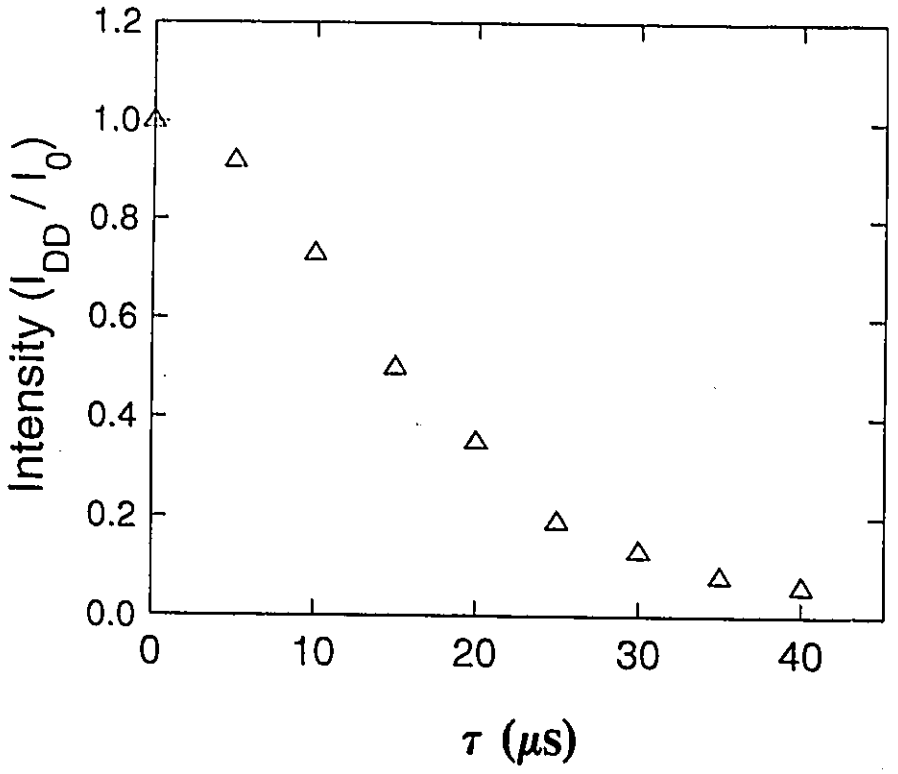

Figure 4.11: Plot of I_{DD}/I_O versus dipolar dephasing time (τ) for the ^{13}C DD/MAS spectra acquired for Kao-PEG 3400 **4-8-A** product (see Figure **4.10**).

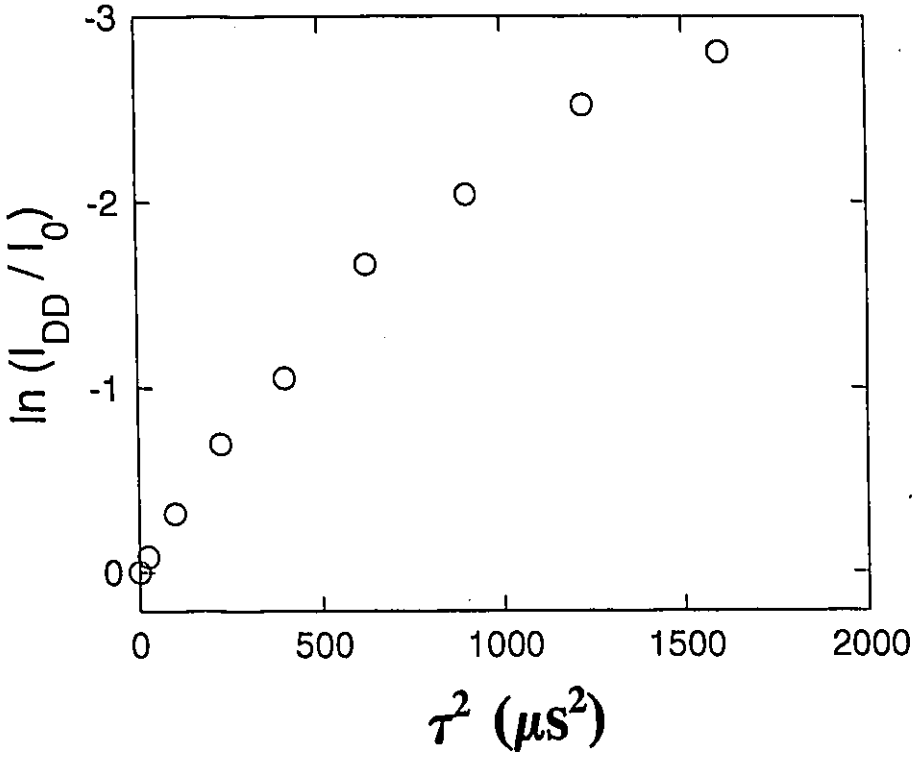

Figure 4.12: Plot of $\ln(I_{DD}/I_O)$ vs. the square of the dipolar dephasing time (τ^2) for the ^{13}C DD/MAS spectra acquired for Kao-PEG 3400 **4-8-A** product (see Figure **4.10**).

Crown Ether Intercalates: The dipolar dephasing behaviour of Kao-18C6 is shown in Figure **4.13**. The small peak at 180 ppm assigned to a carbonyl impurity of some sort, remained strong after 40 μs dephasing time ($I_{DD}/I_O = 0.85$). This is in accord with what one would expect for a carbon which is not directly bonded to a proton [211]. In contrast, the resonances at 62 and 70 ppm, assigned to oxyethylene carbons showed only a residual signal after 40 μs of dipolar dephasing, indicating that the oxyethylene carbons are in a rigid environment. The DMSO methyl resonance at 41 ppm is much less affected by dipolar dephasing.

4.2.4.3 State of Residual Co-Intercalated DMSO

As implied earlier, information regarding the interlayer environment of residual DMSO in the oxyethylene based organokaolinites can obtained with ^{13}C CP/MAS. In the liquid and solid states, the two methyl groups in DMSO give degenerate resonances at respectively 40.3 ppm [43] and 40.0 ppm [42]. For ordered Kao-DMSO, the two methyl groups are degenerate, yielding two resonances at approximately 43.1 and 44.2 ppm [42-45]. In this work, it was confirmed that the Kao-DMSO starting material had two ^{13}C resonances, only the resonances were found at 43.7 and 42.7 ppm (Table **4.2**). The linewidths of these resonances were estimated to be in the range of about 80 Hz, despite some uncertainty due to peak overlap. ^{13}C DD/MAS NMR using a 40 μs dipolar dephasing time showed that both resonances had an I_{DD}/I_O ratio of about 0.60.

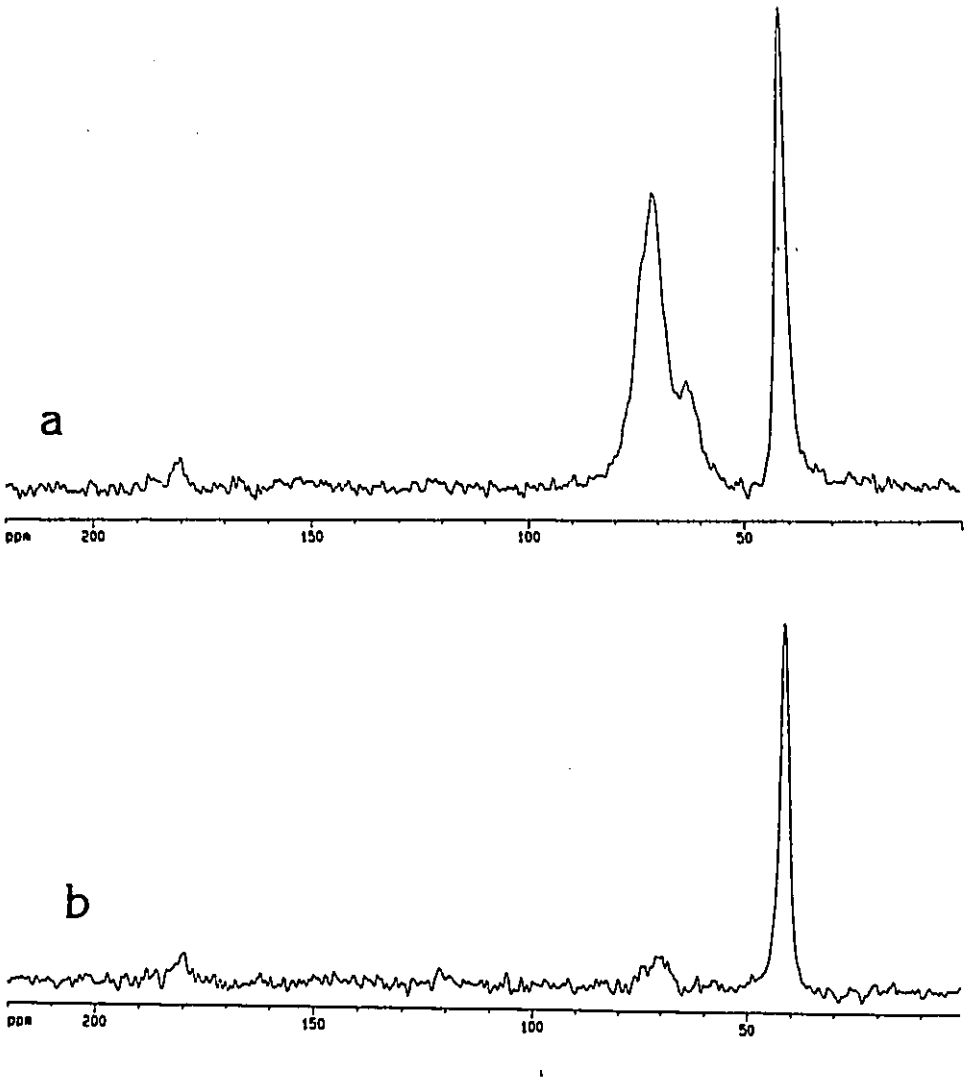

Figure 4.13: Solid State ^{13}C CP/MAS NMR spectra for Kao-18C6 **4-6-A**: (**a**) no dipolar dephasing; (**b**) DD/CP-MAS (τ= 40 μs).

For all the oxyethylene-based organokaolinites where DMSO was present in the interlayers as unreacted starting material, only one ^{13}C resonance could be observed at about 42 ppm with a linewidth between 115 and 150 Hz. The I_{DD}/I_O ratio for the DMSO resonance in these cases, varied from 0.48 for Kao-PEG 3400 to 0.85 for Kao-15C5. For Kao-DiEG and Kao-TriEG, no residual DMSO was observed, presumably due the large excess of reactant and high temperature used in the preparation procedure.

The presence of only one DMSO methyl resonance for residual DMSO in the oxyethylene based organokaolinites, as well as the different DD/MAS results when compared to the pure Kao-DMSO intercalate imply that the DMSO molecules are in different local environments. This is to be expected if one considers that the DMSO is probably randomly entangled in the oxyethylene-kaolinite 2-D matrix, and not found in discrete Kao-DMSO and Kao-oxyethylene layers. This is probably the reason why the intercalated DMSO is so difficult to completely remove. For example, even after heating at 150 °C for 16 hrs, some traces of intercalated DMSO could still be found in Kao-PEG 3400 and Kao-PEG 1000.

4.3.5 TGA\DSC Analysis

Thermal analysis of oxyethylene based organokaolinites by TGA and DSC revealed that they do not behave as typical organokaolinite intercalates such as Kao-DMSO or Kao-NMF, which upon heating would first evolve the intercalated DMSO or NMF in one or two discrete steps at temperatures less than 250 °C to yield the deintercalated kaolinite [215-218], followed by decomposition of the kaolinite itself. Instead, it was found that the organic

Sample	Temperature Range	TGA Weight Loss[1]	DSC Thermal Events	Total TGA Weight Loss[1]	Total Calcination Weight Loss[2]
	°C	%	°C	%	%
Kaolinite	0-300		-		
N_2	300-600		538(endo.)	13.1	14.1
	600-950	-	-		
	950-1050	-	1003(exo.)		
Kao-DMSO	25-152	16.6	131(endo.)		
N_2	152-258	14.5	215(endo.)		
	258-444	1.3	-	40.0	41.5
	444-648	7.6	527(endo.)		
	648-1050	-	1009(exo.)		
Kao-NMF	25-120	1.1	103(endo.)		
N_2	120-250	13.9	196(endo.)		
	250-450	1.0	-		
	450-650	10.2	534(endo.)	27.5	27.3
	650-950	1.0	-		
	950-1200	0.3	1003(exo.)		
Kao-EG 10.8 Å	25-100	-	-		
(4-1-A)	100-240	5.4	160(endo.)		
N_2	240-440	5.1	426(endo.)	24.1	-
	44-620	9.4	524(endo.)		
	620-1200	4.2	1004(exo.)		
			1026(exo.)		
Kao-DiEG	25-200	4.1	72(endo.)		
(4-2-A)	200-430	8.3	410(endo.)		
N_2	430-600	8.5	478(endo.)	24.9	26.5
			520(endo.)		
	600-950	1.5	-		
	950-1200	2.5	1005(exo.)		
			1027(exo.)		
Kao-DiEG	25-200	4.6	102(endo.)		
(4-2-A)	200-440	8.3	402(endo.)		
air	440-650	7.3	482(endo.)	21.8	26.5
			514(endo.)		
	650-950	0.2	-		
	950-1100	1.4	1007(exo.)		
			1024(exo.)		

Kao-TriEG	25-200	1.8	160(endo.)		
(4-3-A)	200-300	1.0	-		
N_2	300-450	9.0	429(endo.)		
	450-600	9.7	518(endo.)	25.5	28.2
	600-950	1.9	-		
	950-1200	2.1	1004(exo.)		
			1026(exo.)		
Kao-TriEG	25-220	1.4	161(endo)		
(4-3-B)	220-300	1.0	-		
air	300-410	10.8	390(exo.)		
	410-650	10.7	470(endo.)	25.1	28.2
			510(endo.)		
	650-950	0.3	1009(exo.)		
	950-1100	0.9	1023(exo.)		
Kao-TetraEG	25-300	3.6	-		
(4-4-A)	300-423	8.2	384(exo.)		
air	423-650	8.7	477(endo.)	21.1	27.3
	650-950	0.1	-		
	950-1100	0.5	1008(exo.)		
			1024(exo.)		
Kao-PEG 3400	25-100	1.0	-		
(4-8-B)	100-200	0.7	-		
N_2	200-340	8.3	324(endo.)	26.3	30.4
	340-440	7.3	405(endo.)		
	440-650	8.7	474(endo.)		
	650-950	-	-		
	950-1050	0.3	1010(exo.)		
			1025(exo.)		
Kao-PEG 3400	25-100	1.2	-		
(4-8-B)	100-200	0.6	-		
air	200-340	9.5	328(exo.)	27.0	30.4
	340-440	5.8	480(endo.)		
	440-650	8.6	-		
	650-950	0.3	-		
	950-1050	1.0	1010(exo.)		
			1021(exo.)		
PEG 3400	25-193	-	65(endo.)		
air	193-414	95.7	342(exo.)	99.2	-
	414-1050	3.5	537(exo.)		

Table 4.3: Summary of TGA/DSC results for the thermal decomposition of kaolinite, Kao-DMSO, Kao-NMF, PEG 3400 and some oxyethylene based organokaolinites. (1) Problems were encountered with the TGA baseline drift, during many of these runs, so the % weight losses for the TGA results are only approximate. (2) The calcination weight loss was the total % weight loss upon air calcination at 1100 °C for 2 hrs.

component was not entirely removed from the oxyethylene based organokaolinites until much higher temperatures (> 1000 °C), and the thermal decompositions followed multistep processes which were dependant to some extent on the atmosphere which was used during the TGA/DSC run (Table 4.3). In contrast with Kao-DMSO or Kao-NMF, it was difficult to discriminate between the decomposition of the organic oxyethylene guest and the inorganic kaolinite host.

In general, weight losses at less than 250 °C were attributed to the loss of weakly adsorbed or intercalated water and small organic molecules. Some of the residual DMSO or NMF from the starting material was also lost in this temperature range as judged by IR spectra taken before and after heating at 160 °C. Much of the co-intercalated DMSO appeared to remain trapped in the interlayers until higher temperatures (>200 °C).

Between about 250 and 400 °C, some of the organic material was lost as a result of either deintercalation, pyrolysis or combustion processes. Between 400 and 650 °C, one observed an additional weight loss due to the continued decomposition of the organic component as well as to the dehydroxylation reaction of kaolinite itself. At higher temperatures (>650 °C), a very gradual weight loss was often observed, although this may be masked by the influence of a drifting baseline, which affected many of the TGA runs. Some of this weight loss may be attributable to the continued slow pyrolytic decomposition of residual carbonaceous material. This is supported by the observation that the samples remained black in both nitrogen and air atmospheres until at least 1000 °C. Between 1000°C and 1030 °C, two exothermic events were generally seen for the decomposition of the oxyethylene based organokaolinites.

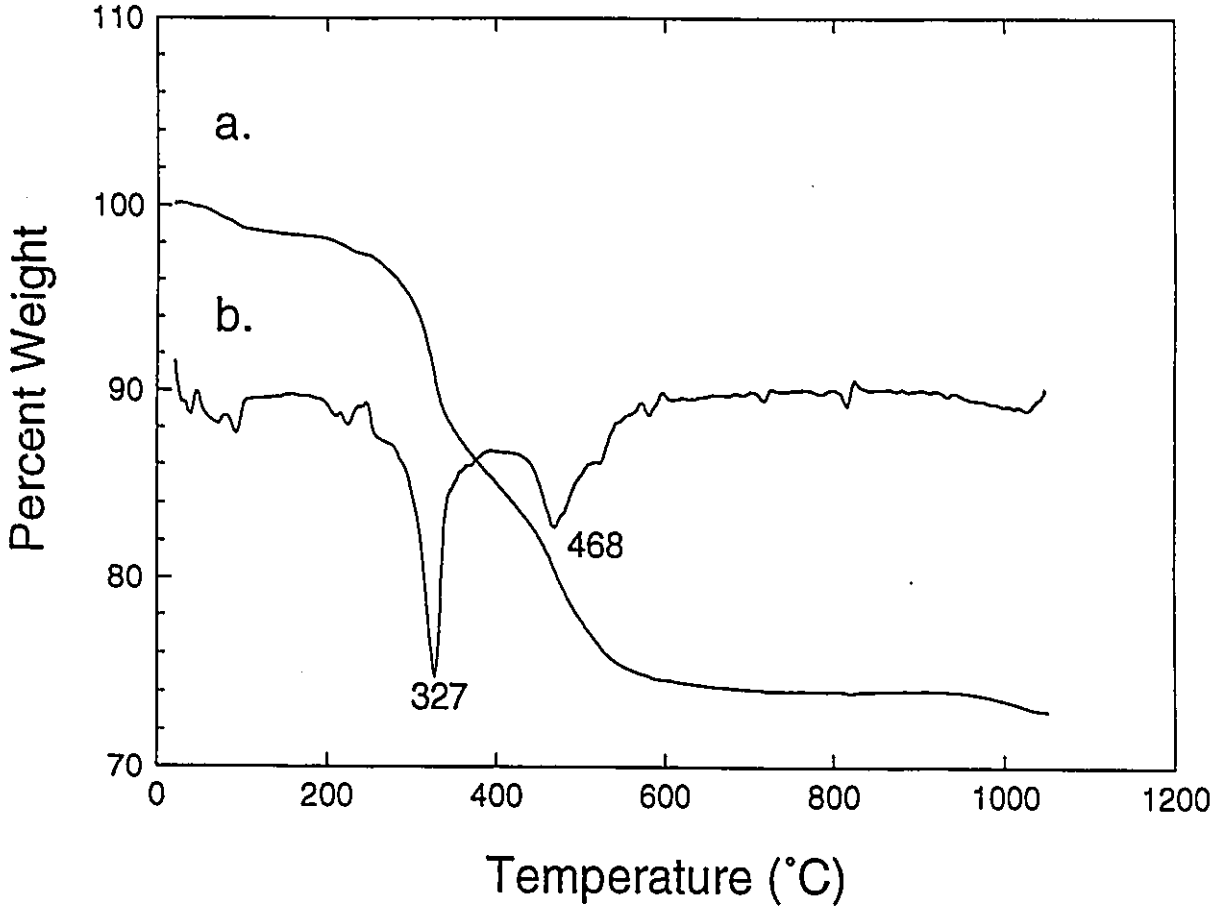

Figure 4.14: TGA (a) and corresponding DGA (b) curve (20-1050 °C) for Kao-PEG 3400 **4-8-B**.

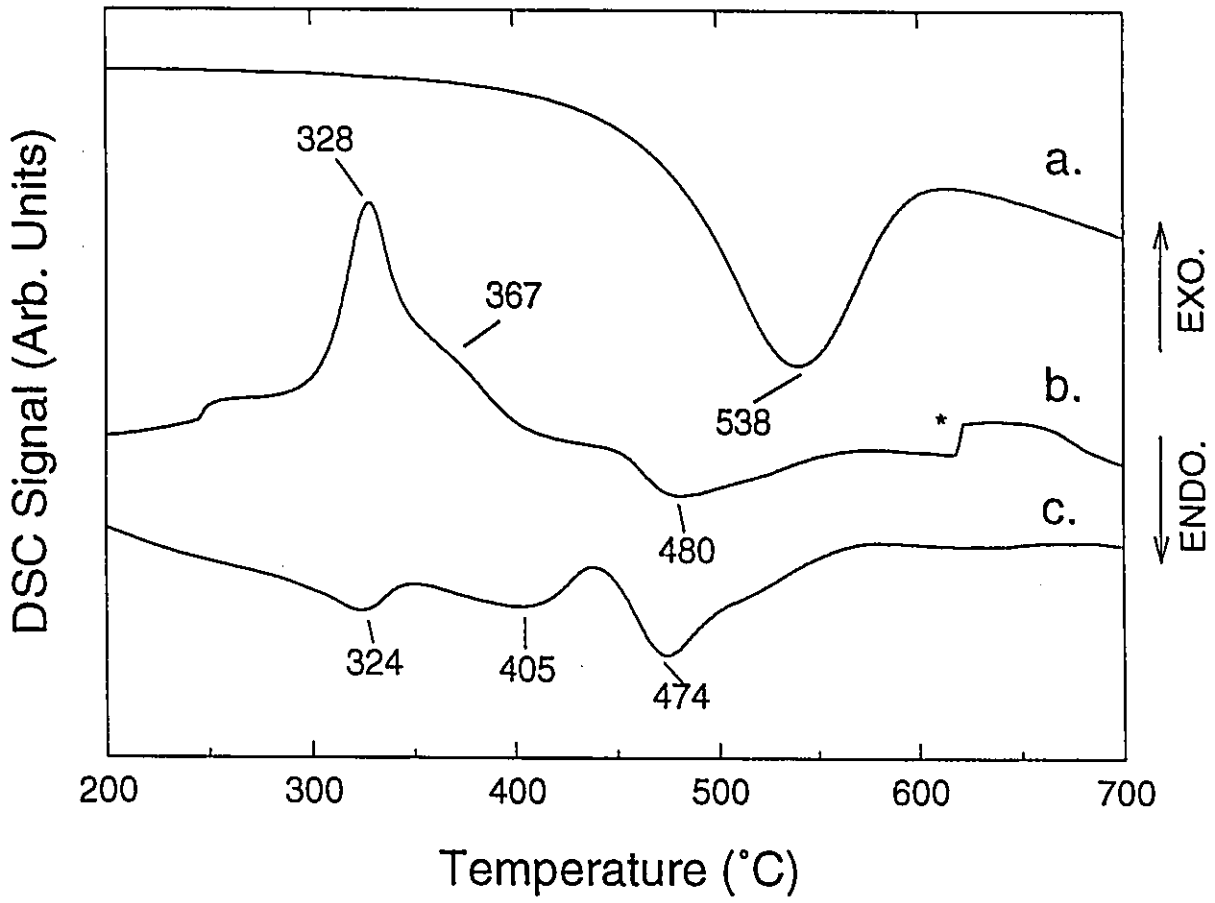

Figure 4.15: DSC traces (200-700 °C) for Kaolinite (**a**) and Kao-PEG 3400 **4-8-B** in air (**b**) and N_2 (**c**). (*) instrumental error.

The thermal decomposition of Kao-PEG 3400 in air atmosphere can be observed in Figure **4.14**. The decomposition followed a complicated multistep process where some of the decomposition steps overlapped. The total weight loss for the TGA run up to 1050 °C was found to be 27.0 % which is significantly lower than the 30.4 % that was found upon calcination of the same product at 1100 ° C for 3 hrs. This discrepancy may be attributed to either the presence of significant amounts of carbonaceous residual material, or to a drifting TGA baseline.

Initially, there was a 1.2 % weight loss from 25-100 °C due to the loss of surface adsorbed volatiles followed by a further 0.6 % weight loss from 100-200 °C. Aranda and Ruiz-Hitzky observed that the characteristic endothermic DTA peak associated with the melting of PEO at 72 °C was missing in the DTA of PEO/M^{n+}-montmorillonite [116]. This was also found to be the case for Kao-PEG 3400 where the endothermic DSC melting peak of PEG 3400 at 65 °C (Table **4.3**) was not observed for Kao-PEG 3400. This confirms that the polymer chains in the bulk and intercalated states are in different "aggregation states".

From 200-340 °C, one observes a 9.5 % weight loss attributable to the combustion of organic material (Figure **4.14**). This was supported by the DSC run which indicated a very strong exothermic event with a peak of 328 °C (Figure **4.15 b**). For comparison, it was found that for the thermal decomposition of pure PEG 3400 in air atmosphere, a very strong exotherm was observed centered at 342 °C corresponding to a 95.7 % combustion weight loss. In contrast, no thermal event for kaolinite was detected in this region (Figure **4.15 a**), and for Kao-PEG 3400 in nitrogen atmosphere, one observed an endothermic event with a peak at 324 °C (Figure **4.15 c**) probably due to the pyrolytic decomposition of the organic

component. For the N_2 atmosphere decomposition of Kao-PEG 3400 one observes an additional endothermic peak at 405 °C (Figure **4.15 c**), whereas for the air decomposition of Kao-PEG 3400, an exothermic shoulder at 367 °C is evident (Figure **4.15 b**), suggesting a multistep combustion process.

Aranda and Ruiz-Hitzky found that for PEO intercalated into M^{n+}-montmorillonite in nitrogen atmosphere, the initial PEO endothermic DTA decomposition peaks occur at lower temperature than for the bulk PEO [116]. Depending on the nature of the interlayer cation, they observed either a 1 step pyrolysis process (Na^+, Li^+) or a two step process (Ba^{2+}) for the decomposition of the intercalated PEO. It was rationalized that for divalent cations, there would exist both coordinated and uncoordinated oxyethylene units due to packing considerations. Since kaolinite does not have interlayer cations which may coordinate to oxyethylene units, another factor must account for the multistep pyrolysis of PEG which is observed for Kao-PEG 3400.

Overlapping with the weight loss associated with the organic decomposition reactions of Kao-PEG 3400, is the weight loss associated with the dehydroxylation reaction of kaolinite itself between 440-650 °C (Figure **4.14**). This was the case for both air and nitrogen TGA runs for all of the oxyethylene based organokaolinites analyzed. For Kao-PEG 3400 in air, the dehydroxylation reaction of kaolinite was estimated to involve an 8.6 % weight loss, compared to a weight loss of 13.1 % found for the kaolinite starting material (theoretical weight loss = 14.0 %). The dehydroxylation reaction for kaolinite exhibits an endothermic peak at 538 °C, whereas it appears at 480 °C and 474 °C for Kao-PEG 3400 in air and nitrogen atmospheres respectively. It would appear that the presence of PEG in the

interlayers of kaolinite has the effect of reducing the dehydroxylation temperature to a significant extent. It should be noted however, that the dehydroxylation reaction does not appear to be complete until about 600 °C. This is reflected in the slow tailing off of the DSC signals between 500-600 °C (Figures **4.15 b** and **4.15 c**).

Finally, there occur two separate exothermic events for Kao-PEG 3400 between 950-1050 °C (Figure **4.16**). These occur at 1010 °C and 1021 °C in air atmosphere with a small 1.0 % weight loss associated with these events (Figure **4.14**). In nitrogen atmosphere, the two exotherms were present at 1010 °C and 1025 °C, but a corresponding weight loss was less evident, and appeared simply as an extension of the negative sloping baseline. In contrast, kaolinite exhibits one sharp exothermic peak at 1003 °C, which has been attributed to a structural reorganization forming either mullite nuclei and spinel (Γ-Al_2O_3) or both [219-221].

It is evident that the intercalation of oxyethylene species into the interlamellar spaces of kaolinite has dramatically altered the decomposition sequence of kaolinite, in a manner which is very much different from other intercalates like Kao-DMSO and Kao-NMF. This is seen in the reduced temperatures of kaolinite dehydroxylation as well as the appearance of an additional exothermic peak between 950-1050 °C.

It is believed that the complete combustion of the oxyethylene species cannot occur once the structure has collapsed after the initial decomposition reactions before 400 °C. Structural collapse followed by the dehydroxylation of the kaolinite itself then causes the residual interlayer carbonaceous material to be trapped within a metakaolinite matrix. This is interesting since carbon-aluminosilicate nanocomposite materials may have some technological uses [107-109] (see Section **1.4.3**).

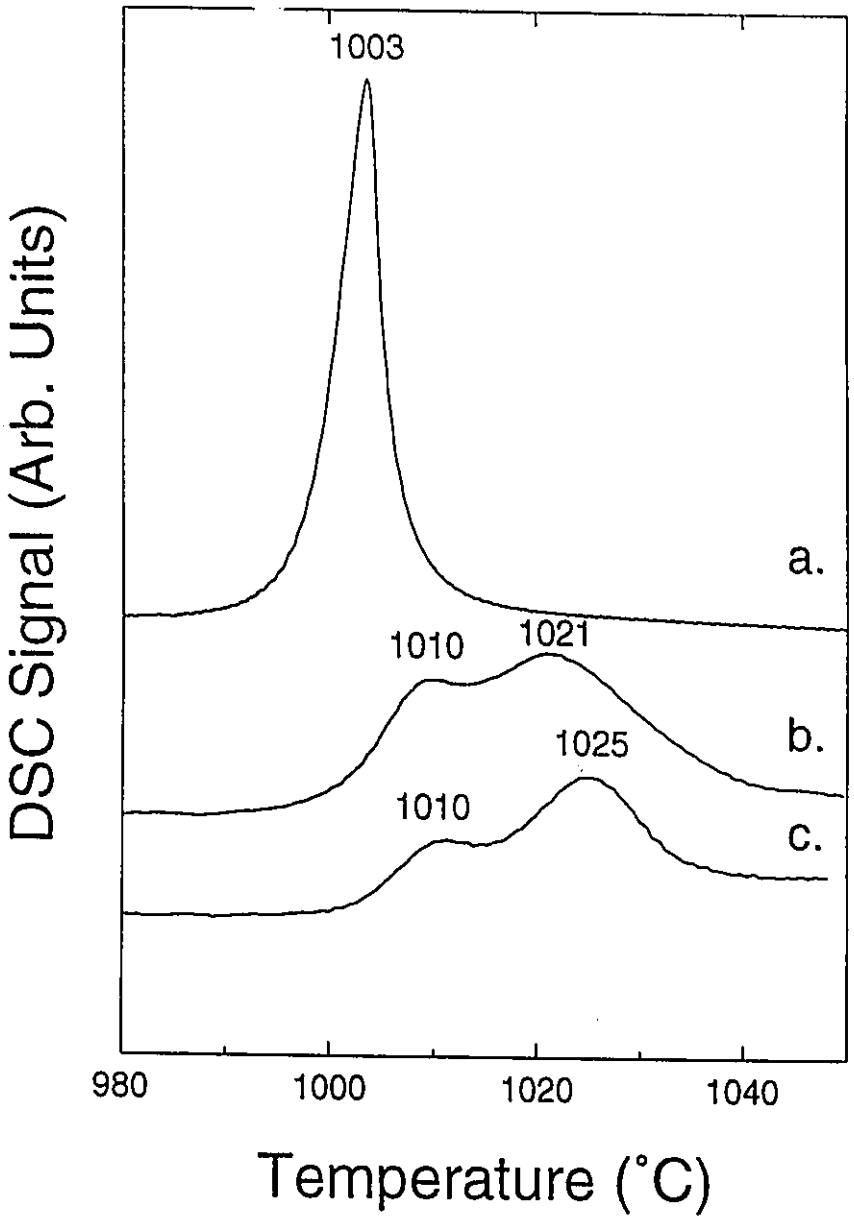

Figure 4.16: DSC traces (980-1050 °C) for Kaolinite (a); Kao-PEG 3400 **4-8-B** in air (b) and N_2 (c).

Some of this carbonaceous material may be released once the material undergoes structural reorganization between 1000-1030 °C. In air atmosphere, this is then combusted relatively fast and a weight loss is observed associated with a structural reorganization which normally should have no associated weight loss. In nitrogen atmosphere, combustion does not occur, so no sudden weight loss is observed, beyond the limits of the baseline drift. It is noteworthy, that for all of the nitrogen atmosphere TGA runs involving oxyethylene based organokaolinites, the colour of the product was black. Upon completion of the air atmosphere TGA runs, the products were greyish in colour.

4.3.6 Effects of Water Washing

The stability of some of the oxyethylene based organokaolinites was studied with respect to leaching with water. This stability is an indication of the strength of the host-guest interaction. Most intercalates of kaolinite, such as Kao-KOAc, Kao-hydrazine, Kao-DMSO and Kao-NMF may be leached out relatively easily by simply washing with water at room temperature [37,63,184]. Typically, a disordered collapsed kaolinite results from this leaching although "hole" water may sometimes be trapped in the interlayers [68,70]. It was found that it is sometimes possible to wash Kao-EG 10.8 Å with water to yield an 8.4 Å hydrate of kaolinite (see Section **3.2.4**). In contrast, some organokaolinites such as Kao-EG 9.4 Å were found to be highly resistant to leaching with water. For example, heating Kao-EG 9.4 Å with excess water in an autoclave at 200 °C for 72 hrs failed to fully collapse the structure (see Section **3.2.3**).

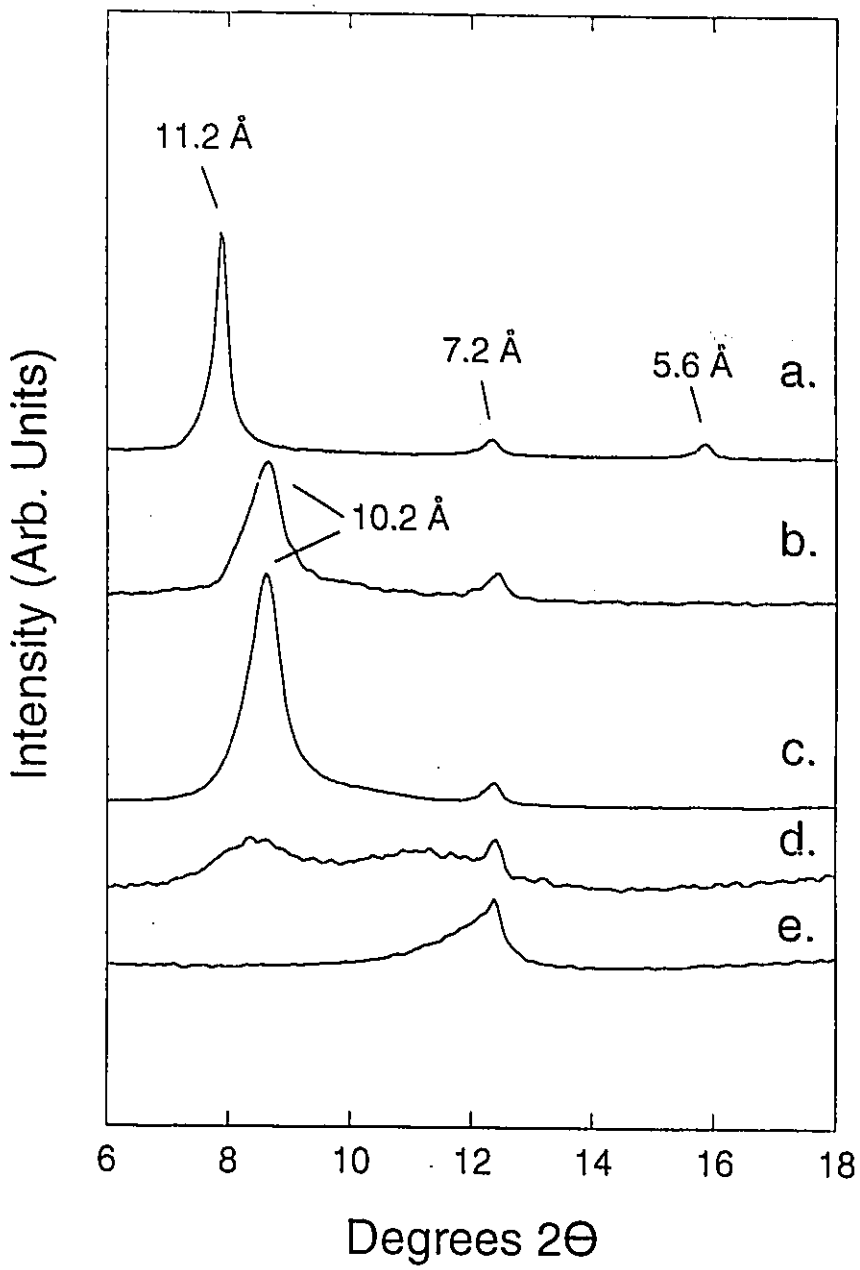

Figure 4.17: XRD patterns (6-18 °2Θ) for Kao-PEG 3400 **4-8-A** (**a**); (**a**) refluxed 40 hrs in excess water (**b**); (**b**) refluxed an additional 42 hrs in excess water (**c**); (**c**) heated at 180 °C for 20 hrs (**d**); (d) heated at 400 °C for 3 hrs (**e**).

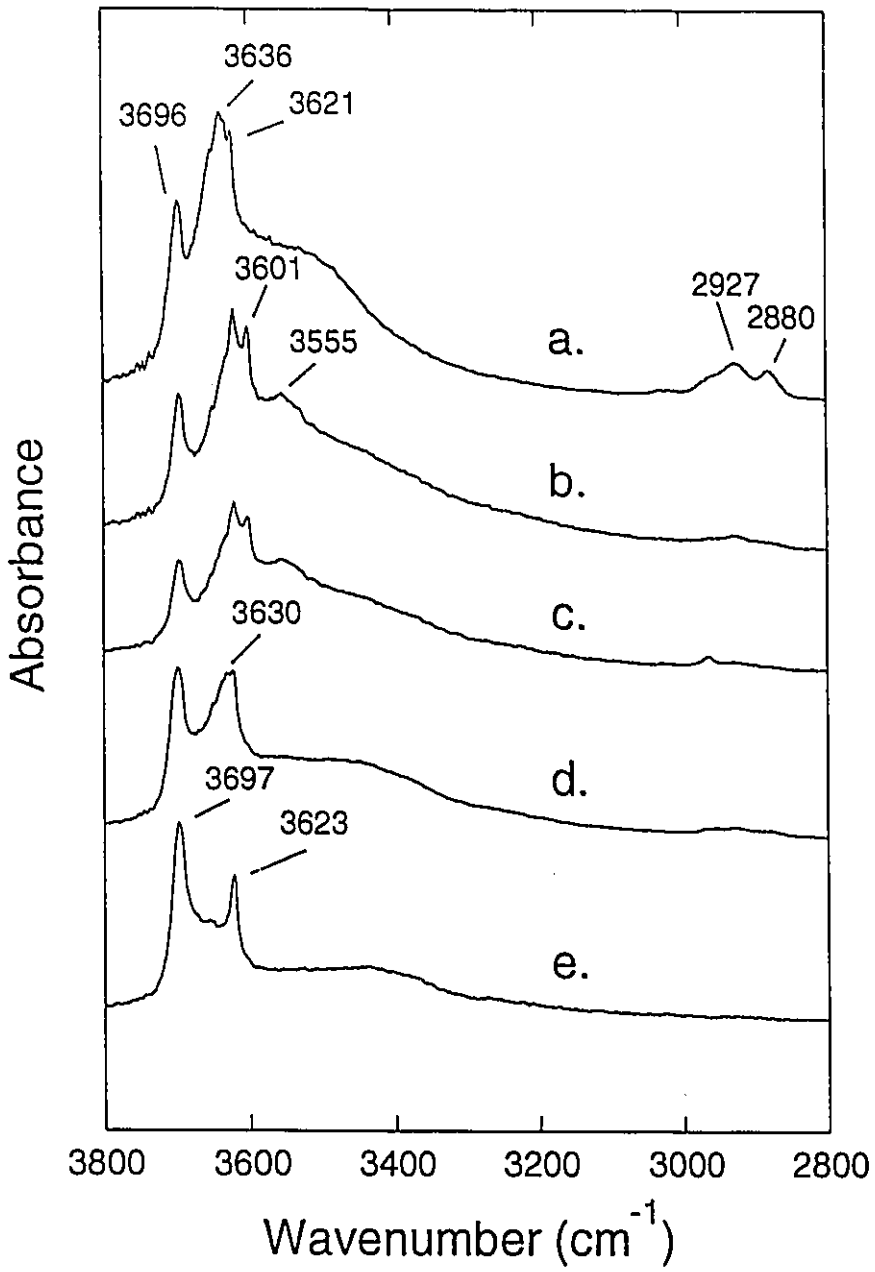

Figure 4.18: FTIR patterns (3800-2800 cm^{-1}) for Kao-PEG 3400 **4-8-A** (**a**); (**a**) refluxed 40 hrs in excess water (**b**); (**b**) refluxed an additional 42 hrs in excess water (**c**); (**c**) heated at 180 °C for 20 hrs (**d**); (**d**) heated at 400 °C for 3 hrs (**e**). Note: The relative absorbance scales of the spectra have been adjusted in order to facilitate comparison.

For Kao-PEG 3400, it was found that most of the interlayer organic material could be washed out through prolonged refluxing in water. The last traces were extremely resistant to water leaching, plausibly due to the collapse of some of the kaolinite layers along the crystal edges, with pockets of polymer encapsulated further within the interlayers. Once collapse occurs, the interlayers are inaccessible to water, and the polymers may not be washed out with water. For the most part however, removal of the organic material by water washing did not lead to the structural collapse to unexpanded kaolinite, but instead, a hydrate of kaolinite was formed with traces of the organic material still in the interlayers. This hydrate was stable with respect to heat treatment, and was very difficult to collapse back down to a 7.2 Å disordered kaolinite. All of this is illustrated in Figure **4.17**, which shows the effects of water leaching and thermal treatments on the XRD patterns (6-18 °2Θ) of Kao-PEG 3400. The corresponding IR patterns for the materials resulting from these treatments are shown in Figure **4.18**.

Upon refluxing 60 mg of Kao-PEG 3400 in 10 ml water for 40 hrs, The d_{001} reflection of Kao-PEG 3400 was shifted from d= 11.2 Å to d= 10.2 Å. A 10 Å d-spacing is consistent with the formation of a kaolinite dihydrate since Costanzo *et al.* have previously reported the preparation of a 10 Å synthetic dihydrate of kaolinite [66], and the related clay mineral halloysite often exists in nature as a 10 Å hydrated phase [37].

Infrared spectroscopy also confirms that a hydrate of kaolinite was formed when Kao-PEG 3400 was refluxed in water (Figure **4.18 b**). O-H stretching bands are present as sharp bands at 3696 cm^{-1} (m), 3620 cm^{-1} (s) and 3601 cm^{-1} (s) and a broader band at 3555 cm^{-1}. It also reveals significant traces of residual organic material in the interlayers of kaolinite as

shown by the presence of C-H stretching intensity at 2800-3000 cm^{-1}. The O-H stretching pattern of this hydrate is almost identical to that which was observed sometimes when Kao-EG 10.8 Å was washed with excess water to yield an 8.4 Å hydrate of kaolinite (Section **3.2.4**). It is thus surprising that for Kao-PEG 3400 leached with water, it is a 10.2 Å hydrate which is formed and not the 8.4 Å hydrate reported previously.

It should be noted that for the 8.4 Å hydrate formed from Kao-EG 10.8 Å, the product was somewhat disordered as seen from the broad d_{001} reflection, and the IR patterns which were obtained were not always reproducible. It was hypothesized that inhomogeneities in the bulk sample caused by inconsistent drying and insufficient mixing may have led to these phenomena. It is conceivable that some 10 Å hydrate phase may have been present with the 8.4 Å phase, and this was not detected in the XRD which is sensitive to long range ordering, but was detected in some of the IR samples which is sensitive to local effects and uses a much smaller sample size than was used for the XRD measurements. The FTIR spectra are remarkably similar in not only the O-H stretching pattern, but in the other regions as well. For example, in both cases, bands appear at 970 cm^{-1}, which is assigned to the bending deformation of inner surface Al-O-H groups hydrogen bound to interlayer water molecules [184].

Once the hydrate is formed, it is very difficult to fully collapse the structure. Even after heat treatment at 200 °C, the structure had not fully collapsed (Figure **4.17 d**). It was not until heating at 400 °C that the structure collapsed to a very disordered kaolinite (Figure **4.17 e**). IR confirmed that a disordered kaolinite type material was produced, with many of the characteristic lattice vibration bands still present. The signature O-H stretching pattern

of kaolinite was replaced with a pattern suggestive of a disordered kaolinite structure (Figure 4.18 e). Almost no residual C-H stretching intensity could be detected, presumably indicating that the residual organics had been combusted or pyrolysed at this temperature.

Kao-DiEG, Kao-TriEG and Kao-PEG 1000 also exhibited similar behaviour upon refluxing in excess water for 40-48 hrs (Table 4.4).

Sample	Before Water Treatment		After Water Treatment[1]	
	d_{001} (Å)	Int.Ratio[2]	d_{001} (Å)	I.R.[2]
Kao-DiEG **(4-2-B)**	10.74	0.98	10.14	0.95
Kao-TriEG **(4-3-B)**	10.79	0.95	10.30	0.75
Kao-TetraEG **(4-3-B)**	10.83	0.95	7.35[3]	-
Kao-PEG 1000 **(4-7-A)**	11.06	0.95	10.21	0.88
Kao-PEG 3400 **(4-8-A)**	11.18	0.96	10.23	0.90

Table 4.4: Summary of XRD results for the effects of refluxing in water for some oxyethylene based organokaolinites. (1) Water treatment consisted of refluxing 20-80 mg of the organokaolinite in 10-20 ml of water for 40-48 hrs, followed by a workup consisting of centrifugation, washing with water, centrifuging a second time and air drying on an XRD glass slide after dispersing the sample again in water; (2) intercalation ratio; (3) This peak overlaps with the d_{001} reflection of fully collapsed kaolinite at 7.2 Å.

Once again, the (001) XRD reflections were shifted to about 10 Å and the FTIR spectra all showed that hydrates had been formed with nearly identical patterns to those observed for the water leached Kao-PEG 3400 product (Figure **4.18 b**). O-H stretching bands were present at 3601 cm^{-1} (m), and 3555 cm^{-1} (m), the δ(HOH) band was at 1635 cm^{-1} (w) and an Al-O-H inner surface deformation band was found shifted to 968 cm^{-1} due the influence of hydrogen bonding with interlayer water. Residual organic molecules were shown to be present by the very weak C-H stretching and deformation bands.

Interestingly, Kao-TetraEG did not behave in the same manner as the other oxyethylene based organokaolinites. When Kao-TetraEG was refluxed in excess water for 48 hrs, and then allowed to dry, a 7.35 Å partial hydrate of kaolinite resulted. This was confirmed by IR which showed characteristic absorption bands at 3550 cm^{-1} (w) and 1655 cm^{-1} (vw) due to the presence of residual intercalated water. The other absorption bands were almost identical those of the fully collapsed kaolinite parent mineral. The reason for this difference in behaviour with respect to water leaching may be related to lower reaction temperature, which was used in the preparation of Kao-TetraEG from Kao-NMF (**4-4-A**), or perhaps to the presence of residual co-intercalated NMF in the interlayers which was absent in the other samples studied.

4.3.7 Structural Model for Kao-PEG

4.3.7.1 Chemical Formula

Kao-PEG 3400 (**4-8-A**) and Kao-PEG 1000 (**4-7-A**) were analyzed for % C and % H. This was performed at high temperature (> 1000 C) to ensure the complete combustion of the nanocomposite. The chemical formula for samples **4-7-A** and **4-8-A** were calculated based on the basis of the CP/MAS results and the calcination weight losses at 1100 °C for the samples. CP/MAS NMR (Section **4.2.4.2**) showed that the OEU/DMSO ratio for **4-7-A** and **4-8-A** were approximately 2.8 and 5.9 respectively, and the calcination weight losses were 29.1 and 29.4 % respectively (Table **4.3**). Using these data sample, the formula for sample **4-7-A** was estimated to be $Al_2Si_2O_5(OH)_4(-OCH_2CH_2-)_{0.767}(DMSO)_{0.274}$ and similarly sample **4-8-A** was estimated to be $Al_2Si_2O_5(OH)_4(-OCH_2CH_2-)_{0.985}(DMSO)_{0.167}$.

The calculated formula for both samples is consistent with one unit of oxyethylene or DMSO per $Al_2Si_2O_5(OH)_4$ unit. This stoichiometry is similar to that which one obtains for Kao-DMSO where TGA measurements indicate that for every $Al_2Si_2O_5(OH)_4$ unit there is close to 1.0 intercalated DMSO molecule [42,215].

If one wishes to know how much surface area, one $Al_2Si_2O_5(OH)_4$ unit provides for an intercalated oxyethylene unit, it is important to know the unit cell dimensions of kaolinite. Based on recently published unit cell dimensions [24], the surface area of one interlamellar face of one $Al_2Si_2O_5(OH)_4$ unit is calculated to be 23.0 $Å^2$. The approximate area, based on CPK models, that one side of a flattened oxyethylene unit occupies is about 14 $Å^2$, so it would

appear to a first approximation that there remains some void space in the interlamellar regions of kaolinite.

4.2.7.2 Polymer Conformation

The 3.9 Å expansion along the (001) direction due to the polymer incorporation is indicative of a flattened monolayer arrangement of the polymer chains in the interlamellar space. A schematic representation of this is given in Figure **4.19**. Similar layer expansions have been reported for polyethylene glycols incorporated into other layered structures. An expansion of 4.5 Å was observed for polyethylene oxide incorporated into V_2O_5 [193], and 2.8 Å for polyethylene glycol intercalated into α-zirconium phosphate [192].

The actual conformation that the polymer adopts with respect to the kaolinite host material is very difficult to ascertain. Intuitively, one expects the oxygens of the polymer chains to orient themselves such that they may hydrogen bond with the hydroxylated aluminate surface of kaolinite. Indeed, this is likely the main driving force for the intercalation reaction. In order to obtain maximum hydrogen-bonding interaction, it would also be useful for the polymer to adopt a conformation such that the oxygens of the polymer chain line up in a repeating manner so that they match up with the surface hydroxyl groups of the kaolinite. This means that the distances between oxygens in the polymer chain, be roughly comparable to the distances between hydroxyl groups in kaolinite. If one assumes that the interhydroxyl distance is fixed at about 2.8 Å based on the refined kaolinite

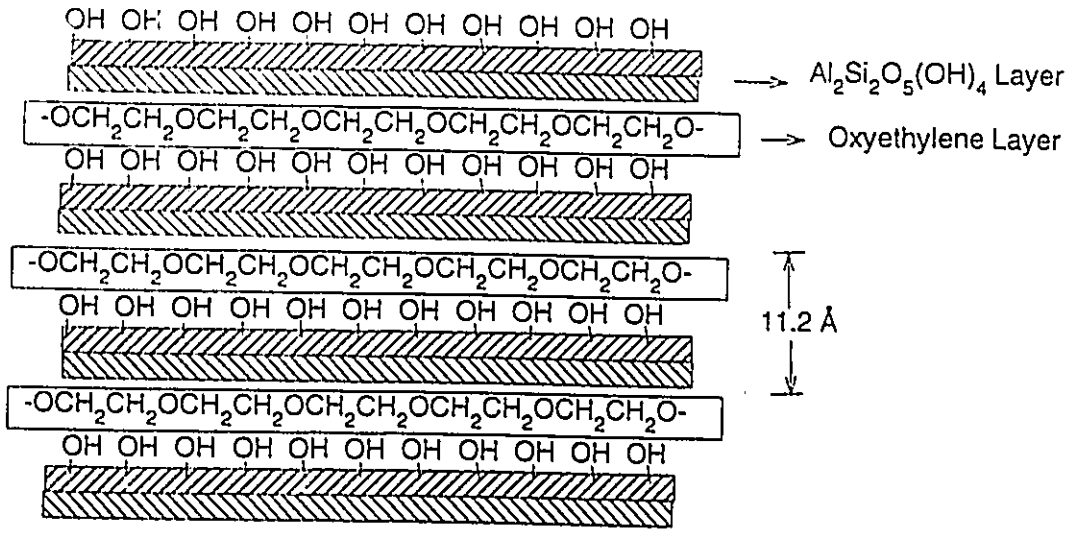

Figure 4.19: Schematic representation of an oxyethylene based organokaolinite nanocomposite material. The polyethylene oxide chains are intercalated in a flattened monolayer arrangenment.

structure[23], then it is expected that a polymer conformation where ethyleneoxy groups repeat every 2.8 Å with the oxygens all facing towards the hydroxyl surface would be particularly favourable. This type of polymer conformation has been described previously in a polyethylene oxide-$HgCl_2$ complex [222,223]. It has been given the designation PEO-$HgCl_2$ type II complex and has been found to be nearly in the form TG_2TG_2; that is:

$$\begin{array}{l} -\,CH_2\,-(-\,O\,-\,CH_2\,-\,CH_2\,-\,O\,-\,CH_2\,-\,CH_2\,-)_n- \\ \quad\;\; 167^\circ\;\; 81^\circ\;\; 73^\circ\;\; -167^\circ\;\; -81^\circ\;\; -73^\circ \end{array}$$

With this conformation, the repeat unit per oxyethylene group is 2.94 Å, and all the oxygens are lined up on one side of the chain. It is conceivable, that with a little more bending and twisting, it would be possible to obtain a decent fit for the kaolinite hydroxyl surface and the polymer chain.

4.3 Conclusion

It has been shown that it is possible to intercalate a wide array of molecules based on the oxyethylene unit (-CH_2CH_2O-) into the interlayers of kaolinite. These include the intercalation of simple oligomers of kaolinite such as diethylene glycol, triethylene glycol and tetraethylene glycol, but also extends to include the much larger molecules PEG 1000 and PEG 3400. Preliminary results also show that the intercalation of two crown ethers, 18-crown-6 and 15-crown-5 was also achieved. A complicating feature for many of the products was the presence of residual DMSO and NMF in the interlayers. This was especially evident for the organokaolinite products obtained when a large excess of the oxyethylene species was not used. This was the case for Kao-18C6, Kao-15C5 and Kao-PEG 1000 and Kao-PEG 3400.

A common unifying feature for all of the oxyethylene based organokaolinites studied, was the similarity of the XRD and IR patterns for all of these materials. XRD shows that all of the intercalated oxyethylene species were arranged in a flattened monolayer arrangement, such that the interlayer expansion was between 3.6 Å and 4.0 Å. Infrared analysis of Kao-

PEG 3400 supported the assignment of a trans conformation to at least a portion of the ($O\text{-}CH_2CH_2\text{-}O$) groups of the PEG polymer while ^{13}C DD/MAS NMR suggested that the polymer was intercalated intact and was more constrained in the interlamellar spaces of kaolinite than it was in its bulk form. ^{13}C CP/MAS results for products obtained by the intercalation of smaller oxyethylene molecules such as EG, DiEG and TriEG, were consistent with an intercalation process which does not include the condensation of the end alcohol groups to yield a long chain polymer intercalated into kaolinite.

Water leaching experiments confirmed that most of the interlayer oxyethylene species, may be washed by refluxing in water, although it was very difficult to remove the last traces of polymer from the interlayers. In many instances water refluxing of the oxyethylene based organokaolinites led to the formation of a 10 Å dihydrate of kaolinite with residual amounts of organic oxyethylene material trapped in the interlayers. This was difficult to collapse to the completely anhydrous kaolinite.

TGA/DSC analysis revealed that the complete decomposition of the organic component of the oxyethylene based organokaolinites did not occur until greater than 1000 °C. For all of the oxyethylene based organokaolinites analyzed, a small weight loss was observed for the air atmosphere TGA/DSC runs associated with the two exothermic transitions between 990 and 1040 °C. This was not evident for the N_2 atmosphere runs. This weight loss was thought to be the result of the release of carbonaceous material trapped within a metakaolinite matrix during the structural reorganization of metakaolinite which takes place above 1000 °C.

Especially studied was the Kao-PEG product obtained from the reaction of Kao-DMSO or Kao-NMF with polyethylene glycol MW 1000 and MW 3400. This represents the first example of the direct intercalation of a polymer into the interlamellar surface of kaolinite, and this material may prove to have interesting intercalation properties, since both kaolinite and PEO are known to intercalate various alkali salts. A Kao-PEG salt complex would represent a second generation nanocomposite material, whereby within the rigid inorganic kaolinite lattices, the intercalated PEG polymer could in turn aid in the complexation of the salt. This material would then be a suitable candidate to act as an anisotropic solid electrolytic material. Materials derived from the intercalation of crown ether into the structure of kaolinite may also fulfil this role.

Chapter 5

Exploratory Work on the Preparation of Other Types of Organokaolinites

5.1 Introduction

In Chapters 2 and 3 it was shown that it is possible to rigidly fix small alcohol moieties onto the interlamellar surface of kaolinite, most likely through the grafting reaction of the alcohol group to the Al-O-H surface of the kaolinite. The kaolinite-diol system was especially studied. These materials are interesting in that they are true organomineral composites where the organic units are covalently attached to the inorganic substrate in an ordered stacking of organomineral layers. It would be of interest to expand this chemistry to include other systems than just the alcohol/diol organokaolinite system. It may be possible for example, to attach an organic unit which would contain a pendant functionality which may then be used to attach another reactant molecule. One may thus envisage rationally assembling sophisticated anisotropic organomineral materials based on asymmetric kaolinite layers.

With the diol based organokaolinites, the interlayer cohesive forces for these new materials prevented easy layer swelling. This was presumably due to the strong hydrogen bonding between the pendant hydroxyl groups of the diols and the silicate surface of the kaolinite layers. As a result, even though the alcohol functionality of the diol unit offers an attractive site for further interlayer modification reactions, it is inaccessible to attacking

species. Other types of organokaolinites, preferably with weaker interlayer cohesion and consequently greater swelling properties are required if one wishes to use them as the first step in the development of more sophisticated structures.

This was the rationale for exploring new types of kaolinite modification reactions beyond those involving molecules with only alcohol and ether functionalities. In this chapter, the modification reactions involving a wide range of reactant species are investigated. Specifically, modification with amines (section **5.2.1**), carboxylic acid derivatives (section **5.2.2**) and other reactants (**5.2.3**) are examined.

5.2 Results and Discussion

5.2.1 Amino Functionalized Organokaolinites (Kao-EOA)

Part of the appeal in attaching molecules with pendant amine groups in the interlayer space of kaolinite lies with the possibility of using the free amine group to attach larger molecules to the interlayer surface kaolinite. Amines are chemically reactive and would, for example, provide an ideal site for the attachment of a carbonyl functionalized molecule (R1-C=O) to the amino functionalized interlayer surface of kaolinite ($\equiv$Al-O-R2-NH_2) via an $\equiv$Al-O-R2-N=C-R1 linkage obtained through a condensation reaction.

Organokaolinites with organic guests possessing amino groups have been previously reported. One of the most commonly used organokaolinite intercalates is kaolinite-hydrazine (Kao-Hz) [36,51-53,56]. This material is easily prepared with reaction kinetics which are typically

much faster than those of Kao-DMSO or Kao-NMF. Kao-Hz is much less stable than either Kao-DMSO or Kao-NMF, decomposing in ambient conditions within less than an hour. This ease of formation and inherent instability is used to advantage as an intermediate in the preparation of other organokaolinites via the displacement method [56,224,225]. The fact that hydrazine does intercalate into kaolinite is an indication that there exists some affinity of kaolinite for the amino group, and it should be possible to prepare other amino based organokaolinites. Recently, Inoue *et al* have prepared a series of aminoalcohol based organoboehmite materials in which they proposed that the organic units were attached to the boehmite via Al-O-$(CH_2)_nNH_2$ bonds [157]. This suggests that it may be possible to do the same for kaolinite.

5.2.1.1 Preparation

A series of amines were reacted with Kao-DMSO and Kao-NMF (Table 5.1). These included the aminoalcohols ethanolamine (EOA) and 3-amino-1-propanol (3,1 AP) which formed new organokaolinite intercalates. The reactions involving ethylene diamine (**5-1-5**), DL-1-amino-2-propanol (**5-1-7**) and nitroaniline (**5-1-8**) were unsuccessful and yielded only collapsed unmodified kaolinite and Kao-DMSO starting material.

For Kao-3,1 AP (**5-1-6**), the modified phase had a basal spacing of 11.1 Å, and the intercalation ratio (I.R.) was only 0.58. IR results for this material definitely show that the Kao-DMSO starting material has been altered, and one observes bands attributable to the 3-amino-1-propanol guest species. For example faint ν(NH) bands were detected at 3426 cm^{-1}

(vw), 3364 cm^{-1} (vw), ν(CH) bands at 2941 cm^{-1} (w) and 2878 cm^{-1} (w), and deformation bands at 1574 cm^{-1} (w), 1482 cm^{-1} (w) and 1322 cm^{-1}. The fact that 3-amino-1-propanol formed an intercalate with kaolinite whereas DL-1-amino-2-propanol did not, may be due to the higher reaction temperature for Kao-3,1 AP formation (187 °C vs 160 °C), which permitted a more rapid diffusion of 3-amino-1-propanol into the interlayers of kaolinite before structural collapse could occur. Alternately, the presence of an end methyl group in 1-amino-2-propanol may have also made interlayer diffusion more difficult and contributed to a weaker host-guest interaction.

Starting Material	Reactant	Rxn Code[1]	Basal Spacing[2] (Å)	I.R.[3]
Kao-DMSO	Ethanolamine	**5-1-1**	10.7	0.98
Kao-NMF	Ethanolamine	**5-1-2**	10.5	0.96
Kaolinite	Ethanolamine	**5-1-3**	NR	
Hal-DMSO	Ethanolamine	**5-1-4**	10.6	1.0
Kao-DMSO	Ethylene Diamine	**5-1-5**	NR	
Kao-DMSO	3-Amino-1-Propanol	**5-1-6**	11.1	0.58
Kao-DMSO	DL-1-Amino-2-Propanol	**5-1-7**	NR	
Kao-DMSO	Nitroaniline	**5-1-8**	NR	

Table 5.1: Summary of the organokaolinite products formed from the treatment of amines with kaolinite. (1) see Section **6.8.1** for reaction details and characterizations; (2) This refers to the basal spacing of the principal modified product phase; (3) Intercalation ratio.

It is surprising that ethylene diamine was unable to form an organokaolinite product via the displacement of DMSO in view of the fact that ethylene diamine may intercalate into halloysite, to form an 11.7 Å intercalation complex [33,34]. Reaction with para-nitroaniline was also unsuccessful, presumably due to the hydrophobic nature of para-nitroaniline and the weaker basicity of paranitroaniline compared to primary amines, which would adversely affect the hydrogen bonding interactions with the kaolinite host.

Clearly, the greatest success was achieved using ethanolamine as the reactant, and this product (Kao-EOA) will be examined is some detail. It was possible to form nearly identical Kao-EOA products from both Kao-DMSO (**5-1-1**) and Kao-NMF (**5-1-2**) starting materials but not from unexpanded kaolinite (**5-1-3**). This indicates that the intercalating agent (DMSO or NMF) which was used to provide access to the interlamellar space of kaolinite plays a passive role and is not involved in the actual chemical reaction between ethanolamine and the interlamellar surface of kaolinite. DMSO and NMF are required only to pry open the clay layers.

The Kao-EOA product exhibited a remarkable crystallinity as exhibited by the strong reflections of the XRD pattern (Figure **5.1**). The main product had a basal spacing of 10.67 Å. This product was found to be stable with respect to vacuum drying over phosphorus pentoxide for 24 hrs at 25 °C, but was unstable when washed with water overnight, reverting slowly back to the parent kaolinite 7.2 Å phase.

It was also possible to form the halloysite analogue of Kao-EOA (Hal-EOA), by reacting Hal-DMSO with ethanolamine (**5-1-4**). These materials exhibited similar basal spacings and IR patterns. Hal-EOA was much less crystalline than Kao-EOA, as evidenced

by the very broad diffraction peaks. This was presumably due to the turbostratic nature of halloysite and Hal-EOA compared to kaolinite and Kao-EOA. No residual unexpanded parent mineral could be detected for the Hal-EOA, so it appears that 100 % modification was achieved. This was not the case for Kao-EOA, where a reflection at 7.2 Å representing 1.5 % relative intensity indicates the presence of a small amount residual unexpanded kaolinite.

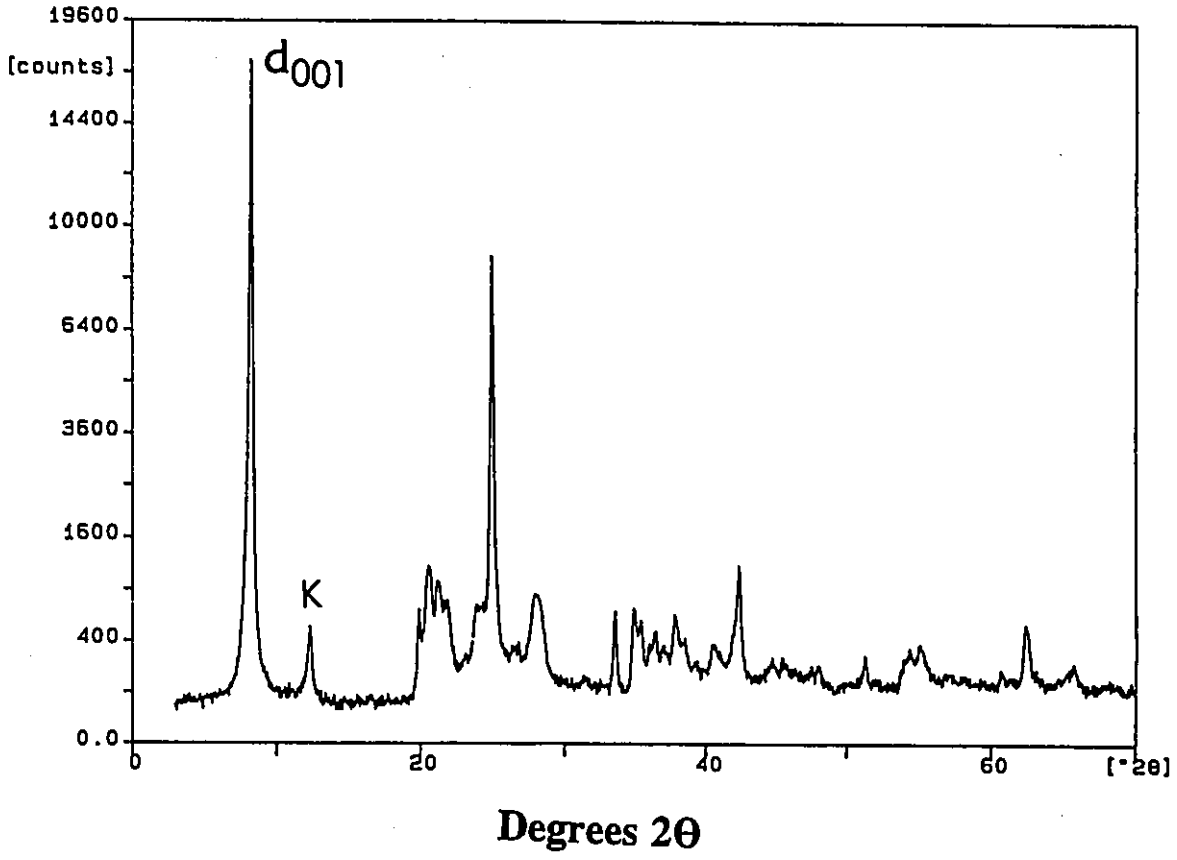

Figure 5.1: XRD pattern for Kao-EOA (2-70 °2θ). (K) indicates residual kaolinite.

An ethanolamine derivative (intercalate or otherwise) of kaolinite has never been reported in the literature. Ethanolamine has however been reported intercalated in halloysite[34]. In this example a material with a basal spacing of 10.7 Å was reported, which is similar to what is reported here (**5-1-4**). This corresponded to a layer expansion of 3.5 Å which is less than the 4.0 Å minimum clearance space which was calculated for ethanolamine. This is in accord with many other intercalates which show a smaller than expected basal spacing due to some keying in of the guest (see Chapter 2).

5.2.1.2 IR Analysis

The IR patterns of Hal-EOA and Kao-EOA were nearly identical with both materials showing strong evidence of modification of the respective host minerals. In particular, the O-H stretching region was greatly perturbed and additional N-H stretching bands could be seen due to the ethanolamine units (Figure **5.2**). The ν(OH) bands of kaolinite normally found at 3695 cm^{-1}, 3670 cm^{-1}, 3652 cm^{-1} and 3620 cm^{-1} have been replaced by bands at 3693 cm^{-1}, 3628 cm^{-1}, 3558 cm^{-1} and 3486 cm^{-1} for Kao-EOA. These last two bands represent significant red shifts, indicating the effects of increased hydrogen bonding between the kaolinite host and ethanolamine guest.

The inner hydroxyl kaolinite peak at 3620 cm^{-1} peak has been blue shifted to 3628 cm^{-1}. A similar blue shift phenomena for an evacuated (0.01 torr) hydrazine intercalated kaolinite has previously been attributed to keying of the $-NH_2$ moiety of hydrazine into the siloxane ditrigonal cavity of kaolinite [53]. A partial collapse of the hydrazine intercalate from

10.4 Å to 9.6 Å was associated with this phenomena. This 8 cm^{-1} shift of the inner hydroxyl V(OH) band, therefore provides strong evidence for the keying in of the $-NH_2$ group of ethanolamine into the $(Si\text{-}O\text{-})_6$ macroring of kaolinite.

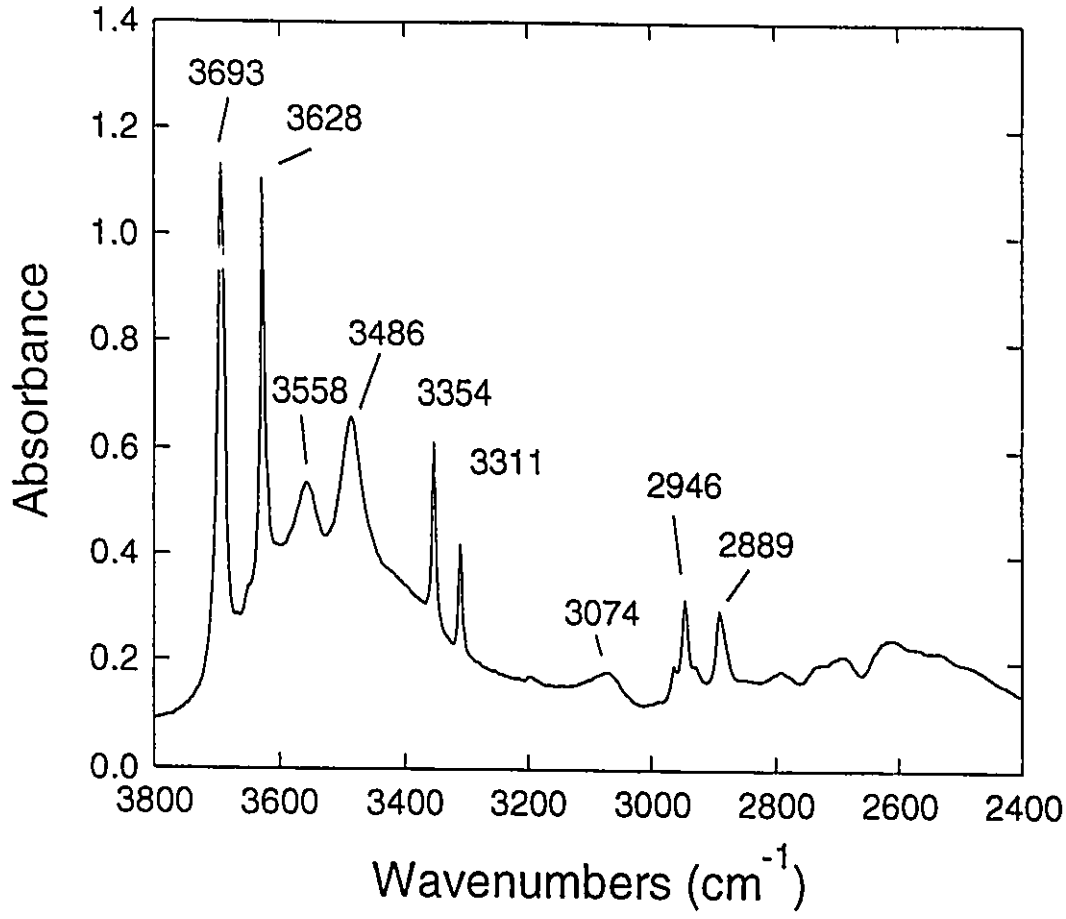

Figure 5.2: IR spectra of Kao-EOA (3800-2400 cm^{-1}).

In addition to the O-H stretching region, further evidence for ethanolamine modification includes the presence of two sharp N-H stretching bands at 3354 cm^{-1} and 3311 cm^{-1}. The position of these bands indicate that the amino group is experiencing hydrogen bonding. In addition, one observes C-H stretching bands at 2946 cm^{-1} and 2889 cm^{-1} (Figure **5.2**), which may be attributed to the intercalated ethanolamine unit.

In the deformation region (Figure **5.3**), an NH bending band at 1613 cm^{-1}, a δ(CH) band at 1476 cm^{-1}, and a C-N stretching band at 1353 cm^{-1} could all be observed.

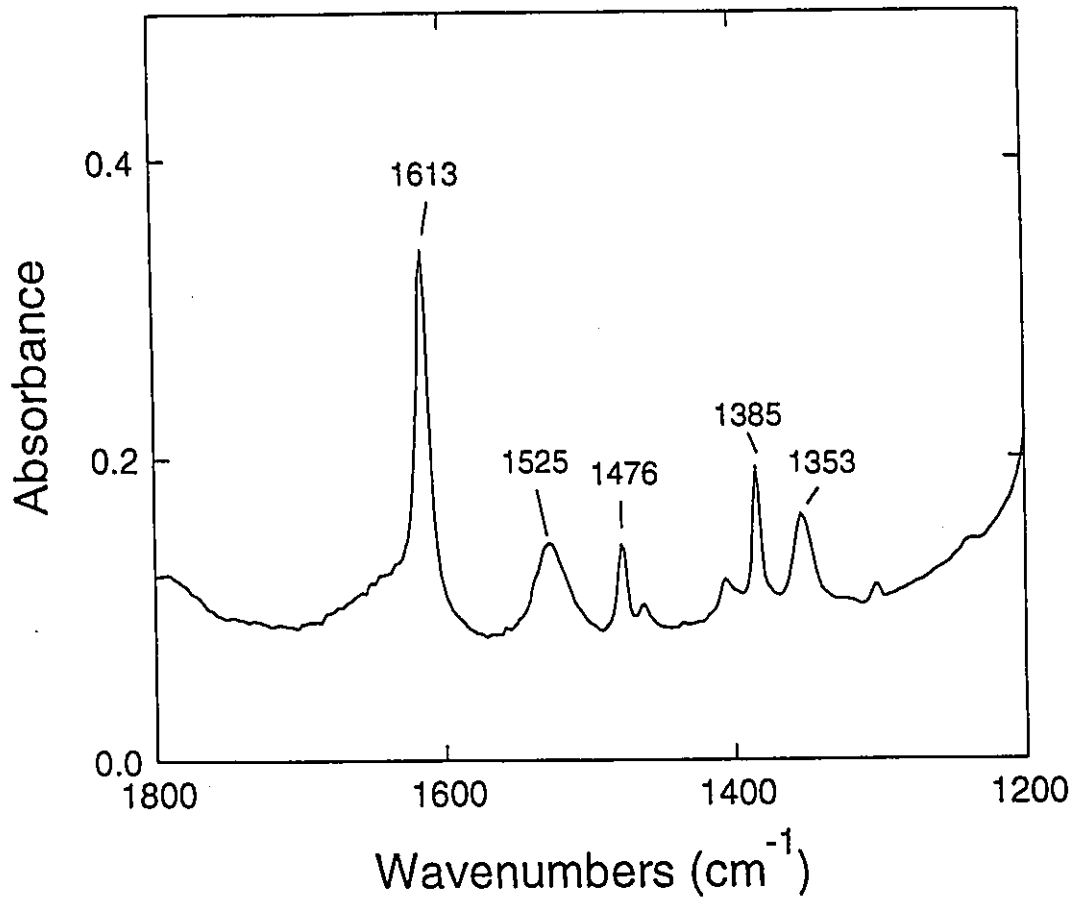

Figure 5.3: IR spectra of Kao-EOA (1800-1200 cm^{-1}).

The kaolinite host material also showed signs of perturbation in the lattice vibrations region (Figure **5.4**). The very strong in-plane Si-O-Si stretching vibrations of kaolinite at 1010 cm^{-1} and 1033 cm^{-1} [26] are shifted to higher frequencies in Kao-EOA to 1016 cm^{-1} and 1045 cm^{-1}. The δ(Al-OH) band of the inner hydroxyl of kaolinite is shifted from 915 cm^{-1} to 908 cm^{-1}, and the δ(Al-OH) band of the inner surface kaolinite hydroxyls is replaced by a band at 974 cm^{-1}. All this indicates strong host-guest interactions between kaolinite and the ethanolamine moiety.

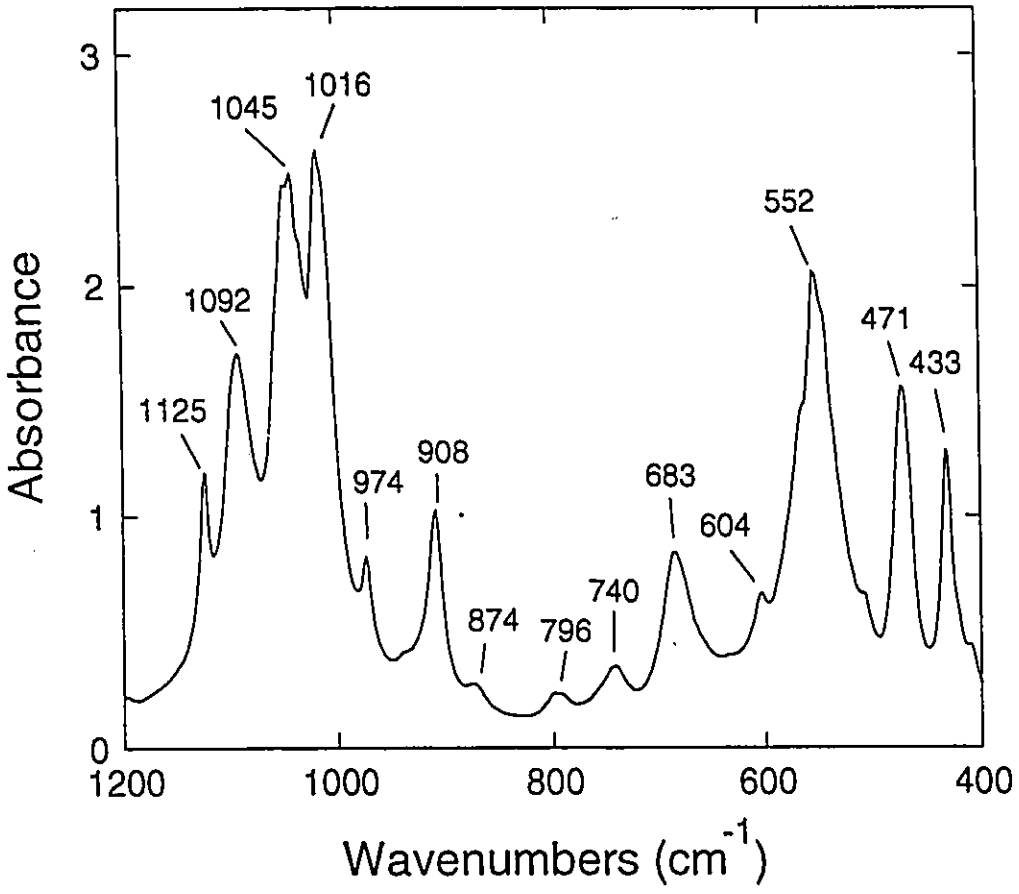

Figure 5.4: IR spectra of Kao-EOA (1200-400 cm^{-1}).

5.2.1.3 ^{13}C NMR Analysis

The solid state ^{13}C CP/MAS NMR (45.3 MHz) showed two broad resonances, one at 43 ppm and the other at 60.5 ppm corresponding respectively to the ^{13}C-NH_2 carbon and the ^{13}C-O- carbon of the ethanolamine unit. This was consistent with the insertion of the ethanolamine units in the interlayers of kaolinite. A dipolar dephasing experiment (40 μs interrupted decoupling) showed that no signal could be detected after 200 scans. This indicated that the ethanolamine species is very rigid on the ^{13}C NMR timescale. This is consistent with the existence of a rigidly bound ethanolamine unit, plausibly grafted to the aluminate interlamellar surface via $\equiv$Al-O-CH_2CH_2-NH_2 linkages.

5.2.1.4 Thermogravimetric Analysis

Thermal Analysis of Kao-EOA shows that decomposition does not occur until about 150 °C, and then there appears to be a three step decomposition ending at 600 °C (Figure 5.5). The total calcination weight loss after heating to 1100 °C in air for 3 hours is 27.5 %. Hal-EOA differs from Kao-EOA in that there is a preliminary decomposition step (7.6 % weight loss) beginning almost immediately upon heating (Section **6.8.1.4**).

The thermal decomposition in nitrogen between 150 °C to 600 °C is characterized by endothermic peaks at 225 °C, 377 °C and 503 °C (Figure **5.6 a**). The peaks at 225 °C and 377 °C are assigned to the endothermic pyrolysis of the interlayer organic material, and the peak at 503 °C is assigned to the dehydroxylation of the kaolinite host. In air atmosphere

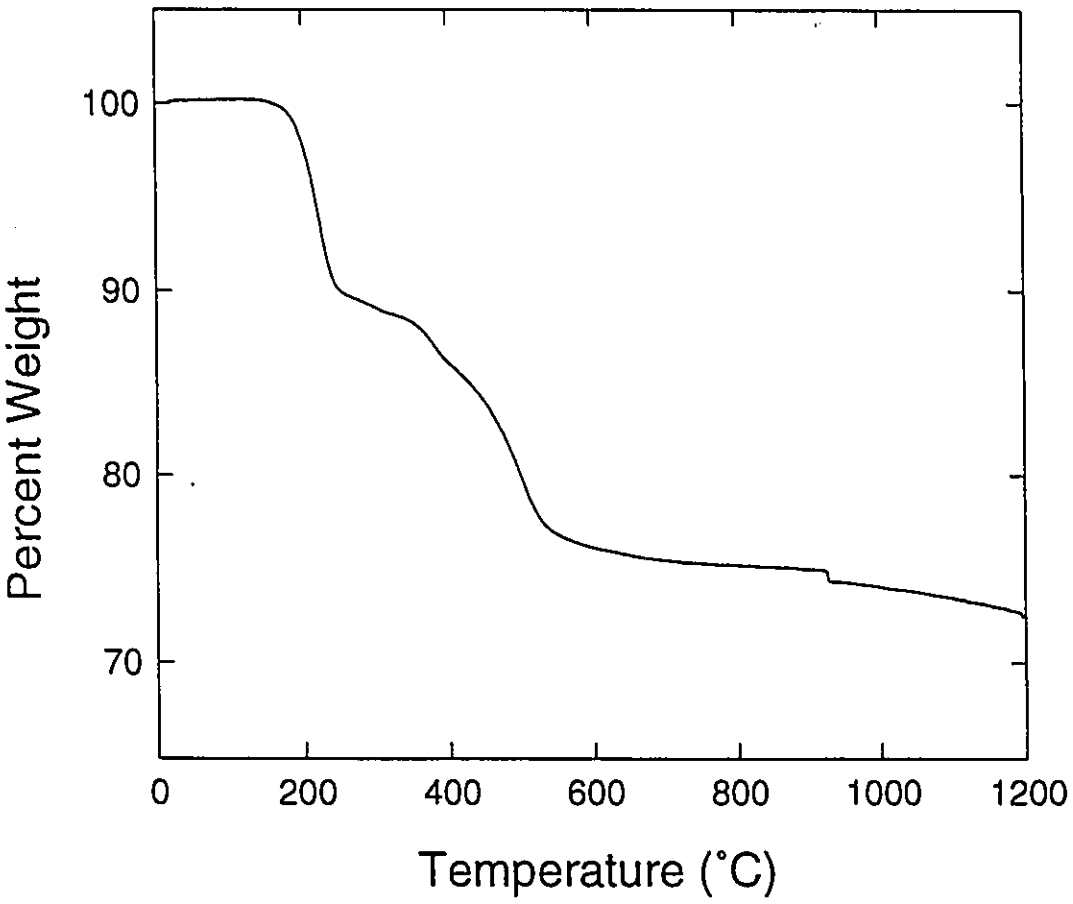

Figure 5.5: TGA run (20-1200 °C) for Kao-EOA in N_2 atmosphere (40 cm^3/min).

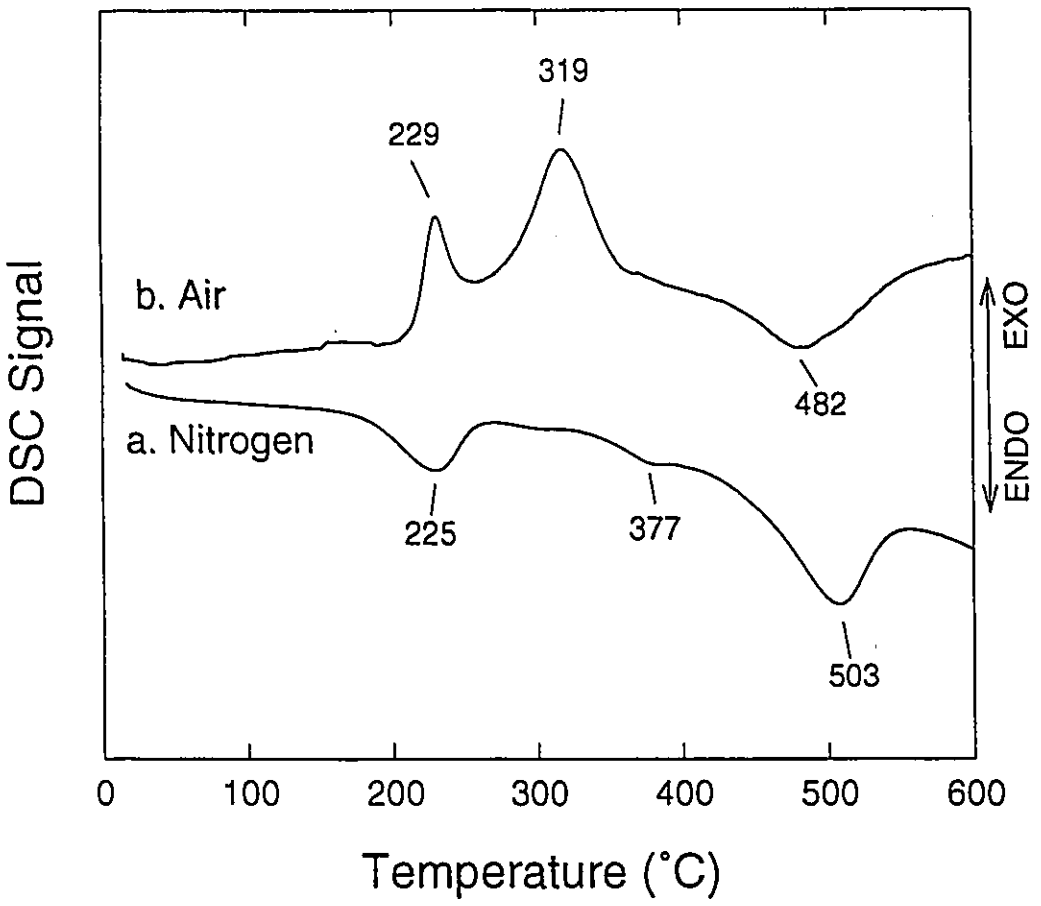

Figure 5.6: DSC run for Kao-EOA in nitrogen (a) and air (b) atmospheres.

(Figure **5.6 b**), one observes an endothermic peak at 482 °C assigned to the dehydroxylation of the kaolinite host material. However, instead of two endothermic events corresponding to the decomposition of interlayer organic material, one sees two exotherms with peaks at 229 °C and 319 °C. These exotherms are assigned to the exothermic combustion of the interlayer organic material. When the TGA/DSC run was done in air atmosphere, the product after heating to 1100 °C was white, indicating that complete combustion of the interlayer organic material had occurred.

Based on elemental analysis of Kao-EOA, one can assign the following approximate formula: $Al_2Si_2O_5(OH)_{3.0}(OCH_2CH_2NH_2)_{1.0}$ (%C: calc. 7.97, found 8.16; %N: calc. 4.65, found 4.12; %H: calc. 2.99, found 2.72; calcination wt. loss (%): calc. 26.2, found 27.5). Here one assumes that grafting has occurred via the condensation reaction of the alcohol group of the ethanolamine with the interlamellar Al-O-H groups of kaolinite. This is consistent with the model for the aminoalcohol derivatized organoboehmites of Inoue *et al*[157]. Here, there exists one ethanolamine unit per $Al_2Si_2O_5(OH)_4$ structural unit of kaolinite, which would allow each amino group to key into one $(Si\text{-}O\text{-})_6$ macroring of the silicate surface of the adjacent layer. Alternately, if one were to consider an ethanolamine unit which is intercalated into the interlamellar surface of kaolinite without grafting one could assign a chemical formula of $Al_2Si_2O_5(OH)_4.(CH_2OHCH_2NH_2)_{1.0}$ (%C: calc. 7.52, found 8.16; %N: calc. 4.39, found 4.12; %H: calc. 3.45, found 2.72, calcination wt. loss (%): calc. 30.4, found 27.5). The large discrepancy between the calculated (3.45 %) and found (2.72 %) values for the %H of this last assignment would seem to indicate that the chemical formula

based on the grafting of ethanolamine units ($Al_2Si_2O_5(OH)_{3.0}(OCH_2CH_2NH_2)_{1.0}$) is a better representation of the structure.

5.2.1.5 Structural Model

The model which best fits all of the characterization data is that of an organokaolinite material where ethanolamine units are attached to the aluminate interlamellar surface of kaolinite via $\equiv$Al-O-$CH_2CH_2NH_2$ covalent linkages, in much the same way that was proposed by Inoue *et al* for aminoalcohol based organoboehmites [157]. Only, in the organokaolinite case, the pendant NH_2 group is keyed into the $(SiO\text{-})_6$ macroring of the adjacent silicate surface. This model explains both the rigidity of the ethanolamine units (^{13}C CP/MAS NMR results) and the thermal stability of Kao-EOA. Elemental analysis and IR are also consistent with this structure.

Regarding Hal-EOA, the short range structure of this intercalate appears to be quite similar to Kao-EOA judging from the similarity in the IR patterns of the two products. The long range ordering as evident from XRD, indicates that Hal-EOA is arranged in a turbostratic manner whereas Kao-EOA appears to have some three dimensional ordering. This is what might be expected on the basis that the parent materials show this same difference in long range ordering.

5.2.2 Functionalization of Kaolinite with Carboxylic Acid Derivatives

The purpose of this work was to extend the type of interlayer surface reactions in kaolinite to include other surface grafting methods beyond the alcohol condensation reactions. For carboxylic acids (RCOOH), it was believed that under appropriate conditions, it would be possible to functionalize the aluminate surface of kaolinite via surface ester linkage ($\equiv$Al-O_2CR), with water being a reaction product. Acid chlorides (RCOCl) could react with surface aluminol groups in a similar way to yield $\equiv$Al-O_2CR linkages with HCl being a reaction product.

Recent work involving alumoxanes has shown that it is possible to create carboxylate derivatives of alumoxanes with Al-O_2CR linkages [226-230]. For example the reaction of boehmite with carboxylic acids was found to give alumoxanes with the following formula: $[Al(O)_x(OH)_y(O_2CR)_z]_n$ where $2x + y + z = 3$ and R= C1-C13 [226,230]. This work suggests that a similar type of reactivity may be expected from kaolinite, and some exploratory work concerning the reactions of carboxylic acid derivatives with kaolinite is outlined in the following section.

5.2.2.1 Reactions with Acetic Acid

The reaction of kaolinite with a variety of carboxylic acid derivatives was attempted, and these are summarized in Table 5.2. The modification of Kao-DMSO (5-2-1) and Kao-NMF (5-2-2) with acetic acid at high temperatures (approximately 200 °C) in an autoclave

Starting Material	Reactant	Rxn Code[1]	Basal Spacing[2] (Å)	Relative Intensity[3]
Kao-DMSO	Acetic Acid	**5-2-1**	10.2 9.5 7.0[4] 6.2	46 100 28 83
Kao-NMF	Acetic Acid	**5-2-2**	9.4 7.0[4] 6.2	6 20 100
Kaolinite	Acetic Acid	**5-2-3**	7.2[4]	100
Kao-DMSO	Chloroacetyl Chloride	**5-2-4**	11.2 9.5 7.2[4]	100 (sh) 11
Kao-DMSO	Acetyl Chloride	**5-2-5**	8.6 7.2[4]	100 16
Kao-DMSO	Propionic Acid	**5-2-6**	11.0 7.2[4]	100 4
Kao-NMF	Propionic Acid	**5-2-7**	7.2[4]	100
Kao-DMSO	Propionyl Chloride	**5-2-8**	11.4 7.2[4]	100 7

Table 5.2: Summary of the organokaolinite products formed from the treatment of carboxylic acid derivatives with kaolinite. (1) see Section **6.8.2** for reaction details and characterizations; (2) This refers to the basal spacing of the principal modified product phases at low diffraction angle (between 2 and 16 °2Θ); (3) The peak intensities were normalized such that the most intense peak was set to 100; (4) unexpanded kaolinite.

led to the removal of the DMSO and NMF swelling agents and the modification of the kaolinite host material. In contrast, no modification was achieved when unexpanded kaolinite was directly reacted with acetic acid at 200 °C (**5-2-3**). This shows that pre-swelling of the kaolinite layers is necessary in order for modification to occur.

The products of reaction **5-2-1** (Kao-HOAc-1) and **5-2-2** (Kao-HOAc-2) were found to differ considerably. Four XRD peaks were observed for Kao-HOAc-1 between 2-16 °2Θ. the peak at d= 10.2 Å appeared as a shoulder of the most intense peak at d= 9.5 Å. This 10.2 Å peak disappeared when washed with water (see section **6.8.2.1**). It is thought that this peak indicates the presence of an intercalated acetic acid phase whereas the peak at 9.5 Å is the acetic acid functionalized phase. The assignment of the 9.5 Å reflection was also supported by the observation of a d_{002} reflection at 4.77 Å which is consistent with the formation of a layered organokaolinite. Water washing would plausibly serve to remove intercalated acetic acid but not grafted acetic acid in much the same way that was observed for the two ethylene glycol phases of kaolinite (see Chapter 3). It is noteworthy that an 11.6 Å halloysite-acetic acid intercalation complex has been reported by Carr and Chih [34]. The large basal spacing of this acetic acid based organohalloysite compared to the 9.5 Å basal spacing of Kao-HOAc suggests that the acetic acid units in these organominerals are in different states. The XRD peak at 7.0 Å is assigned to unexpanded kaolinite, and the peak at 6.2 Å is due to an unknown phase.

For Kao-HOAc-2, one does not observe a phase at 10.2 Å and one sees instead a weak reflection at 9.5 Å assigned once again to the acetic acid modified phase of kaolinite. A residual kaolinite peak at 7.0 Å was observed and the strongest reflection was the

reflection at 6.2 Å. The differences in the relative intensities of all the XRD reflections compared to Kao-HOAc-1 may be due to the longer reaction time employed for the preparation of Kao-HOAc-2 (23 hours versus 70 hours). Longer reaction times appear to favour the formation of the 6.2 Å phase.

The nature of the 6.2 Å phase is unknown, although it was initially believed that boehmite (AlOOH) may be responsible for this reflection since it is characterized by a basal spacing of 6.1 Å [231] and is in equilibrium with kaolinite under hydrothermal conditions [232]. This notion was refuted by the IR results which showed no ν(OH) absorption bands at 3295 cm^{-1} and 3092 cm^{-1} which are indicative of boehmite [233,234]. Moreover, it was found that upon prolonged water washing (5 days), the peak at 6.2 Å slowly disappeared, suggesting that the phase responsible for this reflection was water soluble. Boehmite should not exhibit this type of solubility behaviour. The 6.2 Å unidentified phase is therefore assumed to be a slightly water soluble decomposition product of the reaction of kaolinite with acetic acid, probably some sort of silicon or aluminum acetate species, such as the insoluble tricarboxylate $Al(O_2CH_3)_3$, which was reported to form when gibbsite ($Al(OH)_3$) was reacted with excess acetic acid [230].

IR Analysis: IR data indicates that the 6.2 Å phase is characterized by strong bands at 1576 cm^{-1} and 1480 cm^{-1} which can be assigned respectively to the antisymmetric ν(COO) and symmetric ν(COO) bands of an acetate ligand. This is assigned on the basis that these bands were much more intense for Kao-HOAc-2 where the relative intensity of the 6.2 Å phase was also much greater than product Kao-HOAc-1 (Table **5.2**). In addition, when the

6.2 Å phase was removed from the Kao-HOAc-1 product by prolonged water washing, these bands were not observed at all (Section **6.8.2.1**). The 96 cm^{-1} difference in these bands suggest that the acetate ligand is acting as a bidentate chelating ligand [235]. In comparison, for the alumoxane product $[Al(O)_x(OH)_y(O_2CH_3)_z]_n$ (where $2x + y + z = 3$), obtained from the reaction of acetic acid with boehmite [226,230], The ν(COO) bands appear at 1586 cm^{-1} and 1466 cm^{-1} (120 cm^{-1} difference) which they attribute as being consistent with a bridging mode of coordination. The presence of a carboxylate which is chelating, that is, in which both oxygens in the O_2R carboxylate ligand are bound to the same aluminum is dubious due to the ring strain that would accompany such a structure [230]. As a result, all aluminum carboxylate complexes were thought to have either terminal monodentate or bridging ligation.

The bands at 1657 cm^{-1} (s), 1421 cm^{-1} (w), 1380 cm^{-1} (w) and 1300 cm^{-1} (m) were associated with the presence of the 9.5 Å phase, since these bands remained after water washing to remove the 6.2 Å phase. The bands at 1657 cm^{-1} and 1300 cm^{-1} are assigned to the antisymmetric and symmetric COO stretching modes of an intercalated acetate moiety, and the large 357 cm^{-1} difference between these two bands is indicative of an acetate in unidentate coordination [235]. In recent work dealing with the sol-gel chemistry of aluminum alkoxides, bands at 1654 cm^{-1} and 1354 cm^{-1} (difference = 300 cm^{-1}) were also assigned to monodentate acetate coordinated to an octahedrally coordinated aluminum. This provides strong evidence for the formation of an interlayer $\equiv Al\text{-}O_2CH_3$ surface ester linkage. By contrast, if acetic acid and not unidentate acetate were the intercalating species, one would

expect to see a v(C=O) band close to the 1720 cm^{-1} which one observes for liquid acetic acid [171].

One also observes in the infrared spectra of the water washed Kao-HOAc-1 sample, Si-O lattice vibration bands at 1060 cm^{-1} (vs) and 1038 cm^{-1} (vs) indicating a substantial perturbation compared to kaolinite where these bands appear at 1032 cm^{-1} (vs) and 1010 cm^{-1} (vs). Two very weak v(CH) bands are also observed at 2950 cm^{-1} and 2925 cm^{-1}. For comparison, kaolinite which has been intercalated with hydrated potassium acetate (Kao-KOAc 14 Å), also has very weak v(CH) bands between 2970 cm^{-1} and 2930 cm^{-1} which appear as a shoulder on the low frequency side of the broad v(OH) band between 3000-3550 cm^{-1} (section **6.4.4**).

Thermogravimetric Analysis: The TGA data indicates that Kao-HOAc-1 is stable up to greater than 250 °C. XRD and IR confirmed that heating the product at 200 °C for 2 hours followed by cooling to room temperature did not affect either the IR or XRD patterns. Decomposition of Kao-HOAc occurs between 250 and 600 °C in what appears to be a two step process characterized by endothermic events at 322 °C (m) and 433 °C (s). One also observes endotherms in this range for product Kao-HOAc-2, except that in this case the endotherm near 322 °C is very strong and the endotherm near 435 °C is very weak. This suggests that the endotherm at around 322 °C is due to the 6.2 Å phase (which is the dominant phase in Kao-HOAc-2) and the one at approximately 435 °C is due to the 9.5 Å phase assigned to the acetate grafted organokaolinite (which is the dominant phase in Kao-HOAc-1). These decomposition steps are plausibly due to the decarboxylation of the acetate

ligands. Kao-KOAc for example experiences a decarboxylation at an endothermic peak temperature of 375 °C [236] (see also section **6.4.4**). In both Kao-HOAc-1 and Kao-HOAc-2 one observes weak endotherms near 500 °C due to the endothermic dehydroxylation of residual kaolinite. The weight loss after heating to 1000 °C in air atmosphere was 29 % for Kao-HOAc-1 and 45 % for Kao-HOAc-2. The large weight loss for Kao-HOAc-2 is consistent with the assignment of the 6.2 Å phase to a molecular acetate species.

^{13}C CP/MAS NMR: Further proof for the assignment of the 9.5 Å phase to an organokaolinite in which acetate units are grafted to the interlayer aluminate surface is provided from ^{13}C CP/MAS NMR (Bruker CXP-180, 45.27 MHz). For Kao-HOAc-1 one observes two carbonyl resonances at 185.9 ppm and 179.5 in addition to a methyl resonance at 25.1 ppm with a shoulder near 21 ppm. This suggests that there are two types of carbonyl species. The fact that for Kao-HOAc-2, where there is relatively little 9.5 Å phase present, one only observes resonances at 179.6 ppm and 25.3 ppm indicates that these resonances are probably due to the 6.2 Å phase. The resonances at 185.9 and 21 ppm therefore are assigned respectively to the carbonyl and methyl groups of the monodentate acetate unit in the 9.5 Å organokaolinite phase. A carbonyl resonance at 179 ppm has been attributed to an acetate ligand linked monodentate to an octahedrally coordinated aluminum [171,237] and $[Al(O)_x(OH)_y(O_2CH_3)_z]_n$ also has a ^{13}C carbonyl resonance at 179.3 ppm [230].

5.2.2.2 Reactions with Propionic Acid

Reaction of Kao-DMSO with propionic acid under refluxing conditions (**5-2-6**) led to the formation of an 11.0 Å organokaolinite product (Kao-PrOAc). Reaction of Kao-NMF with propionic acid was not successful (**5-2-7**) probably due to the structural collapse of Kao-NMF to kaolinite before reaction with propionic acid could occur. Carr and Chih [34] had previously reported the existence of a 12.1 Å intercalated halloysite-propionic acid phase which was unstable in vacuum. This 1.1 Å difference in basal spacings compared to Kao-PrOAc (**5-2-6**) suggests that the propionic acid units are in different interlayer environments.

Evidence for propionic acid incorporation was found from ^{13}C CP/MAS NMR (75.48 MHz) which showed resonances at 182, 22 and 10 ppm, attributable to the three carbons (a-c), respectively of intercalated propionic acid ($C_aH_3C_bH_2C_cOOH$). One also observes a resonance at 41 ppm due to the presence of residual co-intercalated DMSO. IR bands at 1751 cm^{-1} (w) and especially 1651 cm^{-1} (m) also confirmed the presence of an interlayer carbonyl species, although the nature of this species is unknown. As a comparison, for the propionic acid carboxylate-alumoxane product $[Al(O)_x(OH)_y(O_2CH_2CH_3)_2]_n$, IR bands were reported at 1589 cm^{-1} and 1473 cm^{-1} and at ^{13}C carbonyl resonance was reported at 180.0 ppm [230].

TGA data for Kao-PrOAc in N_2 atmosphere (Section **6.8.2.6**) showed that there was a substantial 29.4 % wt. loss up to 1200 °C, indicating the presence of substantial interlayer organic material. Up to 200 °C there was a small 3.6 % wt. loss ($T_{endo.}$ = 115 °C) due plausibly to weakly adsorbed surface water and propionic acid. Between 200-428 °C, decomposition of the interlayer organic material occurred in what appeared to be a two step

process characterized by a total weight loss of 12.7 % with endothermic peaks at 313 °C and 406 °C. The high temperature at which this decomposition occurs indicates that the interlayer propionic acid species is tightly bound to the kaolinite. This supports the hypothesis that there is some grafting (at least in part) of the propionic acid species to the aluminate surface of kaolinite. A 10.1 % weight loss attributable mainly to the dehydroxylation of kaolinite host is observed between 428-650 °C ($T_{endo.}$=483 °C), and there is a further gradual 3.0 % weight loss between 650-1200 °C.

5.2.2.3 Reactions with Acid Chlorides

The reaction of two acetyl chlorides (Reactions **5-2-4** and **5-2-5**) with Kao-DMSO were carried out in order to see if any reaction occurs. Reaction of Kao-DMSO with acetyl chloride (**5-2-5**) led initially to the formation of an 8.6 Å phase. The nature of this phase was unknown, since the presence of IR bands at 3548 cm^{-1} (m) and 1650 cm^{-1} (w) were somewhat suggestive of intercalated water, whereas the presence of a ν(C=O) band at 1690 cm^{-1} (m,br) suggested that some acetyl chloride units is also intercalated. Interestingly, it was found that when another XRD pattern was taken of the sample after sitting in a closed container for one year, diffraction peaks were observed at 10.7 Å and 8.2 Å along with the residual kaolinite reflection, indicating perhaps a phase segregation. Reaction with chloroacetyl chloride ($ClCH_2COCl$) yielded a disordered 11.1 Å organokaolinite. Some of the chloroacetyl chloride units appeared to have been intercalated as evidenced by the infrared ν(CO) bands at 1755 cm^{-1} (w,sh), and 1723 cm^{-1} (m).

The reaction of Kao-DMSO with propionyl chloride (Rxn **5-2-7**) yielded a product which consisted essentially of Kao-DMSO as observed by IR and XRD characterizations (Section **6.8.2.8**). The failure to form a propionyl chloride derived organokaolinite was probably due to the difficulty in diffusing propionyl chloride into the interlayer spaces of kaolinite under the conditions employed (stirring at 20 °C for 7 days).

5.2.3 Other Functionalization Reactions with Kaolinite

A number of other attempts were made to prepare new organokaolinite materials (Table **5.3**). Some of these such as the reaction with thiols were clearly unsuccessful (Reactions **5-3-3** and **5-3-4**), yielding collapsed kaolinite (basal spacing= 7.2 Å) as the only product. Other reactions were more successful. Reaction with 2-chloroethanol for example yielded a 10.9 Å phase as the principal phase. A 10.8 Å intercalated phase was previously reported for the reaction of halloysite with 2-chloroethanol [33,34].

Reactions of Kao-DMSO with chlorotrimethylsilane (**5-3-5**) and chlorodimethylethylsilanes (**5-3-6**) yielded 10.8 Å products which were thermally stable above 200 °C. The nature of these reaction products was however unclear.

Finally, reaction of Kao-DMSO with an excess of the phenyl phosphonic acid melt at 180-190 °C caused the irreversible decomposition of kaolinite. A very complicated reaction product exhibiting many XRD diffraction peaks was observed (Section **6.8.3.7**). The characteristic ν(OH) pattern of kaolinite was replaced by a medium intensity very broad band between 3650-3100 cm^{-1}. Water washing of the product removed most of the XRD

diffraction peaks. A broad intense reflection remained at 14.4 Å, indicative of a poorly ordered unknown reaction product. It is noteworthy that trimethyl phosphate is also known to cause the irreversible decomposition of kaolinite at 100 °C [238].

Starting Material	Reactant	Rxn Code[1]	Basal Spacing[2] (Å)	Relative Intensity[3]
Kao-DMSO	2-Chloroethanol	**5-3-1**	10.9 8.9 7.2[4]	100 9(sh) 4
Kao-DMSO	3-Chloro-1,2-propanediol	**5-3-2**	11.2 7.5[4]	36 60
Kao-DMSO	2-Thiolethanol	**5-3-3**	7.2[4]	100
Kao-DMSO	1,2-Ethanedithiol	**5-3-4**	7.2[4]	100
Kao-DMSO	Chlorotrimethyl silane	**5-3-5**	10.8 7.2[4]	100 12
Kao-DMSO	Chlorodimethylethyl silane	**5-3-6**	10.8 7.2[4]	100 8
Kao-DMSO	Phenylphosphonic Acid	**5-3-7**	14.9 12.3 11.5 10.5 7.5 7.1[4]	24 100 19 2 8 0.5

Table 5.3: Summary of the organokaolinite products formed from an assortment of treatments. (1) see Section **6.8.3** for reaction details and characterizations. (2) This refers to the basal spacing of the principal modified product phases at low diffraction angle (between 2 and 16 °2Θ). (3) The peak intensities were normalized such that the most intense peak was set to 100. (4) unexpanded kaolinite.

5.3 Conclusions

Exploratory work involving the modification of the interlamellar surface of kaolinite using reactants other than molecules with only alcohol and/or ether functionalities was performed. A well-ordered material, Kao-EOA, resulted from the reaction of ethanolamine with both Kao-DMSO and Kao-NMF. It was proposed that this material is made up of ethanolamine units attached to kaolinite via $\equiv$Al-O-$CH_2CH_2NH_2$ linkages. This would be consistent with what was observed for some aminoalcohol functionalized organoboehmites[157]. It was also shown that it was possible to obtain what was thought to be an acetate functionalized organokaolinite, where the acetate unit was linked via $\equiv$Al-O_2CH_3 interlayer surface groups.

While most of the work shown in this chapter has been of an exploratory nature, clearly, the potential exists to expand the chemistry of kaolinite and to include its use as a precursor material in the preparation of new asymmetric layered structures.

Chapter 6

Experimental Section

6.1 Solvents and Reagents

All chemicals used were of reagent grade quality and were not further purified unless otherwise specified. If additional drying of the solvents or liquid reagents was required, this was accomplished by either fractional distillation (amines), distilling from CaH_2 (alcohols), or by treatment with activated molecular sieves.

Most of the crude clays were obtained from the Source Clay Repository of the Clay Mineral Society (Department of Geology, University of Missouri, USA). Additional purification, primarily by standard sedimentation procedures was required to remove coarse impurities in most of the clays [239].

6.2 Instrumentation

6.2.1 Infrared Spectroscopy

Infrared spectra were obtained on a Bomem Michelson MB 100 FTIR spectrometer using 30-50 averaged scans at 4 cm^{-1} resolution. The samples were prepared as KBr pellets (0.25-0.50 % by weight in KBr), as neat liquids trapped between NaCl plates, or occasionally in a fluorocarbon mulling agent (Fluorolube). Peak positions (in

cm^{-1}) were either determined manually or automatically using the available FTIR software.

6.2.2 X-Ray Diffraction (XRD)

XRD powder patterns were performed on one of two instruments. Both instruments used Cu Kα radiation (wavelength = 1.5416 Å). The Philips PW 1050/81 automated diffractometer was located in the laboratory of Dr. Chao, Department of Earth Sciences, Carleton University. It was equipped with a graphite monochromator and the XRD patterns were obtained using a generator voltage of 40 kV and a generator current of 40 mA.

Operation of the Philips PW 3710 diffractometer was performed using a generator voltage of 45 kV and a generator current of 40 mA. Typically, a step size of 0.04 °2Θ was used with a dwell time of 0.5 seconds per step. The sample was spun during pattern acquisition, and an automatic divergent slit and a 0.1 mm receiving slit was used without employing any mask.

Samples were normally prepared on a circular glass disk although in some instances a low background silicon circular disk was employed. Samples were prepared in one of two ways. Directly mounting the samples on the disks using a small amount of vaseline as an adhesive tended to provide a more randomly oriented. Dispersing 20-30 mg of sample with 1 ml of an appropriate solvent, followed by sonification for 10

seconds and application on a glass slide tended to provide an oriented sample once the solvent had evaporated.

For the product characterizations in the experimental sections, not all of the XRD reflections were indicated. Only those reflections which are most important or prominent are given for most of the products. All the d-values are given in Angstrom units (Å), with the relative intensities given in brackets on a scale where 100 is the intensity of the most intense reflection. When residual kaolinite reflections are observed the notation (K) is used to indicate this. Anatase is a common impurity and can be observed as a reflection at d= 3.52 Å.

The notation I.R. is used for the intercalation ratio (see Section **1.3.3**), and the c-spacing or basal spacing is calculated based on the indexed (00l) reflections (See Section **1.3.3**). In some instances, for the more important materials, additional XRD information is provided.

6.2.3 Thermogravimetric Analysis (TGA and DSC)

Unless otherwise indicated, all thermal analysis (TGA and DSC) runs were done on a Polymer Labs 1500H under either flowing nitrogen or air (20-90 cm^3/min) and a heating rate of 10-20 °C per minute. Approximately 10 mg of sample was used for each run using alumina sample and reference pans. Calibration of the thermocouple was performed by using the known endothermic melting transitions of lead, zinc and gold.

Baseline drift, probably caused by the excessive gas flow rates used in many of the TGA runs (< 80 cm^3/min) caused significant uncertainty in the TGA weight losses for many runs. It was indicated when baseline drift was a problem. The baseline drift was sometimes corrected to some extent by either subtracting from each of the runs a blank TGA run of an equal quantity of calcined alumina powder or by adjusting the baseline digitally. It should be stressed that in most cases, the TGA weight loss data was only approximate, and during the course of a TGA run, the total weight loss could be in error by as much as 5-7%. This was ascertained by comparing the given TGA weight loss to the accurately weighed samples before and after the TGA run. The given TGA weight loss was generally lower than what was actually determined.

6.2.4 Nuclear Magnetic Resonance Spectroscopy (NMR)

^{13}C CP/MAS and DD/MAS experiments were performed on a number of instruments with spinning rates ranging from 3-5 kHz. These included Bruker instruments: ASX-200 (50.32 MHz), ASX-200 (50.29 MHz) and CXP-180 (45.27 MHz). All ^{13}C CP/MAS spectra were referenced to hexamethylbenzene at 14.9 ppm unless otherwise indicated.

^{29}Si CP/MAS NMR experiments were done on either a Bruker CXP-180 (35.76 MHz) or a Bruker ASX-200 (39.76 MHz) with a spinning rate of approximately 4 KHz). All ^{29}Si CP/MAS spectra were referenced to tetramethylsilane (TMS) at 0.0 ppm.

Solution state NMR (^1H and ^{13}C) were performed on either a Gemini-200, Varian XL-300 or a Bruker AMX-500, and both ^1H and ^{13}C chemical shifts are reported relative to $SiMe_4$ in $CDCl_3$ unless otherwise stated.

6.2.5 Particle Size Analysis

A Micromeritics Sedigraph 5100 was employed for all particle size analysis measurements. A 0.05 % sodium metaphosphate solution was used as both the background liquid and as dispersant solution. The solvent parameters for pure water were employed for the software data treatment. A beamsplit sample cell calibration was performed before each run, as well as a solvent background correction. The densities of the samples were either estimated from literature values, or were measured using a helium pycnometer (see below), and the particle size analysis was done at temperatures ranging from 30-40 °C. Bubble detection was set to low and pump speed was set to high.

Typically 1.5 g of clay was added to 40 ml of 0.05 % sodium metaphosphate solution in a beaker, and this was sonified until a homogeneous solution was obtained (about 10 minutes). One drop of Photoflow (from Kodak) was added to help prevent bubble formation and this was then added to the sample mixing chamber. An additional 5-10 ml of 0.05 ml sodium metaphosphate solution was used to rinse the beaker to ensure that all of the sample was transferred. A high speed run ranging from 50-0.1 μm usually took 4 hrs to complete.

6.2.6 Pycnometer Density Measurements

The densities of powders were measured using a Micromiretics pycnometer using helium as the filler gas. Calibration of the sample container volumes was done using metal spheres whose volumes were accurately known. The powders were repeatedly purged with helium in order to remove as much nitrogen and oxygen as possible from the sample and the container as possible.

6.3 Purification and Characterization of Clays

6.3.1 Kaolinite

Well crystallized Georgia KGa-1 kaolinite was purchased from the Source Clay Repository of the Clay Mineral Society (University of Missouri). This was purified based on previously reported sedimentation techniques [239-242]. Typically, 60 g of the crude product was mixed with 4.0 litres of deionized water. This gave a strongly flocculated suspension with a pH ranging from 4.5-6.0. Vigorous stirring was maintained and the pH was adjusted to 9.0 through the careful dropwise addition of 0.1 N NaOH solution. At this pH, the particles were no longer flocculated, but were in the form of a suspension. At this point, the stirring was stopped, the 4 litre beaker was covered with a watch glass, and the sedimentation was allowed to proceed. After 6 hrs the top 15 cm of the mixture

were carefully siphoned off. This process was repeated one more time with the remaining sediment. The supernatant colloidal solution from this was combined with that of the previous batch. The coarse sediment was then discarded.

The pH of the combined dispersed supernatant was then adjusted to pH= 6.0 through the careful dropwise addition of 0.1 N HCl, upon which the dispersion flocculated. Flocculation was allowed to occur until a well defined sediment was formed with a clear supernatant solution above the sediment. The supernatant was then siphoned off and discarded. The sediment was suction filtered and washed with deionized water until the washings showed no trace of chloride from saturated $AgNO_3$ solution. The purified kaolinite was then air dried followed by drying for at least 8 hrs in an oven at 100 °C. The product was then characterized by particle size analysis, XRD, elemental analysis (XRF), FTIR and TGA/DSC which all supported previously reported literature data on KGa-1 kaolinite [243].

- XRD (Philips PW 3710, vaseline mounted, indexing modified from Bailey [2] based on the following C1 triclinic unit cell parameters: a= 5.146 Å, b= 8.946 Å, c= 7.388 Å, α= 91.7°, ß= 104.7°, Γ=89.8°): d_{001}= 7.132 (100); d_{020}= 4.459 (8.9); $d_{1\text{-}10}$, d_{110}= 4.351 (11); $d_{11\text{-}1}$= 4.170 (10); $d_{1\text{-}1\text{-}1}$= 4.120 (6.6); $d_{02\text{-}1}$= 3.840 (4.8); d_{021}= 3.740 (2.7); d_{002}= 3.573 (65); Anatase (TiO_2) impurity, 3.512 (6.4); d_{111}= 3.371 (2.6); $d_{11\text{-}2}$= 3.243 (0.7); $d_{1\text{-}1\text{-}2}$= 3.093 (0.6); d_{022}= 2.745 (0.6); $d_{1\text{-}30}$, $d_{20\text{-}1}$= 2.560 (3.8); $d_{13\text{-}1}$= 2.528 (2.6); $d_{1\text{-}3\text{-}1}$, d_{200}= 2.493 (4.7); d_{003}= 2.381 (5.7); $d_{20\text{-}2}$, $d_{1\text{-}31}$= 2.338 (7.0); d_{131}= 2.290 (4.1); $d_{13\text{-}2}$= 2.245 (0.6); d_{201}= 2.184 (0.6); $d_{02\text{-}3}$= 2.126 (0.2); $d_{20\text{-}3}$, $d_{1\text{-}32}$= 1.991 (1.7); d_{132}= 1.939 (0.8); $d_{13\text{-}3}$= 1.893 (0.9); $d_{1\text{-}3\text{-}3}$, d_{202}= 1.834 (0.5); d_{004}= 1.788 (1.4); $d_{24\text{-}1}$=

1.688 (0.5); $d_{20\text{-}4}$, $d_{1\text{-}33}$, $d_{1\text{-}5\text{-}1}$= 1.665 (1.8); $d_{1\text{-}51}$, d_{133}= 1.619 (0.9); $d_{13\text{-}4}$= 1.583 (0.4); $d_{2\text{-}2\text{-}4}$, $d_{1\text{-}3\text{-}4}$, $d_{31\text{-}3}$, d_{203}= 1.543 (0.5); d_{060}, $d_{33\text{-}1}$, $d_{3\text{-}3\text{-}1}$= 1.490 (1.5); $d_{3\text{-}32}$, $d_{15\text{-}3}$, $d_{3\text{-}30}$, d_{061}= 1.451 (0.2); d_{005}= 1.429 (0.2); d_{242}, $d_{20\text{-}5}$= 1.398 (0.1)

- FTIR (in cm^{-1}): ν(O-H): 3694 (s), 3669 (m), 3653 (m), 3621 (s), 3450 (w,br); δ(HOH): 1631 (vw,br); Si-O; 1114 (s), 1099 (s), 1032 (vs), 1010 (vs); δ(Al-OH): 938 (m,sh), 915 (s); other bands: 791 (w), 755 (m), 694 (m), 650 (w), 545 (s), 475 (s), 432 (s).

- TGA/DSC (90 cm^3/min N_2, TGA wt. losses are approximate): 0-300 °C: 0.5 % wt. loss; 300-600 °C: 13.1 % wt. loss, $T_{endo.}$= 538 °C (s); 600-950 °C: 0.0 % wt. loss; 950-1200 °C: 0.0% wt. loss, $T_{exo.}$= 1003 °C (s). Total TGA weight loss = 13.6 %. Calcination wt. loss (3 hours at 1100 °C in air atmosphere): 14.14 %.

- Elemental Analysis (XRF, calculated on the basis of $Si_2Al_2O_5(OH)_4$): % SiO_2: calc. 46.58, found 44.73; % Al_2O_3: calc. 39.52, found 38.48; % Fe_2O_3: calc. 0.00, found 0.28; % MgO: calc. 0.00, found 0.04; % CaO: calc. 0.00, found 0.09; % Na_2O: calc. 0.00, found 0.00; % K_2O: calc. 0.00, found 0.01; % TiO_2: calc. 0.00, found 1.85; % P_2O_5: calc. 0.00, found 0.07; % H_2O (based on wt. loss during fusion): calc. 13.95, found 14.36; Si/Al= 0.99.

Helium pycnometer measurements showed that the crude KGa-1 kaolinite had a density of 2.66 g/cm^3 which is in accord with previously published values [244]. This density value was used for the particle size analysis (Sedigraph 5100) which showed for

all batches that at least 98 % of the sample was less than 2 μm esd. This confirmed that the coarser fractions were removed by sedimentation.

XRD showed the presence of slight quantity of residual anatase (TiO_2) by a sharp reflection at d= 3.51 Å. Otherwise, XRD confirmed the well-crystallized nature of kaolinite [2,10]. FTIR analysis of the O-H stretching region also confirmed the crystallinity of the purified material [25,243]. TGA/DSC showed a 13-14 % weight loss upon calcination, with a strong endothermic event corresponding to the dehydroxylation reaction of kaolinite at 538 °C and a strong exothermic event corresponding to a structural reorganization of metakaolinite at 1003 °C. This is in accord with what one expects from literature studies on KGa-1 kaolinite [243].

6.3.2 Halloysite

Halloysite from Eureka, Utah (Halloysite #13) was obtained from Ward's Natural Science Establishment Inc. (Rochester, NY) in the form of hard rocklike chunks. The material was purified by first grinding up the chunks to the consistency of a coarse powder. Significant quantities of quartz were detected in this crude form by powder XRD (XRD quartz reflections: d(Å)= 4.24, 3.33 etc.). 40 g of this was mixed with 1 litre of water and stirred vigorously for 24 hrs followed by one hour of sonification. The sample was then purified by sedimentation in the same manner as with kaolinite. The yield from 40 g of coarse product was 8 g of an off-white powder. This was characterized by XRD, FTIR and TGA/DSC.

- XRD (Philips PW 3710, H_2O dispersed: d_{001} = 7.32 (100), 4.44 (99), d_{002} = 3.58 (32).

- FTIR (in cm^{-1}): ν(O-H): 3696 (s), 3623 (m), 3600-3300 (m,br); δ(HOH): 1632 (w,br); Si-O; 1110 (s,sh), 1087 (s), 1032 (vs); δ(Al-OH): 941 (m, sh), 911 (s); other bands: 790 (w), 754 (m), 688 (s), 541 (s), 469 (s), 433 (s).

- TGA/DSC (90 cm^3/min N_2, TGA weight losses are approximate): 20-200 °C: 2.3 % wt. loss, $T_{endo.}$ = 70 °C (m); 200-350 °C: 0.4 % wt. loss; 350-650 °C: 11.7 % wt. loss, $T_{endo.}$ = 519 °C (s); 650- 1100 °C: $T_{exo.}$ = 1007 °C (m). Total TGA weight loss = 14.4 %.

Helium pycnometer density analysis of the crude material was found to be 2.66 g/cm^3 which is identical to what was obtained for kaolinite. Using this value for the particle size analysis of the purified material revealed that 100 mass % of the particles were finer than 10 μm, 92 % finer than 1.0 μm, and 35 % finer than 0.1 μm.

6.3.3 Dickite

Dickite from St. George, Utah (Dickite # 16) was obtained from Ward's Natural Science Establishment Inc. (Rochester, NY) in the form of hard rocklike chunks. This was broken up with a mortar and pestle and ground up to give a coarse powder. Significant amounts of rocky and sandy material were found to be mixed with a much finer material.

A preliminary rapid sedimentation was performed to remove the small rocks and sand. This consisted of mixing 10 g of the material with 100 ml of deionized water, followed by vigorous stirring for 1 hr and then sedimentation. After two minutes of sedimentation time, the very coarse impurities were removed, and the remaining suspension was filtered, washed with water and air dried.

This material was found to contain significant traces of quartz (XRD quartz reflections: d(Å)= 4.24, 3.33 etc.) and at least one other unidentified impurity. This impurity was evident as a very intense FTIR ν(O-H) band at 3487 cm^{-1}, interfering with the O-H stretching pattern of dickite, and as a number of sharp intense XRD reflections at d(Å)= 5.74, 5.66, 4.93, 3.47, 2.97, 2.88, 2.29, 1.92, 1.90, 1.50.

IR bands associated with the presence of Dickite were found at 3694 cm^{-1}(m), and 3622 cm^{-1}(m), 940 cm^{-1} (w,sh) and 913 cm^{-1}. Bands at 1237 cm^{-1} (s), 1082 cm^{-1} (vs), 1029 cm^{-1} (vs) are probably due to the overlap of absorption bands of both dickite and impurities.

TGA/DSC also confirmed that a significant portion of the material was in the form of an impurity which decomposes in N_2 atmosphere between 700-850 °C (20 % weight loss, $T_{endo.}$= 787 °C). In contrast, the dehydroxylation weight loss of dickite component was found to be 11 % of the total (T_{endo}= 528 °C). On the basis of the TGA results, it can be estimated as first approximation that roughly 70-75 weight % of the product is in the form of dickite with the remaining 20-25 % in the form of an unknown material which decomposes almost entirely upon calcination above 850 °C.

It was decided not to use this material, due to the large amounts of impurities as evidenced by XRD, FTIR and TGA/DSC.

6.3.4 Sudoite

Crude sudoite labelled Kb-227 (from Anhée, Belgium) was obtained from Dr. Annik Anceau (Université de Liège, Belgium). Previous elemental analysis and XRD results performed on the bulk fraction showed this material contained 24.1 % quartz and 1.8 % goethite (Fe_2O_3) impurities [245]. The chemical formula for the sudoite phase was estimated to be $(Al_{2.84}Mg_{1.79}Fe_{0.19}^{3+}Fe_{0.03}^{2+}Li_{0.02})Si_{3.24}Al_{0.76})O_{10}(OH)_8 0.46H_2O$. This is in fairly good approximation with the idealized sudoite formula of $Al_2(Si_3Al)O_{10}(OH)_2(Mg_2Al)(OH)_8$. A preliminary sedimentation was performed to remove the very coarse sandy fraction, and the resulting material was analyzed by XRD, TGA/DSC and FTIR. XRD analysis was fully consistent with that which had been previously reported [245]. A number of unsuccessful attempts were made to expand the interlayers of the purified sudoite using hydrazine, DMSO and potassium acetate.

- XRD (Philips PW 3710, H_2O dispersed, indexing based on literature assignments[245]): d_{001}= 14.03 (40), d_{002}= 7.05 (47); d_{003}= 4.71 (100); d_{110}= 4.49 (18), Quartz 4.24 (27), d_{004}= 3.54 (46); Quartz 3.33 (90); d_{005}= 2.84 (13); $d_{13\text{-}1}$= 2.60 (3); etc..

- FTIR (in cm^{-1}): ν(O-H): 3611 (s), 3514 (s), 2280 (m,sh); δ(HOH): 1633 (w); Si-O; 1016 (vs); other bands: 695 (s), 526 (s), 472 (vs), 459 (vs).

- TGA/DSC (90 cm^3/min N_2, TGA weight losses are approximate): 20-485 °C: 3.0 % wt. loss, $T_{endo.}$ = 64 °C (w); 485-700 °C: 8.5 % wt. loss $T_{endo.}$ = 586 °C (s); 700-1000 °C: $T_{exo.}$ = 806 °C (w), $T_{endo.}$ = 875 °C (w), $T_{exo.}$ = 938 °C (w).

6.3.5 Sepiolite

6.3.5.1 Sep-Spain: A Crude sample of Spanish sepiolite (labelled Tolsa S.A. Madrid) was ground up with a mortar and pestle to yield 27 g of a beige powder. FTIR, XRD and TGA all showed this material to be relatively pure, and conformed to literature data [243].

- XRD (Philips PW 1050/81, H_2O dispersed): d_{110}= 13.02 (100); d_{130}= 7.9 (3); d_{200}=6.9 (5); 4.62 (8); d_{060}= 4.40 (11); 3.83 (8); d_{080}= 3.39 (6); etc..

- FTIR (in cm^{-1}): ν(O-H): 3682 (w), 3622 (m), 3562 (s), 3410 (s,br), 3245 (m,br); δ(HOH): 1653 (m), 1628 (m); Si-O; 1075 (s), 1027 (vs), 985 (vs); other bands: 1201 (m), 788 (w), 690 (w), 653 (w).

- TGA/DSC (85 cm^3/min N_2, TGA wt. losses are approximate): 20-200 °C: 12.1 % wt. loss, $T_{endo.}$ = 101 °C (s); 200-350 °C: 2.9 % wt. loss, $T_{endo.}$ = 300 °C (w); 350-650 °C: 2.0 % wt. loss; 650-1000 °C: 1.3 % wt. loss, $T_{exo.}$ = 847 °C (s). Total TGA weight loss = 18.3 %.

6.3.5.2 Sep-Nevada: Sepiolite from Nevada (labelled Sep-Nev) was obtained from the Source Clays Repository in the form of a hard rocklike material. The characterization of

this material has been previously described [246]. This material was broken up into small pieces followed by wet grinding with a mortar and pestle. 30 g of this material was vigorously mixed with 4 litres of 1 N NaCl (maintained at approximately pH 4.0 with HCl addition) for 16 hours in a 4 litre beaker. Upon removal of the stirring action, the mixture quickly flocculated, due to the presence of NaCl in solution. After settling for one day, the supernatant was siphoned off and discarded. The beaker was once again filled to the 4 litre mark with deionized water and the process was repeated until eventually the supernatant liquid was shown not to contain chloride ion as judged by a negative $AgNO_3$ test.

At this point, deionized water was again added to the stable colloidal suspension in order to fill the beaker to the 4 litre mark. Sedimentation was allowed to occur after 5 minutes of vigorous stirring. This was allowed to proceed for 4 hours, after which the top 15 cm (out of 20 cm) of colloidal dispersion was siphoned off. The beaker was refilled with deionized water and the process was repeated one more time, with the sediment being discarded at the end of this second time and the siphoned colloidal dispersion being combined with that of the first batch.

The collected colloidal dispersion was centrifuged and the sediments were allowed to air dry. Upon air drying, first at room temperature, and then later in an oven at 100 °C, a flexible fibrous material was formed which could be torn apart in small pieces. This was characterized by FTIR, XRD and TGA. FTIR and XRD characterizations were in accord with those in the literature [246,247].

- XRD (Philips PW 1050/81, H_2O dispersed, d-values in Å and relative intensities in brackets): d_{110}= 12.79 (100); d_{200}= 6.91 (5); d_{060}= 4.53 (3); d_{080}= 3.39 (9); etc.

- FTIR (in cm^{-1}): ν(O-H): 3690 (m), 3620 (s,sh), 3566 (s), 3423 (s,br), 3260 (s,br); δ(HOH): 1655 (m); Si-O; 1078 (s), 1021 (vs), 979 (vs); other bands: 1211 (m), 785 (w), 764 (w), 691 (w), 647 (w), 471 (s), 440 (s).

- TGA/DSC (85 cm^3/min N_2, TGA wt. losses are approximate): 20-200 °C: 8.8 % wt. loss, $T_{endo.}$= 87 °C (s); 200-350 °C: 3.1 % wt. loss, $T_{endo.}$= 300 °C (w); 350-650 °C: 5.9 % wt. loss; 650-1000 °C: 1.7 % wt. loss, $T_{exo.}$= 848 °C (s). Total TGA weight loss = 19.5 %.

6.3.6 Palygorskite

Palygorskite (also known as attapulgite) from Florida was obtained from the Clay Minerals Repository at the University of Missouri (labelled PFl-1) and has been previously characterized [243]. XRD and FTIR patterns of the crude material were in accord with those which were previously reported and traces of quartz could be readily observed in the XRD pattern.

- XRD (Philips PW 3710, H_2O dispersed,): d_{110}= 10.76 (100); d_{200}= 6.52 (13); d_{130}= 5.47 (7); d_{040}= 4.50 (17); Quartz 4.28 (7); d_{221}= 3.68 (6); Quartz 3.36 (22); d_{311}= 3.25; etc.

- FTIR (in cm^{-1}): ν(O-H): 3615 (s), 3582 (s), 3547 (s), 3402 (s,br), 3280 (m,sh); δ(HOH): 1655 (m); Si-O vibrations: 1193 (m), 1120 (s,sh), 1090 (s), 1030 (vs), 986 (vs); other bands: 911 (m), 647 (m), 510 (s), 482 (s), 444 (s).

6.4 Preparation and Characterization of Organomineral Starting Materials

6.4.1 Kaolinite-Dimethyl Sulfoxide (Kao-DMSO)

The preparation and characterization of Kao-DMSO has been extensively examined [36]. The dimethyl sulfoxide intercalate of kaolinite was prepared by mixing typically 20 g of the purified kaolinite with 100 ml of DMSO in a closed vessel (usually a sealed jar) and allowing sufficient time (2 months) for maximum intercalation to occur. This was determined by measuring the XRD patterns of the sample smeared onto a glass slide and comparing the peak intensities of the intercalated versus the non-intercalated d_{001} peaks. The mixture was occasionally stirred during the course of the intercalation reaction. The intercalated product was then filtered and washed with 50 mL 1,4 dioxane to remove excess DMSO. After air drying for 4 hours, approximately 30 g of white powder was collected and characterized by XRD, FTIR, TGA/DSC and ^{13}C CP/MAS NMR. A number of batches were prepared by this method, and the intercalation ratio

(I.R.) as estimated by powder XRD was generally between 0.92-0.98. The full characterization of a typical Kao-DMSO batch is given below.

- XRD (Philips PW 3710, MeOH dispersed): d_{001}= 11.140 (100); d_{001} (K)= 7.138 (2.2); d_{002}= 5.585 (2.3); 4.460 (1.2); 4.308 (1.0); 4.198 (2.0); 4.110 (1.7); 4.024 (2.3); 3.977 (2.2); d_{003}= 3.728 (19); d_{002} (K)= 3.572 (2.4); Anatase 3.511 (1.1); 3.334 (0.5); 3.051 (0.5); d_{004}= 2.797 (0.7); 2.570 (0.5); 2.496 (0.5); 2.457 (0.5); 2.378 (0.4); 2.339 (0.4); 2.292 (0.4); d_{005}= 2.237 (1.1); d_{006}= 1.866 (0.5); d_{060}= 1.490 (0.2). d= 11.18 ± 0.03, I.R.= 0.978.

- FTIR (in cm^{-1}): ν(O-H): 3695 (m), 3662 (s), 3621 (s), 3538 (m), 3505 (m); ν(C-H): 3023 (w), 2937 (w), 2819 (w); δ(HOH): 1636 (vw); δ(C-H): 1433 (w), 1408 (w), 1394 (w), 1319 (w); Si-O: 1122 (s), 1095 (s), 1040 (vs), 1030 (vs,sh), 1019 (vs); δ(Al-OH): 958 (m), 940 (w,sh) 905 (s); other bands: 789 (w), 743 (m), 720 (w), 682 (m), 607 (w), 551 (s), 466 (s), 434 (s).

- TGA/DSC (90 cm^3/min N_2): 25-152 °C: 16.6 % wt. loss, $T_{endo.}$= 131 °C (s); 152-258 °C: 14.5 % wt. loss, $T_{endo.}$= 215 °C (s); 258-444 °C: 1.3 % wt. loss; 444-648: 7.6 % wt. loss, $T_{endo.}$= 527 °C (s): 648-1050 °C: 0 % wt. loss, $T_{exo.}$= 1009 °C (s). Total TGA weight loss = 40.0 %. Calcination weight loss (2 hrs at 1100 °C in air atmosphere)= 41.5 %.

^{13}C CP/MAS NMR (Bruker CXP-180, 45.27 MHz): 43.7 (CH_3), 42.7 (CH_3).

6.4.2 Kaolinite-N-Methylformamide (Kao-NMF)

The preparation and characterization of Kao-NMF has been previously reported [36]. Typically, Kao-NMF was prepared by mixing 20 g of the purified kaolinite with 100 ml of N-methyl formamide (NMF) in a closed container and allowing sufficient time (1 months) for maximum intercalation to occur. The extent of intercalation was monitored in the same way as for Kao-DMSO. The sample was then filtered and washed with 50 mL dioxane to remove excess NMF. After air drying for 4 hours, 28 g of white powder was collected and characterized by XRD, FTIR and TGA/DSC. A number of batches were prepared by this method, and the intercalation ratio (I.R.) as estimated by powder XRD was generally between 0.85-0.98. The full characterization of a typical Kao-NMF batch is given below.

- XRD (Philips PW 1050/81, methanol dispersed): d_{001}= 10.79 (100); d_{001} (K)= 7.18 (7.6); d_{003}= 3.58 (51). d= 10.76 ± 0.04, I.R.= 0.93.

- FTIR (in cm^{-1}): v(O-H): 3690 (s), 3620 (s), 3585 (m,br); v(N-H): 3418 (s); v(C-H): 2942 (vw), 2908 (w); v(C=O): 1681 (s); deformation region: 1530 (m), 1420 (w), 1380 (w), 1238 (vw); Si-O vibrations: 1101 (s), 1034 (s), 1009 (vs); δ(Al-OH): 944 (w), 907 (s); other bands: 789 (w,sh), 745 (w), 687 (m), 551 (s), 470 (s), 431 (s).

- TGA/DSC (40 cm^3/min N_2): 25-120 °C: 1.1 % wt. loss, $T_{endo.}$= 103 °C (w); 120-250 °C: 13.9 % wt. loss, $T_{endo.}$= 196 °C (s); 250-450 °C: 1.0 % wt. loss; 450-650: 10.2 % wt. loss, $T_{endo.}$= 534 °C (s): 650-1200 °C: 0.8 % wt. loss, $T_{exo.}$= 1003 °C (s).

Total TGA weight loss = 27.0 %. Calcination weight loss (2 hrs at 1100 °C in air atmosphere)= 27.3 %.

6.4.3 Kaolinite-Hydrazine (Kao-Hz)

The formation of Kao-Hz was based on preparations previously described in the literature [36,51]. 5 g of KGa-1 kaolinite (98 % < 5 μm) was added to 20 ml of anhydrous hydrazine (Aldrich, N_2H_4) in a 50 ml round bottomed flask fitted with a septum. This was allowed to stand with occasional stirring for three weeks or more. Gas was evolved during the course of intercalation due to the decomposition reaction of hydrazine yielding N_2 and H_2. Filtering, washing with 2-propanol and air drying for 2 hrs yielded 6.6 g of an off-white powder. XRD and FTIR were in accord with previous literature characterizations [36,51].

- XRD (Philips PW 3710): d_{001}= 10.26 (100); d_{001} (K)= 7.13 (2.7); d_{002}=5.15 (0.9); d_{003}= 3.45 (16); d=10.30 ± 0.05; I.R.= 0.97.

- FTIR (in cm^{-1}): ν(O-H): 3694 (m), 3654 (m), 3620 (s), 3599 (m), 3565 (m,br), 3469 (m,br); ν(N-H): 3364 (m), 3309 (w), 2989 (m,br); δ(N-H): 1618 (m,br), 1305 (w); Si-O; 1100 (s), 1038 (vs), 1011 (vs); δ(Al-OH): 906 (m); other bands: 787 (w), 748 (w), 688 (m), 559 (s), 470 (s), 433 (s).

- TGA/DSC (85 cm^3/min N_2): 20-86 °C: 6.1 % wt. loss, $T_{endo.}$= 79 °C (w); 86-172 °C: 5.7 % wt. loss, $T_{endo.}$= 152 °C (m); 172-432 °C: 1.7 % wt. loss; 432-640 °C:

9.8 % wt. loss, $T_{endo.}$ = 526 °C (s); 640-1200: $T_{exo.}$ = 1009 °C (s). Total TGA weight loss = 23.3 %.

6.4.4 Kaolinite-Potassium Acetate (Kao-KOAc)

The intercalation reaction of potassium acetate with kaolinite was performed by literature methods [35,51]. 0.2 g of kaolinite (KGa-1; 98 % < 5 μm) was ground together for 5-10 minutes with 0.2 g of potassium acetate (KOAc) using a mortar and pestle. Due to the hygroscopic nature of KOAc, the mixture quickly became pasty. The grinding was occasionally repeated during a two week period after which the mixture was washed with 15 ml of 2-propanol to remove excess KOAc, followed by centrifugation. Air drying yielded 0.28 g of an off-white powder. XRD, FTIR and TGA were in accord with previous literature characterizations [35,36,51].

- XRD (Philips PW 3710, vaseline mounted): d_{001} = 13.97 (100); d_{001} (K) = 7.13 (13.5); d_{003} = 4.68 (0.6); d = 14.00 ± 0.05; I.R. = 0.88.

- FTIR (in cm^{-1}): ν(O-H): 3695 (s), 3652 (m), 3620 (s), 3606 (m), 3479 (s,br); ν(COO^-): 1602 (s,asym), 1420 (m,sym); δ(HOH): 1655 (w,sh); Si-O vibrations: 1114 (s), 1033 (vs), 1014 (vs); δ(Al-OH): 941 (m), 911 (s), 904 (m); other bands: 1349 (vw), 796 (w), 753 (m), 696 (s), 652(m), 545(s), 475 (s), 430 (s).

- TGA/DSC (90 cm^3/min N_2, TGA wt. losses are only approximate due to problems with baseline drift): 20-100 °C: 8.0 % wt. loss, $T_{endo.}$ = 77 °C (s); 100-300 °C: 1.0 % wt. loss; 300-440 °C: 9.4 % wt. loss, $T_{endo.}$ = 381 °C (s); 440-650 °C: 5.4 % wt.

loss, $T_{endo.}$ = 489 °C (m); 650-1000: 0 % wt. loss, $T_{endo.}$ = 683 °C (w). Total TGA weight loss = 23.8 %.

6.4.5 Halloysite-Dimethyl Sulfoxide (Hal-DMSO)

2.0 g of purified halloysite was mixed with 10 ml of DMSO in a sealed jar and stirred for 1 week. This was then filtered, washed with 1,4 dioxane and air dried for 3 hrs.

- XRD (Philips PW 3710, vaseline mounted): d_{001} = 11.16 (100); d_{002} = 5.59 (1.6); d_{003} = 3.73 (19). d= 11.18 ± 0.02 Å; I.R.=1.0.

- FTIR (in cm^{-1}): ν(O-H): 3699 (m), 3663 (s), 3623 (s), 3539 (s), 3502 (s); ν(C-H): 3022 (w), 2939 (w), 2821 (w); δ(HOH): 1630 (w,br); δ(C-H): 1434 (w), 1409 (w), 1320 (w); Si-O vibrations: 1123 (s,sh), 1094 (s), 1028 (vs); δ(Al-OH): 957 (s), 903 (s); other bands: 788 (w), 744 (m), 680 (m), 533 (s), 464 (s), 438 (s).

- TGA/DSC (90 cm^3/min N_2, TGA wt. losses are approximate): 20-140 °C: 12.1 % wt. loss, $T_{endo.}$ = 64 °C (w), $T_{endo.}$ = 106 °C (s); 140-300 °C: 16.6 % wt. loss, $T_{endo.}$ = 211 °C (s); 300-650 °C: 8.5 % wt. loss, $T_{endo.}$ = 502 °C (s); 650-1100 °C: $T_{exo.}$ = 1007 °C (s). Total TGA weight loss = 37.2 %.

6.5 Experimental for Chapter 2

6.5.1 Modification of Kaolinite with Monoalcohols

6.5.1.1 Kao-DMSO + Methanol (Rxn 2-1-1): 5.0 g of Kao-DMSO (I.R. = 0.97; 31 % DMSO) was mixed with 160 ml of methanol (0.03% water by Karl-Fischer titration) in a glass-lined autoclave, sealed and placed in a silicone oil bath. This was maintained at an oil bath temperature ranging from 190-270 °C for 89 hrs. The autogenous pressure which developed ranged from 200 to 630 psig. The reaction vessel was then allowed to cool to ambient temperature, opened up, and the reaction mixture was filtered and washed with 40 ml of methanol. This was dried at 100 °C for 1 hr. The final yield was 3.3 g of an off-white powder (some product was lost during the filtration step).

The water content of the mother liquor as determined by Karl-Fischer titration was found to be 2.2 % by weight compared to 0.03 % for the original methanol solvent. GC-MS confirmed the presence of traces of dimethylether (DME) in the mother liquor (m/e: 46 (M^+, 50); 45 (M^+-H, 100)) although quantitative data for DME was not obtained due to the overlap with the very large methanol peak. GC-MS also showed significant traces of another compound probably 2-methoxyethanol (m/e: 76 (M^+, 1.8); 75 (M^+-H, 71); 62 (M^+-CH_2, 19); 47 (M^+-CH_2CH_3, 20); 45 (M^+-OCH_3, 100); 31 (OCH_3^+, 10); 29 ($CH_2CH_3^+$, 24). Proton NMR (300 MHz, D_2O) of the mother liquor showed the presence of methanol (3.39 ppm, s) and another resonance (2.52 ppm, broad) due perhaps to

residual DMSO. The solid product was characterized by XRD, FTIR, TGA/DSC, elemental analysis (Carbon, Hydrogen) and ^{13}C CP/MAS NMR.

- XRD (Philips PW 3710, methanol dispersed): d_{001}= 8.20 (100); d_{001} (K)= 7.15 (12); 4.46 (6); 4.22 (7.8); d_{002}= 4.08 (16); d_{002} (K)= 3.58 (11); Anatase, 3.51 (3.7); 3.01 (0.9); d_{003}= 2.717 (1.9); 2.56 (0.8); 2.52 (1.7); 2.38 (1.0); 2.33 (0.7); 2.29 (1.3); 2.04 (0.7); 1.97 (0.4); 1.89 (0.3); 1.79 (0.2); 1.69 (0.5); 1.67 (0.5); 1.62 (0.1); d_{060}=1.488 (0.5). d-spacing= 8.17 ± 0.03 Å; I.R.= 0.89.

- FTIR (cm^{-1}): ν(O-H): 3696 (m), 3646 (m), 3620 (m), 3496 (w,vb); ν(C-H): 2957 (w), 2927 (w), 2849 (w); δ(HOH): 1643 (w); δ(C-H): 1460 (vw); Si-O vibrations: 1127 (s), 1050 (vs), 1032 (vs); δ(Al-OH): 910 (s); other bands: 810 (vw), 801 (w), 744 (w), 678 (m), 529 (vs), 472 (s), 431 (s).

- TGA/DSC (80 cm^3/min air; TGA % wt. losses are only approximate): 20-370 °C: 0.2 % wt. loss; 370-640 °C: 12.1 % wt. loss, $T_{endo.}$= 515 °C (s); 640-920 °C: 0.5 % wt. loss; 920-1049 °C: 1.4 % weight loss, $T_{exo.}$=1009 (s). Total TGA wt. loss = 14.2 %. Calcination weight loss (3 hrs at 1100 °C in air atmosphere): 17.85%.

- NMR: ^{13}C CP-MAS (Bruker ASX-200, 50.32 MHz) 51.1 ppm ($\nu_{1/2}$= 75 Hz); ^{29}Si CP-MAS (Bruker ASX-200, 39.76 MHz) -92.6 ppm ($\nu_{1/2}$= 100Hz); ^{27}Al MAS (Bruker ASX-200, 52.15 MHz): -10.7 ppm ($\nu_{1/2}$= 2000 Hz)

- Elemental analysis (calculated for $Al_2Si_2O_5(OH)_{3.13}(OCH_3)_{0.87}$). %C: Found 2.17, Calc. 3.86; %H: Found 2.00, Calc. 2.12; Si/Al (XRF): found 1.13, calc. 1.0.

6.5.1.2 Kao-DMSO + Methanol (Rxn 2-1-2): 1.0 g of Kao-DMSO (I.R.= 0.96) was mixed with 15 ml methanol in an autoclave and sealed, followed by heating in an oil bath between 200-230 °C for 35 hrs (550 psig maximum autogenous pressure). This yielded 0.54 g of an off-white powder, after filtering, washing with methanol and air drying.

- XRD (Philips PW 3710, methanol dispersed): d_{001}= 8.63 (100); d_{001} (K)= 7.17 (8.0); 4.46 (7.5); d_{002}= 4.32 (8.1); 3.96 (2.3); d_{002} (K)= 3.58 (5.3); Anatase 3.52 (1.8); d_{003}= 2.88 (1.8); d_{060}= 1.489 (0.4). d-spacing= 8.63 ± 0.01; I.R.= 0.93.

- FTIR: ν(O-H) 3695 (m), 3645 (m), 3621 (m), 3538 (m,br); ν(C-H): 2956 (w), 2921 (w), 2845 (w).

- TGA/DSC (90 cm^3/min N_2, TGA % wt. losses are approximate): 70-393 °C: 2.3 % wt. loss; 393-673 °C: 11.8 % wt. loss, $T_{endo.}$= 513 °C (s); $T_{exo.}$= 1018 °C (s). Total TGA weight loss = 14.1 %.

- TGA/DSC (90 cm^3/min air, TGA % wt. losses are approximate): 30-306 °C: 2.2 % wt. loss; 306-661 °C: 12.1 % wt. loss, T_{endo}= 510 °C (s); 940-1060 °C: 1.3 % wt. loss, $T_{exo.}$= 963 °C (w, sh), $T_{exo.}$= 1011 °C (s). Total TGA wt. loss = 15.6 %.

6.5.1.3 Kao-DMSO + Methanol (Rxn 2-1-3) Other preparation methods were less successful. Heating 1.5 g of Kao-DMSO with 25 ml of methanol in an autoclave for 42 hrs at 155-160 °C (temperature of silicone oil bath), yielded a material with significant amounts of DMSO and possibly water in the interlayers.

- XRD (Philips PW 3710, methanol dispersed): 11.26 Å (100); 9.17 Å (12); 7.15 Å (6.5).

- FTIR (cm^{-1}): ν(O-H): 3694 (m), 3626 (m), 3538 (m,br); C-H: 3020 (w), 2940 (w), 2843 (w); δ(HOH): 1645 (w); δ(C-H): 1434 (vw), 1406 (vw), 1320 (vw).

6.5.1.4 Kao-NMF + Methanol (Rxn 2-1-4): 1.0 g of Kao-NMF (I.R.= 0.93) was mixed with 15 ml methanol in an autoclave and sealed, followed by heating in an oil bath between 190-200 °C for 20 hrs (400 psig autogenous pressure). After filtering, washing with methanol and air drying, this yielded 0.87 g of an off-white powder.

- XRD (Philips PW 3710, methanol dispersed): d_{001}= 8.56 (100); d_{001} (K)= 7.15 (10); 4.46 (11); 4.35 (9.4); d_{002}= 4.25 (12); 4.17 (9.2); 3.96 (4.1); d_{002} (K)= 3.57 (11); Anatase 3.51 (5.2); d_{003}= 2.84 (1.8); d_{060}= 1.489 (0.8). d-spacing= 8.53 ± 0.04 Å; I.R.= 0.91.

- FTIR: ν(O-H) 3695 (m), 3646 (m), 3621 (m), 3523 (m,br); ν(C-H): 2955 (w), 2922 (w), 2843 (w).

- TGA/DSC (80 cm^3/min air; TGA % wt. losses are approximate): 20-270 °C, 2.3 % wt. loss; 270-640 °C, 12.9 % wt. loss, $T_{endo.}$= 523 °C (s); 969-1096 °C, 1.3 % weight loss, $T_{exo.}$= 1014 °C (s).

6.5.1.5 Kaolinite + Methanol (Rxn 2-1-5): 1.0 g of kaolinite was mixed with 20 g of dry methanol (<0.05 % water by Karl-Fischer titration) in an autoclave, sealed, and heated in an oil bath between 200-215 °C for 120 hrs. After filtering, washing with

methanol and air drying, this afforded an off-white powder. This was shown by XRD to be unreacted kaolinite. The water content of the mother liquor was 0.62 % by Karl-Fischer titration.

6.5.1.6 Kao-NMF + Ethanol (Rxn 2-1-6): 2.0 g of Kao-NMF (I.R.= 0.91) was mixed with 60 ml of reagent grade ethanol in an autoclave and sealed, followed by heating in an oil bath between 200-230 °C for 18 hrs. After filtering, washing with ethanol and air drying, this afforded 1.4 g of an off-white powder. This was shown by XRD and FTIR to be mainly collapsed kaolinite, with a trace of residual Kao-NMF, evident by the FTIR peaks at 3420 (w) and 1683 (w).

- XRD (Philips PW 1050/81, ethanol dispersed): d_{001} (K)= 7.20 (69); 4.46 (14); 4.37 (10); 4.18 (7); d_{002} (K)= 3.58 (100).

6.5.1.7 Kao-DMSO + n-Decanol (Rxn 2-1-7): 3.0 g of Kao-DMSO (I.R. = 0.95) was refluxed with 100 ml of benzyl alcohol (Aldrich, BP: 231 °C) in open atmosphere for 6 hrs. Bumping proved to be a problem, so a few boiling chips were added to the refluxing mixture. This was cooled and the mixture was washed/centrifuged with ethanol to remove excess decanol. The product was air dried to yield 1.7 g of a greyish powder. The FTIR pattern of the product was almost identical to that of unreacted kaolinite. XRD confirmed that most of the product was in the form of a very disordered 7.2 Å kaolinite phase, but traces of an additional phase characterized by a reflection at d= 9.5 Å could also be observed.

6.5.1.8 Kao-DMSO + Benzyl Alcohol (Rxn 2-1-8): 1.7 g of Kao-DMSO was refluxed with 65 ml of benzyl alcohol (BP: 202-206 °C) in open atmosphere for 20 hrs. This was cooled to 40 °C and the mixture was filtered while still warm, followed by washing with acetone to remove excess benzyl alcohol. The product was dried in an oven at 70 °C for 1 hr to yield 1.0 g of product. FTIR showed that the Kao-DMSO starting material had collapsed to give the parent kaolinite material.

6.5.1.9 Treatment of Kao-MeOH 8.2 Å with Water (Rxn 2-1-9): 0.3 g of Kao-MeOH was mixed with 10 ml of water and stirred for 14 days at room temperature. Upon centrifugation and washing one time with water, the sample was collected and characterized.

- XRD (Philips PW 3710, methanol dispersed): d_{001}= 8.62 Å (100); d_{001} (K)=7.14 Å (16); 4.45 (5.8); d_{002}= 4.26 (5.5); d_{002} (K)= 3.57 (9.8); Anatase 3.51 (3.5); 3.36 (0.7); 3.05 (0.3); 2.56 (0.9); 2.53 (0.8); 2.38 (1.3); 2.34 (0.8); 2.29 (0.5); 2.10 (0.3); 1.89 (0.2); 1.79 (0.3); 1.66 (0.2); 1.62 (0.1); d_{060}= 1.488. I.R.= 0.86.

- FTIR (cm^{-1}): ν(O-H): 3695 (m), 3644 (m), 3623 (m), 3549 (m); ν(C-H): 2956 (w), 2927 (w), 2844 (w); δ(HOH): 1646 (w); δ(C-H): 1460 (vw); Si-O vibrations: 1089 (s), 1080-1000 (vs); δ(Al-OH): 910 (s); other bands: 796 (w), 750 (w), 682 (m), 541 (s), 473 (s), 431 (s).

When a portion of the water washed Kao-MeOH product (d_{001}= 8.62 Å.; I.R.= 0.86) was heated at 150 °C for 4 hours a partial structural collapse resulted as observed by XRD (d(Å)= 8.10 (100); 7.14 (22)). The FTIR pattern was also consistent with the

formation of a product resembling the original Kao-MeOH 8.2 Å product, only in this case the ν(C-H) bands were less intense than previously.

6.5.2 Modification of Kaolinite with Simple Polyols

6.5.2.1 Kao-DMSO + Ethylene Glycol (Rxn 2-2-1): 2.0 g of Kao-DMSO (I.R.=0.97) was refluxed with 100 ml of ethylene glycol (<0.05 % H_2O by Karl-Fischer titration, BP 196-198 °C) under N_2 atmosphere for 18 hrs. Centrifugation, washing with methanol and air drying yielded 1.2 g of an off-white powder.

- XRD (Philips PW 1050/81, methanol dispersed): d_{001}= 9.45 (100); d_{001} (K)= 7.18 (3.5); d_{002}= 4.69 (9); 4.47 (5); 4.18 (8); 4.03 (2); d_{002}(K)=3.58 (3); Anatase 3.52 (1); 3.38 (1); d_{003}=3.13 (1.9). d-spacing= 9.40 ± 0.04; I.R.= 0.97.

- FTIR (cm^{-1}): ν(O-H): 3693 (m), 3665 (m), 3620 (s), 3572 (s), 3396 (s); ν(C-H): 2968 (w), 2945 (w), 2894 (w); δ(HOH): 1630 (vw); δ(C-H): 1462 (vw), 1384 (w), 1324 (w), 1279 (vw), 1237 (w), 872 (w); Si-O vibrations: 1120 (s), 1086 (s), 1045 (vs); δ(Al-OH): 910 (s); other bands: 794 (w), 750 (w), 674 (m), 545 (vs), 470 (s), 434 (s).

- TGA/DGA (TA Instruments 2950 TGA, 10 °C/min, 100 cm^3/min N_2): 20-200 °C: 0.8 % wt. loss; 200-440 °C: 9.7 % wt. loss, DGA peaks= 355 °C (sh) and 400 °C ; 470-640 °C: 7.2 % weight loss, DGA peaks= 471 °C (sh) and 482 °C; 640-1000 °C: negligible wt. loss. Total TGA wt. loss = 17.7 %.

DTA (TA Instruments 2910 DSC, 10 °C/min, 40 cm^3/min N_2): $T_{endo.}$= 380 °C (m); $T_{endo.}$= 449 °C (m); $T_{exo.}$= 494 °C (m); $T_{endo.}$= 555 °C (m).

6.5.2.2 Kao-DMSO + Ethylene Glycol (Rxn 2-2-2): This reaction was scaled up by refluxing 18 g of Kao-DMSO (I.R.= 0.92) with 300 ml of EG for 44 hrs. Washing with methanol and air drying yielded 13 g of product. The FTIR pattern of the product was nearly identical to that previously reported.

- XRD (Philips PW 1050/81, methanol dispersed): d_{001}= 9.43 (100); d_{001} (K)= 7.18 (8); d_{002}= 4.69 (5); 4.46 (6); 4.18 (9); 4.03 (5); d_{002} (K)= 3.58 (6); 3.38 (2); d_{003}= 3.12 (13). d-spacing= 9.40 ± 0.03; I.R.= 0.92.

- Density (Micromiretics helium pycnometer): 2.40 ± 0.04 g/cm^3.

- NMR: ^{13}C CP/MAS (Bruker CXP-180, 45.3 MHz) 64.1 ppm ($v_{1/2}$= 150 Hz); ^{29}Si CP/MAS (Bruker CXP-180, 35.8 MHz) -92.4 ppm ($v_{1/2}$= 90 Hz).

Preparation of composite membranes using Kao-EG 9.4 Å and PDMS: Kaolinite and Kao-EG 9.4 Å (2-2-2) were incorporated into a polydimethylsiloxane (PDMS) matrix to form a composite membrane (40 % by weight of kaolinite) for use in gas separation testing. The preparation of these membranes was based on procedures described elsewhere [248,249]. Briefly, 2.40 g of kaolinite or Kao-EG 9.4 Å were mixed with 3.27 g of vinylmethylpolysiloxane (silicone rubber compound RTV615, General Electric Silicones) and 2 ml of hexane. The mixture was dispersed by vigorous mechanical stirring and then by sonification, followed by addition of 0.33 g of the curing agent (RTV615B, General Electric Silicones). After 2 minutes of mechanical stirring, the membrane was cast on a clean glass plate to a thickness of 0.2 mm, followed by heating at 100 °C overnight. The membrane was then carefully pealed off. Preliminary tests

performed on the membranes for the separation of benzene from water were not very promising, so no further tests were done.

6.5.2.3 Kao-NMF + Ethylene Glycol (Rxn 2-2-3): 2.0 g of Kao-NMF (I.R.=0.90) was refluxed with 100 ml of ethylene glycol (<0.05 % H_2O by Karl-Fischer titration, BP 196-198 °C) under N_2 atmosphere for 20 hrs. Centrifugation, washing with methanol and air drying yielded 1.3 g of an off-white powder. FTIR showed the product to be almost identical to that obtained with Kao-DMSO as the starting material.

-XRD (Philips PW 1050/81, 1,4 dioxane dispersed): d_{001}= 9.51 (100); d_{001} (K)= 7.18 (16); d_{002}= 4.69 (4); 4.46 (7); 4.18 (9); 4.04 (5); d_{002} (K)= 3.58 (10); 3.39 (2); 3.30 (2); d_{003}= 3.14 (8). d-spacing= 9.43 $\pm$ 0.07; I.R.= 0.86.

6.5.2.4 Kao-NMF + Ethylene Glycol (Rxn 2-2-4): 1.0 g of Kao-NMF (I.R.=0.91) was refluxed with 2.5 ml of ethylene glycol in a 5 ml round bottom under open atmosphere for 17 hours. Filtering and washing with ethanol provided as off-white powder. The FTIR pattern was characteristic of a high intercalation ratio Kao-EG 9.4 Å (I.R $\approx$ 0.9).

6.5.2.5 Kaolinite + Ethylene Glycol (Rxn 2-2-5): 2.2 g of purified kaolinite (98 % < 5 μm) was refluxed with 100 ml of ethylene glycol for 18 hrs under N_2 atmosphere. Filtering and washing with methanol yielded a product whose IR spectrum was identical with unmodified kaolinite.

6.5.2.6 Kao-DMSO + 1,3 Propanediol (Rxn 2-2-6): 0.6 g of Kao-DMSO was refluxed with 30 ml of 1,3 propanediol (BP: 214 °C) for 22 hrs under nitrogen atmosphere, followed by cooling, filtering and washing with methanol. An off-white powder was collected, air dried and then vacuum dried over P_2O_5 at 40 °C for 3 hrs.

- XRD (Philips PW 1050/81, methanol dispersed): d_{001}= 9.84 (100); d_{001} (K)= 7.18 (3); d_{002}=4.90 (5); 4.47 (4); 4.20 (3); d_{002} (K)= 3.58 (4); Anatase 3.52 (1); d_{003}=3.27 (8). d-spacing= 9.82 ± 0.02; I.R.= 0.97.

- FTIR (in cm^{-1}): ν(O-H): 3694 (m), 3632 (m), 3621 (m), 3550 (m,br), 3440 (m,br); ν(C-H): 2968 (w), 2890 (w); δ(HOH): 1640 (w)

- TGA (N_2 atm., 20 °C/min., Perkin-Elmer TGA 7): 50-200 °C: 3.1 % wt. loss; 200-460 °C: 7.8 % wt. loss; 460-650 °C: 6.8 % wt loss; 650-1000 °C: 1.4 % wt. loss. Total weight loss = 19.0 %.

- NMR: ^{13}C CP/MAS (Bruker CXP-180, 45.3 MHz) 62.2 ppm ($\nu_{1/2}$= 300 Hz), 30.5 ppm ($\nu_{1/2}$= 400 Hz); ^{29}Si CP/MAS (Bruker CXP-180, 35.8 MHz) -92.7 ppm ($\nu_{1/2}$= 85 Hz).

6.5.2.7 Kao-NMF + 1,3 Propanediol (Rxn 2-2-7): 1.0 g of Kao-NMF (I.R. 0.91) was refluxed with 50 ml of 1,3 propanediol (BP: 214 °C) for 18 hrs under nitrogen atmosphere, followed by cooling, filtering and washing with 1,4 dioxane. After air drying, 0.85 g of an off-white powder was collected. This showed substantially smaller signs of modification as seen by FTIR than for the same product using DMSO as the

starting material (Reaction 6). The v(C-H) stretching patterns of the two products were practically identical.

- TGA/DSC (N_2 40 cc/min): 20-200 °C: 1.0 % wt. loss; 200-450 °C: 7.3 % wt. loss, $T_{endo.}$ = 411 °C (m); 450-650 °C: 10.4 % wt loss, $T_{endo.}$ = 517 °C (s); 650-950 °C: 1.4 % wt. loss; 950-1200 °C: 2.2 % wt. loss, $T_{exo.}$ = 1006 °C (m), $T_{exo.}$ = 1026 °C (w,sh). Total weight loss = 22.3 %.

6.5.2.8 Kao-DMSO + 1,2 Propanediol (Rxn 2-2-8): 0.6 g of Kao-DMSO (I.R.= 0.97) was refluxed with 30 ml of 1,2 propanediol (BP: 187 °C) for 20 hrs under nitrogen atmosphere, followed by cooling, filtering and washing with methanol. The product was air dried, followed by vacuum drying at 120 °C for 3 hrs.

- XRD (Philips PW 1050/81, methanol dispersed): d_{001}= 10.90 (100); d_{001} (K)= 7.16 (1.8); d_{002}= 5.43 (1.5); 4.45 (1.5); 4.31 (1.5); 4.12 (1.9); 3.95 (0.5); d_{003}= 3.61 (11); 3.34 (0.6); 3.25 (1.2); d_{004}= 2.71 (1.4); d_{005}=2.16 (1.3). d-spacing= 10.84 ± 0.03; I.R.= 0.98.

- FTIR (in cm^{-1}): v(O-H) 3694(m), 3641(s), 3621 (w), 3609(w), 3490 (m,br); v(C-H) 2971 (w), 2937 (w), 2880 (w,sh).

- TGA/DSC (N_2 35 cc/min): 20-200 °C: 3.2 % wt. loss, $T_{endo.}$= 116 °C (w); 200-455 °C: 11.5 % wt. loss, $T_{endo.}$= 405 °C (s); 455-650 °C: 8.0 % wt loss, $T_{endo.}$= 517 °C (m); 650-950 °C: 1.4 % wt. loss; 950-1200 °C: 2.2 % wt. loss, $T_{exo.}$= 1003 °C (w), $T_{exo.}$= 1024 °C (w). Total weight loss = 26.3 %.

- NMR: ^{13}C CP/MAS (Bruker CXP-180, 45.3 MHz) 70.2 ppm ($\nu_{1/2}$= 215 Hz), 21.4 ppm ($\nu_{1/2}$= 150 Hz); ^{29}Si CP/MAS (Bruker CXP-180, 35.8 MHz) -93.2 ppm ($\nu_{1/2}$= 65 Hz).

6.5.2.9 Kao-NMF + 1,2 Propanediol (Rxn 2-2-9): 1.0 g of Kao-NMF (I.R. =0.91) was refluxed with 50 ml of 1,2 propanediol (BP: 187 °C) for 16 hrs under nitrogen atmosphere, followed by cooling, filtering and washing with 1,4 dioxane. 0.9 g of product was recovered after air drying. This was shown by FTIR to be very similar to the product obtained from Kao-DMSO starting material (Rxn **2-2-8**), only the extent of modification was somewhat less, and there were traces of residual NMF.

- TGA/DSC (N_2 40 cm^3/min): 20-200 °C: 2.2 % wt. loss, $T_{endo.}$= 101 °C (w); 200-445 °C: 8.3 % wt. loss, $T_{endo.}$= 410 °C (m); 445-650 °C: 9.9 % wt loss, $T_{endo.}$= 517 °C (m); 650-950 °C: 1.5 % wt. loss; 950-1200 °C: 2.0 % wt. loss, $T_{exo.}$= 1005 °C (m), $T_{exo.}$= 1025 °C (w,sh). Total weight loss = 23.9 %

6.5.2.10 Kao-DMSO + 1,4 Butanediol (Rxn 2-2-10): 1.6 g of Kao-DMSO (I.R.= 0.97) was refluxed with 30 ml of 1,4 butanediol (BP: 230 °C) for 19 hrs, followed by cooling, filtering and washing with ethanol. The product was air dried to yield 1.2 g of an off-white powder. Characterization by XRD and FTIR showed that the product consisted primarily of the starting material, Kao-DMSO.

- XRD (Philips PW 3710, vaseline mounted): d_{001}=11.39 (100), d_{001} (K)= 7.24 (16), d_{003}= 3.71 (76); d-spacing= 11.26 ± 0.18, I.R.= 0.86.

- FTIR (in cm^{-1}): v(O-H) 3698 (m), 3663 (m), 3623 (m), 3545 (m, br), 3510 (m,br); v(C-H) 3020 (w), 2934 (w).

Vacuum drying at 120 °C over P_2O_5 for 3 hrs, exhibited an FTIR pattern consistent with a disordered almost completely collapsed kaolinite. Water washing of the product (overnight in excess water) showed an IR v(OH) pattern typical of a hydrated kaolinite with v(OH) bands at 3693 (m), 3618 (m), 3600 (m), 3553 (m), and almost no absorption in the v(C-H) region. A substantial δ(HOH) band was found at 1635 cm^{-1}, and a band at 970 cm^{-1} due plausibly to the bending of inner surface Al-OH groups H-bonded to interlayer water could also be detected. XRD showed what appeared to be the presence of three phases with reflections at d(Å)= 9.9, 8.3 and 7.2. The reflections at d= 9.9 Å was thought to be due to a dihydrate of kaolinite, the one at d= 8.3 Å to the monohydrate of kaolinite, and finally the reflection at d= 7.2 Å was thought to be due residual kaolinite.

Subsequent attempts using both Kao-DMSO and Kao-NMF as starting materials to form a 1,4 butanediol organokaolinite were unsuccessful.

6.5.2.11 Kao-DMSO + (±) 1,2 Butanediol (Rxn 2-2-11): 1.0 g of Kao-DMSO (I.R.= 0.98) was refluxed with 50 ml of (±) 1,2 butanediol (Aldrich, BP 191-192 °C) for 16 hrs under N_2 atmosphere, followed by cooling, filtering and washing with ethanol. The product was air dried to yield 0.6 g of an off-white powder.

- XRD (Philips PW 3710, vaseline mounted): d_{001} = 11.30 (100); d_{001} (K) = 7.15 (2.2); d_{002} = 5.68 (1.3); 4.44 (6.4); 4.14 (4.3); 3.96 (3.2); d_{003} = 3.79 (11.3), d_{002} (K) = 3.57 (1.8); Anatase 3.51 (1.7); d_{004} = 2.84 (1.3); d_{005} = 2.28 (1.5); d_{006} = 1.89 (0.3). d = 11.36 ± 0.04; I.R. = 0.98.

- FTIR (in cm^{-1}): ν(O-H) 3695 (m), 3648 (m), 3621 (m), 3490 (m, br); ν(C-H): 2966 (w), 2938 (w), 2883 (w); δ(HOH): 1637 (w); δ(C-H): 1463 (vw): Si-O vibrations: 1125 (s), 1060-1010 (vs); δ(Al-OH): 913 (s); other bands: 745 (w), 676 (m), 541 (vs), 475 (vs), 429 (s).

- TGA/DSC (90 cm^3/min N_2, weight losses approximate due to baseline drift): 20-200 °C: 4.6 % wt. loss, $T_{endo.}$ = 59 °C (w), $T_{endo.}$ = 138 °C (w); 200-440 °C: 13.5 % wt. loss, $T_{endo.}$ = 386 °C (s); 440-650 °C: 10.3 % wt. loss, $T_{endo.}$ = 513 °C (m); 650-1050 °C: 1.5 % wt. loss, $T_{exo.}$ = 1012 °C (w), $T_{exo.}$ = 1027 °C (m); Total weight loss: 29.9 %.

6.5.2.12 Kao-NMF + (±) 1,2 Butanediol (Rxn 2-2-12): 1.0 g of Kao-NMF (I.R. = 0.91) was refluxed with 50 ml of (±) 1,2 butanediol (Aldrich, BP 191-192 °C) for 16 hrs under N_2 atmosphere, followed by cooling, filtering and washing with ethanol. The product was air dried to yield 0.8 g of an off-white powder. The FTIR pattern of the product was virtually identical to that of unmodified kaolinite.

6.5.2.13 Kao-DMSO + 1,3 Butanediol (Rxn 2-2-13): 1.0 g of Kao-DMSO (I.R. = 0.98) was refluxed with 50 ml of (±) 1,3 butanediol (Aldrich, BP 203-204 °C)

for 20 hrs under N_2 atmosphere, followed by cooling, filtering and washing with ethanol. The product was air dried to yield 0.5 g of an off-white powder.

- XRD (Philips PW 3710, vaseline mounted): d_{001}= 11.30 (100); d_{001} (K)= 7.12 (2.2); d_{002}= 5.68 (1.2); 4.45 (9.2); 4.16 (7.2); d_{003}= 3.79 (9.0); d_{002} (K)= 3.57 (2.9); Anatase 3.51 (3.6); d_{004}= 2.85 (0.9); d_{005}= 2.28 (0.6); d_{006}= 1.89 (0.5); d_{007}= 1.62 (0.1). d= 11.36 ± 0.04; I.R.= 0.98.

- FTIR (in cm^{-1}): ν(O-H) 3695 (m), 3646 (m), 3621 (m), 3604 (w), 3549 (m, br), 3425 (m, br); ν(C-H); 2974 (w), 2935 (w), 2888 (w, sh); δ(HOH): 1637 (w); δ(C-H): 1458 (vw), 1386 (vw), 858 (vw): Si-O vibrations: 1120 (s), 1086(s), 1051 (vs), 1035 (vs); δ(Al-OH): 911 (s); other bands: 800 (w), 746 (w), 679 (m), 541 (s), 472 (s), 431 (s).

- TGA/DSC (90 cm^3/min N_2, weight losses approximate due to baseline drift): 20-100 °C: 3.4 % wt. loss, $T_{endo.}$= 60 °C (w); 100-250 °C: 5.1 % wt. loss; 250-450 °C: 13.1 % wt. loss, $T_{endo.}$= 387 °C (s); 450-650 °C: 9.0 % wt. loss, $T_{endo.}$= 497 °C (m); 650-1050 °C: $T_{exo.}$= 1012 °C (m), $T_{exo.}$= 1029 °C (m); Total weight loss: 30.6 %.

6.5.2.14 Kao-NMF + 1,3 Butanediol (Rxn 2-2-14): 1.0 g of Kao-NMF (I.R.= 0.91) was refluxed with 50 ml of (±)-1,3 butanediol (Aldrich, BP 203-204 °C) for 20 hrs under N_2 atmosphere, followed by cooling, filtering and washing with ethanol. The product was air dried to yield 0.9 g of an off-white powder. FTIR and XRD showed that the product was mostly a collapsed kaolinite, with traces of an additional phase.

- XRD (Philips PW 3710, vaseline mounted): d_{001} = 11.50 (30); $d_{\bar{1}01}$ (K)= 7.12 (77); d_{002} (K)=3.57 (100). I.R. = 0.28.

- FTIR (in cm^{-1}): ν(O-H) 3697 (s), 3668 (w), 3654 (w), 3621 (m), 3421 (w, br); ν(C-H); 2974 (w), 2935 (w), 2888 (w, sh); δ(HOH): 1657 (vw); Si-O vibrations: 1115 (s), 1085 (s), 1043 (vs,sh) 1033 (vs), 1011 (vs); δ(Al-OH): 915 (s), 940 (m, sh); other bands: 792 (w), 754 (w), 691 (m), 542 (vs), 471 (s), 430 (s).

- TGA/DSC (90 cm^3/min N_2, weight losses approximate due to baseline drift): 20-200 °C: 4.4 % wt. loss, $T_{endo.}$ = 124 °C (m); 200-400 °C: 1.0 % wt. loss; 400-650 °C: 12.9 % wt. loss, $T_{endo.}$ = 519 °C (s); 650-1050 °C: $T_{exo.}$ = 1012 °C (s). Total weight loss =18.3 %.

6.5.2.15 Kao-DMSO + 2,3 Butanediol (Rxn 2-2-15): 1.0 g of Kao-DMSO (I.R.= 0.98) was refluxed with 40 ml of 2,3 butanediol (Aldrich, BP 183-184 °C) for 20 hrs under N_2 atmosphere, followed by cooling, filtering and washing with ethanol. The product was air dried to yield 0.6 g of an off-white powder. The FTIR pattern of the product was virtually identical to that of unmodified kaolinite.

6.5.2.16 Kao-NMF + 1,3 Butanediol (Rxn 2-2-16): 1.0 g of Kao-NMF (I.R.= 0.91) was refluxed with 40 ml of 2,3 butanediol (Aldrich, BP 183-184 °C) for 20 hrs under N_2 atmosphere, followed by cooling, filtering and washing with ethanol. The product was air dried to yield 0.7 g of an off-white powder. The FTIR pattern of the product was virtually identical to that of unmodified kaolinite.

6.5.2.17 Kao-DMSO + 1,5 Pentanediol (Rxn 2-2-17): 1.5 g of Kao-DMSO (I.R.= 0.98) was refluxed with 50 ml of 1,5 pentanediol (BP: 242 °C) for 16 hrs, followed by cooling, filtering and washing with methanol. The product was air dried to yield 1.0 g of an off-white powder. Characterization by FTIR showed that the product was kaolinite, which was regenerated upon collapse of Kao-DMSO.

6.5.2.18 Kao-NMF + 1,5 Pentanediol (Rxn 2-2-18): 1.5 g of Kao-NMF (I.R.= 0.91) was refluxed with 50 ml of 1,5 pentanediol (BP: 242 °C) for 16 hrs, followed by cooling, filtering and washing with methanol. The product was air dried to yield 1.0 g of an off-white powder. Characterization by FTIR showed that the product was kaolinite, which was regenerated upon collapse of the Kao-NMF starting material.

6.5.2.19 Kao-DMSO + Glycerol (Rxn 2-2-19): 0.2 g of Kao-DMSO was mixed with 15 ml of glycerol in a glass vial, and the viscous mixture was sonified to ensure dispersion. Sonification resulted in the reaction mixture heating up to about 100 °C. The reaction mixture was then sealed with parafilm and stored with occasional agitation for 40 days. This was then washed with methanol, air dried and analyzed by FTIR and XRD.

- XRD (Philips PW 1050/81, ethanol dispersed): d_{001}= 11.07 (100); d_{001} (K)= 7.18 (4); d_{002}= 5.54 (1); 4.46 (2); 4.34 (3); 4.14 (4); 3.91 (1); d_{003}=3.68 (14); d_{002} (K)= 3.57 (2); Anatase 3.52 (0.5); 3.22 (1); d_{004}= 2.75 (1.5); 2.55 (1). d=11.06 $\pm$ 0.02; I.R.= 0.96.

- FTIR (in cm^{-1}): v(O-H): 3694 (m), 3620 (m), 3600 (m), 3543 (m,br), 3400 (m,br); v(C-H): 2948 (w), 2897 (w).

6.5.2.20 Kao-NMF + Glycerol (Rxn 2-2-20): 0.2 g of Kao-NMF was mixed with 15 ml of glycerol in a glass vial, and the viscous mixture was sonified to ensure dispersion. Sonification resulted in the reaction mixture heating up to about 100 °C. The reaction mixture was then sealed with parafilm and stored with occasional agitation for 40 days. This was then washed with methanol, air dried and analyzed by FTIR and XRD.

- XRD (Philips PW 1050/81, ethanol dispersed): d_{001}=11.04 (100), d_{001}(K)=7.18 (18), 4.45 (11); 4.34 (6); 4.13 (8); d_{003}=3.67 (22); d_{002} (K)= 3.57 (15); Anatase 3.52 (5). d=11.03 ± 0.03; I.R.= 0.85.

- FTIR (in cm^{-1}): v(O-H): 3692 (m), 3619 (m), 3600 (m), 3546 (m,br), 3418 (m,br); v(C-H): 2947 (w), 2890 (w).

6.5.3 Modification of Kaolinite with Ether Alcohols

6.5.3.1 Kao-DMSO + 2-Methoxyethanol (Rxn 2-3-1): 12.8 g of Kao-DMSO (I.R. =0.80) was refluxed with 500 ml of 2-methoxyethanol (BP. 124 °C) for 67 hrs under open atmosphere. This was then cooled, filtered and washed with methanol followed by vacuum drying at 120 °C over P_2O_5 for 3 hrs to yield 12.3 g of an off-white powder.

- XRD (Philips PW 1050/81, 1,4 dioxane dispersed): d_{001}=10.60 (100); d_{001} (K) =7.18 (18); d_{002}= 5.28 (2); 4.47 (5); 4.36 (1); 4.11 (1); d_{002} (K)= 3.57 (13); d_{003}=3.52 (14). d=10.57 ± 0.03; I.R.= 0.85.

- FTIR (in cm^{-1}): ν(O-H): 3694 (m), 3649 (m), 3620 (m), 3470 (m,br); ν(C-H): 3018 (vw), 2970 (w), 2935 (w), 2908 (w), 2878 (vw), 2847 (w), 2820 (vw); δ(HOH) 1638 (w); δ(C-H); 1475(vw), 1455 (vw), 1440 (vw), 1264(w), 1199 (w); other bands: 1114 (s), 1000-1100 (vs), 940 (w,sh), 914 (s), 838 (w), 797 (w), 751 (w), 690 (m), 540 (s), 471 (s), 431 (s).

- TGA/DSC (40 cm^3/min N_2): 20-200 °C: 1.1 % wt. loss; 200-440 °C: 6.9 % wt. loss, $T_{endo.}$= 412 °C (s); 440-475 °C: 2.8 wt. loss, $T_{endo.}$= 464 °C (m); 475-650: 6.7 % wt loss, $T_{endo.}$= 528 °C (s); 650-950 °C; 1.1 % wt. loss; 950-1200 °C: 1.9 % wt loss, $T_{exo.}$= 1002 °C (m). Total weight loss = 20.5 %.

- NMR: ^{13}C CP/MAS (Bruker CXP-180, 45.3 MHz) 74.2 ppm ($\nu_{1/2}$= 240 Hz), 62.0 ppm ($\nu_{1/2}$= 180 Hz); ^{29}Si CP/MAS (Bruker CXP-180, 35.8 MHz) -91.57 ppm ($\nu_{1/2}$= 75 Hz, residual kaolinite), -93.1 ppm ($\nu_{1/2}$= 55 Hz).

6.5.3.2 Kao-NMF + 2-Methoxyethanol (Rxn 2-3-2): 1.0 g of Kao-NMF (I.R. =0.91) was refluxed with 50 ml of freshly distilled 2-methoxyethanol (124-125 °C fraction) for 22 hrs under nitrogen atmosphere. This was then cooled, filtered and washed with 1,4 dioxane followed by air drying to yield 0.90 g of an off-white powder. FTIR indicated that this was essentially the same product as that obtained from Kao-DMSO,

with the exception that some trace amounts of NMF could be detected (ν(NH) 3415 cm^{-1}, ν(C=O) 1654 cm^{-1}).

6.5.3.3 Kao-DMSO + Diethyleneglycol Monobutyl Ether (Rxn 2-3-3): 2.0 g of Kao-DMSO (I.R. =0.97) was refluxed with 200 ml of diethylene glycol mono n-butyl ether (BP. 231 °C) for 19 hrs under open atmosphere. This was then cooled, filtered and washed with methanol. After drying on a hot plate (low setting), 2.0 g of an off-white powder was recovered.

- XRD (Philips PW 3710, vaseline mounted): d_{001}=10.84 (100); 8.54 (0.7); d_{001} (K)= 6.99 (1.8); d_{002}= 5.47 (1.0); 4.42 (6.2); 4.13 (4.9); 4.06 (4.4); 3.95 (5.3); d_{003}= 3.69 (12). d=10.94 ± 0.11; I.R.= 0.98.

- FTIR (in cm^{-1}): ν(O-H): 3694 (m), 3630 (s), 3621 (s), 3555 (s,br); ν(C-H): 2940 (w), 2880 (w); δ(HOH) 1635 (w); Si-O: 1120 (s,sh), 1088 (s,sh), 1050 (vs), 1021 (vs); δ(Al-OH): 950 (w,sh), 910 (s); other bands: 1600 (w), 1365 (vw), 797 (w), 746 (w), 682 (m), 548 (vs), 470 (s), 431 (s).

- TGA/DSC (90 cm^3/min air, TGA % wt. loss values are approximate): 20-200 °C: 2.9 % wt. loss, DGA peak= 95 °C (w); 200-400 °C: 8.1 % wt. loss, DGA peak= 317 °C (s), $T_{exo.}$= 317 °C (s); 400-650 °C: 7.5 % wt. loss, DGA peak= 473 °C (m), $T_{endo.}$= 482 °C (m); 950-1200 °C: 1.6 % wt loss, $T_{exo.}$= 1007 °C (w). Total TGA weight loss = 20.1 %.

6.5.3.4 Kao-NMF + Diethyleneglycol Monobutyl Ether (Rxn 2-3-4): 1.0 g of Kao-NMF (I.R. =0.91) was refluxed with 50 ml of freshly distilled diethylene glycol mono n-butyl ether (Fisher, BP 231 °C) for 22 hrs under nitrogen atmosphere. This was then cooled, filtered and washed with 1,4 dioxane followed by air drying to yield 0.90 g of an off-white powder. FTIR indicated that very little modification had been achieved, although there was some weak absorption in the C-H stretching region (2800-3100 cm^{-1}).

6.5.3.5 Kao-NMF + Triethyleneglycol Monomethyl Ether (Rxn 2-3-5): 1.0 g of Kao-NMF (I.R. =0.91) was refluxed with 40 ml of triethyleneglycol monomethyl ether (Aldrich, 95 %, BP >200 °C) for 27 hrs under open atmosphere. This was then cooled, filtered and washed with methanol, followed by air drying to yield 0.94 g of a greyish powder.

- XRD (Philips PW 1050/81, 1,4 dioxane dispersed): d_{001}=11.03 (100); 8.48 (2); d_{001} (K)= 7.18 (11); d_{002}= 5.51 (4); 4.46 (19); 4.14 (11); d_{003}=3.65 (55); d_{004}= 2.74 (1); d_{005}= 2.20 (1). d=10.99 ± 0.04 Å, I.R.= 0.95.

- FTIR (in cm^{-1}): ν(O-H): 3695 (s), 3650 (s), 3622 (s), 3475 (m,br); ν(C-H): 2932 (w), 2878 (w); δ(HOH) 1655 (w); δ(C-H) 1462 (vw), 1252 (vw), 850 (vw); Si-O: 1127 (m), 1050 (vs), 1025 (vs); δ(Al-OH): 915 (s); other bands: 801 (vw), 750 (w), 690 (m), 550 (vs), 482 (s), 430 (s).

6.6 Experimental for Chapter 3

6.6.1 Preparation of Kao-EG 10.8 Å

6.6.1.1 Rxn 3-1-1: 1 g of Kao-DMSO (I.R. > 95 %) was mixed with 1 ml reagent grade ethylene glycol (BDH) in a 2 ml glass ampoule and then sealed. The ampoule was placed in an oven and maintained at 140-190 °C for 3 days. This was opened up, filtered and washed with methanol, followed by air drying for 4 hours, yielding a white powder.

- XRD (Philips PW 3710, vaseline mounted): d_{001}= 10.74 (100); d_{001} (K)= 7.12 (1.7); d_{002}= 5.41 (0.7); 4.45 (4.9); 4.13 (5.9); 3.74 (1.8); d_{003}= 3.61 (19); Anatase 3.51 (2.2); 3.36 (0.7); d_{004}= 2.71; (0.6), 2.57 (1.1); 2.49 (1.3); 2.33 (1.1); 2.29 (0.5); 2.23 (0.4); d_{005}= 2.17 (0.9); 2.09 (0.2); 1.89 (0.2); d_{006}= 1.81 (0.3); 1.69 (0.2); 1.55 (0.1); d_{060}= 1.489 (0.8). d-spacing (Kao-EG 10.8 Å)= 10.83 ± 0.05 Å; I.R.= 0.98.

- FTIR (in cm^{-1}): ν(O-H) 3693 (m), 3638 (s), 3620 (s), 3601 (m), 3554 (m,br), 3280 (m,sh); ν(C-H); 3016 (vw), 2966 (w), 2934 (w), 2883 (w); δ(HOH): 1640 (w); δ(C-H): 1459 (w), 1408 (w), 1362 (w), 1325 (vw): Si-O vibrations: 1122 (s), 1080 (s), 1048 (vs), 1029 (vs); δ(Al-OH): 959 (m), 912 (s); other bands: 885 (w,sh), 803 (w), 747 (w), 681 (m), 545 (s), 470 (s), 430 (s).

- TGA/DSC (85 cm^3/min N_2, TGA wt. losses are approximate): 20-210 °C: 5.6 % wt. loss, $T_{endo.}$= 168 °C (m); 210-345 °C: 5.4 % wt. loss, $T_{endo.}$= 305 °C (w); 345-466 °C: 5.7 % wt. loss, $T_{endo.}$= 432 °C (m); 466-650 °C: 6.5 % wt. loss, $T_{endo.}$= 512

°C (m); 650-1050 °C: $T_{exo.}$ = 1012 °C (m), $T_{exo.}$ = 1030 °C (w,sh); Total TGA weight loss: 23.2 %.

25 mg of this product (Kao-EG 10.8 Å) was heated at approximately 150 °C overnight followed by characterization by FTIR and XRD.

- XRD (Philips 1050/81; 1,4 dioxane dispersed): 9.2 (sh); d_{001}=8.0 (100,br).

- FTIR (in cm^{-1}): ν(O-H) 3697 (s), 3625 (s), 3550 (m); δ(HOH): 1641 (w); Si-O vibrations: 1090 (s), 1038 (vs), 1012 (vs); δ(Al-OH): 912 (s); other bands: 792 (w), 750 (w), 686 (m), 542 (s), 472 (s), 431 (s).

6.6.1.2 Rxn 3-1-2: 0.5 g of Kao-Hydrazine (I.R.= 0.97) was mixed with 15 ml of EG in a round bottom flask for 8 days in an oil bath maintained at 60-70 °C under N_2 atmosphere. This was filtered, washed with methanol and air dried to give 0.5 g of an off-white powder.

- XRD (Philips PW 3710, 1,4 dioxane dispersed): d_{001}= 10.66 (100), d_{001} (K)= 7.10 (10), d_{002}= 5.40 (1.2). I.R.= 0.91.

- FTIR (in cm^{-1}): ν(O-H): 3697 (s), 3751 (w), 3622 (s), 3602 (w,sh), 3600-3200 (m,br); ν(C-H): 2945 (w), 2886 (w); Si-O vibrations: 1086 (s), 1045 (vs), 1035 (vs), 1011 (vs); δ(Al-OH): 914 (s).

100 mg of this sample was washed with 2 ml of D_2O, heated briefly to 100 °C for 1 minute and then allowed to stand at room temperature in a sealed container for 3 days. The mixture was centrifuged and the supernatant was examined by ^1H NMR. This confirmed that ethylene glycol was present in significant quantities in the supernatant

(Varian XL-300: 3.65 ppm (s)). The sediment was quickly dried on a hot plate and examined by FTIR. The FTIR pattern of the product was consistent with that of a fully collapsed kaolinite with significant amounts of deuterium exchanged inner surface hydroxyls (ν(O-D): 2727 cm^{-1} (m), 2672 cm^{-1} (w)).

6.6.1.3 Rxn 3-1-3 and Rxn 3-1-4: 100 mg of Kao-DMSO (**Rxn 3-1-3**; I.R= 0.96) and Kao-NMF (Rxn **3-1-4**; I.R.= 0.91) were placed on a glass slide in a glass bell jar containing 100 ml of ethylene glycol. The bell jar was closed, and the samples were exposed to a saturated atmosphere of ethylene glycol for 48 hours at room temperature. Examination of the FTIR patterns of the products revealed that there was no change in the Kao-DMSO and Kao-NMF starting materials.

6.6.2 Effects of Water Concentration on the Formation of Kao-EG 9.4 Å Versus Kao-EG 10.8 Å

6.6.2.1 Rxn 3-2-1 (0 % water): 1.0 g of Kao-DMSO (I.R. = 0.92) was refluxed with 50.0 ml of freshly distilled ethylene glycol (BP 194-199 °C, < 500 ppm H_2O by Karl-Fischer titration) for 16 hrs under N_2 atmosphere. The yield after 1,4 dioxane washing and air drying was 0.5 g of an off-white powder.

- XRD (Philips PW 1050/81, methanol dispersed, 1 day after preparation): d_{001} (Kao-EG 9.4 Å)= 9.55 (100); d_{001} (K)= 7.19 (10); d_{002} (Kao-EG 9.4 Å)= 4.72 (6); 4.47

(8); 4.19 (14); 4.04 (6); d_{002} (K)= 3.58 (9); Anatase 3.53 (4); 3.40 (3); 3.24 (1); d_{003} (Kao-EG 9.4 Å)= 3.13 (11); d-spacing= 9.46 ± 0.08; I.R.= 0.91.

- XRD (Philips PW 3710, methanol dispersed, 25-30 days after preparation): d_{001} (Kao-EG 9.4 Å)= 9.46 (100); d_{001} (K)= 7.15 (6.7); d_{002} (Kao-EG 9.4 Å)= 4.70 (2.9); 4.46 (2.5); 4.18 (3.8); 4.04 (2.2); d_{002} (K)= 3.57 (4.1); Anatase 3.52 (1.5); 3.39 (1.2); 3.23 (0.9); d_{003} (Kao-EG 9.4 Å)= 3.13 (4.9); 2.75 (0.1); 2.57 (0.5); 2.52 (0.6); 2.45 (0.4); 2.43 (0.4); 2.38 (0.5); d_{004} (Kao-EG 9.4 Å)= 2.34 (0.8); 2.30 (0.6); 2.17 (0.3); 2.04 (0.1); 1.99 (0.1); 1.94 (0.1); 1.89 (0.2); 1.88 (0.2); 1.79 (0.2); 1.69 (0.1); 1.67 (0.2); 1.62 (0.1); 1.55 (0.1); d_{060}= 1.487 (0.2). d-spacing= 9.40 ± 0.04; I.R.= 0.94.

- FTIR (cm^{-1}, 1 day after preparation): ν(O-H): 3695 (m), 3667 (m), 3622 (m), 3574 (m), 3394 (m); ν(C-H): 2969 (w), 2945 (w), 2894 (w); δ(HOH): 1630 (vw); δ(C-H): 1462 (w), 1324 (w), 1280 (vw), 1237 (w), 872 (w); Si-O vibrations: 1119 (s), 1085 (s), 1044 (vs); δ(Al-OH): 912 (s); other bands: 794 (w), 749 (w), 600 (m,sh), 672 (m), 545 (s), 518 (s,sh), 470 (s), 441 (s,sh), 432 (s).

- TGA/DSC (40 cm^3/min N_2): 20-200 °C: 1.9 % wt. loss, $T_{endo.}$= 104 °C (w), $T_{endo.}$= 147 °C (w); 200-470 °C: 9.8 % wt. loss, $T_{endo.}$= 444 °C (s); 470-620 °C: 7.2 % wt. loss, $T_{endo.}$= 509 °C (w), $T_{exo.}$= 528 °C (w), $T_{endo.}$= 554 °C (m); 640-1200 °C: 4.3 % wt. loss, $T_{exo.}$= 1004 °C (m), $T_{exo.}$= 1029 °C (m). Total TGA wt. loss = 23.2 %.

- TGA/DSC (85 cm^3/min air, TGA % wt. losses are approximate): 20-200 °C: 1.9 % wt. loss; 200-486 °C: 9.2 % wt. loss, $T_{endo.}$= 444 °C (s); 486-623 °C: 5.8 % wt. loss, $T_{exo.}$= 532 °C (w), $T_{endo.}$= 556 °C (w); 950-1100 °C: 1.9 % wt. loss, $T_{exo.}$= 973 °C (w,sh), $T_{exo.}$= 1007 °C (m), $T_{exo.}$= 1025 °C (s).

- ^{13}C CP/MAS NMR (Bruker MSL-200, 50.29 MHz, spinning rate of 4 KHz): One resonance at 65 ppm ($\nu_{1/2}$= 120 Hz).

- Elemental analysis (calculated for $Al_2Si_2O_5(OH)_{3.2}(OCH_2CH_2OH)_{0.8}$). Carbon (%): Found 6.51, Calc. 6.55; Hydrogen (%): Found 2.48 , Calc. 2.46. XRF data: SiO_2 (%): Found 39.7, Calc. 40.9; Al_2O_3 (%): Found 34.4, Calc. 34.8; TiO_2 (%): 1.52; Fe_2O_3 (%): 0.19.

6.6.2.2 Rxn 3-2-2 (1% water): 1.0 g of Kao-DMSO was refluxed with a solution made up of 49.5 ml of freshly distilled ethylene glycol and 0.5 ml of deionized water for 19 hrs under N_2 atmosphere. The yield after 1,4 dioxane washing and air drying was 0.5 g of an off-white powder.

- XRD (Philips PW 1050/81, methanol dispersed, 1 day after preparation): d_{001} (Kao-EG 9.4 Å)= 9.48 (100); d_{001} (K)= 7.20 (6); d_{002} (Kao-EG 9.4 Å)= 4.70 (6); 4.47 (10); 4.37 (1); 4.19 (16); 4.04 (9); 3.91 (3); d_{002} (K)= 3.58 (7); Anatase 3.52 (3); 3.44 (4); d_{003} (Kao-EG 9.4 Å)= 3.13 (11); d-spacing= 9.42 ± 0.06; I.R.= 0.94.

- XRD (Philips PW 3710, methanol dispersed, XRD pattern was taken 25-30 days after preparation): d_{001} (Kao-EG 10.8 Å)= 10.82 (53); d_{001} (Kao-EG 9.4 Å)= 9.40 (100); d_{001} (Kao-H_2O)= 8.53 (4.1); d_{001}(K)= 7.15 (6.3); d_{002} (Kao-EG 10.8 Å)= 5.43 (0.3); d_{002} (Kao-EG 9.4 Å)= 4.68 (2.9); 4.46 (2.9); 4.36 (1.1); 4.18 (3.7); 4.03 (2.2); 3.91 (0.8); d_{003} (Kao-EG 10.8 Å)= 3.62 (5.0); d_{002} (K)= 3.57 (4.2); Anatase, 3.52 (1.9); 3.38 (1.3); d_{003} (Kao-EG 9.4 Å)= 3.12 (4.6); d_{060}=1.489 (0.2). d-spacings= 10.85 ± 0.03

(Kao-EG 10.8 Å); 9.37 ± 0.03 (Kao-EG 9.4 Å); I.R.= 0.96 (calculated by considering all of the intercalated phases).

- FTIR (cm^{-1}, 1 day after preparation): v(O-H): 3694 (m), 3667 (m), 3622 (m), 3574 (m), 3392 (m); v(C-H): 2970 (w), 2944 (w), 2894 (w).

- FTIR (cm^{-1}, 3 months after preparation): v(O-H): 3694 (m), 3669 (m), 3650 (m), 3622 (m), 3599 (m), 3573 (m), 3392 (m); v(C-H): 2970 (w), 2944 (w), 2894 (w).

- TGA/DSC (90 cm^3/min N_2, TGA wt. losses are approximate): 20-220 °C: 2.8 % wt. loss, $T_{endo.}$= 145 °C (m); 220-480 °C: 8.4 % wt. loss, $T_{endo.}$= 449 °C (s); 480-650 °C: 5.2 % wt. loss, $T_{endo.}$= 504 °C (m,sh), $T_{exo.}$= 540 °C (w), $T_{endo.}$= 557 °C (m).

6.6.2.3 Rxn 3-2-3 (2% water): 1.0 g of Kao-DMSO was refluxed with a solution made up of 49.0 ml of freshly distilled ethylene glycol and 1.0 ml of deionized water for 19 hrs under N_2 atmosphere. The yield after washing with 1,4 dioxane and air drying was 0.6 g of an off-white powder.

- XRD (Philips PW 1050/81, methanol dispersed, 1 day after preparation): d_{001} (Kao-EG)= 9.69 (100); d_{001} (K)= 7.23 (14); 4.47 (12); 4.20 (10); 4.05 (8); d_{002} (K)= 3.58 (9); Anatase 3.53 (5); 3.38 (1); d_{003} (Kao-EG)= 3.12 (3); I.R.= 0.88.

- XRD (Philips PW 3710, methanol dispersed, 25-30 days after preparation, d-values in Å and relative intensities in brackets): d_{001} (Kao-EG 10.8 Å)= 10.83 (72); d_{001} (Kao-EG 9.4 Å)= 9.64 (100); d_{001} (K)= 7.14 (14); d_{002} (Kao-EG 10.8 Å)= 5.54 (0.2); d_{002} (Kao-EG 9.4 Å)= 4.74 (1.2); 4.46 (11); 4.18 (10.7); 4.03 (8.2); 3.85 (3.2); d_{002} (K)= 3.57 (16); Anatase 3.51 (7.7); 3.38 (3.5); 3.24 (3.5); d_{003} (Kao-EG 9.4 Å)= 3.11

(3.1); d_{060}= 1.490 (0.9). I.R.= 0.92 (calculated by considering all of the intercalated phases).

- FTIR (cm^{-1}, 4 days after preparation): ν(O-H): 3695 (m), 3667 (m), 3623 (m), 3576 (m), 3394 (m); ν(C-H): 2970 (w), 2944 (w), 2893 (w); δ(HOH): 1637 (w); δ(C-H): 1461 (w), 1325 (w), 1280 (vw), 1236 (w), 872 (w); Si-O vibrations: 1120 (s), 1100-1000 (vs); δ(Al-OH): 912 (s); other bands: 794 (w), 749 (w), 677 (m), 545 (s), 475 (s), 441 (s), 432 (s).

6.6.2.4 Rxn 3-2-4 (5% water): 1.0 g of Kao-DMSO was refluxed with a solution made up of 47.5 ml of freshly distilled ethylene glycol and 2.5 ml of deionized water for 16 hrs under N_2 atmosphere. The yield after 1,4 dioxane washing and air drying was 0.6 g of an off-white powder.

- XRD (Philips PW 1050/81, methanol dispersed, 1 day after preparation): d_{001} (Kao-EG)= 10.94 (100); 9.84 (58); d_{001} (K)= 7.22 (50); 4.47 (41); 4.20 (33); 3.62 (71); Anatase 3.53 (21). I.R.= 0.76.

- XRD (Philips PW 3710, methanol dispersed, 25-30 days after preparation): d_{001} (Kao-EG 10.8 Å)= 10.83 (100); d_{001} (K)= 7.15 (15); d_{002} (Kao-EG 10.8 Å)= 5.44 (0.6); 4.46 (6.1); 4.36(4.8); 4.12 (5.6); d_{003} (Kao-EG 10.8 Å)= 3.62 (23); d_{002} (K)= 3.57 (17); Anatase 3.51 (5.8); 3.13 (0.3); d_{004} (Kao-EG 10.8 Å)= 2.71 (0.2); 2.56 (1.7); 2.49 (1.9); 2.38 (1.4); 2.34 (2.4); 2.29 (1.3); 2.18 (0.7); 2.12 (0.3); 1.99 (0.4); 1.89 (0.7); 1.79 (0.2); 1.68 (0.4); 1.67 (0.6); 1.62 (0.2); 1.55 (0.2); d_{060}=1.490 (0.7). d-spacing (Kao-EG 10.8 Å)= 10.86 ± 0.02 Å; I.R.= 0.87.

- FTIR (cm^{-1}, 1 day after preparation): ν(O-H): 3696 (s), 3623 (s), 3575 (m), 3398 (m,sh), 3285 (m,sh); ν(C-H): 2968 (w,sh), 2947 (w), 2888 (w); δ(HOH): 1640 (vw); δ(C-H): 1458 (w), 1367 (w), 1324 (vw), 1236 (vw), 875 (vw,sh); Si-O vibrations: 1125 (s,sh), 1080 (s,sh), 1048 (vs), 1037 (vs), 1015 (s,sh); δ(Al-OH): 913 (s); other bands: 796 (w), 750 (w), 686 (m), 542 (s), 472 (s), 430 (s).

- FTIR (cm^{-1}, 3 months after preparation): ν(O-H): 3696 (s), 3651 (m), 3640 (m), 3621 (s), 3601 (m), 3553 (m), 3500-3200 (m,br), 3398 (m,sh), 3285 (m,sh); ν(C-H): 2950 (w), 2885 (w);

- TGA/DSC (40 cm^3/min N_2): 20-200 °C: 4.7 % wt. loss, $T_{endo.}$ = 157 °C (m); 200-467 °C: 7.9 % wt. loss, $T_{endo.}$ = 437 °C (m); 467-640 °C: 7.4 % wt. loss, $T_{endo.}$ = 518 °C (m); 640-1200 °C: 3.8 % wt. loss, $T_{exo.}$ = 1005 °C (m), $T_{exo.}$ = 1025 °C (w,sh). Total TGA wt. loss = 23.8 %.

100 mg of this sample was washed with 2 ml of D_2O, heated briefly to 100 °C for 1 minute and then allowed to stand at room temperature in a sealed container for 3 days. The mixture was centrifuged and the supernatant was examined by ^1H NMR. This confirmed that ethylene glycol was present in significant quantities in the supernatant (Varian XL-300; 3.65 ppm (s)). The sediment was quickly dried on a hot plate and examined by FTIR. The FTIR pattern of the product was consistent with that of a fully collapsed kaolinite with significant amounts of deuterium exchanged inner surface hydroxyls (ν(O-D): 2728 cm^{-1} (m), 2674 cm^{-1} (w)).

6.6.2.5 Rxn 3-2-5 (10% water): 1.0 g of Kao-DMSO was refluxed with a solution made up of 45.0 ml of freshly distilled ethylene glycol and 5.0 ml of deionized water for 16 hrs under N_2 atmosphere. The yield after 1,4 dioxane washing and air drying was 0.5 g of an off-white powder.

- XRD (Philips PW 1050/81, methanol dispersed, 1 day after preparation): d_{001} (Kao-EG 10.8 Å)= 11.00 (100); d_{001} (K)= 7.22 (16); 4.47 (9); 4.15 (6); d_{003} (Kao-EG 10.8 Å)= 3.63 (32); d_{002} (K)= 3.59 (18,sh); Anatase 3.53 (5). I.R.= 0.86.

- XRD (Philips PW 3710, methanol dispersed, XRD pattern was taken 25-30 days after preparation, d-values in Å and relative intensities in brackets): d_{001} (Kao-EG 10.8 Å)= 10.75 (100); d_{001} (K)= 7.10 (14); d_{002} (Kao-EG 10.8 Å)= 5.41 (0.6); 4.43 (2.7); 4.14 (2.9); d_{003} (Kao-EG 10.8 Å)= 3.61 (26); d_{002} (K)= 3.56 (19); Anatase 3.50 (3.6); d_{004} (Kao-EG 10.8 Å)= 2.71 (0.4); 2.55 (0.9); 2.49 (1.2); 2.37 (1.2); 2.33 (1.5); 2.28 (0.9); d_{005} (Kao-EG 10.8 Å)= 2.17 (0.6); 1.98 (0.2); 1.93 (0.2); 1.89 (0.4); 1.81 (0.3); 1.79 (0.3); 1.66 (0.4); 1.61 (0.1); 1.54 (0.1); d_{060}=1.487 (0.5). d-spacing (Kao-EG 10.8 Å)= 10.82 ± 0.04 Å; I.R.= 0.88.

- FTIR (cm^{-1}, 1 day after preparation): ν(O-H): 3695 (s), 3641 (s), 3621 (s), 3600 (w,sh), 3550 (m,br), 3285 (m,sh); ν(C-H): 2947 (w), 2883 (w); δ(HOH): 1630 (vw); δ(C-H): 1457 (w), 1412 (vw), 1364 (w), 1337 (vw), 1327 (vw), 1247 (vw,sh), 879 (w,sh); Si-O vibrations: 1118 (s,sh), 1080 (s,sh), 1050 (vs), 1043 (vs), 1036 (vs), 1024 (vs,sh), 1013 (s,sh); δ(Al-OH): 960 (w), 938 (w,sh), 913 (s); other bands: 796 (w), 750 (w), 685 (m), 545 (s), 472 (s), 430 (s).

- FTIR (cm^{-1}, 3 months after preparation): v(O-H): 3695 (s), 3644 (m), 3621 (s), 3599 (m), 3550 (m), 3500-3200 (m,br); v(C-H): 2945 (w), 2882 (w).

- TGA/DSC (40 cm^3/min N_2): 20-240 °C: 5.4 % wt. loss, $T_{endo.}$ = 160 °C (m); 240-440 °C: 5.1 % wt. loss, $T_{endo.}$ = 426 °C (m); 440-620 °C: 9.4 % wt. loss, $T_{endo.}$ = 524 °C (m); 620-1200 °C: 4.2 % wt. loss, $T_{exo.}$ = 1004 °C (m), $T_{exo.}$ = 1026 °C (w,sh). Total TGA wt. loss = 24.1 %.

- TGA/DSC (85 cm^3/min air, TGA % wt. losses are approximate): 20-212 °C: 5.3 % wt. loss, $T_{endo.}$ = 168 °C (m); 212-480 °C: 7.5 % wt. loss, $T_{endo.}$ = 425 °C (m); 480-630 °C: 6.3 % wt. loss, $T_{endo.}$ = 533 °C (m); 950-1100 °C: 1.0 % wt. loss: $T_{exo.}$ = 1009 °C (m), $T_{exo.}$ = 1021 °C (m). Calcination wt. loss (1100 °C in air atm. for 3 hours): 24.5 %.

- Elemental analysis (calculated for $Al_2Si_2O_5(OH)_4(HOCH_2CH_2OH)_{0.58}$ based on 24.5 % calcination wt. loss). Carbon (%): Found 5.22, Calc. 4.74 %; Hydrogen (%): Found 2.57, Calc. 2.54.

- ^{13}C CP/MAS NMR (Bruker MSL-200, 50.29 MHz, spinning rate of 4 KHz): One resonance at 65 ppm ($v_{1/2}$ = 55 Hz).

6.6.2.6 Rxn 3-2-6 (20% water): 1.0 g of Kao-DMSO was refluxed with a solution made up of 40.0 ml of freshly distilled ethylene glycol and 10.0 ml of deionized water for 19 hrs under N_2 atmosphere. The yield after 1,4 dioxane washing and air drying was 0.5 g of an off-white powder.

- XRD (Philips PW 1050/81, methanol dispersed): 14.63 (7); 7.37 (100,asym); 4.48 (25); 4.39 (10); 4.19 (10); 3.60 (80).

- XRD (Philips PW 3710, methanol dispersed): d_{001} (Kao-EG 10.8 Å)= 10.79 (27); 7.32 (90,sh); d_{001} (K)= 7.15 (100); 4.46 (8.0); 4.36 (5.9); 4.18 (5.3); d_{002} (K)= 3.58 (77); Anatase 3.51 (13); 2.74 (0.3); 2.56 (2.7); 2.49 (3.1); 2.38 (4.2); 2.34 (4.7); 2.29 (2.3); 2.19 (0.5); 1.99 (0.9); 1.89 (0.9); 1.79 (1.6); 1.67 (1.2); 1.62 (0.4); 1.54 (0.2); d_{060}= 1.488 (0.5). I.R.= 0.12.

- FTIR (cm^{-1}, 1 day after preparation): ν(O-H): 3696 (s), 3671 (w), 3653 (m), 3621 (s), 3550 (m,br), 3600-3200 (m,br); ν(C-H): 2942 (w), 2885 (w); δ(HOH): 1650 (w); Si-O vibrations: 1094 (s), 1080-1000 (vs); δ(Al-OH): 938 (m,sh), 914 (s); other bands: 792 (w), 753 (w), 691 (m), 545 (s), 470 (s), 430 (s).

6.6.3 Attempts at Expansion of Kao-EG 9.4 Å with Organic Solvents

6.6.3.1 Initial Attempts: Portions of 0.1 g of Kao-EG 9.4 Å (from Rxn **2-2-2**, I.R. 0.92) were mixed with 2.5 ml samples of DMSO, ethyl acetate, 1,4 dioxane, methanol, hexane and acetic acid at room temperature for 14 days in glass vials. The product was then filtered and the product was air dried on a glass XRD slide. XRD patterns were taken shortly after the product appeared to be dry. In all cases no evidence for the intercalation of organic solvents was observed as judged by the presence of the strong reflections due to the Kao-EG 9.4 Å starting material. In another experiment 0.2 g of Kao-EG 9.4 Å (from Rxn **2-2-2**, I.R.=0.92) was refluxed in 50 ml of toluene (BP 110

°C) for 5 hrs, followed by washing with methanol and air drying. The FTIR pattern of the product confirmed that the Kao-EG 9.4 Å starting material remained unchanged. A similar experiment, whereby 0.1 g of Kao-EG 9.4 Å (from Rxn **2-2-2**, I.R.= 0.92) was refluxed in 50 ml of 1,2-dimethoxyethane (BP 85 °C) for 2 hours also confirmed that the FTIR pattern of the starting material remained unchanged. Refluxing 0.5 g of Kao-EG 9.4 Å (from Rxn **2-2-2**) in 50 ml of 90:10 mixture of ethylene glycol:water for 16 hours also failed to alter the product.

6.6.3.2 Kao-EG 9.4 Å + DMSO/H_2O (95/5): 0.5 g of Kao-EG 9.4 Å (from Rxn **2-2-2**, I.R.= 0.92) was refluxed in 50 ml of 95 % DMSO (roughly 5 % water by Karl-Fischer titration) for 24 hrs. An unknown white material was deposited on the inside of the reflux condenser. The contents of the reaction mixture were filtered and washed with ethanol, followed by characterization by XRD and FTIR.

- XRD (Philips PW 1050/81, 1,4 dioxane dispersed): d_{001} (Kao-DMSO)= 11.32 (100); d_{001} (Kao-EG 9.4 Å)= 9.55 (49); d_{001} (K)= 7.23 (14).

- FTIR (cm^{-1}): v(O-H): 3693 (m), 3665 (m), 3620 (s), 3547 (m.br), 3508 (m,br), 3402 (m,sh); v(C-H): 3019 (w), 2967 (w), 2936 (w), 2895 (w).

Upon heating at 150 °C for 24 hours, this product reverted to a low intercalation ratio Kao-EG 9.4 Å product as evidenced by FTIR which indicated the presence of peaks attributable to Kao-EG 9.4 Å, albeit at weaker intensities, and the absence of bands attributable solely to Kao-DMSO.

6.6.4 Calcination of Kao-EG 9.4 Å at 700 °C

0.5 g of kaolinite and Kao-EG 9.4 Å (from reaction 2, I.R. = 0.92) were placed in a muffle furnace and heated between 600-700 °C for 2 hours. The Kao-EG 9.4 Å calcined product (**KEG-C700**) was black, whereas the calcined kaolinite product (Metakaolinite) product was off-white. Upon cooling the two products were analyzed by XRD and FTIR.

Metakaolinite: FTIR (cm^{-1}): ν(OH): 3444 (m,br); δ(HOH): 1640 (w); Si-O: 1086 (vs); other bands: 822 (s,br), 683 (s,br), 466 (s). XRD: amorphous, small reflection at d=3.52 Å due to anatase impurity.

KEG-C700: FTIR (cm^{-1}): ν(OH): 3440 (m,br); c(CH): 2962 (vw), 2925 (vw), 2872 (vw); δ(HOH): 1605 (w); Si-O: 1072 (vs); other bands: 820 (s,br), 650 (m,sh), 464 (s). XRD: amorphous, small reflection at d= 3.52 Å due to anatase impurity. ^{13}C CP/MAS NMR (Bruker CXP-180, Acquisition time = 1 hr): no signal detected.

6.6.5 Hydrolysis of Kao-EG 9.4 Å

6.6.5.1 Water Treatment at 100 °C: 0.7 g of Kao-EG 9.4 Å (I.R. = 0.92) was refluxed in 50 ml of water for 48 hours. Filtering, water washing and air drying yielded 0.5 g of an off-white powder. FTIR analysis indicated that very little decomposition of the Kao-EG 9.4 Å starting material had occurred.

6.6.5.2 D_2O Washing of Kao-EG 9.4 Å: 100 mg of this sample (Kao-EG 9.4 Å, I.R. 0.92) was washed with 2 ml of D_2O, heated briefly to 100 °C for 1 minute and then allowed to stand at room temperature in a sealed container for 3 days. The mixture was centrifuged and the supernatant was examined by ^1H NMR. This confirmed that ethylene glycol was the principal organic product present in the supernatant (Varian XL-300; 3.65 ppm (s)). The sediment was quickly dried on a hot plate and examined by FTIR. This showed almost no collapse of the Kao-EG 9.4 Å product, but some minimal deuterium exchange could be observed.

- FTIR (cm^{-1}): v(O-H): 3695 (m), 3667 (m), 3622 (s), 3573 (m), 3393 (m); v(C-H): 2970 (w), 2946 (w), 2895 (w); v(O-D): 2755 (vvw), 2735 (vvw), 2707 (vw), 2675 (vw), 2637 (vw), 2519 (vw).

6.6.5.3 Water Treatment at 200 °C: More severe hydrolysis conditions were employed in this attempts at hydrolysis. 1.0 g of Kao-EG 9.4 Å (I.R.= 0.92) was placed in a sealed autoclave with 10 ml of deionized water, followed by heating in an oil bath maintained between 200-210 °C for 72 hours. This was cooled down, filtered, washed with methanol and air dried to yield 0.9 g of an off-white powder. Analysis of the aqueous mother liquor by ^{13}C NMR (Bruker AMX-500, 125.77 MHz, 10 % D_2O, referenced to the methyl resonance of acetone at 31.1 ppm) showed that the only organic component present was ethylene glycol (62.24 ppm). A standard EG/H_2O sample confirmed this assignment (62.22 ppm). Both FTIR and XRD indicated an incomplete collapse of the Kao-EG 9.4 Å structure.

- XRD (Philips PW 3710, vaseline mounted, d-values in Å and relative intensities in brackets): d_{001} =9.10 (83); d_{001} (K)= 7.08 (100). I.R.= 0.45.

- FTIR (cm^{-1}): ν(O-H): 3696 (s), 3623 (s), 3569 (m), 3390 (m); ν(C-H): 2971 (w), 2945 (w), 2894 (w); δ(HOH): 1633 (w); δ(C-H): 1463 (vw), 1325 (w), 1237 (w); Si-O vibrations: 1150-1000 (vs); δ(Al-OH): 914 (s); other bands: 792 (w), 752 (w), 690 (m), 545 (vs), 470 (s), 429 (s).

6.6.6 Effects of Water Washing on Kao-EG 10.8 Å

A 100 mg portion of Kao-EG 10.8 Å (from Rxn **3-1-1**, I.R.= 0.98) was washed with approximately 10 ml of water, followed by centrifugation and air drying for three hours on a glass XRD slide. The product was analyzed by XRD, FTIR and TGA/DSC. Three consecutive FTIR spectra were taken of the sample, once it had been scraped off the XRD slide.

- XRD (Philips PW 3710, vaseline mounted): d_{001} (Kao-H_2O 8.4 Å)= 8.38 (100); d_{001} (K)= 7.11 (15); 4.45 (29); d_{002} (Kao-H_2O 8.4 Å)= 4.21 (17); 3.96 (12); 3.67 (14); d_{002} (K)= 3.57 (16); Anatase 3.51 (13); 3.32 (9.0); 3.08 (3.3); d_{003} (Kao-H_2O 8.4 Å)= 2.81 (1.8); 2.56 (12); 2.52 (7.5); 2.39 (7.4); 2.38 (9.7); 2.34 (5.7); 2.29 (3.2); 2.23 (2.5); d_{004} (Kao-H_2O 8.4 Å)= 2.11 (3.3); 1.99 (1.2); 1.95 (0.4); 1.89 (1.4); 1.81 (0.7); 1.79 (0.6); 1.68 (1.4); 1.67 (1.7); 1.61 (0.8); 1.54 (0.5); d_{060}= 1.489 (4.8); 1.47 (1.1). d-spacing (Kao-H_2O 8.4 Å)= 8.42 ± 0.03 Å, I.R.= 0.87.

- FTIR (cm^{-1}, first try, KBr pellet): ν(O-H): 3694 (m), 3620 (s), 3599 (s), 3550 (m); δ(HOH): 1635 (w,br); Si-O vibrations: 1110 (s), 1025 (vs), 1007 (vs); δ(Al-OH): 970 (s), 910 (s); other bands: 793 (w), 761 (w), 703 (m), 676 (m), 560 (vs), 472 (s), 432 (s).

- FTIR (cm^{-1}, second try, KBr pellet): ν(O-H): 3696 (s), 3621 (s), 3549 (m); δ(HOH): 1654 (w); Si-O vibrations: 1095 (s), 1037 (vs), 1012 (vs); δ(Al-OH): 947 (w,sh), 911 (s); other bands: 795 (w), 751 (w), 680 (m), 542 (vs), 471 (s), 431 (s).

- FTIR (cm^{-1}, third try, fluorolube mull): ν(O-H): 3695 (s), 3668 (w), 3654 (w), 3647 (w), 3620 (s), 3547 (s); δ(HOH): 1653 (m).

- TGA/DSC (85 cm^3/min N_2, TGA wt. losses are approximate): 20-400 °C: 4.3 % wt. loss, $T_{endo.}$ = 150 °C (w); 400-650 °C: 13.0 % wt. loss, $T_{endo.}$ = 526 °C (s); 650-1100 °C: $T_{exo.}$ = 1009 °C (m). Total TGA wt. loss = 17.3 %.

6.6.7 Reaction of Halloysite-DMSO with EG

1.0 g of Hal-DMSO was refluxed with 55 ml of ethylene glycol (BDH, < 0.1 % H_2O) for 40 hours under N_2 atmosphere. This was then filtered and washed with methanol to remove excess EG. Air drying yielded 0.69 g of an off-white powder.

- XRD (Philips PW 3710, methanol dispersed): d_{001} = 9.49 (100); d_{002} = 4.71 (2.1); d_{003} = 3.11 (4.4); d=9.4 ± 0.1 Å; I.R.=1.0.

- FTIR (in cm^{-1}): ν(O-H): 3700 (m), 3657 (m), 3628 (s), 3578 (s,br), 3505 (s,br); ν(C-H): 2965 (w), 2947 (w), 2892 (w);

6.7 Experimental for Chapter 4

6.7.1 Preparation of Kao-EG 10.8 Å

The preparation method for this material was similar that previously described in section **6.6.2.4**. Briefly, 1.0 g of Kao-DMSO was refluxed in 50 g of a 95:5 (vol/vol) ethylene glycol:water mixture for 20 hrs followed by filtering and washing with 1,4 dioxane to remove excess ethylene glycol. The product, **4-1-A**, was air dried and characterized by XRD, FTIR, and TGA/DSC. It was found to be almost identical to the material described in section **6.6.2.4**.

6.7.2 Preparation of Kaolinite-Diethylene Glycol (Kao-DiEG)

This product was prepared, starting from both Kao-DMSO (Rxn **4-2-A**) and Kao-NMF (Rxn **4-2-B**) as the starting materials. 1.0 g of either Kao-DMSO or Kao-NMF was mixed with 50 ml of reagent grade diethylene glycol (Aldrich BP 245 °C) at room temperature. This was then refluxed for 26 hrs. Workup consisted of cooling, filtering and washing with 30 ml of methanol to remove excess diethylene glycol. The off-white powder was air dried overnight before storage and subsequent characterization. Characterization by XRD, FTIR and TGA/DSC showed that both starting materials (Kao-DMSO and Kao-NMF) yielded nearly identical products, **4-2-A** and **4-2-B**. No traces of

residual DMSO or NMF were observed by IR. ^{13}C CP-MAS of **4-2-A** also showed no traces of residual interlayer DMSO. The characterization for **4-2-A** is given below.

- XRD (Philips PW 3710, methanol dispersed): d-spacing= 10.86 ± 0.04 Å; I.R.=0.97.

- FTIR (in cm^{-1}): ν(OH): 3692 (m), 3638 (m), 3620 (m), 3605 (w,sh), 3600-3200 (m,br); ν(C-H): 2944 (w), 2885 (w); δ(HOH): 1634 (w); δ(C-H): 1460 (w), 1366 (w); Si-O vibrations: 1118 (s), 1084 (s), 1060-960 (vs); δ(Al-OH): 960 (w), 914 (s); other bands: 800 (w), 754 (w), 685 (m), 550 (s), 477 (s), 433 (s).

- Calcination weight loss (three hours at 1100 °C in air atmosphere): 26.5 %.

- ^{13}C CP/MAS (Bruker ASX-200, 50.33 MHz, spinning speed= 4 KHz): CH_2 ether: 68 ppm, $\nu_{1/2}$= 415 Hz; CH_2 alcohol: 59 ppm, $\nu_{1/2}$= 380 Hz.

6.7.3 Preparation of Kaolinite-Triethylene Glycol (Kao-TriEG)

Both Kao-DMSO (Rxn **4-3-A**) and Kao-NMF (Rxn **4-3-B**) were used as the starting material in two separate reactions. The reaction and workup conditions were identical to those in the preparation of Kao-DiEG, except that this time, the temperature of reflux was 285 °C. Characterization by XRD, FTIR and TGA/DSC again showed that both Kao-DMSO or Kao-NMF yielded nearly identical products, **4-3-A** and **4-3-B** respectively. No traces of residual interlayer DMSO or NMF were detected by IR for these products. ^{13}C CP-MAS also confirmed the absence of DMSO in product **4-3-A**. The characterization for **4-3-A** is given below.

- XRD (Philips PW 3710, methanol dispersed): d-spacing= 10.93 ± 0.04 Å; I.R.=0.96.

- FTIR (in cm^{-1}): ν(OH): 3694 (m), 3650 (m), 3621 (m), 3600-3200 (m,br); ν(C-H): 2939 (w), 2880 (w); δ(HOH): 1635 (w); δ(C-H): not examined; Si-O vibrations: 1121 (s), 1077 (s), 1051 (vs), 1029 (vs); δ(Al-OH): 912 (s); other bands: 801 (w), 746 (w), 681 (m), 540 (s), 474 (s), 430 (s).

- Calcination weight loss (3 hours at 1100 °C in air atmosphere): 29.9 %.

- ^{13}C CP/MAS (Bruker ASX-200, 50.33 MHz, spinning speed= 4 KHz): CH_2 ether: 71 ppm, $\nu_{1/2}$= 420 Hz; CH_2 alcohol: 62 ppm, $\nu_{1/2}$= 275 Hz.

6.7.4 Preparation of Kaolinite-Tetraethylene Glycol (Kao-TetraEG)

1 g of Kao-NMF was mixed with 40 g of tetraethylene glycol (TetraEG) and heated to approximately 150 °C for 48 hrs. Workup consisted of cooling and washing with 1,4 dioxane to yield an off-white powder, **4-4-A**. This was characterized by XRD, FTIR, TGA/DSC and ^{13}C CP/MAS. Residual interlayer NMF was detected by IR and ^{13}C CP/MAS spectroscopies.

- XRD (Philips PW 3710, methanol dispersed): d-spacing= 10.99 ± 0.04 Å; I.R.=0.96.

- FTIR (in cm^{-1}): ν(OH): 3693 (m), 3645 (m), 3620 (m), 3600-3200 (m,br), 3412 (w); ν(C-H): 2938 (w), 2885 (w); ν(C=O): 1660 (w); δ(C-H and N-H): 1535 (vw), 1459 (w), 1419 (w), 1375 (w), 1354 (w), 1315 (w), 1266 (w), 1248 (w); Si-O vibrations: 1122

(s), 1095 (s,sh), 1060-960 (vs); δ(Al-OH): 915 (s); other bands: 840 (w), 802 (w), 753 (w), 687 (m), 540 (s), 470 (s), 431 (s).

- Calcination weight loss (3 hours at 1100 °C in air atmosphere): 27.3 %.

- ^{13}C CP/MAS (Bruker ASX-200, 50.33 MHz, spinning speed= 4 KHz): CH_2 ether + alcohol: 67 ppm, $v_{1/2}$= 730 Hz; CH_3 NMF: 27 ppm, $v_{1/2}$= 115 Hz; C=O NMF: 165 ppm, $v_{1/2}$= 200 Hz.

6.7.5 Preparation of Kaolinite-15-Crown-5 (Kao-15C5)

2.4 g of 15-Crown-5 (Aldrich) was placed in a 10 ml round-bottomed flask and heated to 155 °C in a silicone oil bath. While stirring vigorously, 0.5 g of Kao-DMSO was added at once, and the reaction mixture was stirred for an additional 45 hrs, maintaining a reaction temperature of 155-160 °C. The mixture was then cooled to room temperature, and washed 3 X with methanol, centrifuging each time. Drying over P_2O_5 in a desiccator yielded 0.35 g of an off-white powder, **4-5-A**, which was then characterized by FTIR and XRD and ^{13}C CP-MAS NMR. Large amounts of residual interlayer DMSO were observed in the NMR spectrum.

- XRD (Philips PW 3710, methanol dispersed): d-spacing= 11.15 ± 0.04 Å; I.R.= 0.96.

- FTIR (in cm^{-1}): ν(OH): 3693 (m), 3630 (m), 3620 (m), 3600-3300 (m,br); ν(C-H): 3022 (w), 2955 (w,sh), 2929 (w), 2879 (w); δ(HOH): 1648 (w); δ(C-H): 1460 (w), 1433 (w), 1405 (w), 1368 (w), 1358 (w), 1320 (w), 1256 (w); Si-O vibrations: 1126 (s),

1086 (s), 1050 (vs), 1026 (vs); δ(Al-OH): 957 (w), 939 (w), 910 (s); other bands: 859 (w), 796 (w), 747 (w), 683 (m), 545 (s), 470 (s), 431 (s).

- Calcination weight loss (three hours at 1100 °C in air atmosphere): 28.4 %.

- ^{13}C CP/MAS (Bruker ASX-200, 50.33 MHz, spinning speed= 4 KHz): CH_2 ether: 70 ppm, $\nu_{1/2}$= 400 Hz, 62 ppm (sh); CH_3 DMSO: 42 ppm, $\nu_{1/2}$= 110 Hz.

6.7.6 Preparation of Kaolinite-18-Crown-6 (Kao-18C6)

An unsuccessful attempt to prepare Kao-18C6 following the procedure described above for Kao-15C5 was made. It was believed that the reaction kinetics for the preparation of Kao-18C6 from Kao-DMSO were slower than for the corresponding case for Kao-15C5, so it was decided to try the reaction at a greater temperature.

1.3 g of 18-crown-6 (Aldrich) was placed in a 25 ml round bottom flask and heated to 190 °C in a silicone oil bath. While stirring vigorously with a magnetic stirrer, 0.21 g of Kao:DMSO was added at once to the 18-crown-6 melt. After 16 hrs reaction, the mixture was allowed to cool, followed by washing with isopropyl alcohol and centrifugation. This was repeated 3 times. The product was air dried, first at 25 °C for 2 hrs and then in an oven for 30 min at 90 °C to yield an off-white powder, **4-6-A**. Characterization was then performed by XRD, FTIR and ^{13}C CP/MAS NMR. Large amounts of interlayer DMSO were detected by ^{13}C NMR.

- XRD (Philips PW 3710, methanol dispersed): d-spacing= 11.15 ± 0.04 Å; I.R.= 0.97.

- FTIR (in cm^{-1}): ν(OH): 3695 (m), 3636 (m), 3621 (m), 3600-3300 (m,br); ν(C-H): 3024 (w), 2955 (w,sh), 2928 (w), 2879 (w); δ(HOH): 1641 (w); δ(C-H): 1457 (w), 1434 (w), 1403 (w), 1359 (w), 1319 (w), 1257 (w); Si-O vibrations: 1124 (s), 1085 (s), 1049 (vs), 1028 (vs); δ(Al-OH): 954 (w), 938 (w), 912 (s); other bands: 797 (w), 746 (w), 684 (m), 543 (s), 471 (s), 431 (s).

- Calcination weight loss (3 hours at 1100 °C in air atmosphere): 29.6 %.

- ^{13}C CP/MAS (Bruker ASX-200, 50.33 MHz, spinning speed= 4 KHz): CH_2 ether: 70 ppm, $\nu_{1/2}$= 390 Hz, 62 ppm (sh); CH_3 DMSO: 41 ppm, $\nu_{1/2}$= 130 Hz; C=O unknown: 180 ppm.

6.7.7 Preparation of Kaolinite-Polyethylene glycol 1000 (Kao-PEG 1000)

Five reactions were performed involving the formation of Kao-PEG 1000 product. The first reaction (Rxn **6-7-A**) used Kao-DMSO as the starting material, the second (Rxn **6-7-B**) used Kao-NMF, the third reaction (Rxn **6-7-C**) was a control experiment where kaolinite itself was used as the starting material. The last two reactions involved refluxing mixtures of Kao-NMF and PEG 1000 in 1,4 dioxane (Rxn **6-7-D**) and water (Rxn **6-7-E**).

6.7.7.1 Rxn 6-7-A: In the first reaction, 10 g of polyethylene glycol 1000 (Aldrich) was heated to 155 °C in a 50 ml round bottom flask placed in a silicone oil bath. To this viscous melt, 2.0 g of Kao-DMSO was added at once and the reaction was allowed to proceed for a total of 216 hrs (9 days). At selected times during the reaction,

small aliquots were removed with a pipette, quenched by cooling and worked up by repeatedly washing with methanol to remove excess polyethylene glycol. Typically, after workup, each aliquot yielded 40-60 mg of product. FTIR spectra and XRD patterns were taken for these aliquots in order to monitor the extent of reaction. The remaining final product was worked up by washing/centrifuging in methanol 3 times, followed by air drying at 25 °C and then drying in an oven at 100 °C for three days. This yielded an off-white powder, **6-7-A**, which was then characterized by XRD, FTIR, TGA/DSC, ^{13}C CP/MAS NMR and elemental analysis (% C,H). Residual interlayer DMSO was detected by ^{13}C CP/MAS NMR.

- XRD (Philips PW 3710, methanol dispersed): d-spacing= 11.12 ± 0.04 Å; I.R.= 0.95.

- FTIR (in cm^{-1}): ν(OH): 3695 (m), 3650 (m), 3633 (m), 3621 (m), 3600-3300 (m,br); ν(C-H): 3020 (w), 2959 (w,sh), 2924 (w), 2878 (w); δ(HOH): 1645 (w); δ(C-H): 1461 (w), 1407 (w), 1356 (w), 1318 (w), 1268 (w), 1249 (w); Si-O vibrations: 1124 (s), 1087 (s), 1049 (vs), 1026 (vs); δ(Al-OH): 955 (w), 939 (w), 911 (s); other bands: 852 (w), 838 (w), 815 (w), 798 (w), 748 (w), 685 (m), 542 (s), 472 (s), 430 (s).

- Calcination weight loss (3 hours at 1100 °C in air atmosphere): 29.1 %.

- ^{13}C CP/MAS (Bruker ASX-200, 50.33 MHz, spinning speed= 4 KHz): CH_2 ether: 70 ppm, $\nu_{1/2}$= 415 Hz; CH_3 DMSO: 42 ppm, $\nu_{1/2}$= 115 Hz.

- Elemental Analysis: Carbon 7.90 %; Hydrogen 2.63 %.

6.7.7.2 Rxn 6-7-B: When Kao-NMF was used as the starting material for the reaction with PEG 1000, it was found that at 155 °C structural collapse to unexpanded kaolinite would occur since Kao-NMF is not as thermally stable as Kao-DMSO, and is subject to thermal decomposition at lower temperatures than Kao-DMSO [215,216]. It was therefore decided to gently ramp up the reaction temperature in order to allow reaction with PEG 1000 to occur before the structural collapse of Kao-NMF might occur.

10 g of polyethylene glycol 1000 was allowed to melt in a 50 ml round bottom flask by placing the flask and its contents in a silicone oil bath at 70 °C. 1.5 g of Kao-NMF was added at once, maintaining vigorous stirring. The reaction mixture was maintained at 70 °C for 6 days followed by slowly increasing the reaction temperature to 160 °C over the course of an additional 4 days. Finally the reaction mixture was maintained at 160 °C for 3 more days. Aliquots were removed and analyzed at various times to monitor the extent of reaction as was previously described for Rxn 7A. The remaining final product was collected and worked up after a total reaction time of 312 hrs to yield an off-white powder, **6-7-B**, which was characterized by XRD and FTIR. Residual traces of interlayer NMF were observed in the IR.

- XRD (Philips PW 3710, methanol dispersed): d-spacing= 11.01 ± 0.05 Å; I.R.= 0.78.

- FTIR (in cm^{-1}): ν(OH): 3698 (m), 3651 (m,sh), 3623 (m), 3600-3300 (m,br), 3412 (w); ν(C-H): 2929 (w,sh), 2882 (w); ν(C=O): 1661 (w); δ(C-H): 1463 (w), 1417 (vw), 1377 (vw), 1358 (w), 1314 (w), 1247 (w); Si-O vibrations: 1121 (s), 1087 (s),

1044 (vs), 1026 (vs), 1012 (vs); δ(Al-OH): 913 (s); other bands: 797 (w), 751 (w), 687 (m), 541 (s), 470 (s), 428 (s).

- Calcination weight loss (3 hours at 1100 °C in air atmosphere): 23.5 %.

6.7.7.3 Rxn 6-7-C: The control experiment involved placing 5 g of PEG 1000 in a 50 ml round bottom flask, heating to 200 °C, adding 0.6 g of kaolinite, and stirring the mixture under nitrogen atmosphere at this temperature for a total of 6 days. Workup consisted of washing with methanol to remove excess PEG 1000, followed by air drying to yield product **6-7-C** which was then characterized by XRD and FTIR. This showed that there was no detectable change in the nature of the unexpanded kaolinite starting material.

6.7.7.4 Rxn 6-7-D: 1.0 g of Kao-NMF (I.R. = 0.91) was mixed with a solution consisting of 4.0 g of PEG 1000 dissolved in 40 mls of 1,4 dioxane. This was refluxed for 162 hrs in open atmosphere. After filtering, washing with 1,4 dioxane and air drying, 0.81 g of an off-white powder was collected. The FTIR spectra of this product showed that no polymer incorporation had been achieved, and instead one observed a pattern consistent with a partially collapsed Kao-NMF (ν(N-H)=3419 cm^{-1}, ν(C=O)= 1688 cm^{-1}).

6.7.7.5 Rxn 6-7-E: 1.0 g of Kao-NMF (I.R. = 0.91) was mixed with a solution consisting of 4.0 g of PEG 1000 dissolved in 40 mls of water. This was refluxed for 162

hrs in open atmosphere. After filtering, washing with 1,4 dioxane and air drying, 0.87 g of an off-white powder was collected. The FTIR spectra of this product was consistent with a fully collapsed kaolinite.

6.7.8 Kaolinite-Polyethylene glycol 3400 (Kao-PEG 3400)

Three reactions were performed involving the formation of Kao-PEG 3400 product. Reactions **6-8-A** and **6-8-B** were performed at 155 °C and 195 °C respectively, and reaction **6-8-C** was a control experiment where kaolinite itself was used as the starting material.

6.7.8.1 Rxn 6-8-A: 10 g of polyethylene glycol 3400 (Aldrich) was heated to 155 °C in a 50 ml round bottom flask placed in a silicone oil bath. This reaction was treated in exactly the same way as described for Rxn 7A in the preparation of Kao-PEG 1000. The final product, **6-8-A**, was an off-white powder which was then characterized by XRD, FTIR, TGA/DSC, ^{13}C CP/MAS NMR and elemental analysis (% C,H). The product contained significant quantities of residual interlayer DMSO.

- XRD (Philips PW 3710, methanol dispersed): d-spacing= 11.16 ± 0.04 Å; I.R.= 0.96.

- FTIR (in cm^{-1}): ν(OH): 3696 (m), 3650 (m,sh), 3636 (m), 3620 (m), 3600-3300 (m,br); ν(C-H): 3022 (w), 2956 (w,sh), 2927 (w), 2880 (w); δ(HOH): 1647 (w); δ(C-H):

1465 (w), 1407 (w), 1358 (w), 1318 (w), 1268 (w,sh), 1248 (w); Si-O vibrations: 1124 (s), 1086 (s), 1050 (vs), 1026 (vs); δ(Al-OH): 955 (w), 938 (w), 912 (s); other bands: 852 (w), 797 (w), 747 (w), 684 (m), 545 (s), 470 (s), 430 (s).

- Calcination weight loss (3 hours at 1100 °C in air atmosphere): 29.4 %.

- ^{13}C CP/MAS (Bruker ASX-200, 50.33 MHz, spinning speed= 4 KHz): CH_2 ether: 70 ppm, $v_{1/2}$= 450 Hz; CH_3 DMSO: 42 ppm, $v_{1/2}$= 150 Hz.

- Elemental Analysis: Carbon 8.09 %; Hydrogen 2.73 %.

6.7.8.2 Rxn 6-8-B: 10 g of polyethylene glycol 3400 (Aldrich) was heated to 195 °C in a 50 ml round bottom flask placed in a silicone oil bath. 2.5 g of Kao-DMSO was added at once to the melt and the reaction was allowed to proceed for a total of 116 hrs. Small aliquots were removed at given times during the course of reaction to monitor product formation. After 116 hrs reaction time, the final product, **6-8-B**, was an off-white powder which was characterized by XRD and FTIR. This showed that product **6-8-B** was virtually identical to product **6-8-A**. Residual DMSO was observed in the interlayers by FTIR.

- XRD (Philips PW 3710, methanol dispersed): d-spacing= 11.19 ± 0.04 Å; I.R.= 0.97.

- Calcination weight loss (3 hours at 1100 °C in air atmosphere): 30.4 %.

6.7.8.3 Rxn 6-8-C: The control experiment was done in exactly the same way as described for Rxn **6-7-C**, with the exception that PEG 3400 was used instead of PEG

1000. The final product, **6-8-C**, was characterized by XRD and FTIR, which showed that the kaolinite starting material remained unexpanded.

6.8 Experimental for Chapter 5

6.8.1 Reactions of Kaolinite with Amines

6.8.1.1 Kao-DMSO + Ethanolamine (Rxn 5-1-1): The reaction of Kao-DMSO with ethanolamine was repeated a number of times and in all cases nearly identical materials resulted. The following is a typical example. 1.0 g of Kao-DMSO (I.R.=0.97) was refluxed with 50 ml of freshly distilled ethanolamine (EOA) for 22 hours under N_2 atmosphere. This was then filtered and washed with 1,4 dioxane to remove excess EOA. Air drying at 40 °C for 2 hrs yielded 0.76 g of an off-white powder.

- XRD (Philips PW 3710, vaseline mounted): d_{001}= 10.64 (100); d_{001} (K)= 7.14 (1.5); d_{002}= 5.34 (0.1); 4.46 (1.4); 4.34 (2.3); 4.28 (2.1); 4.20 (2.0); 4.15 (1.4); 3.72 (1.2); d_{003}= 3.56 (16.5); 3.32 (0.5); 3.19 (1.2); 3.14 (0.9); 2.84 (0.1); d_{004}= 2.67 (0.7); d_{005}= 2.13 (1.2); d_{006}= 1.78 (0.2); d_{060}= 1.487 (0.3). d= 10.67 ± 0.03 Å, I.R.=0.985.

- FTIR (in cm^{-1}): ν(O-H): 3693 (s), 3628 (s), 3558 (m), 3486 (s), ν(NH): 3354 (m), 3311 (m); ν(C-H): 3074 (w,br), 2964 (vw), 2946 (w), 2935 (vw), 2889 (w); δ(HOH): 1663 (w); δ(C-H, N-H): 1613 (w), 1525 (w), 1476 (w), 1353 (w), 1197 (w); Si-O vibrations: 1125 (s), 1092 (s), 1045 (vs), 1016 (vs); δ(AlOH): 974 (m), 908 (s);

other bands: 2792 (vw), 2691 (w), 2612 (w), 1385 (w,impurity), 874 (w), 796 (w), 740 (w), 683 (m), 604 (w,sh), 552 (s), 471 (s), 433 (s).

- TGA/DSC (40 cm^3/min N_2): 20-300 °C: 11.1 % wt. loss, $T_{endo.}$ = 225 °C (m); 300-430 °C: 4.4 % wt. loss, $T_{endo.}$ = 377 °C (w); 430-650 °C: 9.1 % wt. loss, $T_{endo.}$ = 503 °C (s); 650-1200 °C: 2.8 % wt. loss, $T_{exo.}$ = 1004 °C (m). Total TGA weight loss = 27.5 %.

- TGA/DSC (90 cm^3/min air, TGA % wt. loss values are approximate): 20-252 °C: 6.3 % wt. loss, $T_{exo.}$ = 229 °C (m); 252-400 °C: 7.2 % wt. loss, $T_{exo.}$ = 319 °C (s); 400-612 °C: 10.6 % wt. loss, $T_{endo.}$ = 482 °C (s); 612-1100 °C: 2.0 % wt. loss, $T_{exo.}$ = 1011 °C (w,sh), $T_{exo.}$ = 1032 °C (m).

- ^{13}C CP/MAS NMR (Bruker CXP-180, spinning speed= 6 KHz, 45.27 MHz, δ(ppm)): 42 ($-CH_2NH_2$), 60 ($-CH_2O-$); no dipolar dephasing signal detected after 40 μs dephasing time for either resonance.

- Elemental Analysis: % C: 8.06; % H: 2.72; % N: 4.12. Calcination weight loss (air atmosphere at 1100 °C for three hours): 27.5 %.

A portion of this sample (**5-1-1**) was then heated in an oven at 150 °C for 80 minutes.

- XRD (Philips PW 3710, vaseline mounted, d-values in Å and relative intensities in brackets): d_{001} = 10.48 (100), d_{001} (K)= 7.04 (6.5); I.R.=0.94.

Effects of D_2O washing on Kao-EOA: 0.1 g of Kao-EOA (**5-1-1**) was mixed with 2.0 g of D_2O in a glass vial. This was gently heated to the boiling point, and the

mixture was allowed to sit at room temperature for 5 days. The supernatant was then removed and examined by ^{1}H NMR.

^{1}H NMR, Varian-300, δppm (D_2O): 2.81 (t,2H,J=5.5 Hz); 3.15 (t,2H,J=5.6 Hz); 3.37 (m,1H); 3.59 (t,3H,J=5.6 Hz); 3.64 (t,8H,J=5.6 Hz).

The solid was washed once more with 2 ml D_2O (overnight at room temperature) followed by centrifugation and drying in an oven at 100 °C for 1 hr. This was then examined by FTIR.

-FTIR (in cm^{-1}): ν(OH): 3693 (m), 3650 (w), 3621 (s), 3550 (w,br); ν(OD): 2726 (s), 2711 (m,sh), 2698 (m,sh), 2676 (m,sh), 2635 (m,sh), 2635 (w), 2595 (w); Si-O vibrations: 1096 (s), 1036 (vs), 1012 (vs); δ(Al-OH): 913 (s); other bands: 700 (s), 534 (s), 472 (s), 433 (s).

6.8.1.2 Kao-NMF + Ethanolamine (Rxn 5-1-2): 2.0 g of Kao-NMF (I.R.=0.91) was refluxed with 60 ml of ethanolamine (freshly distilled) for 23 hours under N_2 atmosphere. This was then filtered and washed with 1,4 dioxane to remove excess ethanolamine. Air drying yielded 2.0 g of an off-white powder. The FTIR and XRD patterns proved to be nearly identical to the Kao-EOA product obtained from Kao-DMSO.

- XRD (Philips PW 3710, vaseline mounted, vacuum dried 40 °C 3 hrs: d_{001}= 10.36 (100); d_{001} (K)= 7.02 (3.7); 4.41 (7.5); 4.31 (9.8); 4.25 (11); 4.15 (9.1); 4.00 (5.6); 3.69 (5.9); d_{003}= 3.53 (23); d=10.5 ± 0.2 Å; I.R.=0.96.

- FTIR: nearly identical to Kao-EOA from Rxn 5-1-1)

- TGA/DSC (35 cm^3/min N_2): 20-175 °C: 5.1 % wt. loss; 175-285 °C: 7.3 % wt. loss, $T_{endo.}$ = 228 °C (m); 285-400 °C: 4.3 % wt. loss, $T_{endo.}$ = 377 °C (m); 400-650 °C: 9.4 % wt. loss, $T_{endo.}$ = 491 °C (s); 650-1000 °C, 3.2 % wt. loss, $T_{exo.}$ = 1006 °C (m), $T_{exo.}$ = 1015 °C (w,sh). Total TGA weight loss = 29.3 %.

- TGA/DSC (80 cm^3/min air; vacuum dried over P_2O_5 at 50 °C for 3 hrs; TGA % wt. losses only approximate): 20-265 °C: 6.7 % wt. loss, $T_{exo.}$ = 236 °C (m); 265-389 °C: 5.4 % wt. loss, $T_{exo.}$ = 316 °C (s); 389-723 °C: 11.5 % wt. loss, $T_{endo.}$ = 510 °C (s); 650-1000 °C: 1.9 % wt. loss, $T_{exo.}$ = 1010 °C (w,sh), $T_{exo.}$ = 1028 °C (m).

6.8.1.3 Kaolinite + Ethanolamine (Rxn 5-1-3): 1.0 g of kaolinite was refluxed with 50 ml of ethanolamine in a round bottom flask fitted with a reflux condenser for 17 hrs under nitrogen atmosphere. After filtering and washing the reaction mixture with methanol, the product was air dried, yielding 0.9 g of a light grey product. The FTIR pattern of this product was indicative of the well-crystallized kaolinite starting material.

6.8.1.4 Hal-DMSO + Ethanolamine (Rxn 5-1-4): 1.0 g of Hal-DMSO (see section **6.4.5** for full description of Hal-DMSO) was refluxed with 40 ml of ethanolamine (freshly distilled) for 20 hours under N_2 atmosphere. This was then filtered and washed with ethanol to remove excess ethanolamine. Air drying yielded 0.70 g of an off-white powder.

- XRD (Philips PW 3710, vaseline mounted): d_{001} = 10.61 (100); d_{003} = 3.55 (13). d=10.6 ± 0.1 Å; I.R.=1.0.

- FTIR (in cm^{-1}): ν(O-H): 3695 (s), 3630 (s), 3558 (s), 3491 (s), ν(NH): 3356 (m), 3313 (m); ν(C-H): 3076 (w,br), 2948 (w), 2889 (w); ν(C=O): 1614 (m); δ(C-H, N-H): 1478 (vw), 1355 (vw): Si-O: 1125 (s), 1035 (vs); δ(AlOH): 908 (s); other bands: 2620 (w), 744 (w), 680 (m), 551 (s), 468 (s), 434 (s).

- TGA/DSC (85 cm^3/min N_2, TGA weight losses are approximate): 20-153 °C: 7.6 % wt. loss, $T_{endo.}$ = 72 (m,sh), $T_{endo.}$ = 113 °C (m); 153-297 °C: 10.0 % wt. loss, $T_{endo.}$ = 238 °C (s); 297-417 °C: 4.4 % wt. loss, $T_{endo.}$ = 380 °C (w); 417-650 °C: 8.6 % wt. loss, $T_{endo.}$ = 493 °C (s).

6.8.1.5 Kao-DMSO + Ethylene Diamine (Rxn 5-1-5): 1.2 g of Kao-DMSO (I.R.=0.97) was refluxed with 60 ml reagent grade ethylene diamine (Aldrich, BP 118 °C) in a round bottom flask fitted with a reflux condenser for 18 hrs under nitrogen atmosphere. After filtering and washing the reaction mixture with 1,4 dioxane, the product was air dried yielding 0.8 g of a light grey product. The FTIR pattern of this product was indicative of partially collapsed Kao-DMSO.

6.8.1.6 Kao-DMSO + 3-Amino-1-Propanol (Rxn 5-1-6): 1.0 g of Kao-DMSO (I.R.= 0.97) was refluxed with 50 ml of 3-amino-1-propanol (Aldrich, $NH_2(CH_2)_3OH$, BP 187-188 °C) for 19 hrs under N_2 atmosphere. Workup consisted of cooling, filtering and washing with methanol. 0.82 g of an off-white powder were recovered after air drying for 1 hr. XRD and FTIR patterns were indicative of a partially modified product.

- XRD (Philips PW 3710, vaseline mounted): d_{001}= 11.07 (90), d_{001} (K)= 7.10 (66). I.R.= 0.58.

- FTIR (in cm^{-1}): ν(O-H) 3698 (s), 3652 (m), 3622 (s), 3626 (w,br); ν(NH): 3364 (vw); ν(C-H): 2941 (w), 2878 (w); δ(C-H, N-H): 1574 (w), 1482 (w), 1322 (vw); Si-O vibrations: 1110 (s,sh), 1085 (s), 1046 (vs), 1032 (vs), 1013 (vs); δ(Al-OH): 914 (s); other bands: 791 (w), 752 (w), 685 (m), 539 (s), 472 (s), 431 (s).

6.8.1.7 Kao-DMSO + DL-1-Amino-2-Propanol (Rxn 5-1-7): 1.0 g of Kao-DMSO (I.R.= 0.97) was refluxed with 50 ml of DL-1-amino-1-propanol (Aldrich, $NH_2CH_2CH_2OHCH_3$, BP 160 °C) for 19 hrs under N_2 atmosphere. Workup consisted of cooling, filtering and washing with methanol. 0.72 g of an off-white powder were recovered after air drying for 1 hr. FTIR indicated that no modification had occurred, and the Kao-DMSO starting material had reverted to a collapsed kaolinite.

6.8.1.8 Kao-DMSO + Nitroaniline (Rxn 5-1-8): A preliminary attempt to intercalate nitroaniline into the interlayer space of kaolinite by reacting 1.0 g of Kao-DMSO in 10 g of melted nitroaniline (MP 149°C) at 175 °C for 40 hrs under nitrogen atmosphere. During the course of reaction, the mixture slowly turned black. Workup consisted of repeated washings with methanol to remove as much of the excess organic material as possible. FTIR and XRD patterns were both consistent with a collapsed kaolinite structure.

6.8.2 Reactivity of Kaolinite With Carboxylic Acid Derivatives

6.8.2.1 Kao-DMSO + Acetic Acid (Rxn 5-2-1): 1.0 g of Kao-DMSO (I.R.=0.97) was placed in a stainless steel autoclave with 20 ml acetic acid (< 50 ppm water by Karl-Fischer titration). This was sealed and heated in a silicone oil bath held at 150 °C for 20 hrs and then at 210 °C for 3 hrs. The maximum evolved pressure was 5 bar. After filtering and washing with methanol, the product was air dried to yield 0.95 g of an off-white powder.

- XRD (Philips PW 3710, acetone dispersed): 10.23 (46,sh), 9.50 (100), 7.01 (28), 6.23 (83), 4.77 (5), 4.55 (18), 4.45 (27), 4.23 (17), 4.06 (16), 3.89 (23), 3.57 (11).

- FTIR (in cm^{-1}): v(O-H): 3696 (s), 3624 (s), 3200-3600 (s,br); v(C-H): 2940 (vw); v(C=O): 1657 (s), 1577 (m), 1480 (m), 1421 (w), 1380 (w), 1302 (m); Si-O vibrations: 1127 (s), 1060 (vs), 1038 (vs); δ(AlOH): 976 (s), 948 (s), 930 (s), 916 (m); other bands: 741 (w), 683 (m), 633 (s), 600 (s), 579 (s), 542 (s), 471 (s), 431 (s).

- TGA/DSC (90 cm^3/min N_2, TGA wt. loss values are approximate): 20-100 °C: 1.2 % wt. loss, $T_{endo.}$= 63 °C (w); 100-263 °C: 1.8 % wt. loss, $T_{endo.}$= 131 °C (w); 263-350 °C: 6.8 % wt. loss, $T_{endo.}$= 322 °C (m); 350-600 °C: 13.1 % wt. loss, $T_{endo.}$= 433 °C (s), $T_{endo.}$= 499 °C (w,sh); 600-1100 °C: $T_{exo.}$= 1012 °C (w,sh), $T_{exo.}$= 1022 °C (m).

- ^{13}C CP/MAS NMR (Bruker CXP-180, 45.27 MHz, δ(ppm)): 21 (sh, CH_3), 25.1 (CH_3), 179.5 (COO), 185.9 (COO).

50 mg of Kao-HOAc (**5-2-1**) was washed with 10 ml of water for 3 days. This was filtered and air dried.

- XRD (Philips PW 3710, acetone dispersed): 9.83 (100); 9.50 (73,sh); 7.13 (7.3); 6.24 (7.1); 4.76 (2.9).

This was then washed an additional 2 days in 50 ml of water to give the following product.

- XRD (Philips PW 3710, acetone dispersed): d_{001}= 9.42 (100); d_{001} (K)= 7.14 (9.1); d_{002}= 4.74 (2.1).

- FTIR (in cm^{-1}): ν(O-H): 3695 (s), 3623 (s), 3200-3600 (s,br); ν(C-H): 2950 (vw), 2925 (vw); ν(C=O): 1658 (s), 1421 (w), 1379 (w), 1300 (m); Si-O vibrations: 1135 (s,sh), 1060 (vs), 1037 (vs); δ(AlOH): 947 (s), 930 (s), 916 (m); other bands: 744 (w), 686 (m), 547 (s), 471 (s), 431 (s).

6.8.2.2 Kao-NMF + Acetic Acid (Rxn 5-2-2): 1.25 g of Kao-NMF (I.R.=0.91) was placed in a glass lined stainless steel autoclave with 20 ml acetic acid (< 50 ppm water by Karl-Fischer titration). This was sealed and heated in a silicone oil bath with temperature between 170-200 °C for 70 hrs. The maximum evolved pressure was 7 bar. After filtering, the product was ground up and washed with methanol and then filtered again. Grinding was necessary since the product contained some agglomerations of particles which were difficult to break up. Air drying yielded 1.4 g of an off-white powder.

- XRD (Philips PW 3710, methanol dispersed): 9.36 (6.0); 6.98 (20); 6.21 (100); 4.54 (15); 3.88 (17); 3.35 (14); 2.47 (6.8).

- FTIR (in cm^{-1}): ν(O-H): 3697 (s), 3621 (s), 3200-3600 (s,br); ν(C-H): 2940 (vw); ν(C=O): 1657 (s), 1576 (vs), 1479 (vs), 1430 (m), 1409 (m), 1361 (w), 1303 (w); Si-O vibrations: 1127 (m,sh), 1062 (vs), 1036 (vs); δ(AlOH): 976 (vs), 915 (m); other bands: 699 (s), 678 (s), 655 (s), 625 (m), 600 (s), 543 (s), 510 (s), 471 (s), 433 (s).

- TGA/DSC (90 cm^3/min N_2, TGA wt. loss values are approximate): 20-200 °C: 7.0 % wt. loss, $T_{endo.}$ = 55 °C (m); 200-360 °C: 19.7 % wt. loss, $T_{endo.}$ = 326 °C (s); 360-650 °C: 13.4 % wt. loss, $T_{endo.}$ = 435 °C (w), $T_{endo.}$ = 505 °C (m); 600-1000 °C: $T_{exo.}$ = 910 °C (w). Total TGA weight loss = 40.1 %.

- ^{13}C CP/MAS NMR (Bruker CXP-180, 45.27 MHz, δ(ppm)): 25.3 (sh, CH_3), 179.6 (COO).

A small portion of this sample was heated to 200 °C for 2 hours in an oven. There was no apparent change in either the FTIR or XRD pattern.

6.8.2.3 Kaolinite + Acetic Acid (Rxn 5-2-3): 1.0 g of kaolinite was mixed with 30 ml of acetic acid (< 50 ppm water by Karl-Fischer titration) in a glass-lined stainless steel autoclave. This was sealed and heated in a silicone oil bath with temperature maintained between 180-220 °C for 48 hrs. After filtering, the product was washed with methanol to give 0.65 g of an off-white powder. The XRD pattern of this product was indicative of well crystallized kaolinite, indicating that no modification was achieved.

6.8.2.4 Kao-DMSO + Chloroacetyl Chloride (Rxn 5-2-4): 1.0 g Kao-DMSO (I.R. = 0.96) was refluxed with 40 ml of chloroacetyl chloride (Fluka, $ClCH_2COCl$, BP 105-106 °C) for 6 hours under open atmosphere. The mother liquor gradually turned yellow as the reaction progressed. After filtering and washing with 1,4 dioxane, 0.87 g of a yellowish powder was recovered and characterized by XRD and FTIR.

- XRD (Philips PW 1050/81, 1,4 dioxane dispersed): d_{001}= 11.21 (100); 9.52 (sh); d_{001} (K)= 7.21 (11); d_{002}= 5.57 (4); d_{003}= 3.65. d=11.10 ± 0.13 Å; I.R. = 0.90.

- FTIR (in cm^{-1}): ν(O-H): 3693 (s), 3634(s), 3625 (s), 3462 (m), 3400 (m,br); ν(C-H): 3015 (w), 2964 (w), 2872 (w); ν(C=O): 1755 (w,sh), 1723 (m); δ(HOH) 1638 (w); δ(C-H) 1462 (vw), 1404 (w), 1358 (w), 1309 (w,br), 1218 (w); Si-O vibrations: 1119 (m), 1081 (s), 1051 (vs), 1036 (vs); δ(Al-OH): 962 (vw), 913 (s); other bands: 794 (w), 750 (w), 685 (m), 545 (vs), 473 (s), 431 (s).

6.8.2.5 Kao-DMSO + Acetyl Chloride (Rxn 5-2-5): 0.20 g Kao-DMSO (I.R. = 0.96) was stirred with 5 ml of acetyl chloride (Aldrich, CH_3COCl, BP 52 °C) in a round bottom flask fitted with a reflux condenser and a calcium chloride drying tube for 7 days at room temperature. After filtering and washing with dichloromethane 0.11 g of an off-white powder was recovered. Some product was lost due to spillage during the washing step.

- XRD (Philips PW 1050/81, dichloromethane dispersed): d_{001}= 8.61 (100); d_{001} (K)= 7.23 (16). I.R. =0.86.

- FTIR (in cm^{-1}): v(O-H): 3696 (m), 3645 (m,sh), 3620 (s), 3548 (m), 3400 (m,br); v(C=O): 1690 (m,br); δ(HOH) 1655 (w); δ(C-H) 1476 (vw), 1298 (w); Si-O: 1086 (s), 1038 (vs), 1012 (vs); δ(Al-OH): 911 (s); other bands: 1620 (vw), 785 (vw), 751 (w), 685 (m), 547 (vs), 471 (s), 430 (s).

- TGA/DSC (85 cm^3/min N_2, TGA wt. loss values are approximate): 20-250 °C: 8.9 % wt. loss, $T_{endo.}$= 78 °C (m), $T_{endo.}$= 153 °C (m); 250-600 °C: 11.3 % wt. loss, $T_{endo.}$= 431 °C (m), $T_{endo.}$= 498 °C (s); 600-1000 °C: $T_{exo.}$= 1011 °C (s).

After storing the product in a stoppered vial for 11 months, an XRD was redone. This showed significant difference from the original pattern.

- XRD (Philips PW 3710, vaseline mounted, d-values in Å and relative intensities in brackets): d_{001}= 10.71 (100); 8.17 (72); d_{001} (K)= 7.09 (20).

6.8.2.6 Kao-DMSO + Propionic Acid (Rxn 5-2-6): 1.5 g Kao-DMSO (I.R.=0.96) was refluxed with 55 ml of propionic acid (JT Baker, CH_3CH_2COOH, BP 140-142 °C) for 19 hrs in open atmosphere. This was then filtered and washed with 1,4 dioxane. 1.15 g of an off-white powder was recovered.

- XRD (Philips PW 1050/81, 1,4 dioxane dispersed): d_{001}= 11.03 (100); d_{001} (K)= 7.18 (4); d_{002}= 5.50 (1); d_{003}= 3.65 (20). d-spacing= 10.99 ± 0.04; I.R.= 0.96.

- FTIR (in cm^{-1}): v(O-H): 3693 (w), 3643 (m), 3620 (m), 3560 (m,br), 3417 (m,br); v(C-H): 3000 (vw), 2985 (w), 2950 (w), 2924 (w): v(C=O): 1715 (w,br), 1651 (m); δ(C-H) 1403 (w), 1246 (w); Si-O; 1127 (s), 1058 (vs), 1037 (vs); δ(Al-OH): 950

(m), 915 (m); other bands: 1385 (m), 894 (w,sh), 820(vw), 746 (w), 686 (m), 570 (s), 544 (s), 474 (s), 436 (s).

- TGA/DSC (40 cm^3/min N_2): 20-200 °C: 3.6 % wt. loss, $T_{endo.}$ = 115 °C (m); 200-348 °C: 7.1 % wt. loss, $T_{endo.}$ = 313 °C (m); 348-428 °C: 5.6 % wt. loss, $T_{endo.}$ = 406 °C (m); 428-650 °C: 10.1 % wt. loss, $T_{endo.}$ = 483 °C (m); 650-1200 °C: 3.0 % wt. loss, $T_{exo.}$ = 1006 °C (m). Total TGA weight loss = 29.4 %.

- ^{13}C CP/MAS NMR (Bruker ASX-300, 75.48 MHz): C=O (PA): 182 ppm; CH_2 (PA): 22 ppm; CH_3 (PA): 10 ppm; CH_3 (DMSO): 41 ppm.

A portion (20 mg) of this product was washed with 10 ml of water for 20 hrs, followed by air drying. This did not affect the appearance of the IR pattern to a great extent, although there was some evidence for the slow leaching of the organic component (for example the intensity of the 1651 cm^{-1} is decreased upon water washing).

Heating the product under vacuum at 130 °C for 17 hrs over P_2O_5 also failed to completely collapse the structure. However, heating at 200 °C for 1 hour did appear to fully collapse the structure to the parent kaolinite material as indicated by FTIR.

6.8.2.7 Kao-NMF + Propionic Acid (Rxn 5-2-7): 1.5 g Kao-NMF (I.R.=0.91) was refluxed with 55 ml of propionic acid (JT Baker, CH_3CH_2COOH, BP 140-142 °C) for 19 hrs in open atmosphere. This was then filtered and washed with 1,4 dioxane. 1.15 g of an off-white powder was recovered. XRD and FTIR patterns of the product were both consistent with an almost completely collapsed kaolinite structure, with traces of residual interlayer NMF.

6.8.2.8 Kao-DMSO + Propionyl Chloride (Rxn 5-2-8): 0.21 g Kao-DMSO (I.R.=0.96) was stirred with 5 ml of propionyl chloride (Aldrich, CH_3CH_2COCl, BP 77-79 °C) in a round bottom flask fitted with a reflux condenser and a calcium chloride drying tube for 7 days at room temperature. After filtering and washing with dichloromethane 0.16 g of an off-white powder was recovered. XRD and FTIR suggested that the product was in large part th starting material Kao-DMSO.

- XRD (Philips PW 1050/81, dichloromethane dispersed): d_{001}= 11.41 (100); d_{001} (K)= 7.21 (7); d_{003}= 3.75 (30).

- FTIR (in cm^{-1}): ν(O-H): 3695 (m), 3635 (s), 3620 (s), 3578 (s), 3545 (m,br), 3435 (m,br); ν(C-H): 3015 (w), 2915 (w); δ(C-H) 1430 (w), 1410 (w), 1322 (w); Si-O vibrations; 1124 (s), 1082 (s), 1060-1000 (vs); δ(Al-OH): 955 (m), 910 (s); other bands: 798 (w), 748 (w), 687 (m), 543 (vs), 468 (s), 431 (s).

- TGA/DSC (85 cm^3/min N_2, TGA wt, loss values are approximate): 20-200 °C: 5.0 % wt. loss, $T_{endo.}$= 71 °C (w,sh), $T_{endo.}$= 133 °C (m); 200-350 °C: 12.9 % wt. loss, $T_{endo.}$= 293 °C (m); 350-600 °C: 8.2 % wt. loss, $T_{endo.}$= 502 °C (s); 650-1050 °C: $T_{exo.}$= 1010 °C (m).

6.8.3 Other Attempts at Functionalizing Kaolinite

6.8.3.1 Kao-DMSO + 2-Chloroethanol (Rxn 5-3-1): 1.0 g Kao-DMSO (I.R.= 0.97) was refluxed with 45 ml of 2-chloroethanol (Aldrich, BP 129 °C) for 41 hrs under

N_2 atmosphere. The mother liquor was brownish. After filtering and washing with 1,4 dioxane, 0.76 g of a grey powder was recovered.

- XRD (Philips PW 3710, vaseline mounted): d_{001}= 10.92 (100), 8.94 (8.8,sh), d_{001} (K)= 7.15 (3.9), d_{003}= 3.68 (20). d= 10.98 ± 0.09 Å; I.R.= 0.89.

- FTIR (in cm^{-1}): v(O-H): 3693 (m), 3619 (s), 3600 (s), 3555 (s,br), 3440 (m,vbr); v(C-H): 2949 (vw), 2880 (vw); δ(HOH) 1638 (w, br.); δ(C-H) 1462 (vw), 1306 (vw); Si-O vibrations: 1109 (s), 1096 (s), 1050-1000 (vs); δ(Al-OH): 969 (m), 911 (s); other bands: 792 (w), 759 (w), 688 (m), 554 (vs), 479 (s), 438 (s).

- TGA/DSC (85 cm^3/min N_2, TGA % wt. loss values are approximate): 20-170 °C: 6.1 % wt. loss, $T_{endo.}$= 74 °C (m); 170-379 °C: 7.0 % wt. loss; 379-636 °C: 9.8 % wt. loss, $T_{endo.}$= 478 °C (m); 650-1200: $T_{exo.}$= 1016 °C (m). Total TGA weight loss = 22.9 %.

6.8.3.2 Kao-DMSO + 3-Chloro-1,2-Propanediol (Rxn 5-3-2): 1.0 g Kao-DMSO (I.R.=0.97) was refluxed with 40 ml of 3-chloro-1,2-propanediol (Aldrich, $CH_2OHCH_2OHCH_2Cl$, BP 213 °C) for 6 hrs under open atmosphere. The mother liquor gradually turned dark brown as the reaction progressed. After filtering and washing with 1,4 dioxane, 0.73 g of a grey powder was recovered.

- XRD (Philips PW 1050/81, 1,4 dioxane dispersed): d_{001}= 11.15 (36); d_{001} (K)= 7.5 (60,assym); d_{002} (K)= 3.68 (100); I.R.= 0.38.

- FTIR (in cm^{-1}): v(O-H): 3697 (s), 3652(w), 3623 (s), 3440 (m,br); v(C-H): 3055 (vw), 2943 (vw), 2880 (vw); δ(HOH) 1634 (w, br.); δ(C-H) 1462 (vw), 1428 (vw); Si-O:

1090 (s), 1050-1000 (vs); δ(Al-OH): 914 (s); other bands: 792 (w), 752 (w), 690 (m), 543 (vs), 478 (s), 431 (s).

6.8.3.3 Kao-DMSO + 2-Thiol-Ethanol (Rxn 5-3-3): 1.2 g of Kao-DMSO (I.R.=0.97) was refluxed with 50 ml 2-thiol-ethanol (Aldrich, BP 157 °C) in a round bottom flask fitted with a reflux condenser for 16 hrs under nitrogen atmosphere. The suspension quickly turned grey upon refluxing. An unknown hard whitish solid material, perhaps the result of a polymerization reaction involving 2-thiol-ethanol, was deposited on the walls of the condenser. After filtering and washing the reaction mixture with 1,4 dioxane, the product was air dried yielding 0.8 g of a light grey product. The FTIR pattern of this product was almost identical to that of unmodified kaolinite, showing no evidence of modification.

6.8.3.4 Kao-DMSO + 1,2-Ethanedithiol (Rxn 5-3-4): 1.25 g of Kao-DMSO (I.R.=0.97) was refluxed with 50 ml 1,2-ethane-dithiol (Aldrich, BP 144-146 °C) for 21 hrs. The suspension quickly turned grey upon reflux conditions. After filtering and washing with 100 ml of 1,4 dioxane, the light grey product was air dried. The FTIR pattern of this product was almost identical to that of unmodified kaolinite, showing no evidence of modification.

6.8.3.5 Kao-DMSO + Chlorotrimethylsilane (Rxn 5-3-5): 4.7 g of Kao-DMSO powder (I.R.=0.96) was refluxed with a mixture of 12 ml chlorotrimethylsilane in 200

ml dioxane for 24 hrs. This was done in air atmosphere with a calcium chloride drying tube fitted to the condenser. Centrifugation of the reaction mixture, washing with 1,4 dioxane, and drying at 100 °C for 1 hour afforded 3.9 g of a grey product.

- XRD (Philips PW 1050/81, 1,4 dioxane dispersed): 10.77 (100); d_{001} (K)= 7.15 (12); 4.45 (16); 4.15 (16); 3.56 (41).

- FTIR (in cm^{-1}): ν(O-H): 3694 (s), 3635 (s), 3621 (s), 3600-3200 (s,br); ν(C-H): 2962 (w), 2932 (w), 2885 (w); δ(HOH): 1634 (m); δ(C-H): 1462 (vw), 1436 (vw), 1384 (vw), 1340 (vw), 1306 (vw), 1252 (vw) 1198 (vw,sh): Si-O: 1100-1000 (vs); δ(AlOH): 913 (s); other bands: 796 (w), 750 (w), 683 (m), 544 (s), 473 (s), 432 (s).

6.8.3.6 Kao-DMSO + Chlorodimethylethylsilane (Rxn 5-3-6): 1.0 g of Kao-DMSO powder (I.R.= 0.92) was refluxed with a mixture of 2.6 ml chlorodimethylethylsilane (Aldrich) in 70 ml dioxane for 22 hours. This was done in air atmosphere with a calcium chloride drying tube fitted to the condenser. Centrifugation of the reaction mixture, washing with 1,4 dioxane, and vacuum drying at 110 °C for 1 hour afforded 0.6 g of a grey product.

- XRD (Philips PW 1050/81, 1,4 dioxane dispersed): 10.77 (100); d_{001} (K)= 7.18 (8); 4.45 (5); 3.68 (15); 3.57 (18).

6.8.3.7 Kao-DMSO + Phenylphosphonic Acid (Rxn 5-3-7): 0.5 g of Kao-DMSO was ground together with 2.0 g of phenylphosphonic acid (Aldrich, MP 163-166 °C) with a mortar and pestle for 5 minutes. An XRD pattern of this mixture was taken.

This was consistent with the superposition of the Kao-DMSO phase (d(Å): 11.05, 5.54, 3.70, etc.) and a phenyl phosphonic acid phase (d(Å): 7.80, 6.39, 5.95, 4.28 etc.). This mixture was then placed in a 50 ml round bottom flask and heated with stirring in a silicone oil bath held between 180-190 °C for 16 hours under N_2 atmosphere. Upon cooling, the pasty reaction product formed a hard brittle material which was ground up. An XRD pattern of this material was taken and showed a very complicated pattern which was indicative of neither phenyl phosphonic acid, kaolinite nor Kao-DMSO. The most prominent peak was an asymmetric reflection at d= 12.3 Å.

The product was washed with methanol to remove excess organic material. This yielded 0.72 g of an off-white powder.

- XRD (Philips PW 3710, methanol dispersed): 14.85 (24); 12.34 (100); 11.47 (19); 10.47 (2.3); 7.49 (7.5); 7.11 (0.5); 6.66 (6.0); 5.40 (1.3); 4.87 (9.4); 4.60 (11); 4.51 (15); 4.27 (14); 4.12 (15); 4.00 (5.5); 3.92 (5.8); 3.68 (10); 3.51 (7.1); 3.39 (9.0); 3.31 (6.0); etc.

- FTIR (in cm^{-1}): v(O-H): 3650-3100 (m,br); v(C-H): 3055 (m); other bands: 1598 (m), 1488 (w), 1440 (m), 1229 (vs), 1174 (vs), 1070 (s), 1034 (s), 929 (m), 746 (m), 693 (m), 566 (s), 493 (m), 419 (s).

- TGA/DSC (90 cm^3/min N_2, TGA % wt. losses are approximate): 20-400 °C: 4 % wt. loss, $T_{endo.}$= 65 °C (w); 400-540 °C: 21 % wt. loss, $T_{endo.}$= 432 °C (w,sh), $T_{endo.}$= 522 °C (m); 540-800 °C: 19 % wt. loss, $T_{endo.}$= 584 °C (m); 800-1100 °C: 13 % wt. loss. Total TGA weight loss = 57 %.

After washing the product with excess water for 10 days at room temperature, the XRD pattern was taken again. This was indicative of a very disordered material with the only well defined peaks being at d= 14.43 Å (100) due to an unknown phase, and a smaller peak at d= 3.51 Å (3.5) due to trace amounts of anatase (TiO_2) impurity.

GENERAL CONCLUSIONS

The interest in using kaolinite as a mineral precursor for the preparation of new nanocomposite materials stems from its unique asymmetric layered structure, which results in a dipolar interlayer environment suitable for the organization of dipolar guest molecules. Moreover, the presence of abundant interlayer aluminol (Al-OH) surface groups offers an attractive chemically reactive site for the interlamellar covalent grafting of organic units.

The principal accomplishments of this work include the demonstration that it is possible to chemically modify the interlayer surface of kaolinite through the attachment of covalently grafted organic groups and that it is possible to directly intercalate a polymer chain (polyethylene glycol) into the interlayer spaces of kaolinite. Both of these contributions represent significant advancements in the intercalation chemistry of the clay mineral kaolinite.

Many of the new organokaolinite materials were prepared through the reaction of small aliphatic alcohols at high temperatures (150-250 °C) with the kaolinite mineral which had been pre-intercalated with either DMSO or NMF (Chapter 2). It was proposed that the alcohols were grafted onto the interlamellar aluminol surface via Al-O-C linkages through the condensation reaction between the alcohol groups of the organic reactants and the interlayer kaolinite aluminol groups. In this manner, new nanocomposite materials were prepared by reacting kaolinite with methanol, polyols and alcohol ethers.

Most of the resultant alcohol modified organokaolinite materials were resistant to both thermal decomposition and solvent leaching. For example, the methoxy functionalized kaolinite (Kao-MeOH) and the ethylene glycol functionalized kaolinite (Kao-EG 9.4 Å) did not decompose until well above 200 °C and were also resistant to decomposition by washing with water and other solvents. This decomposition behaviour is not typical of classical organokaolinite intercalates, such as Kao-DMSO and Kao-NMF which decompose at temperatures less than 200 °C and whose organic guest may be easily washed out in water.

It was found that ethylene glycol may react with kaolinite to give two distinct phases: an intercalated phase (Kao-EG 10.8 Å), and a grafted phase (Kao-EG 9.4 Å) (Chapter 3). Water in the reaction media was shown to favour the Kao-EG 10.8 Å phase at the expense of the Kao-EG 9.4 Å phase. The model which best describes all the properties and characterizations of Kao-EG 9.4 Å is that of an organokaolinite material whose ethylene glycol moieties are attached to the interlamellar aluminate surface at one end via an Al-O-C bond with the remaining pendant alcohol group keyed into the $(Si\text{-}O\text{-})_6$ macroring of the adjacent tetrahedral silicate surface.

Starting from the simplest oxyethylene species (OCH_2CH_2), ethylene glycol, a new class of organokaolinite oxyethylene based nanocomposite materials was developed (Chapter 4). It was possible to intercalate such oxyethylene species as 15-crown-5, 18-crown-6 and polyethylene glycol (MW 3400). The latter represents the first example of the direct incorporation of any polymer into the interlayer space of kaolinite. It was

determined that all of these oxyethylene based nanocomposites were composed of alternating 7 Å layers of kaolinite sandwiched between flattened oxyethylene monolayers.

Exploratory work involving other types of organic reagents showed that there are other promising routes to the interlamellar surface modification of kaolinite (Chapter 5). For example, a robust new material with interlayer amino functionalities was prepared through the reaction of kaolinite with 2-aminoethanol. New organomineral materials may also be prepared using carboxylic acid derivatives. In particular, reaction of kaolinite with acetic acid at high temperatures was proposed to form a new organokaolinite material with Al-O_2CCH_3 groups.

REFERENCES

(1) Moore D. M.; Reynolds R. C. Jr. *X-Ray Diffraction and the Identification and Analysis of Clay Minerals*; Oxford University Press: Oxford, 1989.

(2) Bailey, S. W. In *Crystal Structures of Clay Minerals and their X-ray Identification*; Brindley G. W.; Brown G. Eds.; Mineralogical Society: London, 1984; pp 1-124.

(3) Bailey, S. W. In *Reviews in Mineralogy, Vol. 19: Hydrous Phyllosilicates*; Bailey S. W. Ed.; Mineralogical Society of America: Washington, 1988; pp 9-27.

(4) Martin, R. T.; Bailey, S. W.; Eberl, D. D.; Fanning, D. S.; Guggenheim, S.; Kodama, H.; Pevear, D. R.; Srodon, J.; Wicks, F. J. *Clays Clay Miner.* **1991**, *39*, 333-335.

(5) Guggenheim, S.; Eggleton, R. A. In *Reviews in Mineralogy, Vol. 19: Hydrous Phyllosilicates*; Bailey S. W. Ed.; Mineralogical Society of America: Washington, 1988; pp 675-725.

(6) Jones, B. F.; Galan, E. In *Reviews in Mineralogy, Vol. 19: Hydrous Phyllosilicates*; Bailey S. W. Ed.; Mineralogical Society of America: Washington, 1988; pp 631-674.

(7) Wada, K. In *Minerals in the Soil Environment*; Dixon J. B.; Weeds S. B. Eds.; Soil Science Society of America: 1977; pp 603-638.

(8) Murray, H.H. In *Hydrous Phyllosilicates*; Bailey S. W. Ed.; Mineralogical Society of America: Washington, 1993; pp 67-89.

(9) Zheng, Z.; Lu, D.; Feng, M.; Feng, B.; Jin, T. In *International Clay Conference 1981; Developments in Sedimentology 35*; van Olphen H.; Veniale F. Eds.; Elsevier: Amsterdam, 1982; pp 719-731.

(10) Giese, R. F. In *Hydrous Phyllosilicates*; Bailey S. W. Ed.; Mineralogical Society of America: Washington, 1988; pp 29-66.

(11) Keller, W. A.; Cheng, H.; Johns, W. D.; Meng, C. S. *Clays Clay Miner.* **1980**, *28*, 97-104.

(12) Talibudeen, O.; Goulding, K. W. T. *Clays Clay Miner.* **1983**, *31*, 137-142.

(13) Brindley, G. W. In *Crystal Structures of Clay Minerals and their X-ray Identification*; Brindley G. W.; Brown G. Eds.; Mineralogical Society: London, 1984; pp 125-196.

(14) Merino, E.; Harvey, C.; Murray, H. H. *Clays Clay Miner.* **1989**, *37*, 135-142.

(15) Newnham, R. E. *Mineralog. Mag.* **1961**, *32*, 683-704.

(16) Zvyagin, B. B. *Soviet Phys. Chrystallogr.* **1962**, *7*, 38-51.

(17) Bailey, S. W. *Amer. Mineral.* **1963**, *48*, 1196-1209.

(18) Bailey, S. W. *Clays Clay Miner.* **1969**, *17*, 355-371.

(19) Bookin, A. S.; Drits, V. A.; Plançon, A.; Tchoubar, C. *Clays Clay Miner.* **1988**,

(20) Pauling, L. *Proc. Nat'l. Acad. Sci. U.S.A.* **1930**, *16*, 578-582.

(21) Suitch, P. R.; Young, R. A. *Clays Clay Miner.* **1983**, *31*, 357-366.

(22) Young, R. A.; Hewat, A. W. *Clays Clay Miner.* **1988**, *36*, 225-232.

(23) Bish, D. L.; Von Dreele, R. B. *Clays Clay Miner.* **1989**, *37*, 289-296.

(24) Bish, D. L. *Clays Clay Miner.* **1993**, *41*, 738-744.

(25) Farmer, V. C. In *The Infra-Red Spectra of Minerals*; Farmer V. C. Ed.; Mineralogical Society: London, 1974; pp 331-363.

(26) Farmer, V. C.; Russell, J. D. *Spectrochim. Acta* **1964**, *20*, 1149-1173.

(27) Hess, A. C.; Saunders, V. R. *J. Phys. Chem.* **1992**, *96*, 4367-4374.

(28) Raussell-Colom, J. A.; Serratosa, J. M In *Chemistry of Clays and Clay Minerals*; Newman A. C. D. Ed.; Mineralogical Society: London, 1987; pp 371-422.

(29) Weiss, A.; Becker, H. O.; Orth, H.; Mai, G.; Lechner, H.; Range, K. J. *Proc. Int. Clay Conf. Tokyo* **1969**, *2*, 180-184.

(30) Plançon, A.; Giese, R. F.,Jr.; Snyder, R.; Drits, V. A.; Bookin, A. S. *Clays Clay Miner.* **1989**, *37*, 203-210.

(31) Plançon, A.; Zacharie, C. *Clay Miner.* **1990**, *25*, 249-260.

(32) MacEwan, D. M. C. *Nature* **1946**, *157*, 159-160.

(33) MacEwan, D. M. C. *J. Chem. Soc., Faraday Trans.* **1948**, *44*, 349-367.

(34) Carr, R. M.; Chih, H. W. A. *Clay Miner.* **1971**, *9*, 153-166.

(35) Wada, K. *Amer. Mineral.* **1961**, *46*, 78-91.

(36) Theng, B. K. G. In *The Chemistry of Clay-Organo Reactions*; Adam Hilger: London, 1974; pp 239-260.

(37) MacEwan, D. M. C.; Wilson, M. J. In *Crystal Structures of Clay Minerals and Their X-ray Identification*; Brindley G. W.; Brown G. Eds.; Mineralogical Society: London, 1984; pp 197-248.

(38) Camazano, M. S.; Garcia, S. G. *An. Edafol Agrobiol.* **1966**, *25*, 9-25.

(39) Olejnik, S.; Aylmore, L. A. G.; Posner, A. M.; Quirk, J. P. *J. Phys. Chem.* **1968**, *72*, 241-249.

(40) Olejnik, S.; Posner, A. M.; Quirk, J. P. *Clay Miner.* **1970**, *8*, 421-434.

(41) Johnston, C. T.; Sposito, G.; Bocian, D. F.; Birge, R. R. *J. Phys. Chem.* **1984**, *88*, 5959-5964.

(42) Duer, M. J.; Rocha, J.; Klinowski, J. *J. Am. Chem. Soc.* **1992**, *114*, 6867-6874.

(43) Thompson, J. G.; Cuff, C. *Clays Clay Miner.* **1985**, *33*, 490-500.

(44) Thompson, J. G. *Clays Clay Miner.* **1985**, *33*, 173-180.

(45) Raupach, M.; Barron, P. F.; Thompson, J. G. *Clays Clay Miner.* **1987**, *35*, 208-219.

(46) Lipsicas, M.; Raythatha, R.; Giese, R. F.; Costanzo, P. M. *Clays Clay Miner.* **1986**, *34*, 635-644.

(47) Olejnik, S.; Posner, A. M.; Quirk, J. P. *Clays Clay Miner.* **1971**, *19*, 83-94.

(48) Uwins, P. J. R.; Mackinnon, I. D. R.; Thompson, J. G.; Yago, A. J. E. *Clays Clay Miner.* **1993**, *41*, 707-717.

(49) Cruz, M.; Laycock, A.; White, J. L. *Proc. Int. Clay Conf.* **1969**, *1*, 775-789.

(50) Ledoux, R. L.; White, J. L. *Proc. Int. Clay Conf.* **1966**, *1*, 361-374.

(51) Ledoux, R. L.; White, J. L. *J. Colloid Interf. Sci.* **1966**, *21*, 137-152.

(52) Barrios, J.; Plançon, A.; Cruz, M. I.; Tchoubar, C. *Clays Clay Miner.* **1977**, *25*, 422-429.

(53) Johnston, C. T.; Stone, D. A. *Clays Clay Miner.* **1990**, *38*, 121-128.

(54) Adams, J. M.; Reid, P. I.; Thomas, J. M.; Walters, M. J. *Clays Clay Miner.* **1976**, *24*, 267-269.

(55) Weiss, A.; Thielepape, W.; Orth, H. *Proc. Int. Clay Conf.* **1966**, *1*, 277-293.

(56) Weiss, A.; Thielepape, W.; Göring, G.; Ritter, W.; Schäfer, H. *Proc. Int. Clay Conf.* **1963**, 287-305.

(57) Thompson, J. G.; Uwins, P. J. R.; Whittaker, A. K.; Mackinnon, I. D. R. *Clays Clay Miner.* **1992**, *40*, 369-380.

(58) Michaelian, K. H.; Yariv, S.; Nasser, A. *Can. J. Chem.* **1991**, *69*, 749-754.

(59) Jackson, M. L.; Abdel-Kader, F. H. *Clays Clay Miner.* **1978**, *26*, 81-87.

(60) Thompson, J. G.; Gabbitas, N.; Uwins, P. J. R. *Clays Clay Miner.* **1993**, *41*, 73-86.

(61) Sugahara, Y.; Kitano, S.; Satokawa, S.; Kuroda, K.; Kato, C. *Bull. Chem. Soc. Jpn.* **1986**, *59*, 2607-2610.

(62) Range, K. J.; Range, A.; Weiss, A. *Z. Naturf.* **1968**, *B23*, 1144-1147.

(63) Range, K. J.; Range, A.; Weiss, A. *Proc. Int. Clay Conf.* **1969**, *1*, 3-13.

(64) Costanzo, P. M.; Clemency, C. V.; Giese, R. F. *Clays Clay Miner.* **1980**, *28*, 155-156.

(65) Costanzo, P. M.; Giese, R. F. *Clays Clay Miner.* **1985**, *33*, 415-423.

(66) Costanzo, P. M.; Giese, R. F.; Clemency, C. V. *Clays Clay Miner.* **1984**, *32*, 29-35.

(67) Costanzo, P. M.; Giese, R. F.; Lipsicas, M.; Straley, C. *Nature* **1982**, *296*, 549-551.

(68) Costanzo, P. M.; Giese, R. F.,Jr. *Clays Clay Miner.* **1990**, *38*, 160-170.

(69) Sugahara, Y.; Satokawa, S.; Yoshioka, K.; Kuroda, K.; Kato, C. *Clays Clay Miner.* **1989**, *37*, 143-150.

(70) Costanzo, P. M.; Giese, R. F.; Lipsicas, M. *Clays Clay Miner.* **1984**, *32*, 419-428.

(71) Wada, N.; Raythatha, R.; Minomura, S. *Solid State Comm.* **1987**, *63*, 783-786.

(72) Sugahara, Y.; Satokawa, S.; Kuroda, K.; Kato, C. *Clays Clay Miner.* **1990**, *38*, 137-143.

(73) Sugahara, Y.; Satokawa, S.; Kuroda, K.; Kato, C. *Clays Clay Miner.* **1988**, *36*, 343-348.

(74) Ovramenko, N. A.; Zakharchenko, O. F.; Litovchenko, A. S.; Trachevskii, V. V.; Shutova, V. I.; Ovcharenko, F. D. *Dokl. Akad. Nauk. SSSR. (Chemistry) English* **1989**, *309*, 364-367.

(75) Ruiz-Hitzky, E. *Mol. Cryst. Liq. Cryst. Inc. Nonlin. Opt.* **1988**, *161*, 433-452.

(76) Currell, B. R.; Parsonage, J. R. *J. Macromol. Sci. -Chem.* **1981**, *A16(1)*, 141-166.

(77) Choudary, B. M.; Subba Rao, Y. V.; Prasad, B. P. *Clays Clay Miner.* **1991**, *39*, 329-332.

(78) Ravi Kumar, K.; Choudary, B. M.; Jamil, Z.; Thyagarajan, G. *J. Chem. Soc., Chem. Commun.* **1986**, 130-131.

(79) Choudary, B. M.; Bharathi, P. *J. Chem. Soc., Chem. Commun.* **1987**, 1505-1506.

(80) Ruiz-Hitzky, E.; Fripiat, J. J. *Proc. Int. Clay Conf. (Mexico)* **1975**, 412-413.

(81) Ruiz-Hitzky, E.; Fripiat, J. J. *Clays Clay Miner.* **1976**, *24*, 25-30.

(82) Ruiz-Hitzky, E.; Van Meerbeek, A. *Colloid Polym. Sci.* **1978**, *256*, 135-139.

(83) Van Meerbeek, A.; Ruiz-Hitzky, E. *Colloid Polym. Sci.* **1979**, *257*, 178-181.

(84) Kuroda, K.; Kato, C. *Clays Clay Miner.* **1979**, *27*, 53-56.

(85) Giese, R. F. *Clays Clay Miner.* **1978**, *26*, 51-57.

(86) Giese, R. F. *Bull. Minéral.* **1982**, *105*, 417-424.

(87) Cruz, M.; Jacobs, H.; Fripiat, J. J. *Proc. Int. Clay Conf.* **1973**, 35-46.

(88) Chekin, S. S. *Int. Geol. Rev.* **1982**, *11*, 1338-1346.

(89) Chekin, S. S. *Clays Clay Miner.* **1992**, *40*, 740-741.

(90) Sunagawa, I.; Koshino, Y. *Amer. Mineral.* **1975**, *60*, 407-412.

(91) Pinnavaia, T. J. *Science* **1983**, *220*, 365-371.

(92) Rupert, J. P.; Granquist, W. T.; Pinnavaia, T. J. In *Chemistry of Clays and Clay Minerals*; Newman A. C. D. Ed.; Mineralogical Society: London, 1987; pp 275-318.

(93) Jones, S. L. *Catal. Today* **1988**, *2*, 209.

(94) Jones, W. *Catal. Today* **1988**, 2, 357-367.

(95) Kikuchi, E.; Matsuda, T. *Catal. Today* **1988**, 2, 297-307.

(96) Farfantorres, E. M.; Sham, E.; Grange, P. *Catal. Today* **1992**, *15*, 515-526.

(97) Ohtsuka, K.; Hayashi, Y.; Suda, M. *Chem Mater.* **1993**, *5*, 1823-1829.

(98) Bartley, G. J. J. *Catal. Today* **1988**, 2, 233-241.

(99) Johnson, L. M.; Werpy, T. A.; Pinnavaia, T. J. *J. Am. Chem. Soc.* **1988**, *110*, 8545-8547.

(100) Barrer, R. M.; Hampton, M. G. *Trans. Farad. Soc.* **1957**, 1462-1475.

(101) Barrer, R. M. *Clays Clay Miner.* **1989**, *37*, 385-395.

(102) Barrer, R. M. *Pure Appl. Chem.* **1989**, *61*, 1903-1912.

(103) Barrer R. M. *Zeolites and Clay Minerals as Sorbents and Molecular Sieves*; Academic Press: London, 1978.

(104) Lao, H.; Latieule, S.; Detellier, C. *Chem. Mater.* **1991**, *3*, 1009-1011.

(105) Lao, H.; Detellier, C. *Clays Clay Miner.* **1994**, *4*, 477-481.

(106) Lao, H.; Detellier, C.; Matsuura, T.; Tremblay, A. Y. *J. Mater. Sci. Lett.* **1994**, *13*, 895-897.

(107) Kyotani, T.; Mori, T.; Tomita, A. *Chem. Mater.* **1994**, *6*, 2138-2142.

(108) Kyotani, T.; Suzuki, K. Y.; Sonobe, N.; Tomita, A.; Chida, Y.; Hara, R. *Carbon.* **1993**, *31*, 149-153.

(109) Putyera, K.; Bandosz, T. J.; Jagiello, J.; Schwarz, J. A. *Clays Clay Miner.* **1994**, *42*, 1-6.

(110) Ozin, G. A. *Advan. Mater.* **1992**, *4*, 612-649.

(111) Wang, M. S.; Pinnavaia, T. J. *Chem Mater.* **1994**, *6*, 468-474.

(112) Kojima, Y.; Usuki, A.; Kawasumi, M.; Okada, A.; Kurauchi, T.; Kamigaito, O.; Kaji, K. *J Polym. Sci B-Polym. Phys.* **1994**, *32*, 625-630.

(113) Kojima, Y.; Usuki, A.; Kawasumi, M.; Okada, A.; Kurauchi, T.; Kamigaito, O. *J Polym. Sci. A-Polym. Chem* **1993**, *31*, 1755-1758.

(114) Lan, T.; Kaviratna, P. D.; Pinnavaia, T. J. *Chem. Mater.* **1994**, *6*, 573-575.

(115) Vaia, R. A.; Ishii, H.; Giannelis, E. P. *Chem. Mater.* **1993**, *5*, 1694-1696.

(116) Aranda, P.; Ruiz-Hitzky, E. *Acta Polymer.* **1994**, *45*, 59-67.

(117) Ruiz-Hitzky, E.; Aranda, P. *Adv. Mater.* **1990**, *2*, 545-547.

(118) Aranda, P.; Ruiz-Hitzky, E. *Chem. Mater.* **1992**, *4*, 1395-1403.

(119) Theng B. K. G. *Formation and Properties of Clay-Polymer Complexes: Developments in Soil Science 9*; Elsevier Scientific Publishing Company: Amsterdam, 1979.

(120) Ruiz-Hitzky, E. *Advan. Mater.* **1993**, *5*, 334-340.

(121) Thomas, J. K. *Chem. Rev.* **1993**, *93*, 301-320.

(122) Ogawa, M.; Handa, T.; Kuroda, K.; Kato, C.; Tani, T. *J. Phys. Chem.* **1992**, *96*, 8116-8119.

(123) Ogawa, M.; Takahashi, S.; Kato, C.; Kuroda, K. *J. Mater. Chem.* **1994**, *4*, 519-523.

(124) Ogawa, M.; Takahashi, M.; Kuroda, K. *Chem. Mater.* **1994**, *6*, 715-717.

(125) Kresge, C. T.; Leonowicz, M. E.; Roth, W. J.; Vartuli, J. C.; Beck, J. S. *Nature* **1992**, *359*, 710-712.

(126) Beck, J. S.; Vartuli, J. C.; Roth, W. J.; Leonowicz, M. E.; Kresge, C. T.; Schmitt, K. D.; Chu, C. T-W.; Olson, D. H.; Sheppard, E. W.; McCullen, S. B.; Higgins, J. B.; Schlenker, J. L. *J. Am. Chem. Soc.* **1992**, *114*, 10834-10843.

(127) Inagaki, S.; Fukushima, Y.; Kuroda, K. *J. Chem. Soc. , Chem. Commun.* **1993**, 680-682.

(128) Vartuli, J. C.; Schmitt, K. D.; Kresge, C. T.; Roth, W. J.; Leonowicz, M. E.; McCullen, S. B.; Hellring, S. D.; Beck, J. S.; Schlenker, J. L.; Olsen, D. H.; Sheppard, E. W. *Chem. Mater.* **1994**, *6*, 2317-2326.

(129) Monnier, A.; Schüth, F.; Huo, Q.; Kumar, D.; Margolese, D.; Maxwell, R. S.; Stucky, G. D.; Krishnamurty, M.; Petroff, P.; Firouzi, A.; Janicke, M.; Chmelka, B. F. *Science* **1993**, *261*, 1299-1303.

(130) Huo, Q.; Margolese, D. I.; Ciesla, U.; Desmuth, D.; Feng, P.; Gier, T. E.; Sieger, P.; Firouzi, A.; Chmelka, B. F.; Schüth, F.; Stucky, G. D. *Chem. Mater.* **1994**, *6*, 1176-1191.

(131) Galarneau, A.; Barodawalla, A.; Pinnavaia, T. J. *Nature* **1995**, *374*, 529-531.

(132) Isayama, M.; Sakata, K.; Kunitake, T. *Chem. Lett.* **1993**, 1283-1286.

(133) Isayama, M.; Kunitake, T. *Adv. Mater.* **1994**, *6*, 77-78.

(134) Kleinfeld, E. R.; Ferguson, G. S. *Science* **1994**, *265*, 370-373.

(135) Ruiz-Hitzky, E.; Rojo, J. M. *Nature* **1980**, *287*, 28-30.

(136) Ruiz-Hitzky, E.; Rojo, J. M.; Lagaly, G. *Colloid. Polym. Sci.* **1985**, *263*, 1025-1030.

(137) Sprung, R.; Davis, M. E.; Kauffman, J. S.; Dybowsky, C. *Ind. Eng. Chem. Res.* **1990**, *29*, 213-220.

(138) Nakamoto N. *Infrared and Raman Spectra of Inorganic Compounds*; 3rd ed. Wiley: New-York, 1978.

(139) Kitahara, S. *Bull. Chem. Soc. Jpn.* **1976**, *49*, 3389-3393.

(140) Balard, H.; Sidqi, M.; Papirer, E.; Donnet, J. B.; Tuel, A.; Hommel, H.; Legrand, A. P. *Chromatographia* **1988**, *25*, 707-711.

(141) Sohn, J. R.; Ryu, S. G.; Song, J. H. *J. Mol. Catal.* **1990**, *62*, L1-L4.

(142) Chmielowiec, J.; Morrow, B. A. *J. Colloid Interf. Sci.* **1983**, *94*, 319-327.

(143) Blohowiak, K. Y.; Treadwell, D. R.; Mueller, B. L.; Hoppe, M. L.; Jouppi, S.; Kansal, P.; Chew, K. W.; Scotto, C. L. S.; Babonneau, F.; Kampf, J.; Laine, R. M. *Chem. Mater.* **1994**, *6*, 2177-2192.

(144) Greenler, R. G. *J. Chem. Phys.* **1962**, *37*, 2094-2100.

(145) Boreskov, G. K.; Yu, M.; Shchekochikhin, K.; Makarov, A. D.; Filimonov, V. N. *Dokl. Akad. Nauk. SSSR. (Phys. Chem.) English* **1964**, *156*, 564-566.

(146) Knözinger, H.; Stübner, B. *J. Phys. Chem.* **1978**, *82*, 1526-1532.

(147) Knözinger, H.; Scheglila, A.; Watson, A. M. *J. Phys. Chem.* **1968**, *72*, 2770-2774.

(148) Schiffino, R. S.; Merrill, R. P. *J. Phys. Chem.* **1993**, *97*, 6425-6435.

(149) Busca, G.; Rossi, P. F.; Lorenzelli, V.; Benaissa, M.; Travert, J.; Lavalley, J-C. *J. Phys. Chem.* **1985**, *89*, 5433-5439.

(150) Chin, Y-H.; Ellis, P. D. *J. Am. Chem. Soc.* **1989**, *111*, 7653-7654.

(151) Kubo, T.; Uchida, K. *Kogyo Kaguku Zasshi.* **1970**, *73*, 70-75.

(152) Inoue, M.; Kitamura, K.; Tanino, H.; Nakayama, H.; Inui, T. *Clays Clay Miner.* **1989**, *37*, 71-80.

(153) Inoue, M.; Kominami, H.; Inui, T. *J. Amer. Ceram. Soc.* **1990**, *73*, 1100-1102.

(154) Inoue, M.; Kominami, H.; Inui, T. *J. Chem. Soc., Dalton Trans.* **1991**, 3331-3336.

(155) Inoue, M.; Kondo, Y.; Inui, T. *Chem. Lett.* **1986**, 1421-1424.

(156) Inoue, M.; Kondo, Y.; Inui, T. *Inorg. Chem.* **1988**, *27*, 215-221.

(157) Inoue, M.; Tanino, H.; Kondo, Y. *Clays Clay Miner.* **1991**, *39*, 151-157.

(158) Le Bihan, S.; Guenot, J.; Figlarz, M. *J. Solid State Chem.* **1976**, *17*, 15-25.

(159) Mercier, L.; Facey, G. A.; Detellier, C. *J. Chem. Soc. , Chem. Commun.* **1994**, 2111-2112.

(160) Anderson, M. W.; Klinowski, J. *J. Am. Chem. Soc.* **1990**, *112*, 10-16.

(161) Anderson, M. W.; Klinowski, J. *Nature* **1989**, *339*, 200-203.

(162) Aronson, M. T.; Gorte, R. J.; Farneth, W. E. *J. Catal.* **1987**, *105*, 455-468.

(163) Bronnimann, C. E.; Maciel, G. E. *J. Am. Chem. Soc.* **1986**, *108*, 7154-7159.

(164) Tsiao, C.; Corbin, D. R.; Dybowski, C. *J. Am. Chem. Soc.* **1990**, *112*, 7140-7144.

(165) Aronson, M. T.; Gorte, R. J.; Farneth, W. E.; White, D. *J. Am. Chem. Soc.* **1989**, *111*, 840-846.

(166) Porro, T. J.; Pattacini, S. C. *Appl. Spectrosc.* **1990**, *44*, 1170-1175.

(167) Maeda, K.; Mizukami, F.; Niwa, S.; Toba, M.; Watanabe, M.; Masuda, K. *J. Chem. Soc., Faraday Trans.* **1992**, *88*, 97-104.

(168) Morikawa, Y. *Advances. in Catalysis,. Vol. 39. 39.* **1993**,

(169) Kikkawa, S.; Kanamaru, F.; Koizumi, M. *Inorg. Chem.* **1976**, *15*, 2195-2197.

(170) Ulman, A. *Advan. Mater.* **1990**, 2, 573-582.

(171) Rezgui, S.; Gates, B. C.; Burkett, S. L.; Davis, M. E. *Chem. Mater.* **1994**, *6*, 2390-2397.

(172) Hayashi, S.; Ueda, T.; Hayamizu, K.; Akiba, E. *J. Phys. Chem.* **1992**, *96*, 10922-10928.

(173) Barron, P. F.; Frost, R. L.; Skjemstad, J. O.; Koppi, A. J. *Nature* **1983**, *302*, 49-50.

(174) Yamanaka, S. *Inorg. Chem.* **1976**, *15*, 2811-2817.

(175) Scholzen, G.; Beneke, K.; Lagaly, G. *Z. Anorg. Allg. Chem.* **1991**, *597*, 183-196.

(176) Earnest C. M. *The Application of Differential Thermal Analysis and Thermogravimetry to the Study of Kaolinite Clay Minerals*; Perkin-Elmer: Norwalk,Conn., 1980.

(177) Rouxhet, P. G.; Samudacheata, N.; Jacobs, H.; Anton, O. *Clay Miner.* **1977**, *12*, 171-179.

(178) Guertin, D. L.; Wiberly, S. E.; Bauer, W. H.; Goldenson, J. *J. Phys. Chem.* **1956**, *60*, 1018-1019.

(179) Herreros, B.; Barr, T. L.; Klinowski, J. *J. Phys. Chem.* **1994**, *98*, 738-741.

(180) Stumpfnothof, K.; Weiden, N.; Muller, G. *Z. Kristallogr.* **1992**, *200*, 265-274.

(181) Sugimoto, M.; Kanayama, M.; Nakatsuji, H. *J. Phys. Chem.* **1992**, *96*, 4375-4381.

(182) Lambert, J. F.; Millman, W. S.; Fripiat, J. J. *J. Am. Chem. Soc.* **1989**, *111*, 3517-3522.

(183) Ledoux, R. L.; White, J. L. *Science* **1964**, *145*, 47-49.

(184) Wada, K. *Amer. Mineral.* **1965**, *50*, 924-941.

(185) Ratner, M. A.; Shriver, D. F. *Chem. Rev.* **1988**, *88*, 109-124.

(186) Papke, B. L.; Ratner, M. A.; Shriver, D. F. *J. Phys. Chem. Solids* **1981**, *42*, 493-500.

(187) Parfitt, R. L.; Greenland, D. J. *Clay Miner.* **1970**, *8*, 305-315.

(188) Aranda, P.; Galvan, J. C.; Casal, B.; Ruiz-Hitzky, E. *Electrochim. Acta.* **1992**, *37*, 1573-1577.

(189) Lagadic, I.; Léaustic, A.; Clément, R. *J. Chem. Soc., Chem. Commun.* **1992**, 1396-1397.

(190) Lemmon, J. P.; Lerner, M. M. *Chem Mater.* **1994**, *6*, 207-210.

(191) Ortiz-Avila, C. Y.; Clearfield, A. *Inorg. Chem.* **1985**, *24*, 1773-1778.

(192) Costantino, U.; Marmottini, F. *Mater. Chem Phys.* **1993**, *35*, 193-198.

(193) Liu, Y. J.; DeGroot, D. C.; Schindler, J. L.; Kannewurf, C. R.; Kanatzidis, M. G. *Chem. Mater.* **1991**, *3*, 992-994.

(194) Casal, B.; Aranda, P.; Ruiz-Hitzky, E. *Clay Miner.* **1994**, *29*, 191-203.

(195) Kojima, Y.; Usuki, A.; Kawasumi, M.; Okada, A.; Kurauchi, T.; Kamigaito, O. *J Polym. Sci. A-Polym. Chem* **1993**, *31*, 983-986.

(196) Usuki, A.; Kojima, Y.; Kawasumi, M.; Okada, A.; Fukushima, Y.; Kurauchi, T.; Kamigaito, O. *J. Mater. Res.* **1993**, *8*, 1179-1184.

(197) Kojima, Y.; Usuki, A.; Kawasumi, M.; Okada, A.; Fukushima, Y.; Kurauchi, T.; Kamigaito, O. *J. Mater. Res.* **1993**, *8*, 1185-1189.

(198) Bradley, W. F.; Weiss, E. J.; Rowland, R. A. *Clays Clay Miner. (Tenth National Conf.)* **1963**, *10*, 117-122.

(199) Ruiz-Hitzky, E.; Casal, B. *Nature* **1978**, *276*, 596-597.

(200) Wada, K. *Clay Miner.* **1967**, *7*, 51-61.

(201) Johnston, C. T.; Agnew, S. F; Bish, D. L. *Clays Clay Miner.* **1990**, *38*, 573-583.

(202) Brindley, G. W.; Kao, C-C.; Harrison, J. L.; Lipsicas, M.; Raythatha, R. *Clays Clay Miner.* **1986**, *34*, 239-249.

(203) Prost, R.; Dameme, A.; Huard, E.; Driard, J.; Leydecker, J. P. *Clays Clay Miner.* **1989**, *37*, 464-468.

(204) Olejnik, S.; Posner, A. M.; Quirk, J. P. *J. Colloid Interf. Sci.* **1971**, *37*, 536-547.

(205) Casal, B.; Ruiz-Hitzky, E. *Opt. Pur. Apl.* **1985**, *18*, 49-58.

(206) Yoshihara, T.; Tadokoro, H.; Murahashi, S. *J. Chem. Phys.* **1964**, *41*, 2902-2911.

(207) Matsuura, H.; Miyazawa, T. *Spectrochim. Acta* **1967**, *23A*, 2433-2447.

(208) Tunney, J. J.; Detellier, C. *Clays Clay Miner.* **1994**, *42*, 552-560.

(209) Ballantine, J. A.; Davies, M.; Patel, I.; Purnell, J. H.; Rayanakorn, M.; Williams, K. J. *J. Mol. Catal.* **1984**, *26*, 37-56.

(210) Opella, S. J.; Frey, M. H. *J. Am. Chem. Soc.* **1979**, *101*, 5854-5856.

(211) Alemany, L. B.; Grant, D. M.; Alger, T. D.; Pugmire, R. J. *J. Am. Chem. Soc.* **1983**, *105*, 6697-6704.

(212) Ripmeester, J. A.; Burlinson, N. E. *J. Am. Chem. Soc.* **1985**, *107*, 3713-3714.

(213) Björling, M.; Karlström, G.; Linse, P. *J. Phys. Chem.* **1991**, *95*, 6706-6709.

(214) Roy, A. K.; Inglefield, P. T. *Prog. NMR Spectr.* **1990**, *22*, 569-603.

(215) Adams, J. M.; Waltl, G. *Clays Clay Miner.* **1980**, *28*, 130-134.

(216) Adams, J. M. *Clays Clay Miner.* **1978**, *26*, 169-172.

(217) Breen, C.; Lynch, S. *Clays Clay Miner.* **1988**, *36*, 19-24.

(218) Bain, A. D.; Cramer, J. A. *J. Phys. Chem.* **1993**, *97*, 2884-2887.

(219) Sanchez-Soto, P. J.; Justo, A.; Perez-Rodriguez, J. L. *J. Mater. Sci.* **1994**, *29*, 1276-1283.

(220) Perez-Maqueda, L. A.; Perez-Rodriguez, J. L.; Scheiffele, G. W.; Justo, A.; Sanchez-Soto, P. J. *J Therm. Anal.* **1993**, *39*, 1055-1067.

(221) Mackenzie, K. J. D.; Meinhold, R. H.; Brown, I. W. M.; White, G. V. *J Mater. Sci* **1994**, *29*, 5631-5640.

(222) Takahashi, Y.; Sumita, I.; Tadokoro, H. *J. Polym. Sci.- Polym. Phys.* **1973**, *11*, 2113-2122.

(223) Yokoyama, M.; Ishihara, H.; Iwamoto, R.; Tadokoro, H. *Macromolecules* **1969**, *2*, 184-192.

(224) Sidheswaran, P.; Ram Mohan, S. V.; Ganguli, P.; Bhat, A. N. *Ind. J. Chem.* **1987**, *26A*, 994-998.

(225) Sidheswaran, P.; Bhat, A. N.; Ganguli, P. *Clays Clay Miner.* **1990**, *38*, 29-32.

(226) Apblett, A. W.; Landry, C. C.; Mason, M. R.; Barron, A. R. *Mat. Res. Soc. Symp. Proc.* **1992**, *249*, 75-80.

(227) Kimura, Y.; Sugaya, S.; Ichimura, T.; Taniguchi, I. *Macromolecules* **1987**, *20*, 2329.

(228) Kimura, Y.; Furukawa, M.; Yamane, H.; Kitao, T. *Macromolecules* **1989**, *22*, 79.

(229) Kimura, Y.; Tanimoto, S.; Yamane, H.; Kitao, T. *Polyhedron* **1990**, *9*, 371.

(230) Landry, C. C.; Pappé, N.; Mason, M. R.; Apblett, A. W.; Tyler, A. N.; MacInnes, A. N.; Barron, A. R. *Preprint (submitted for publication)*, **1995**.

(231) Taylor, R. M. In *Chemistry of Clays and Clay Minerals*; Newman A. C. D. Ed.; Mineralogical Society: London, 1987, pp 129-201.

(232) Huang, W. L. *Chem. Geol.* **1993**, *105*, 197-214.

(233) Kiss, A. B.; Gado, P.; Keresztury, G. *Spectrochim. Acta* **1982**, *38A*, 1231-1236.

(234) Fripiat, J. J.; Bosmans, H.; Rouxhet, P. G. *J. Phys. Chem.* **1967**, *71*, 1097-1111.

(235) Nakamoto K. *Infrared and Raman Spectra of Inorganic and Coordination Compounds*; 4th ed. John Wiley and Sons: New York, 1986.

(236) Kristof, J.; Mink, J.; Horvath, E.; Gabor, M. *Vib. Spectrosc.* **1993**, *5*, 61-67.

(237) Rezgui, S.; Gates, B. C. *Chem. Mater.* **1994**, *6*, 2386-2389.

(238) Sanchez-Camazano, M.; Sanchez-Martin, M. J. *Clays Clay Miner.* **1994**, *42*, 221-225.

(239) Jackson, M. L.; Whittig, L. D.; Pennington, R. P. *Soil Sci. Soc. Am. Proc.* **1949**, *14*, 77-81.

(240) Tanner, C. B.; Jackson, M. L. *Soil Sci. Soc. Am. Proc.* **1947**, *12*, 60-65.

(241) van Olphen, H. In *An Introduction to Clay Colloid Chemistry*; John Wiley and Sons: New-York, 1977; 2nd ed. pp 249-253.

(242) Schofield, R. K.; Samson, H. R. *Disc. Faraday Soc.* **1954**, *18*, 135-145.

(243) van Olphen H.; Fripiat J. J. *Data Handbook for Clay Minerals and Other Non-Metallic Minerals*; Pergamon Press: Oxford, 1979.

(244) Deeds, C. T.; van Olphen, H. In *Proceedings of the Tenth National Conference on Clays and Clay Minerals*; Ingerson E. Ed.; Macmillan Company: New-York, 1963; pp 318-328.

(245) Anceau, A. *Clay Miner.* **1992**, *27*, 283-292.

(246) Post, J. L. *Clays Clay Miner.* **1978**, *26*, 58-64.

(247) Caillère S.; Hénin S.; Rautureau M. *Mineralogie des Argiles : 1. Structure et Propriétés Physico-Chimique*; 2nd ed. 1982.

(248) Bai,J. *Performance of Organo-clay-PDMS Membranes in Pervaporation Processes*; MSc. Thesis, University of Ottawa, **1995**.

(249) Lao,H. *Novel Microporous Organo-Clay Materials and Organo-Clay Polymeric Composite Membranes*; PhD. Thesis, University of Ottawa, **1993**.